UC Berkeley
UC Berkeley Electronic Theses and Dissertations

Title
Solute Partitioning and Hindered Diffusion in Hydrogels

Permalink
https://escholarship.org/uc/item/3v41b7zc

Author
Liu, David Ezra

Publication Date
2016

Peer reviewed|Thesis/dissertation

eScholarship.org Powered by the California Digital Library
University of California

Solute Partitioning and Hindered Diffusion in Hydrogels

By

David Ezra Liu

A dissertation submitted in partial satisfaction of the

requirements for the degree of

Doctor of Philosophy

In

Chemical Engineering

in the

Graduate Division

of the

University of California, Berkeley

Committee in charge:

Professor Clayton J. Radke, Chair
Professor Susan J. Muller
Professor Kevin E. Healy

Spring 2016

Abstract

Solute Partitioning and Hindered Diffusion in Hydrogels

by

David Ezra Liu

Doctor of Philosophy in Chemical Engineering

University of California, Berkeley

Professor Clayton J. Radke, Chair

Solute uptake and release govern the efficacy of hydrogels in controlled drug delivery, tissue engineering, and chromatographic separations. In soft contact lenses, uptake and release of wetting, packaging, and care-solution agents is extensively employed to improve on-eye lens performance. Key physical parameters are the equilibrium solute partition coefficient and the solute diffusion coefficient in the gel that dictate the amounts and rates of uptake/release, respectively. To investigate the mechanisms of solute uptake and release in hydrogels, this work experimentally and theoretically determines equilibrium partition and diffusion coefficients of prototypical macromolecules and drugs in hydrogels over a wide range of water contents.

A hydrogel is a crosslinked polymer network with water-filled voids arranged in an unstructured three-dimensional mesh. Solutes (e.g., drugs, sugars, proteins, polymers) typically partition into and diffuse through the water-filled mesh but are excluded from mesh voids smaller than solute size. Consequently, solute size and the distribution of mesh sizes in the hydrogel-polymer network are vital to understand solute uptake and release. Solutes may also exhibit specific interactions with and, accordingly, adsorb to hydrogel polymer chains by hydrogen bonding or counterion binding. Specific solute adsorption to hydrogel-polymer strands results in larger partition coefficients and diminished effective diffusion rates.

To elucidate size effects on aqueous-solute transport rates, diffusion coefficients of large macromolecules in hydrogels with relatively small mesh sizes are investigated experimentally and theoretically. Two photon-confocal microscopy measures transient uptake and release concentration profiles of fluorescently labeled dextrans of varying molecular weight, and fluorescently labeled cationic avidin protein. Dextrans are highly water-soluble polysaccharides. Consequently, they exhibit negligible specific interactions with the hydrogel polymer network. Hydrogel uptake and release follow Fick's second law with almost identical diffusion coefficients in the uptake and release directions. To interpret our data, we implement a Large Pore Effective Medium (LPEM) model taking into account hydrodynamic drag, steric obstruction, and the distribution of mesh sizes available for solute transport. All necessary parameters are measured independently. In all cases, *a priori*-predicted diffusion coefficients by LPEM theory display excellent agreement with

experiment. In contrast to the nonspecific interacting dextrans, cationic avidin protein exhibits near irreversible adsorption with incomplete loading even after 6 days and incomplete release even after two weeks. Avidin protein uptake and release rates clearly highlight the significance of solute-specific adsorption in understanding solute transport rates in hydrogels.

Despite its importance, little attention has been given to how solute-specific interactions affect solute uptake in and release from hydrogels. We measure and theoretically predict partition and diffusion coefficients for prototypical water-soluble drugs in hydrogels where solute-specific binding is pronounced. Hydrogel composition is varied by adjusting the ratio of monomer constituents, 2-hydroxyethyl methacrylate (HEMA) and methacrylic acid (MAA). Partition and diffusion coefficients are obtained through two-photon confocal microscopy and UV/Vis-absorption spectrophotometry upon back extraction. The studied prototypical drugs all exhibit specific adsorption to nonionic MAA and HEMA moieties characterized by greater-than-unity partition coefficients and smaller effective diffusion rates. Conversely, none of the prototypical drugs displayed specific interactions with anionic MAA moieties. To predict equilibrium partition coefficients, we express the partition coefficient as a product of the hydrogel water content and individual enhancement factors for size-exclusion, nonspecific electrostatic interactions, and specific adsorption. Again, all necessary parameters are obtained independently. To predict effective diffusion coefficients, we extend LPEM for specific-solute adsorption and impose local equilibrium. As with the non-interacting dextran solutes, predicted partition and diffusion coefficients are in good agreement with experiment. A framework is now available to predict solute partitioning and diffusion in solute-hydrogel systems that exhibit specific interactions.

The developed theories for solute partitioning are further extended for direct application to silicone-hydrogel contact-lens materials. Silicone hydrogels (SiHy) are microphase-separated materials with silicone domains for oxygen transport and hydrophilic-polymer domains for aqueous-solute transport. Equilibrium silicone-hydrogel water and solute uptake are measured and predicted with an extended partitioning theory assuming that water and aqueous solutes reside only in the hydrophilic-polymer phase, whereas oleophilic solutes partition primarily into the silicone microphase. Excellent agreement is found between theory and experiment. Significantly, our development provides estimation of partitioning properties in silicone hydrogels based solely on synthesis formulation chemistry.

Finally, we deduce compositional properties of a laminated soft contact lens, DAILIES TOTAL 1® (delefilcon A) through measurement of fluorescent solute partition coefficients. Measured partition coefficients and solute-partitioning theory establish (1) the silicone-hydrogel core of the laminated lens is structurally similar to that of a non-laminated commercial SiHy soft contact lens, O_2OPTIX^{TM}, (2) the laminated-lens surface-gel layers are ~10 μm in thickness, (3) the laminated-lens surface-gel layers are of higher water content than the core, and (4) the surface-gel layers of the laminated lens are anionic, whereas the core is nonionic. Importantly, with solute-uptake properties known, our proposed solute-partitioning theory provides a means to elucidate hydrogel physico-chemical properties.

Table of Contents

List of Figures..... v
List of Tables..... viii
Acknowledgments..... ix

Chapter 1: Introduction..... 1
1.1 Motivation..... 1
1.2 Background..... 2
1.2.1 The Equilibrium Solute Partition Coefficient..... 2
1.2.2 The Hindered Diffusion Coefficient..... 4
1.3 Dissertation..... 6
1.4 References..... 8

Chapter 2: Macromolecule Sorption and Diffusion in HEMA/MAA Hydrogels..... 15
2.1 Abstract..... 15
2.2 Introduction..... 16
2.3 Experimental Section..... 17
2.3.1 Gel Synthesis and Characterization..... 17
2.3.2 Solute Characterization..... 18
2.3.3 Gel-Solute Confocal Microscopy..... 19
2.3.4 Nonadsorbing-Solute-Gel Diffusion Coefficients..... 23
2.4 Results..... 24
2.4.1 Nonspecific Interacting Solutes..... 24
2.4.2 Specific-Gel Interacting Counterion Solute..... 25
2.5 Comparison to Theory..... 28
2.5.1 Nonspecific Interacting Solutes..... 28
2.5.2 Large Pore Effective Medium Theory..... 34
2.5.3 Specific Interacting Counterion Solute..... 36
2.6 Conclusions..... 37
2.7 Acknowledgements..... 39

2.8 References..... 39
Appendix 2A: Solution to Linear-Adsorption Kinetics Model..... 46

Chapter 3: Water-Soluble Drug Partitioning and Adsorption in HEMA/MAA Hydrogels..... 47
3.1 Abstract..... 47
3.2 Introduction..... 48
3.3 Materials and Methods..... 50
3.3.1 Chemicals..... 50
3.3.2 Hydrogel Synthesis..... 50
3.3.3 Equilibrium Water Content..... 51
3.3.4 Solute Loading..... 52
3.3.5 Fluorescence Confocal Microscopy..... 52
3.3.6 Back Extraction with UV/Vis-Absorption Spectrophotometry..... 54
3.3.7 Solute Size..... 55
3.4 Experimental Results..... 56
3.5 Theory..... 57
3.6 Discussion..... 60
3.7 Conclusions..... 68
3.8 References..... 68
Appendix 3A: Thermodynamics of Partitioning..... 73
Appendix 3B: Donnan Potential..... 74

Chapter 4: Diffusion of Water-Soluble Sorptive Drugs in HEMA/MAA Hydrogels. 76
4.1 Abstract..... 76
4.2 Body..... 77
4.3 Acknowledgements..... 86
4.4 References..... 86
Appendix 4A: Supporting Information..... 90
S1 Hydrogel Synthesis and Characterization..... 90
S2 Solute Diffusion-Coefficient Measurements..... 90

S3 Theory..... 93

Chapter 5: Equilibrium Water and Solute Uptake in Silicone Hydrogels..... 97

5.1 Abstract..... 97

5.2 Introduction..... 98

5.3 Materials and Methods..... 99

5.3.1 Chemicals..... 99

5.3.2 Hydrogel Synthesis..... 100

5.3.3 Equilibrium Water Content..... 101

5.3.4 Equilibrium Solute Partition Coefficients..... 101

5.4 Experimental Results..... 102

5.5 Theory..... 107

5.6 Discussion..... 109

5.7 Conclusions..... 110

5.8 References..... 110

Chapter 6: Fluorescent Solute-Partitioning Characterization of Layered Soft Contact Lenses..... 113

6.1 Abstract..... 113

6.2 Introduction..... 114

6.3 Materials and Methods..... 114

6.3.1 Soft Contact Lenses..... 114

6.3.2 Attenuated Total-Reflectance Fourier-Transform Infrared Spectroscopy (ATR-FTIR)..... 115

6.3.3 Fluorescent Solutes..... 117

6.3.4 Solute Partition Coefficients..... 117

6.4 Results..... 119

6.5 Discussion..... 125

6.6 Conclusions..... 128

6.7 Acknowledgements..... 129

6.8 References..... 129

Appendix A: Confocal Microscopy Procedure..... 133
A1 Initializing the Laser and Microscope..... 133
A2 Initial Imaging Procedure..... 137
A3 Concentration Detection: 2D Imaging in the Vertical (z-) Direction..... 139
A4 Obtaining Fluorescence Intensities..... 140
A5 Calibration: Ensure Florescence Intensity and Solute Concentration are Linearly Proportional..... 143
A6 Partition Coefficient Measurement..... 143
A7 In-Gel Diffusivity Measurement..... 143

Appendix B: Transient Intensity Profiles Measured by Confocal Microscopy..... 146

Appendix C: Steric Obstruction Factor Derivation..... 149
C1 Single Cylindrical-Cell Diffusion Coefficient:..... 149
C2 Evaluation of the Steric Obstruction Factor..... 154

Appendix D: Hydrodynamic Permeability of Hydrogels..... 159
Abstract..... 159
D1 Experimental Methods..... 160
D1.1 Hydrogel Synthesis..... 160
D1.2 Hydrodynamic Permeability Measurement..... 161
D2 Results and Discussion..... 163
D2.1 Hydrodynamic Permeabilities of HEMA/MAA Homopolymer Hydrogels..... 163
D2.2 Hydrodynamic Permeabilities of HEMA/MAA-based SiHys..... 167
D3 References..... 169

List of Figures

Figure 1.1: Schematic of a hydrogel polymer network..... 3

Figure 2.1: Fluorescence micrographs of FITC-dextran20 absorption into and desorption from a 70-wt% HEMA/ 30-wt% MAA hydrogel with 0.25-wt% cross-link density..... 20

Figure 2.2: Transient intensity profiles of FITC-dextran20 absorption into and desorption from a 70-wt% HEMA/ 30-wt% MAA hydrogel with 0.25-wt% cross-link density..... 22

Figure 2.3: Relative diffusion coefficients of FITC-dextrans in 70-wt % HEMA/ 30-wt % MAA hydrogels as a function of polymer volume fraction..... 26

Figure 2.4: Fluorescence micrographs and transient intensity profiles of Fl-avidin in a 70-wt % HEMA/ 30-wt % MAA hydrogel..... 27

Figure 2.5: Hydrodynamic permeability as a function of water content expressed as $(1-\phi_2)^3 / \phi_2^2$ for hydrogels similar to 70-wt% HEMA/ 30-wt% MAA..... 30

Figure 2.6: Relative diffusion coefficients of FITC-dextran4 in 70-wt % HEMA/ 30-wt % MAA hydrogels as a function of polymer volume fraction..... 31

Figure 2.7: Relative diffusion coefficients of FITC-dextran10 in 70-wt % HEMA/ 30-wt % MAA hydrogels as a function of polymer volume fraction..... 32

Figure 2.8: Relative diffusion coefficients of FITC-dextran20 in 70-wt % HEMA/ 30-wt % MAA hydrogels as a function of polymer volume fraction..... 33

Figure 2.9: Transient loading and release profiles of Fl-avidin in a 70-wt% HEMA/ 30-wt% MAA hydrogel with 0.05-wt % cross-link density..... 38

Figure 3.1: Fluorescence-confocal-microscopy images of sodium fluorescein in HEMA/MAA hydrogels at pH 7.4..... 53

Figure 3.2: Sodium-fluorescein enhancement factor as a function of water volume fraction in HEMA/MAA hydrogels equilibrated in phosphate buffer (pH 7.4) with varying molarity NaCl..... 58

Figure 3.3: Measured solute enhancement factors as functions of water volume fraction for prototypical drugs in HEMA/MAA hydrogels with varying wt % MAA equilibrated in PBS (pH 7.4)..... 62

Figure 3.4: Sodium-fluorescein enhancement factor versus water volume fraction in HEMA/MAA hydrogels equilibrated in PBS (pH 7.4)..... 63

Figure 3.5: Calculated dimensionless Donnan electric potential as a function of water volume fraction for MAA-containing HEMA/MAA hydrogels equilibrated in phosphate buffer (pH 7.4) with varying molarity NaCl..... 64

Figure 3.6: Measured solute enhancement factors as functions of MAA copolymer content for prototypical drugs in HEMA/MAA hydrogels with varying wt % MAA equilibrated in dilute HCl (pH 2)..... 66

Figure 3.7: Sodium-fluorescein enhancement factor as a function of MAA copolymer content in HEMA/MAA hydrogels equilibrated in aqueous HCl (pH 2)..... 67

Figure 4.1: Relative solute diffusion coefficients as functions of polymer volume fraction, for prototypical drugs in HEMA/MAA hydrogels equilibrated in PBS..... 80

Figure 4.2: Relative solute diffusion coefficients as functions of MAA copolymer content for prototypical drugs in HEMA/MAA hydrogels equilibrated in HCl..... 81

Figure 4.3: Parity plot of theoretical and experimental relative solute diffusion coefficients for prototypical drugs in HEMA/MAA hydrogels..... 85

Figure 4A.1: Transient intensity profiles of sodium fluorescein desorption from a 90 wt% HEMA /10 wt% MAA hydrogel..... 91

Figure 4A.2: Release solution absorbance as a function of time for theophylline desorption from a 90 wt% HEMA /10 wt% MAA hydrogel..... 94

Figure 5.1: Equilibrium water volume fraction as a function of the solvent-free volume fraction of hydrophilic monomer for HEMA/MAA-based SiHys..... 103

Figure 5.2: Theophylline partition coefficients as a function of the solvent-free volume fraction of hydrophilic monomer for HEMA/MAA-based SiHys..... 104

Figure 5.3: Caffeine partition coefficients as a function of the solvent-free volume fraction of hydrophilic monomer for HEMA/MAA-based SiHys..... 105

Figure 5.4: Oleophilic-solute partition coefficients as a function of the solvent-free volume fraction of hydrophilic monomer for HEMA/MAA-based SiHys.. 106

Figure 6.1: Truncated ATR-FTIR spectra for PBS solution, DAILIES TOTAL1®, and O2OPTIX™..... 116

Figure 6.2: ATR-FTIR-measured mass water content as a function of known bulk gravimeteric water content for HEMA/MAA synthesized hydrogels..... 118

Figure 6.3: Fluorescence-confocal-microscopy images of FITC-dextran4 at equilibrium in DAILIES TOTAL1® and O2OPTIX™..... 121

Figure 6.4: Hydrophilic solute partition coefficients as a function of hydrodynamic radius at pH 7.4 for FITC-dextrans in DAILIES TOTAL1® and O2OPTIX™..... 122

Figure 6.5: Hydrophilic solute partition coefficients as a function of hydrodynamic radius at pH 4 for FITC-dextrans in DAILIES TOTAL1® and O2OPTIX™..... 123

Figure 6.6: Fluorescence-confocal-microscopy images of Nile Red at equilibrium in DAILIES TOTAL1® and O2OPTIX™..... 126

Figures A.1-A.17: Figures illustrating steps in confocal microscopy.....133-142

Figure B.1: Transient intensity profiles of FITC-dextran20 desorption from 70 wt % HEMA/30 wt % MAA hydrogels with 1 wt % cross-link density at pH 7.4..... 146

Figure B.2: Transient intensity profiles of FITC-dextran20 absorption into 70 wt % HEMA/30 wt % MAA hydrogels with 0.05 wt % cross-link density at pH 7.4..... 147

Figure B.3: Transient intensity profiles sodium fluorescein desorption from 100 wt % HEMA/0 wt % MAA hydrogels with 0.25 wt % cross-link density at pH 2..... 148

Figure C.1: Diagram of cylindrical cell..... . 150

Figure C.2: Diagram of flux through cylindrical cell..... 153

Figure C.3: Diagram of cylindrical cell illustrating r' …..... 155

Figure C.4: The step function, $\sigma\left(r'-(R-a_f)\right)$ as a function of r' 156

Figure D.1: Diagram of the hydrodynamic permeameter apparatus..... 162

Figure D.2: Diagram of the hydrodynamic permeability membrane cell..... 164

Figure D.3: Typical measured hydrodynamic permeabilities as a function of pressure drop for three MAA-based SiHys at pH 7.4..... 165

Figure D.4: Hydrodynamic permeabilities at zero pressure drop as a function of water contents expressed as $(1-\phi_2)^3/\phi_2^{\,2}$ for the HEMA/MAA hydrogels studied in Chapters 2-4 at pH 7.4..... 166

Figure D.5: Hydrodynamic permeabilities at zero pressure drop as a function of the solvent-free volume fraction of hydrophilic monomer for HEMA/MAA-based SiHys at pH 7.4..... . 168

List of Tables

Table 2.1: Hydrogel polymer volume fraction and average mesh size..... 18

Table 2.2: Solute hydrodynamic diameters..... 19

Table 2.3: Solute-hydrogel absorption diffusivities..... 24

Table 2.4: Solute-hydrogel desorption diffusivities..... 25

Table 2.5: Selected gel-diffusion models..... 28

Table 3.1: Hydrogel water volume fractions with varying HEMA:MAA weight ratios..51

Table 3.2: Solute properties in aqueous PBS / HCl.....55

Table 3.3: Enhancement factors with varying HEMA:MAA weight ratios in aqueous PBS / HCl..... 56

Table 3.4: Henry's adsorption constant..... 60

Table 4.1: Hydrogel water contents and solute partition coefficients with varying HEMA:MAA weight ratios in aqueous PBS/HCl..... 78

Table 4.2: Solute bulk-aqueous diffusion coefficients and hydrodynamic radii..... 79

Table 4A.1: Henry's adsorption constant..... 96

Table 5.1: SiHy composition and hydrophilic-monomer volume fraction.....100

Table 5.2: Overall solute enhancement factors for the conventional hydrogels.....108

Table 6.1: Solute properties in aqueous pH 7.4.....117

Table 6.2: Water content of DAILIES TOTAL1® and O2OPTIX™ at aqueous pH 7.4 / 4.....120

Table 6.3: Partition coefficients of FITC-avidin and FITC-dextran20 in DAILIES TOTAL1® and O2OPTIX™ at pH 7.4.....124

Table 6.4: Oleophilic Solute Partition Coefficients in DAILIES TOTAL1® and O2OPTIX™.....125

Table D.1: SiHy composition and hydrophilic-monomer volume fraction.....161

Acknowledgements

This dissertation is one of many thanks. I cannot describe in words how grateful I am to everyone who has helped me attain my goals.

Professional

To Clay for taking me into the Radke Laboratory and teaching me the science (and art) of performing fundamental research. His mentorship made me the researcher I am today, and our fruitful impassioned discussions about science and my project were vital to the work presented in this dissertation. Clay, I really appreciate your guidance in delving deep into thermodynamics and diffusion, and don't believe I would have learned or grown so much with any other adviser.

To the Radke Laboratory past and present: To Colin Cerretani and Sam Maurer for being amazing 5th years when I first joined and showing me the ropes of working in the lab. Their advice still resonates even now when I am graduating. To Cheng-Chun Peng for in-depth conversations about contact lenses and for helpful recommendations on conducting independent research. To Tom Dursch for our dialogue and insight in chemical engineering and transport phenomena, for help managing the day-to-day workings in the lab throughout the years, and whose collaborations on our many projects were integral to their success. To Andrew Crothers, for providing good company and for engaging in riveting scientific (and nonscientific) discussions with me. To Tatyana Svitova for guidance, for knowing where everything is in the lab, and for being extremely helpful whenever I needed something.

To the many undergraduate students I've had the distinct pleasure of working with: Nicole Taylor, Himani Nadgauda, Yoobin Oh, Kevin Hou, Sophia Chan, Daniel Bregante, Nina Widjaja, Shuo Wang, Neil Razdan, Tyler Field, and others who taught me the importance of mentorship and collaboration in research.

To Prof. Prausnitz for co-advising the membrane vapor extraction project and whose helpful teachings in phase equilibria thermodynamics and interesting stories about Berkeley were fundamental to completing this endeavor. And to Jialing Chen whose collaboration on the membrane vapor extraction project led to a working prototype apparatus.

To the Chemical & Biomolecular Engineering Department administration: Carlet Altamirano, Joel Adlen, Kristin Stangl, and many others. They are truly the people who help the department run smoothly and make bureaucracy manageable to graduate students.

To my dissertation committee for taking the time to review this dissertation and provide helpful comments. To Alcon Laboratories and Chevron Corporation for funding the work presented in this dissertation and the research on membrane vapor extraction, respectively.

I really appreciate all of the help everyone has given me throughout the years.

Friends and Confidants

To my house-mates of the Channing Institute: Stan Herrmann, Allie Landry, Chris Jakobson, Pete Lobaccaro, and Kevin Wujcik for making graduate school enjoyable and fun, for being so supportive, and for helping through the good times (and the bad). The parties at the house, video game sessions, outings in the city, family dinners, scientific discussions, and house practice qualifying exams really made my graduate school experience. I don't know where I would be without you guys. To the visiting scholar Leah Sibener for her scholarly contributions and festivity. And to recent additions: Markita Landry and Dan Robbins for showing me professorial life and the "real world" can be cool. Looking forward to my next steps.

To Dan and Elizabeth Lorenc, Eddie Buehler, and Ellie Hass for amazing times and adventures: for joining me at the best pizza places and hangout spots in Berkeley (after lab), weekends away (escaping lab), and lending an ear to listen to my craziness (about lab). And to the dogs, Barley and Jazzy for making everyone happy even when research is going rough.

To my fellow Chemical Engineering entering class of 2011 for being so close-knit and for great memories that I will never forget: The potlucks, Vegas after prelims, get-togethers after each person's qualifying exam and colloquium, College of Chemistry Softball League, Annual Harley/Hannemann Not-A-Christmas-Movie Movie Night, and birthday celebrations are moments I treasure. And on that note, a special thanks to Rachel Licht and Lin Louie for always baking something for my birthday and for being great friends.

And to many others not explicitly stated for helping me (stay sane) in completing my doctoral work at UC Berkeley.

Family

Finally, and most importantly, to my parents, Audrey and Paul, and to my sister, Rebecca for always being there and supporting me to reach all of my endeavors big or small, through the highs and the lows, near or far (2500 miles away from NY to CA). My family is the foundation that grounds me, providing support when I need it most, helping me climb higher (sometimes into the clouds) to achieve my dreams and aspirations.

Chapter 1

Introduction

1.1 Motivation

Hydrogels, hydrophilic polymeric networks swollen in aqueous media,[1,2] are of interest in a wide variety of applications including bioseparations,[3,4] biosensing,[5-8] and encapsulation of cells for tissue engineering.[9-11] Due to their biocompatibility, hydrogels are also extensively used in pharmaceutical applications for controlled delivery of bioactive agents.[2,12-24] Soft contact lenses (SCLs), a widespread application of hydrogels, can be employed as delivery vehicles for drugs and for comfort/wetting agents to the eye.[25-30]

One major challenge in developing separation, sensing, or delivery systems is controlling the amount and rates of solute uptake and release. Hydrogels are especially important because: (1) they provide protection from harmful environments and (2) they undergo swelling/deswelling in response to external stimuli, allowing for regulated and extended uptake/release in specific conditions.[2,24,31] If successfully employed, controlled and targeted release using hydrogels can significantly impact clinical treatment of disorders and diseases, such as in administering insulin in diabetes.[32-34] Likewise, in SCLs, surfactants, drugs, and polymeric agents can potentially be delivered through the lens to prevent adhesion to the eye, to protect against bacterial adhesion, and to provide comfort.[25,30,35,36]

In all applications, the amounts and rates of solute uptake/release are governed by the equilibrium solute partition coefficient and in-gel diffusion coefficient, respectively.[1,2,37-41] This dissertation develops a mechanistic understanding of solute partitioning and diffusion in hydrogels, exploring the effects of solute size, mesh size, electrostatics, and specific adsorption. Equilibrium partition coefficients and diffusion coefficients of prototypical macromolecules and drugs are experimentally measured and theoretically predicted in hydrogels over a wide range of water contents and pH. The developed mechanistic physical models are then extended for direct application to SCL-material design and characterization. To understand more fully the mechanisms of solute uptake in and release from hydrogels, the following sections provide context for the key physical parameters involved: the equilibrium solute partition coefficient and the hindered diffusion coefficient.

1.2 Background

1.2.1 The Equilibrium Solute Partition Coefficient

The amount of solute uptake and release is governed by the equilibrium partition coefficient, k_i, of dilute solute i given by

$$k_i \equiv \frac{C_i^{gel}}{C_i^{bulk}}, \tag{1}$$

where C_i^{gel} and C_i^{bulk} are the solute concentrations in the equilibrated swollen hydrogel and in the surrounding aqueous bulk solution respectively.[42-46] Eq. 1 is restricted to reversible solute uptake and release. Additionally, the partition coefficient remains independent of surrounding bulk solute concentration only in dilute solution where solute-solute interactions are negligible.[37,42]

The structure of a hydrogel is a crosslinked polymer network with water-filled voids arranged in an unstructured three-dimensional mesh.[1,47,48] Figure 1.1 displays a schematic of a hydrogel with prototypical solutes partitioning into the water-filled mesh voids. For ideal point solutes that do not interact with the hydrogel-polymer chains, the partition coefficient and the hydrogel water-volume fraction, ϕ_1, are equivalent. The ideal point solute has access to all water-filled space not taken up by polymer. However, typical solutes (e.g., drugs, sugars, proteins, polymers) are of finite size and charge, and may even specifically interact with hydrogel-polymer chains. To describe deviations from ideality, an enhancement factor[37] may be defined, or

$$E_i \equiv \frac{k_i}{\phi_1}. \tag{2}$$

$E_i < 1$ indicates rejection due to finite solute size and/or from electrostatic repulsion (for coionic solutes and charged hydrogel-polymer chains). $E_i > 1$ arises from specific-solute interactions with hydrogel polymer chains, including counterion complexation and hydrogen bonding. $E_i = 1$ reflects ideality or apparent ideality from competing interactions of size exclusion, electrostatics and specific adsorption. $E_i = 0$ occurs when a solute is too large to enter the water-filled voids of the hydrogel polymer network.

A key length scale determining solute accessibility in the polymer network is the mesh size, ξ, defined as the spacing between crosslinks.[2,40,49] The hydrogel polymer network may also contains a distribution of mesh sizes, as hydrogel synthesis produces a distribution of polymer-strand lengths between crosslinks.[37,46,50,51] Solutes only penetrate water-filled mesh voids with mesh sizes larger than solute size. Additionally, within the gel volume, solutes occupy only a fraction of the space available due to size exclusion. Hence, all else being equal, larger solutes access a smaller fraction of water void space in the polymer network and exhibit smaller enhancement factors.[37,42,44,46]

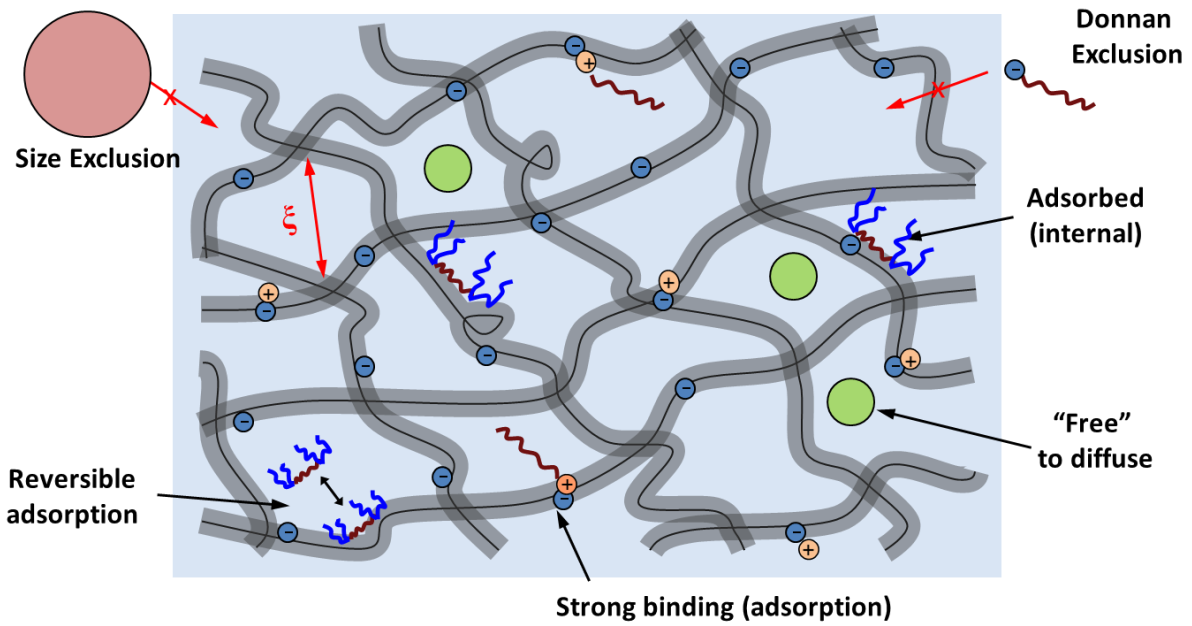

Figure 1.1: Schematic of a hydrogel polymer network. Solutes partitioning and diffusing in the hydrogel may exhibit size exclusion, nonspecific electrostatic interactions, and specific adsorption to hydrogel polymer chains.

Enhancement factors in polyelectrolyte hydrogels are strongly influenced by nonspecific electrostatic interactions.[44-46] For coion-charged solutes, enhancement factors are diminished by electrostatic repulsion between the solute and hydrogel polymer chains. For counterion-charged solutes, enhancement factors are amplified by favorable electrostatic interactions with the hydrogel polymer network. For nonionic solutes, however, electrostatic interactions are missing and enhancement factors are solely determined by size exclusion and specific interaction.

Greater-than-unity enhancement factors often denote specific adsorption to hydrogel polymer chains.[37,43,46] Counterion solutes not only exhibit favorable nonspecific electrostatic interactions, but also undergo specific ion-binding with charged moieties in polyelectrolyte-hydrogels. Nonionic and counterionic solutes also display greater-than-unity enhancement factors when specific interactions overcome size exclusion and/or electrostatic repulsion. Specifically interacting solutes may reversibly or irreversibly bind to hydrogel polymer chains and typically exhibit E_i of $O(1)$ and $E_i >> 1$, respectively.[37] Generally, larger enhancement factors indicate stronger specific solute-polymer-chain interactions and an increasing tendency towards irreversible adsorption.

Because of extensive application, significant effort has been expended on studying equilibrium solute partition coefficients both experimentally and theoretically. Published work primarily falls within three classes: (1) partitioning of nonionic solutes excluded only due to finite solute size;[37,42,43,52-57] (2) partitioning of coionic solutes (in polyelectrolyte hydrogels) excluded by both solute size and electrostatic repulsion;[43-45,58] and (3) partitioning of solutes that specifically interact with hydrogel-polymer strands, including by ion complexation and by hydrogen bonding.[16-19,45,46,58-60] Despite the wide range of interest in equilibrium solute uptake, partition-coefficient prediction is rarely attempted for both the second and third class of solute. Chapter 3 provides a framework quantifying the effects of size exclusion, specific adsorption, and electrostatic interaction on equilibrium solute partitioning.

1.2.2 The Hindered Diffusion Coefficient

The rates of solute uptake and release are governed by the diffusion coefficient, D_i, of dilute solute i. For solutes that do not specifically interact with the hydrogel polymer chains, Fick's law dictates

$$\frac{\partial C_i^{gel}}{\partial t} \equiv \nabla D_i \nabla C_i^{gel}, \tag{3}$$

where t denotes time.[61,62] The diffusion coefficient governs the proportionality between flux and concentration gradient driving force. Further, the diffusion coefficient is constant and independent of surrounding bulk solute concentration only in dilute solution where solute-solute interactions are negligible.[47,48]

Aqueous solutes diffuse through the water-filled voids of the hydrogel polymer network.[18,21,38,39,41,42,63-70] Accordingly, D_i is reduced with respect to that in bulk solution, D_{io}, by interactions with the hydrogel-polymer chains including physical obstruction and

hydrodynamic resistance.[18,21,38,39,41,42,63-70] The distribution of mesh sizes for a given hydrogel is also of critical importance, characterizing the mesh voids accessible for solute transport.[37,50,65] In general, larger polymer-volume-fraction hydrogels with smaller mesh sizes typically exhibit smaller solute diffusion coefficients.

Solute diffusion in hydrogels have been studied extensively both experimentally[17-19,21,38,39,41,42,60,64-73] and theoretically.[18,38,39,41,42,64-71,74-78] Published experimental work typically investigates diffusion of nonspecific-interacting aqueous solutes in high-water-content hydrogels (i.e., >90%).[18,19,21,38,39,41,42,64-72] Available theoretical models focus almost exclusively on nonspecific interactions describing diffusion in hydrogels through three phenomena: (1) available free-volume, (2) hydrodynamic drag, and/or (3) steric obstruction by hydrogel-polymer chains. The first class is collectively known as free-volume theory where diffusion in bulk liquid solution is typically described by a probability of solute jumping through void spaces between solvent molecules.[69,76,77] The jumping probability in hydrogels is altered from that in free solution due to the presence of hydrogel polymer strands. The second class of models are based on hydrodynamics and the increased frictional drag a solute experiences as it diffuses through the hydrogel-polymer network.[73,74,78] Models in the third class describe the increased tortuous path a solute must take and the obstruction of that path by hydrogel polymer chains.[65,68,75,79,80] Although successful at correctly predicting trends, many theories rely on parameters and/or empirical proportionality constants that are difficult to determine through independent measurement.[38,75]

To account for both frictional drag and obstruction by hydrogel-polymer strands, Brady suggested the relative diffusion coefficient, D_i / D_{io}, may be expressed as a product of a hydrodynamic resistance factor and steric obstruction factor.[81] We adopt this approach in Chapter 2 and develop an effective medium model for *a priori* diffusion-coefficient prediction. With all parameters determined independently, macromolecular diffusion coefficients are predicted accounting for hydrodynamic drag, steric obstruction, and the mesh voids available for solute transport.

Little attention has been given to predicting solute diffusion in hydrogels where specific interactions are pronounced. Solute-specific adsorption is often displayed by drugs, polymers and proteins in SCL-material and controlled-release hydrogels.[12,13,17,19,21,45,60,63,64,71] Solute-specific complexation with polymer strands result in diminished release rates. Consequently, solute release rates from hydrogels and application efficacy are often governed by solute-specific interactions with the hydrogel-polymer network.

To correctly account for solute specific adsorption, we distinguish between solute diffusion through the water-filled voids and solute adsorption onto hydrogel-copolymer strands. With this classification, Eq. 3 becomes

$$\phi_1 \frac{\partial C_i^L}{\partial t} + \phi_2 \frac{\partial n_i}{\partial t} = \phi_1 \nabla D_i \nabla C_i^L , \tag{4}$$

where C_i^L and n_i are the concentrations of solute i in the liquid-filled voids and adsorbed on the hydrogel polymer strands, respectively, and ϕ_2 is the hydrogel polymer-volume fraction. Accordingly, an expression describing the kinetics of adsorption is now required as discussed

in Chapter 2. Chapters 2 and 4 provide a framework quantifying the effects of specific adsorption on solute diffusion in hydrogels.

1.3 Dissertation

This dissertation experimentally and theoretically investigates equilibrium partitioning and diffusion of prototypical macromolecules and drugs in hydrogels over a wide range of water contents. Chapters 2-4 establish a fundamental understanding of solute partitioning and hindered diffusion through experiment and model development. Chapters 5-6 extend the theoretical framework developed in prior chapters to other systems of interest including silicone hydrogel biphasic materials and commercial soft contact lenses. Each chapter is summarized below.

Chapter 2: Macromolecule Sorption and Diffusion in HEMA/MAA Hydrogels

Characteristic of SCL-material hydrogels is their relatively low water contents and small mesh sizes.[43] Aqueous diffusing solutes of interest, including polymers and proteins are comparably large.[25,30,59,82] This chapter considers size effects on solute transport rates and investigates macromolecular diffusion coefficients in SCL-material hydrogels where solute size and mesh size are similar. Transient uptake and release concentration profiles of fluorescently labeled macromolecules are measured by two-photon confocal microscopy. Diffusion coefficients are obtained for fluorescently labeled dextrans of varying size and for fluorescently labeled cationic protein avidin. Dextrans are highly water soluble polysaccharides and specific interactions may be neglected. Accordingly, diffusion coefficients are predicted by a large-pore effective-medium (LPEM) model solely accounting for nonspecific interactions and the distribution of mesh sizes available for transport. Using no adjustable parameters, predicted diffusion coefficients are in excellent agreement with experiment. For cationic avidin protein, near irreversible adsorption is observed with gel-loading 3 orders of magnitude slower than that of a dextran of similar size. To interpret our results, a simple linear kinetic model is employed. Absorption and desorption kinetics of cationic avidin protein exemplifies the importance of solute-specific interactions in understanding solute uptake in and release from hydrogels.

Chapter 3: Water-soluble drug partitioning and adsorption in HEMA/MAA hydrogels.

In this chapter, experimentally measured and theoretically predicted prototypical drug partition coefficients are obtained in SCL-material hydrogels where solute specific interactions with the hydrogel polymer chains are pronounced. Two-photon confocal microscopy and back extraction with UV/Vis-absorption spectrophotometry measure equilibrium partition coefficients for acetazolamide, caffeine, hydrocortisone, Oregon Green 488, sodium fluorescein, and theophylline in five soft-contact-lens-material hydrogels over a range of gel polymer composition, water content (40 to 92%), pH (2 to 7.4), and aqueous salinity. Hydrogel composition is adjusted through the relative ratio of monomer constituents, 2-hydroxyethyl methacrylate (HEMA) and methacrylic acid (MAA). At pH 2, MAA is nonionic, whereas at pH 7.4, MAA is anionic. Specific interactions with nonionic MAA and HEMA moieties were exhibited by all studied prototypical drugs. In all cases, $E_i > 1$ was observed in HEMA and nonionic MAA homopolymer hydrogels. In contrast, negligible specific interactions were observed with anionic MAA. For all studied

prototypical drugs, enhancement factors less than unity, $E_i < 1$, were measured in anionic MAA homopolymer hydrogels. To interpret our results, the overall enhancement factor is expressed as a product of individual enhancement factors for size-exclusion, nonspecific electrostatic interactions, and specific adsorption. All necessary parameters were determined independently. Excellent agreement is found between theory and experiment for all studied prototypical drugs.

Chapter 4: Sorption of Water-Soluble Drugs in HEMA/MAA Hydrogels.

This chapter reports experimentally measured and theoretically predicted diffusion coefficients of prototypical drugs in SCL-material hydrogels where solute specific interactions with the hydrogel polymer chains are pronounced. Again, two-photon laser-scanning confocal microscopy and UV/Vis spectrophotometry are employed to detect transient solute concentration profiles and concentration histories respectively. Diffusion coefficients are obtained for theophylline, acetazolamide, sodium fluorescein, and riboflavin in the five SCL-material hydrogels of Chapter 3 as a function of pH (2 and 7.4). As expected, solute release rates are significantly slowed by specific interactions, most apparent when $E_i >> 1$ and adsorption is strong. Effective relative diffusion coefficients (including adsorption) span several orders of magnitude, due to the varying degree of solute interactions with hydrogel polymer chains. We quantitatively predict prototypical drug diffusion coefficient by an LPEM model extended for specific-solute adsorption to each hydrogel copolymer type (HEMA or MAA) and assuming local equilibrium. Again, predictions are determined through independently measured parameters. In all cases, predicted solute diffusivities display good agreement with experiment.

Chapter 5: Equilibrium Water and Solute Uptake in Silicone Hydrogels

Two thirds of all contact lenses prescribed in the United States are silicone-hydrogel (SiHy)-based SCLs.[83-87] Silicone-hydrogels are microphase-separated materials consisting of hydrophilic-polymer domains for aqueous solute transport and hydrophobic-silicone domains for oxygen transport.[88] In this chapter, experimentally measured and theoretically predicted equilibrium water contents and solute partition coefficients are determined for thirty SiHys over a wide range of hydrogel compositions and water contents (3 to 82%). To investigate solute uptake in SiHys, equilibrium partition coefficients for two hydrophilic solutes and two oleophilic solutes are determined. Measured water contents and aqueous-solute partition coefficients rise linearly with increasing solvent-free hydrophilic-polymer volume fraction. Conversely, oleophilic-solute partition coefficients decline linearly with increasing solvent-free hydrophilic-polymer volume fraction. To model equilibrium SiHy water contents and solute partition coefficients, we assume that water and aqueous solutes are confined to the hydrophilic-polymer microphases, whereas oleophilic solutes are distributed predominately into the silicone microphases. Predicted water contents and solute partition coefficients are in excellent agreement with experiment. Importantly, estimation of SiHy water contents and solute partition coefficients is now possible based solely on synthesis formulation and properties of homopolymer hydrogels.

Chapter 6: Fluorescent solute-partitioning characterization of layered soft contact lenses.

In this chapter, solute partitioning is used to elucidate physico-chemical properties of commercial SCLs. Fluorescent-solute partitioning characterizes DAILIES TOTAL 1® (delefilcon A) water-gradient SCLs, which are composed of a laminated SiHy core sandwiched between two thin surface-gel layers. Two-photon fluorescence confocal laser-scanning microscopy and attenuated total-reflectance Fourier-transform infrared spectroscopy (ATR-FTIR) detect partition coefficients of six prototypical fluorescent solutes and surface-gel water contents, respectively. Measured solute fluorescence intensity profiles clearly reveal a laminated structure for the DAILIES TOTAL 1® lenses. Additionally, comparison of fluorescent-solute uptake into the core and surface layers indicates that the SiHy core is structurally similar to O_2OPTIX^{TM}, a commercial non-laminated SiHy SCL. For all studied aqueous solutes, measured partition coefficients are greater in the surface layers than in the SiHy core, revealing higher water content in the surface-gel layers. ATR-FTIR confirms the higher water content of the surface-gel layers (82%) relative to that of the SiHy core (33%). Comparison of water and aqueous-solute uptake at varying pH (4 and 7.4) illustrates that the surface-gel layers are anionic at physiologic pH 7.4, whereas the SiHy core is nonionic. From fluorescent-solute partitioning, we successfully confirm the laminated structure of DAILIES TOTAL 1® and obtain compositional properties of the hydrogel-SCL material.

1.4 References

1. Hoffman, A. S. Hydrogels for biomedical applications. *Advanced Drug Delivery Reviews* **2002,** 64, Supplement, 18-23.
2. Peppas, N. A.; Bures, P.; Leobandung, W.; Ichikawa, H. Hydrogels in pharmaceutical formulations. *European Journal of Pharmaceutics and Biopharmaceutics* **2000,** 50, (1), 27-46.
3. Huang, R.; Kostanski, L. K.; Filipe, C. D. M.; Ghosh, R. Environment-responsive hydrogel-based ultrafiltration membranes for protein bioseparation. *Journal of Membrane Science* **2009,** 336, (1–2), 42-49.
4. Kim, J. J.; Park, K. Smart hydrogels for bioseparation. *Bioseparation* **1998,** 7, (4-5), 177-184.
5. Brahim, S.; Narinesingh, D.; Guiseppi-Elie, A. Bio-smart hydrogels: co-joined molecular recognition and signal transduction in biosensor fabrication and drug delivery. *Biosensors and Bioelectronics* **2002,** 17, (11), 973-981.
6. Lin, G.; Chang, S.; Hao, H.; Tathireddy, P.; Orthner, M.; Magda, J.; Solzbacher, F. Osmotic swelling pressure response of smart hydrogels suitable for chronically implantable glucose sensors. *Sensors and Actuators B: Chemical* **2010,** 144, (1), 332-336.
7. Lin, G.; Chang, S.; Kuo, C.-H.; Magda, J.; Solzbacher, F. Free swelling and confined smart hydrogels for applications in chemomechanical sensors for physiological monitoring. *Sensors and Actuators B: Chemical* **2009,** 136, (1), 186-195.

8. Liu, J. Oligonucleotide-functionalized hydrogels as stimuli responsive materials and biosensors. *Soft Matter* **2011,** 7, (15), 6757-6767.

9. Lee, K. Y.; Mooney, D. J. Hydrogels for tissue engineering. *Chemical Reviews* **2001,** 101, (7), 1869-1880.

10. Drury, J. L.; Mooney, D. J. Hydrogels for tissue engineering: scaffold design variables and applications. *Biomaterials* **2003,** 24, (24), 4337-4351.

11. Khademhosseini, A.; Langer, R. Microengineered hydrogels for tissue engineering. *Biomaterials* **2007,** 28, (34), 5087-5092.

12. Dursch, T. J.; Taylor, N. O.; Liu, D. E.; Wu, R. Y.; Prausnitz, J. M.; Radke, C. J. Water-soluble drug partitioning and adsorption in HEMA/MAA hydrogels. *Biomaterials* **2014,** 35, (2), 620-629.

13. Liu, D. E.; Dursch, T. J.; Oh, Y.; Bregante, D. T.; Chan, S. Y.; Radke, C. J. Equilibrium water and solute uptake in silicone hydrogels. *Acta Biomaterialia* **2015,** 18, 112-117.

14. Peppas, N. A. Hydrogels and drug delivery. *Current Opinion in Colloid & Interface Science* **1997,** 2, (5), 531-537.

15. Gupta, P.; Vermani, K.; Garg, S. Hydrogels: From controlled release to pH-responsive drug delivery. *Drug Discovery Today* **2002,** 7, (10), 569-579.

16. Peng, C.-C.; Burke, M. T.; Chauhan, A. Transport of topical anesthetics in vitamin E loaded silicone hydrogel contact lenses. *Langmuir* **2011,** 28, (2), 1478-1487.

17. Kim, J.; Chauhan, A. Dexamethasone transport and ocular delivery from poly (hydroxyethyl methacrylate) gels. *International Journal of Pharmaceutics* **2008,** 353, (1), 205-222.

18. Stringer, J. L.; Peppas, N. A. Diffusion of small molecular weight drugs in radiation-crosslinked poly (ethylene oxide) hydrogels. *Journal of Controlled Release* **1996,** 42, (2), 195-202.

19. Bettini, R.; Colombo, P.; Peppas, N. A. Solubility effects on drug transport through pH-sensitive, swelling-controlled release systems: Transport of theophylline and metoclopramide monohydrochloride. *Journal of Controlled Release* **1995,** 37, (1–2), 105-111.

20. Kapoor, Y.; Thomas, J. C.; Tan, G.; John, V. T.; Chauhan, A. Surfactant-laden soft contact lenses for extended delivery of ophthalmic drugs. *Biomaterials* **2009,** 30, (5), 867-878.

21. Am Ende, M. T.; Peppas, N. A. Transport of ionizable drugs and proteins in crosslinked poly (acrylic acid) and poly (acrylic acid-co-2-hydroxyethyl methacrylate) hydrogels. II. Diffusion and release studies. *Journal of Controlled Release* **1997,** 48, (1), 47-56.

22. Eckmann, D. M.; Composto, R. J.; Tsourkas, A.; Muzykantov, V. R. Nanogel carrier design for targeted drug delivery. *Journal of Materials Chemistry B* **2014,** 2, (46), 8085-8097.

23. Hoare, T. R.; Kohane, D. S. Hydrogels in drug delivery: Progress and challenges. *Polymer* **2008,** 49, (8), 1993-2007.

24. Qiu, Y.; Park, K. Environment-sensitive hydrogels for drug delivery. *Advanced Drug Delivery Reviews* **2012,** 64, Supplement, 49-60.

25. Tran, V. B.; Sung, Y. S.; Copley, K.; Radke, C. J. Effects of aqueous polymeric surfactants on silicone-hydrogel soft- contact-lens wettability and bacterial adhesion of Pseudomonas aeruginosa. *Contact Lens and Anterior Eye* **2012,** 35, (4), 155-162.

26. Gulsen, D.; Chauhan, A. Ophthalmic drug delivery through contact lenses. *Investigative Ophthalmology & Visual Science* **2004,** 45, (7), 2342-2347.

27. Ciolino, J. B.; Hoare, T. R.; Iwata, N. G.; Behlau, I.; Dohlman, C. H.; Langer, R.; Kohane, D. S. A drug-eluting contact lens. *Investigative Ophthalmology & Visual Science* **2009,** 50, (7), 3346-3352.

28. Peng, C.-C.; Kim, J.; Chauhan, A. Extended delivery of hydrophilic drugs from silicone-hydrogel contact lenses containing Vitamin E diffusion barriers. *Biomaterials* **2010,** 31, (14), 4032-4047.

29. Alvarez-Lorenzo, C.; Hiratani, H.; Concheiro, A. Contact lenses for drug delivery: achieving sustained release with novel systems. *American Journal of Drug Delivery* **2006** 4, (3), 131-151.

30. Ketelson, H. A.; Meadows, D. L.; Stone, R. P. Dynamic wettability properties of a soft contact lens hydrogel. *Colloids and Surfaces B: Biointerfaces* **2005,** 40, (1), 1-9.

31. Reineke, T. M. Stimuli-responsive polymers for biological detection and delivery. *ACS Macro Letters* **2016,** 5, (1), 14-18.

32. Musabayane, C. T.; Munjeri, O.; Bwititi, P.; Osim, E. E. Orally administered, insulin-loaded amidated pectin hydrogel beads sustain plasma concentrations of insulin in streptozotocin-diabetic rats. *Journal of Endocrinology* **2000,** 164, (1), 1-6.

33. Chaturvedi, K.; Ganguly, K.; Nadagouda, M. N.; Aminabhavi, T. M. Polymeric hydrogels for oral insulin delivery. *Journal of Controlled Release* **2013,** 165, (2), 129-138.

34. Kim, B.; Peppas, N. A. In vitro release behavior and stability of insulin in complexation hydrogels as oral drug delivery carriers. *International Journal of Pharmaceutics* **2003,** 266, (1–2), 29-37.

35. Weeks, A.; Boone, A.; Luensmann, D.; Jones, L.; Sheardown, H. The effects of hyaluronic acid incorporated as a wetting agent on lysozyme denaturation in model contact lens materials. *Journal of Biomaterials Applications* **2013,** 28, (3), 323-333.

36. Paterson, S. M.; Liu, L.; Brook, M. A.; Sheardown, H. Poly(ethylene glycol)-or silicone-modified hyaluronan for contact lens wetting agent applications. *Journal of Biomedical Materials Research Part A* **2015,** 103, (8), 2602-2610.

37. Kotsmar, C.; Sells, T.; Taylor, N.; Liu, D. E.; Prausnitz, J. M.; Radke, C. J. Aqueous solute partitioning and mesh size in HEMA/MAA hydrogels. *Macromolecules* **2012,** 45, (22), 9177-9187.

38. Amsden, B. Solute diffusion within hydrogels: Mechanisms and models. *Macromolecules* **1998,** 31, (23), 8382-8395.

39. Bosma, J. C.; Wesselingh, J. A. Partitioning and diffusion of large molecules in fibrous structures. *Journal of Chromatography B: Biomedical Sciences and Applications* **2000,** 743, (1), 169-180.

40. Russell, S. M.; Carta, G. Mesh size of charged polyacrylamide hydrogels from partitioning measurements. *Industrial & Engineering Chemistry Research* **2005,** 44, (22), 8213-8217.

41. Johnson, E. M.; Berk, D. A.; Jain, R. K.; Deen, W. M. Hindered diffusion in agarose gels: test of effective medium model. *Biophysical Journal* **1996,** 70, (2), 1017-1023.

42. Tong, J.; Anderson, J. L. Partitioning and diffusion of proteins and linear polymers in polyacrylamide gels. *Biophysical Journal* **1996,** 70, (3), 1505-1513.

43. Guan, L.; Jiménez, M. E. G.; Walowski, C.; Boushehri, A.; Prausnitz, J. M.; Radke, C. J. Permeability and partition coefficient of aqueous sodium chloride in soft contact lenses. *Journal of Applied Polymer Science* **2011,** 122, (3), 1457-1471.

44. Johnson, E. M.; Berk, D. A.; Jain, R. K.; Deen, W. M. Diffusion and partitioning of proteins in charged agarose gels. *Biophysical Journal* **1995,** 68, (4), 1561-1568.

45. Wu, J.; Sassi, A. P.; Blanch, H. W.; Prausnitz, J. M. Partitioning of proteins between an aqueous solution and a weakly-ionizable polyelectrolyte hydrogel. *Polymer* **1996,** 37, (21), 4803-4808.

46. Fatin-Rouge, N.; Milon, A.; Buffle, J.; Goulet, R. R.; Tessier, A. Diffusion and partitioning of solutes in agarose hydrogels: The relative influence of electrostatic and specific interactions. *The Journal of Physical Chemistry B* **2003,** 107, (44), 12126-12137.

47. Peppas, N. A.; Moynihan, H. J.; Lucht, L. M. The structure of highly crosslinked poly(2-hydroxyethyl methacrylate) hydrogels. *Journal of Biomedical Materials Research* **1985,** 19, (4), 397-411.

48. Anseth, K. S.; Bowman, C. N.; Brannon-Peppas, L. Mechanical properties of hydrogels and their experimental determination. *Biomaterials* **1996,** 17, (17), 1647-1657.

49. Canal, T.; Peppas, N. A. Correlation between mesh size and equilibrium degree of swelling of polymeric networks. *Journal of Biomedical Materials Research* **1989,** 23, (10), 1183-1193.

50. Ogston, A. G. The spaces in a uniform random suspension of fibres. *Transactions of the Faraday Society* **1958,** 54, 1754-1757.

51. Anseth, K. S.; Bowman, C. N. Kinetic gelation predictions of species aggregation in tetrafunctional monomer polymerizations. *Journal of Polymer Science Part B: Polymer Physics* **1995,** 33, (12), 1769-1780.

52. Lazzara, M. J.; Deen, W. M. Effects of concentration on the partitioning of macromolecule mixtures in agarose gels. *Journal of Colloid and Interface Science* **2004,** 272, (2), 288-297.

53. Kosto, K. B.; Panuganti, S.; Deen, W. M. Equilibrium partitioning of Ficoll in composite hydrogels. *Journal of Colloid and Interface Science* **2004,** 277, (2), 404-409.

54. Abbott, N. L.; Blankschtein, D.; Hatton, T. A. Protein partitioning in two-phase aqueous polymer systems. 1. Novel physical pictures and a scaling thermodynamic formulation. *Macromolecules* **1991,** 24, (15), 4334-4348.

55. Sassi, A. P.; Blanch, H. W.; Prausnitz, J. M. Characterization of size-exclusion effects in highly swollen hydrogels: Correlation and prediction. *Journal of Applied Polymer Science* **1996,** 59, (8), 1337-1346.

56. Fatin-Rouge, N.; Wilkinson, K. J.; Buffle, J. Combining small angle neutron scattering (SANS) and fluorescence correlation spectroscopy (FCS) measurements to relate diffusion in agarose gels to structure. *The Journal of Physical Chemistry B* **2006,** 110, (41), 20133-20142.

57. Ratner, B. D.; Miller, I. F. Transport through crosslinked poly(2-hydroxyethyl methacrylate) hydrogel membranes. *Journal of Biomedical Materials Research* **1973,** 7, (4), 353-367.

58. Hirota, N.; Kumaki, Y.; Narita, T.; Gong, J. P.; Osada, Y. Effect of charge on protein diffusion in hydrogels. *The Journal of Physical Chemistry B* **2000,** 104, (42), 9898-9903.

59. Luensmann, D.; Zhang, F.; Subbaraman, L.; Sheardown, H.; Jones, L. Localization of lysozyme sorption to conventional and silicone hydrogel contact lenses using confocal microscopy. *Current Eye Research* **2009,** 34, (8), 683-697.

60. Bengani, L. C.; Leclerc, J.; Chauhan, A. Lysozyme transport in p-HEMA hydrogel contact lenses. *Journal of Colloid and Interface Science* **2012,** 386, (1), 441-450.

61. Bird, R. B.; Stewart, W. E.; Lightfoot, E. N. *Transport phenomena*. 2nd ed.; Wiley: New York, 2006.

62. Deen, W. M. *Analysis of transport phenomena*. Oxford University Press, New York: 1998.

63. Dursch, T. J.; Liu, D. E.; Oh, Y.; Radke, C. J. Fluorescent solute-partitioning characterization of layered soft contact lenses. *Acta Biomaterialia* **2015,** 15, 48-54.

64. Liu, D. E.; Kotsmar, C.; Nguyen, F.; Sells, T.; Taylor, N. O.; Prausnitz, J. M.; Radke, C. J. Macromolecule sorption and diffusion in HEMA/MAA hydrogels. *Industrial & Engineering Chemistry Research* **2013,** 52, (50), 18109-18120.

65. Amsden, B. Solute diffusion in hydrogels: An examination of the retardation effect. *Polymer Gels and Networks* **1998,** 6, (1), 13-43.

66. Phillips, R. J. A hydrodynamic model for hindered diffusion of proteins and micelles in hydrogels. *Biophysical Journal* **2000,** 79, (6), 3350-3353.

67. Johansson, L.; Elvingson, C.; Skantze, U.; Löfroth, J. E. Diffusion and interaction in gels and solutions. In *Trends in Colloid and Interface Science VI*, Helm, C.; Lösche, M.; Möhwald, H., Eds. Springer: New York, 1992; pp 25-29.

68. Ogston, A. G.; Preston, B. N.; Wells, J. D. On the transport of compact particles through solutions of chain-polymers. *Proceedings of the Royal Society of London. A. Mathematical and Physical Sciences* **1973,** 333, (1594), 297-316.

69. Peppas, N. A.; Reinhart, C. T. Solute diffusion in swollen membranes: Part I. A new theory. *Journal of Membrane Science* **1983,** 15, (3), 275-287.

70. Phillips, R. J.; Deen, W. M.; Brady, J. F. Hindered transport in fibrous membranes and gels: Effect of solute size and fiber configuration. *Journal of Colloid and Interface Science* **1990,** 139, (2), 363-373.

71. Merrill, E. W.; Dennison, K. A.; Sung, C. Partitioning and diffusion of solutes in hydrogels of poly(ethylene oxide). *Biomaterials* **1993,** 14, (15), 1117-1126.

72. Russell, S. M.; Belcher, E. B.; Carta, G. Protein partitioning and transport in supported cationic acrylamide-based hydrogels. *AIChE Journal* **2003,** 49, (5), 1168-1177.

73. Pluen, A.; Netti, P. A.; Jain, R. K.; Berk, D. A. Diffusion of macromolecules in agarose gels: Comparison of linear and globular configurations. *Biophysical Journal* **1999,** 77, (1), 542-552.

74. Clague, D. S.; Phillips, R. J. Hindered diffusion of spherical macromolecules through dilute fibrous media. *Physics of Fluids* **1996,** 8, 1720.

75. Hadjiev, N. A.; Amsden, B. G. An assessment of the ability of the obstruction-scaling model to estimate solute diffusion coefficients in hydrogels. *Journal of Controlled Release* **2015,** 199, 10-16.

76. Lustig, S. R.; Peppas, N. A. Solute diffusion in swollen membranes. IX. Scaling laws for solute diffusion in gels. *Journal of Applied Polymer Science* **1988,** 36, (4), 735-747.

77. Yasuda, H.; Peterlin, A.; Colton, C. K.; Smith, K. A.; Merrill, E. W. Permeability of solutes through hydrated polymer membranes: Part III. Theoretical background for the selectivity of dialysis membranes. *Die Makromolekulare Chemie* **1969,** 126, (1), 177-186.

78. Phillips, R. J.; Deen, W. M.; Brady, J. F. Hindered transport of spherical macromolecules in fibrous membranes and gels. *AIChE Journal* **1989,** 35, (11), 1761-1769.

79. Johansson, L.; Elvingson, C.; Löfroth, J. E. Diffusion and interaction in gels and solutions. 3. Theoretical results on the obstruction effect. *Macromolecules* **1991,** 24, (22), 6024-6029.

80. Amsden, B. An obstruction-scaling model for diffusion in homogeneous hydrogels. *Macromolecules* **1999,** 32, (3), 874-879.

81. Brady, J. F. Hindered diffusion. In *Extended Abstracts, AIChE Annual Meeting, San Fransisco, CA, 1994*, AIChE: p 320.

82. Castillo, E. J.; Koenig, J. L.; Anderson, J. M.; Lo, J. Protein adsorption on hydrogels: II. Reversible and irreversible interactions between lysozyme and soft contact lens surfaces. *Biomaterials* **1985,** 6, (5), 338-345.

83. Nichols, J. J. Contact lenses 2011. *Contact Lens Spectrum* **2012,** 27, 20-25.

84. Nichols, J. J. Contact lenses 2012. *Contact Lens Spectrum* **2013,** 28, 24-29.

85. Nichols, J. J. Contact lenses 2013. *Contact Lens Spectrum* **2014,** 29, 22-28.

86. Nichols, J. J. Contact lenses 2014. *Contact Lens Spectrum* **2015,** 30, 22-27.

87. Nichols, J. J. Contact lenses 2015. *Contact Lens Spectrum* **2016,** 31, 18-23.

88. Nicolson, P. C.; Vogt, J. Soft contact lens polymers: An evolution. *Biomaterials* **2001,** 22, (24), 3273-3283.

Chapter 2

Macromolecule Sorption and Diffusion in HEMA/MAA Hydrogels

2.1 Abstract

Transient solute absorption and desorption concentration profiles were measured in a 70-wt% hydroxyethyl-methacrylate (HEMA) /30-wt% methacrylic acid (MAA) anionic hydrogel using two-photon confocal microscopy. Dilute aqueous solutes included fluorescently-labeled dextrans with molecular masses of 4, 10, and 20 kDa, and fluorescently-labeled cationic avidin protein. Cross-linking densities with ethyleneglycol-dimethacrylate (EGDMA) varied from 0 to 1 wt% with polymer volume fractions increasing from 0.15 to 0.25. Average gel mesh sizes, determined from zero-frequency oscillatory shear storage moduli, ranged from about 3.6 to 8.4 nm over the cross-link ratios studied. All solutes exhibit Stokes-Einstein hydrodynamic radii obtained from measured free diffusion coefficients, D_{io}, comparable to or larger than the average gel mesh size. In spite of considerable size-exclusion, the studied solutes penetrate the gels indicating a range of mesh sizes available for transport. Transient uptake and release concentration profiles for FITC-dextrans follow simple diffusion theory with diffusion coefficients, D_i, essentially independent of loading or release characteristic of reversible absorption. Although strongly size-excluded, these solutes do not interact specifically with the polymer network. Diffusivities are accordingly predicted from a large-pore effective-medium (LPEM) model developed to account for solute size, hydrodynamic drag, and distribution of mesh sizes available for transport in the polymer network. For this class of solute, and using no adjustable parameters, diffusivities predicted from the new effective-medium model demonstrate good agreement with experiment.

For the specific-interacting cationic protein, avidin, gel loading is three orders of magnitude slower than that of dextran of similar hydrodynamic radius. Desorption of avidin is not complete even after two weeks of extraction. Based on size alone, avidin is strongly size-excluded, yet it exhibits a partition coefficient of over 20. For the positively charged protein, we observed specific ion binding on the negatively charged carboxylate groups of MAA-decorated polymer strands in the larger mesh spaces. Simple linear sorption kinetics gives an adsorption time constant of 5 min and a desorption time constant of about 20 d suggesting nearly irreversible uptake of cationic avidin on the anionic gel matrix.

Reprint of Liu, D. E.; Kotsmar, C.; Nguyen, F.; Sells, T.; Taylor, N. O.; Prausnitz, J. M.; Radke, C. J. *Industrial & Engineering Chemistry Research* **2013,** 52, (50), 18109-18120.

2.2 Introduction

Diffusion of solute molecules in hydrogels is of interest in a wide variety of applications including chromatographic separations,[1-4] membrane separation,[1,5] and encapsulation of cells in hydrogels for biomedical treatment.[6-8] Due to their biocompatibility, hydrogels are extensively used in pharmaceutics for delivery of bioactive agents,[5,9,10] and for synthesis of artificial organs.[5,11] Soft contact lenses are hydrogels[12-14] and can be used to deliver drugs[15-19] and comfort/wetting agents to the eye.[20,21]

Hydrogels are cross-linked hydrophilic polymers swollen in aqueous media.[5,22-24] Cross-links between chains are formed by physical entanglements, such as van der Waals attraction, hydrogen bonding, ion binding, or, most commonly, by covalent bonds. The three-dimensional structure of a gel is best described by a mesh whose spaces between polymer chains are filled with aqueous solution. Mesh size, ξ, gauges the distance between cross-links in the polymer network.[25] Hydrogels are especially appealing for solute delivery because their mesh sizes can be controlled, for example, by altering temperature[10] or pH.[11]

Solute diffusion in hydrogels occurs primarily through the water fraction. Diffusivities of aqueous solutes in hydrogels are diminished relative to their bulk values by interaction with the polymer chains including hydrodynamic drag, physical obstruction, electro-osmosis, and specific binding.[26-29] The cross-linking process during hydrogel synthesis produces a distribution of polymer-strand molecular weights between cross-links, and correspondingly, a distribution of mesh sizes.[9,30] Thus, in addition to solute-chain interactions, significant size-exclusion can occur when solute size is comparable to gel mesh size.[31]

Because of extensive application, a large effort has been expended on studying solute diffusion in hydrogels both experimentally and theoretically.[2-4,9,17,26-29,32-56] Published work falls into two classes: diffusion of small solutes, such as salts and small sugars, and diffusion of larger solutes, such as polymers, surfactants, and proteins whose sizes are comparable to the mesh size. Most studies are in the first class using a Stokes cell or back extraction; concentration profiles are not available. In most all cases, the hydrogels exhibit relatively large water contents (more than 90 %) and, accordingly, solute size-exclusion is not extreme.

Little attention has been given to diffusion of charged macromolecules in ionic hydrogels of opposite charge. Several investigators have established that oppositely charged macromolecules are adsorbed in ionic hydrogels, especially at low ionic strengths.[1-4] Large counterion solutes provide an opportunity to study the transport rates of solutes that experience both size-exclusion and adsorption to the polymer network.

This work considers application of hydrogels to soft contact lenses,[31] characterized by relatively low water content[45] and, accordingly, small mesh sizes. Conversely, aqueous solutes of interest, including surfactants, polymers, and proteins,[12,13,20,21] are comparably large. Thus, we study diffusion of solutes in a representative soft-contact-lens material with relatively high polymer content where solute and mesh sizes are similar. Two-photon confocal microscopy detects transient fluorescence-intensity profiles within the gel. All diffusivity measurements are performed in sufficient aqueous indifferent electrolyte that electrostatic fields are absent.

Sorption of fluorescently labeled dextrans, and fluorescently labeled avidin is investigated in both loading and release directions. The anionic hydrogels consist of 70-wt% HEMA/ 30-wt% MAA in aqueous phosphate buffer (PBS, pH = 7.4, ionic strength = 0.15 M)

with cross-link densities ranging from 0 to 1 wt%. Average gel mesh size is determined from oscillatory shear rheometry and Gaussian-chain elastic-rubber theory.[31] Solute sizes are determined from independent measurement of the bulk aqueous diffusion coefficient in a restricted diffusion cell[57,58] and Stokes-Einstein theory.[59] Significant size-exclusion is evident with equilibrium solute partition coefficients as low as 0.001 for the largest dextran molecule. To understand nonspecific-interacting dextran diffusivities in the gel, we interpret experimental data using an extended effective-medium theory with all parameters determined independently. For positively charged Fl-avidin, however, uptake and release rates are controlled by specific electrostatic adsorption onto the negatively charged polymer chains. Accordingly, avidin concentration profiles in the gel are determined both by diffusion and adsorption kinetics.

2.3 Experimental Section

2.3.1 Gel Synthesis and Characterization

70-wt % HEMA (#128635, Sigma Aldrich, St. Louis, MO, USA) / 30-wt% MAA (#155721, Sigma Aldrich, St. Louis, MO, USA) hydrogels were synthesized by simultaneous copolymerization and cross-linking of monomers with EGDMA (335681, Sigma Aldrich, St. Louis, MO, USA) as the cross-linking agent at 0 – 1 wt % in aqueous solution.[22,60] Details are described elsewhere. [31] Once synthesized between shimmed glass plates, 6-mm x 6-mm films were cut and placed into scintillation vials filled with phosphate buffer solution (PBS: 0.15 M NaCl, 0.017 M $Na_2HPO_4 \cdot 7H_2O$, and 0.003 M $NaH_2PO_4 \cdot H_2O$; pH = 7.4) for no less than 7 d to allow complete swelling. Because the pK_A of monomeric MAA is 5.5, the synthesized gels are anionic. The Debye length of the background PBS electrolyte is about 0.5 nm so polymer matrix charge is effectively screened. Consequently, nonspecific electrostatic-field effects on solute diffusion fluxes are absent. All experiments were performed at ambient temperature.

Equilibrium swollen gels of varying cross-linked densities were characterized by their water content from thermal gravimetric analysis (TGA, Model 2950, TA Instruments, New Castle, DE, USA) and by their average mesh size obtained from linear oscillatory rheometry (Physica MCR301 Rheometer, Anton-Paar, Ashland, VA, USA).[31] Following Peppas et al.,[22] the measured zero-frequency shear storage modulus, G'(0), for each cross-link density swollen gel was converted to an average mesh size as $\langle \xi \rangle = l_{c-c}\sqrt{2C_n\rho_2 RT/[M_r G'(0)]}\phi_2^{-1/6}$ where l_{c-c} is the length of a covalent carbon-carbon bond in the backbone (0.154 nm), C_n is the Flory characteristic ratio or rigidity factor.[61,62] For HEMA/MAA gels, C_n equals 6.9.[22] M_r is the molecular weight of a repeat unit, 112.7 g/mol for the 70-wt% HEMA/ 30-wt% MAA copolymer, and ρ_2 is the density of the dry polymer (1070 kg/m^3 for 70-wt% HEMA/ 30-wt% MAA). Table 2.1 reports calculated average mesh sizes, $\langle\xi\rangle$, for gels with different cross-link densities and corresponding polymer volume fractions, ϕ_2.[31] Average mesh size increases from 3.6 to 8.3 nm for increasing water volume fractions from 0.74 to 0.86. An extended Ogston mesh-size distribution[30] adequately fits the data in Table 2.1 giving an approximate polymer-strand radius a_f = 2 nm (see Figure 8 of Kotsmar et al.[31])

Table 2.1: Hydrogel Polymer Volume Fraction and Average Mesh Size

Cross-link Density (wt% EGDMA)	ϕ_2 measured with TGA	$\langle\xi\rangle$ **[nm]** calculated*****
0	0.143	8.3
0.01	0.15	7.9
0.025	0.148	8.3
0.05	0.143	8.3
0.1	0.154	7.7
0.25	0.165	7.3
0.5	0.183	6.3
0.75	0.2	5.0
1	0.227	3.6

***** Following Peppas et al.[22]

2.3.2 Solute Characterization

Fluorescein isothiocyanate dextrans (FITC-dextran4, MW = 4000 g/mol; FITC-dextran10, MW = 10,000 g/mol; FITC-dextran20, MW = 20,000 g/mol) were obtained from TdBCons (Uppsala, Sweden). They were extensively dialyzed prior to experiment to remove any free label. Each FITC-dextran solution was placed in a Slide-A-Lyzer Dialysis Cassette (#66212, 2K MWCO, Thermo Scientific) for 1 h at room temperature followed by 1 wk in a commercial refrigerator changing the surrounding PBS dialyzing solution daily. Only FITC-dextran20 showed a decrease in gel diffusivity compared to those of the supplied materials. Avidin fluorescein conjugate (Fl-avidin, #A821) was obtained from Invitrogen (Eugene, OR, USA) and was used as received.

To ascertain the hydrodynamic radii of the chosen solutes, we determined bulk diffusion coefficients in a restricted diffusion cell[57] using UV/Vis absorption.[58] Experimental protocol is described in Kotsmar et al.[31] From the measured diffusion coefficient, the hydrodynamic radius of the aqueous solute was ascertained from the Stokes-Einstein relation.[43,51,59] Our measured bulk diffusivities show good agreement with literature values.[31,55] Table 2.2 displays the hydrodynamic diameters, $2a_{iS}$, of fluorescently labeled dextrans and avidin. Reported diameters suggest that aqueous Fl-avidin is more compact compared to the corresponding branched linear polymers of smaller or comparable molecular weight. Comparison of Tables 2.1 and 2.2 reveals that all solutes are comparable to or larger than the average gel mesh sizes. Nevertheless, all solutes penetrate the gels but with small partition coefficients as low as 0.001 due to significant size-exclusion.[31]

Table 2.2: Solute Hydrodynamic Diameters

Solute	MW [g/mol]	$2a_{iS}$ [nm]
FITC-dextran4	4000	3.1[55]
FITC-dextran10	10000	4.7[55]
FITC-dextran20	20000	6.7[55]
Fl-avidin	68000	7.05[31]

2.3.3 Gel-Solute Confocal Microscopy

Diffusion coefficients of the fluorescently labeled solutes in the hydrogels were determined using two-photon confocal microscopy.[63-66] A distinct advantage of two-photon fluorescence is excitation in a small volume (~0.1 μm^3) allowing minimal photobleaching and permitting transient-profile assessment. At dilute solute concentrations between 10^{-5} and $5x10^{-4}$ M, fluorescence intensity measured both in solution and in the gel was confirmed linearly proportional to dye concentration.[67] Because concentrations are measured in the gel phase, diffusion coefficients are directly ascertained with no need for correction by a partition coefficient. We obtained both loading and unloading profiles to ascertain reversibility of solute uptake and release. A Carl Zeiss (Jena, Germany) 510 LSM META NLO AxioImager Confocal Microscope equipped with a Spectra-Physics (Santa Clara, CA) MaiTai HP DeepSee Laser was used for two-photon imaging at 780 nm. Fluorescence emission was collected with a Plan-Neofluar 10x/0.30 NA objective (Carl Zeiss GmbH) using a 500-550-nm emission filter.

For solute-absorption measurements, 6-mm x 6-mm, 800 to 2500 μm-thick swollen gel sheets were first soaked in the chosen aqueous-PBS/solute solution under magnetic stirring at 400 rpm. At selected times, a gel sheet was removed from solution, lightly blotted on both faces, placed flat on a microscope slide (VWR Micro Slides, 48300-047, VWR International, West Chester, PA, USA), and covered with a microscope cover glass (#12-541-B, Fisher Scientific, Fair Lawn, New Jersey, USA) to prevent water evaporation. Vertical scanning on the microscope was performed downward through the gel at 3-μm intervals over the entire slab thickness at an instrument-set scan rate of about 10 μm/s. To minimize edge effects, scans were performed in the middle of the gel slab. Figure 2.1a shows typical two-photon-confocal fluorescence micrographs of FITC-dextran20 absorbing into a 70-wt% HEMA/ 30-wt% MAA hydrogel slab with 0.25-wt% cross-link density ($\langle\xi\rangle$ = 7.3 nm) at increasing exposure times. FITC-dextran20 permeates the gel from both faces in the expected fashion for diffusive transport. Longer exposure times give more penetration towards the slab center with surface intensities remaining nearly constant. Complete equilibration occurs in less than 1 d for this particular solute/gel combination.

For solute-desorption measurements, nascent swollen gels sheets were first soaked in the pertinent aqueous-solute solution under magnetic stirring for at least 48 h at 400 rpm to guarantee complete saturation. Sample scans confirmed that all solutes, except avidin, reached a uniform-equilibrated concentration profile.[31] Measured water contents of solute-

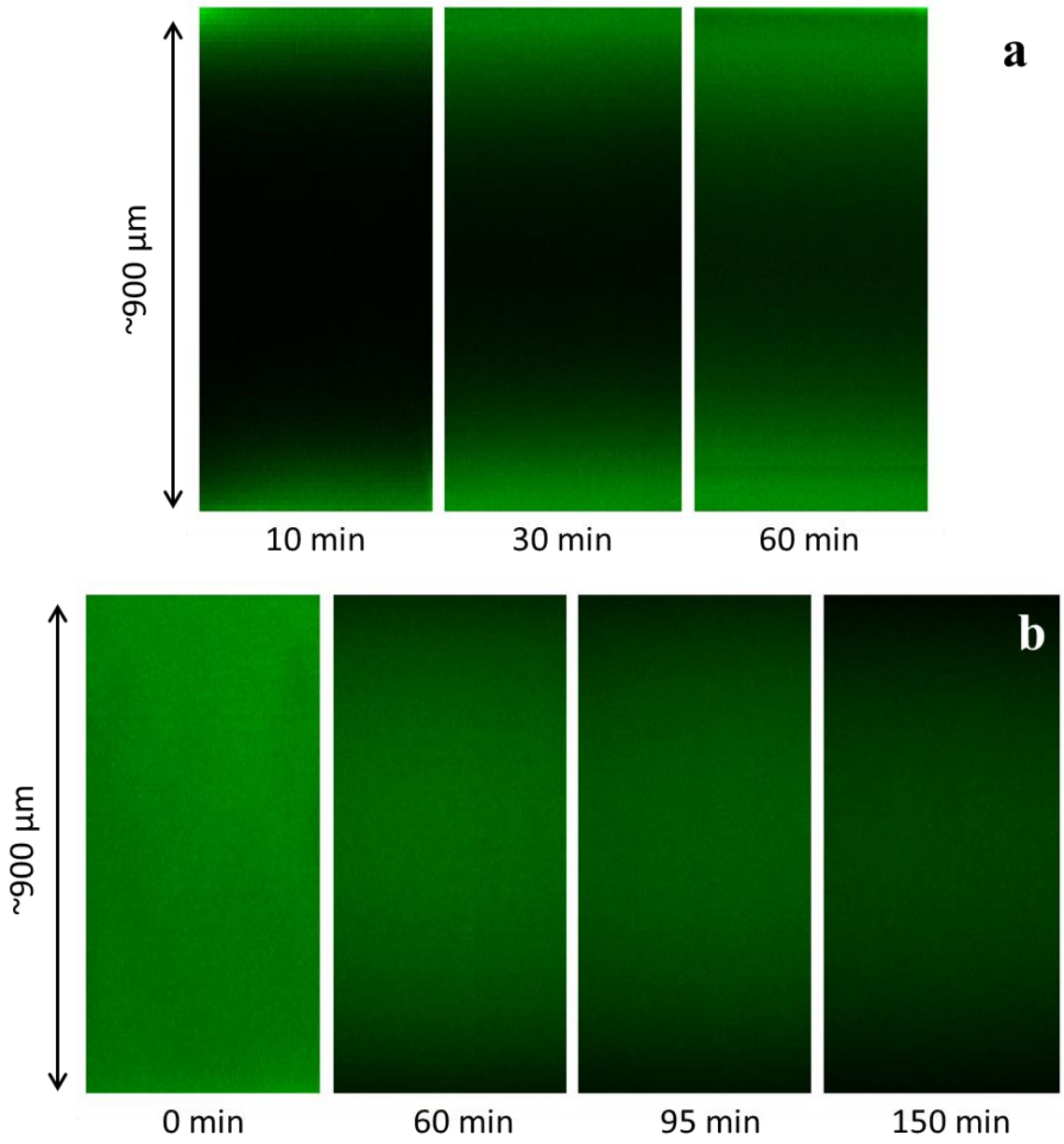

Figure 2.1: (a) Fluorescence micrographs of FITC-dextran20 absorption into a 70-wt% HEMA/ 30-wt% MAA hydrogel with 0.25-wt% cross-link density at different absorption times. (**b)** Fluorescence micrographs of FITC-dextran20 desorption from a 70-wt% HEMA/ 30-wt% MAA hydrogel with 0.25-wt% cross-link density at different desorption times.

loaded and nascent swollen gels were identical. Accordingly, for the dilute solutes employed, solute loading does not alter overall swelling. After equilibration, solute-saturated gel sheets were placed in a large volume of solute-free PBS solution also under magnetic stirring at 400 rpm. At selected release times, a gel sheet was scanned similarly to the absorption measurements, but without blotting. Figure 2.1b shows sample fluorescence micrographs of FITC-dextran20 desorption from a 70-wt% HEMA/ 30-wt% MAA hydrogel with 0.25-wt% cross-link density ($\langle\xi\rangle$ = 7.3 nm). As desorption progresses, fluorescence intensity decreases from the center towards the two surfaces of the gel slab (i.e., top and bottom of the micrographs in Figure 2.1, respectively) as solute diffuses out from the gel and into the surrounding excess PBS solution. After sufficient time, total desorption from the gel is observed, although complete release can take many days depending on the particular solute molecule and gel under study.

As illustrated in Figure 2.2, images obtained from two-photon confocal microscopy were converted into fluorescence-intensity-versus-position profiles. Because fluorescence intensity varies linearly with dye concentration, solute intensity profiles are equivalent to transient concentration profiles in the gel. Typically, four to six different scanned intensity profiles of each micrograph were averaged into one profile. Resulting averaged intensities were then smoothed with the 10 most nearby points by an adjacent-averaging smoothing technique.[14] Background fluorescence intensity was then subtracted.

Figure 2.2a gives loading intensity profiles corresponding directly to the micrographs in Figure 2.1a while Figure 2.2b reflects release intensity profiles corresponding directly to micrographs in Figure 2.1b. The distance scale is from top to bottom of the gel sample. Characteristic diffusion-profile shapes are found for each sorption direction. Because of signal attenuation, intensity profiles are not strictly symmetric with intensities near the bottom of the gel slab slightly lower than those near the top of the slab. This effect is clearly seen in the fully saturated or zero-time profile in Figure 2.2b. Detected fluorescence intensities decline when a thick sample is scanned deeply. Higher solute concentrations are more prone to this decline. To overcome the lack of uniform signal detection at the solute concentrations studied, we evaluated data measured only in the top one-half of the gel where intensities are practically independent of sample depth. For our gel samples, signal attenuation in the top half of the gel is minimal and does not infect solute diffusivities.

A second artifact arises in the experimental intensity data directly at the top surface of the gel, best illustrated by close examination of the absorption profiles in Figure 2.2a. Solute concentrations at the top surface should be large and remain at a single large value during loading. In some cases, however, the maximum fluorescence intensity measured in the gel sample is not exactly at the top surface of the gel, but sometimes is observed downward to a depth of 50 μm. Most likely, the gel surface is locally dried due to the blotting procedure. Consequently, we do not directly use the measured surface intensities in the fitting procedure to obtain solute/gel diffusion coefficients. We find that stirring the surrounding bulk aqueous phase at higher speeds, or even no stirring, has no influence on the measured concentration profiles, confirming negligible external mass-transfer resistance.

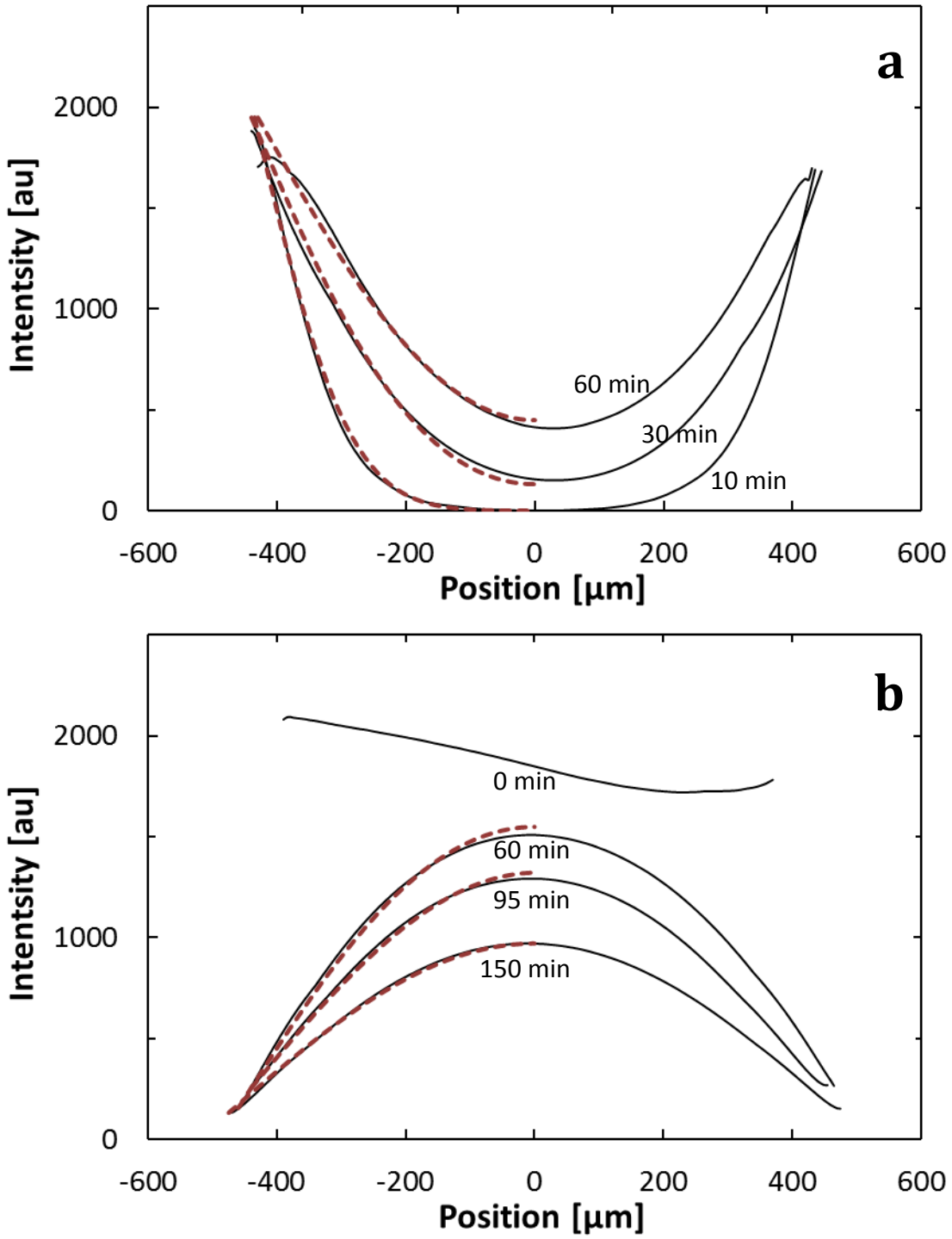

Figure 2.2: (a) Transient intensity profiles of FITC-dextran20 absorption into a 70-wt% HEMA/ 30-wt% MAA hydrogel with 0.25-wt% cross-link density, (**b)** Transient intensity profiles of FITC-dextran20 desorption from a 70-wt% HEMA/ 30-wt% MAA hydrogel with 0.25-wt% cross-link density. Solid and dashed lines represent measured profiles and best fits to Eqs. 2-4, respectively.

2.3.4 Nonadsorbing-Solute-Gel Diffusion Coefficients

At dilute concentration, solute diffusion in a nonadsorbing gel follows Fick's second law with a constant diffusion coefficient

$$\frac{\partial C_i^L(t,x)}{\partial t} = D_i \frac{\partial^2 C_i^L(t,x)}{\partial x^2} \tag{1}$$

where C_i^L is the concentration of dilute solute *i* per unit volume of liquid, *t* denotes time, D_i is the solute diffusivity in the gel, and *x* is the spatial coordinate for a domain thickness *2L* with $x = 0$ locating the center of the gel slab. As highlighted above, only data for $-L < x < 0$ were analyzed. For both loading and release, symmetry is demanded at the centerline. For loading, $C_i^L(t,-L) = C_{i\infty}^{\ L}$ where $C_{i\infty}^{\ L}$ is the final solute concentration in the gel in equilibrium with the bulk aqueous solute solution. For release, $C_i^L(t,-L) = 0$ since the desaturating aqueous solution is devoid of solute and in excess. Initial conditions are $C_i^L(0,x) = 0$ for adsorption and $C_i^L(0,x) = C_{i\infty}^{\ L}$ for desorption because desaturation occurs from the initial equilibrium state.

Let $A_n(t,x;t^*)$ be defined as

$$A_n(t,x;t^*) \equiv 2\frac{(-1)^n}{\lambda_n}\{1-exp[-\lambda_n^2 D_i t^*/L^2]\}exp[-\lambda_n^2 D_i t/L^2]\cos[\lambda_n x/L] \tag{2}$$

where $\lambda_n \equiv (2n+1)\pi/2$ and t^* is a final loading time. Absorption then follows according to

$$\frac{C_i^L(t,x)}{C_{i\infty}^{\ L}} = 1-\sum_{n=0}^{\infty} A_n(t,x;\infty), \tag{3}$$

and desorption from an equilibrated gel at C_∞ obeys the relation

$$\frac{C_i^L(t,x)}{C_{i\infty}^{\ L}} = \sum_{n=0}^{\infty} A_n(t,x;\infty) \tag{4}$$

.

Transient intensity profiles are fit to Equations 2-4 by Levenberg-Marquardt least-square-error minimization[68] to obtain separate diffusion coefficients in the absorption and desorption directions. We use 100 terms in the summations.

For loading profiles, we do not rely on the measured surface intensity at $x = -L$ because of surface blotting. To obtain $C_{i\infty}^{\ L}$, we use an extrapolated concentration from least-squares fitting of the concentration profile and average over all measured profiles in that loading run. All profiles are then adjusted to this average surface concentration and re-fit for the best diffusion coefficient by a second least-square minimization. For any given solute-gel system, no less than four data sets at different absorption times were fit to find the diffusion

coefficient. Resulting diffusion coefficients were then averaged by linearly weighting them by the inverse mean-square error of a particular profile. Likewise, the overall standard deviation of the diffusion coefficient was established by similar linear weighting of the standard deviations for each transient profile.

For the corresponding solute-desorption experiments, initial fluorescence intensity of the dye-saturated gel for each solute-gel system was measured and set as constant and proportional to $C_{i\infty}^{\ L}$. Thereafter, local equilibration with the excess solute-free aqueous solution established the gel surface concentration: $C_i^L(t,-L)=0$. Figure 2.2b, however, illustrates that solute fluorescence at the surface, although small, is not exactly zero after background subtraction. Because this concentration was always less than 5% of the saturated concentration, it was averaged over the measured profiles and subtracted from the measured intensity profiles. Best fitting of the diffusion coefficient and assessment of standard deviation from the desorption profiles was then performed as for the absorption profiles.

2.4 Results

2.4.1 Nonspecific Interacting Solutes

Table 2.3 summarizes diffusion coefficients for absorption measured for the three labeled dextrans in 5 different polymer-content 70-wt% HEMA/ 30-wt% MAA gels at pH = 7.4. In spite of molecular hydrodynamic sizes comparable or larger than the average gel mesh size, all solutes permeate all gels. As expected, diffusivities of the same solute decrease with increasing polymer content (i.e., with decreasing mesh size). In the same cross-link-density gel, solute uptake rates decrease with increasing molecular weight, also as expected.

Table 2.3: Solute-Hydrogel Absorption Diffusivities

Polymer Content ϕ_2	D_i **x10^7 [cm^2/s]**		
	FITC-dextran4	FITC-dextran10	FITC-dextran20
0.143 (0)*	4.44 ± 0.84	2.52 ± 0.94	0.982 ± 0.13
0.154 (0.10)	3.15 ± 0.20	1.64 ± 0.63	0.669 ± 0.17
0.165 (0.25)	2.11 ± 0.086	1.10 ± 0.15	0.675 ± 0.25
0.183 (0.50)	1.16 ± 0.04	0.549 ± 0.079	0.737 ± 0.053
0.227 (1.0)	1.22 ± 0.18	0.689 ± 0.117	0.404 ± 0.12

* numbers in parentheses correspond to wt % cross-linking density

Table 2.4 reports the corresponding solute-gel diffusion coefficients for desorption from the same cross-link-density hydrogels as those for absorption. Trends are identical to those for the loading direction. Comparison of the loading and release diffusion coefficients reveals agreement, although the solute-desorption diffusivities are somewhat smaller than those for absorption. Lack of significant difference between absorption and desorption diffusion coefficients suggests that the solute molecules do not interact strongly with the gel matrix. Loading and release are reversible. Indeed, we find that all dextran solutes are completely extracted from the HEMA/MAA gels to within experimental precision.

Concomitantly, all solutes are size-excluded from a large portion of the liquid void space in the gels.[31] The somewhat smaller desorption diffusion coefficients might be attributed to small interaction with the polymer strands in the larger mesh-size spaces.

Table 2.4: Solute-Hydrogel Desorption Diffusivities

Polymer Content ϕ_2	D_i **x10^7 [cm^2/s]**		
	FITC-dextran4	FITC-dextran10	FITC-dextran20
0.143 (0)*	2.61 ± 0.97	1.25 ± 0.46	0.777 ± 0.063
0.154 (0.1)	2.34 ± 0.47	-	0.809 ± 0.11
0.165 (0.25)	1.84 ± 0.07	1.45 ± 0.20	0.787 ± 0.059
0.183 (0.5)	1.56 ± 0.29	0.63 ± 0.36	0.897 ± 0.15
0.227 (1.0)	1.03 ± 0.07	0.54 ± 0.11	0.617 ± 0.063

* numbers in parentheses correspond to wt % cross-linking density

Figure 2.3 summarizes the loading (closed symbols) and release (open symbols) diffusivities, D_i, in the 70-wt % HEMA/ 30-wt% MAA gels from Tables 2.3 and 2.4 normalized by their corresponding bulk diffusivities, D_{io}, as a function of polymer volume fraction, ϕ_2, for the three labeled dextrans. For comparison, relative macromolecular diffusivities measured in agarose[36] and polyacrylamide[37] gels are shown. Clearly, our dextran-HEMA/MAA data correspond to higher-polymer-content gels where size-exclusion is pronounced. Our data fall in line with those measured by fluorescence recovery after photobleaching (FRAP) by Johnson et al.[36] for proteins in agarose gels, but are somewhat larger than those by Tong and Anderson[37] in polyacrylamide gels. FRAP does not distinguish between diffusion in the uptake or release modes.

2.4.2 Specific-Gel Interacting Counterion Solute

Figure 2.4 shows fluorescence micrographs and transient concentration profiles (solid lines) for Fl-avidin loaded into and released from a 70-wt% HEMA/ 30-wt% MAA hydrogel with 0.05-wt% cross-link density. Loading is far from complete after 6 d compared to at most 3 d for full saturation by dextran solutes of similar size. Desorption was initiated at 6 d and continued for 16 d.

The release profile in Figure 2.4b reveals both farther solute penetration into the gel compared to the loading profile and back extraction into the bulk aqueous solution. After two weeks of leaching, however, only 20 % of the initially loaded solute is released into the surroundings. Application of Fick's law in Eq. 1 to predict loading profiles gives an average absorption diffusion coefficient of 7.2 x 10^{-10} cm^2/s for several repeat runs. This diffusion coefficient is 3 orders of magnitude smaller than those for the dextran solutes in Table 2.3. Apparently, absorption is slowed not only by molecular diffusion, but also by specific attraction of Fl-avidin to the gel matrix.

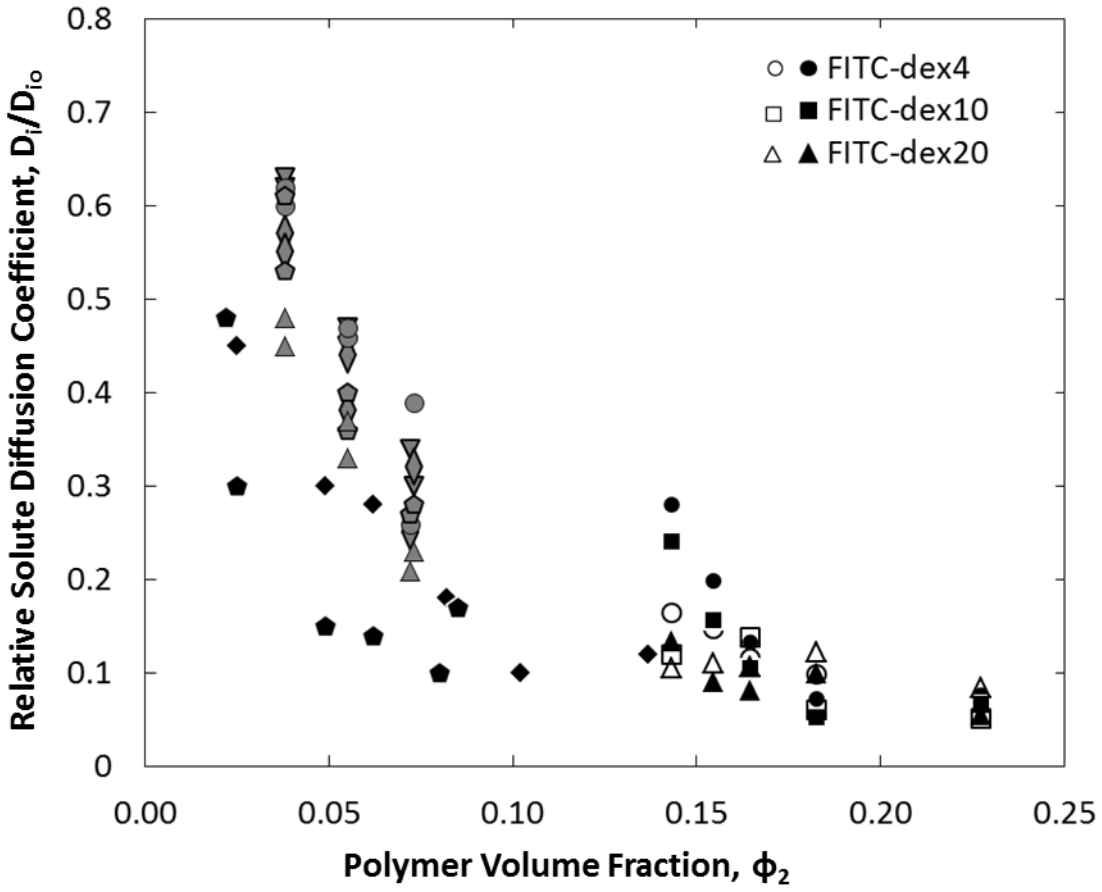

Figure 2.3: Relative diffusion coefficients of FITC-dextran4 (●○), FITC-dextran10 (■ □), and FITC-dextran20 (▲△**)** in 70-wt % HEMA/ 30-wt % MAA hydrogels as a function of polymer volume fraction. Filled symbols correspond to the loading direction while open symbols correspond to the release direction. Also shown are the relative macromolecular diffusion coefficients of Lactalbumin (▽), Ovalbumin (◊), Bovine Serum Albumin (⬟), and Ficolls of molecular weights 21kD (●) and 61kD (▲) in agarose gels,[36] and RNAase (◆) and Bovine Serum Albumin (⬟) in acrylamide gels.[37]

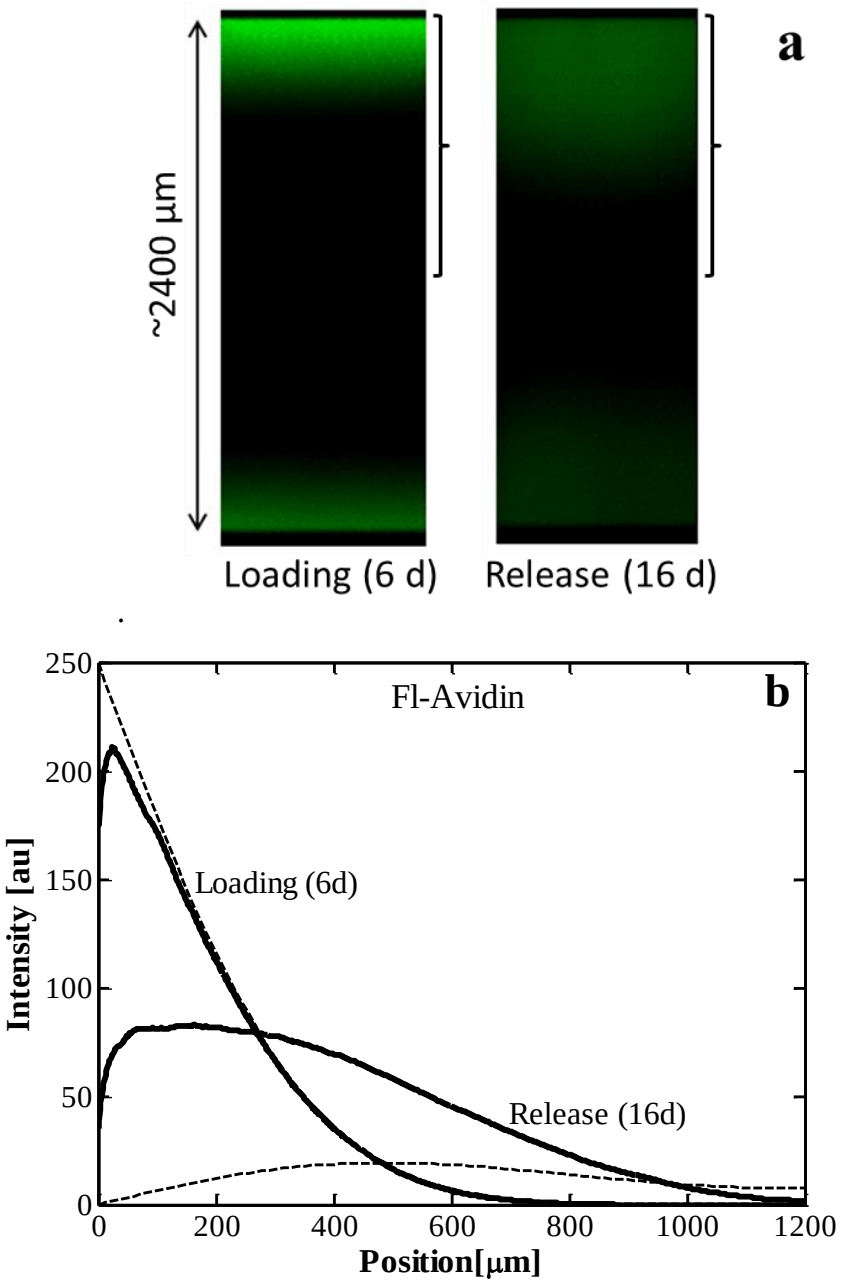

Figure 2.4: (a) Fluorescence micrographs and **(b)** transient intensity profiles (solid lines) of Fl-avidin (0.12 mg/mL solution) in 70-wt% HEMA/ 30-wt% MAA gel with 0.05-wt% cross-link density. a_{iS} = 7.1 nm; $\langle\xi\rangle$ = 8.3 nm. Loading for 6 d followed by release for 16 d. Profiles correspond to the top half of the gel (denoted by brackets in (**a**). Dashed lines are predicted from Eqs. 3 and 4 for loading and release, respectively, with a diffusion coefficient of 7.2 x 10^{-10} cm^2/s best fit from the loading profile.

2.5 Comparison to Theory

2.5.1 Nonspecific Interacting Solutes

Numerous theories are available to quantify solute diffusion when specific interaction with the gel is negligible.[9,32-38,40,41,44] Most all, including free-volume theory,[9,44] however, require empirical adjustable parameters, and do not make use of measured gel mesh size or gel-fiber radius. Table 2.5 displays three current physical-based theories that allow *a priori* prediction of hindered solute diffusion in hydrogels. All follow the suggestion of Brady[41] and express the relative diffusivity as a product of a hydrodynamic-resistance factor, F_i, and a steric or obstruction factor, S_i, related inversely to tortuosity or

$$D_i / D_{io} = F_i S_i \tag{5}$$

where D_i and D_{io} are the diffusion coefficients in the hydrogel and bulk solution, respectively.[33,36,37,40,56] In these expressions, $\alpha \equiv \phi_2(1+a_{iS}/a_f)^2$ where a_{iS} is the solute radius and a_f is the gel fiber radius.

Table 2.5: Selected Gel-Diffusion Models

Model Type	*Expression	Reference
Steric	$\frac{D_i}{D_{io}} = exp\left(-\sqrt{\alpha}\right)$	Ogston[35]
Hydrodynamic and Steric	$\frac{D_i}{D_{io}} = exp\left(-a\phi_2^{\,b}\right)exp(-0.84\alpha^{1.09})$	Phillips[33]
Computational		Claque and Phillips[48]
		Johansson and Löfroth[49]
Hydrodynamic and Steric	$\frac{D_i}{D_{io}} = \left[1+(a_{iS}/\sqrt{\kappa})+\frac{1}{9}(a_{iS}/\sqrt{\kappa})^2\right]^{-1}$	Solomentsev and Anderson[69]
Brinkman-Effective-Medium	$\times\left[e^{-\alpha}+\alpha^2 e^{\alpha}E_1(2\alpha)\right]$	Johansson et al.[34]

$^*\alpha \equiv \phi_2(1+a_{iS}/a_f)^2$; $\quad a = 3.727 - 2.460(\frac{a_f}{a_{iS}}) + 0.822(\frac{a_f}{a_{iS}})^2$;

$b = 0.358 + 0.366(\frac{a_f}{a_{iS}}) - 0.0939(\frac{a_f}{a_{iS}})^2$; $E_1(x) = \int_x^{\infty}\frac{e^{-u}}{u}du$

Hydrodynamic drag is ignored (i.e., $F_i = 1$) in the Ogston expression for D_i/D_{io}, entry 1 of Table 2.5. Conversely, Clague and Phillips[48] simulated hydrodynamic drag on a sphere in a random arrangement of cylindrical fibers giving $F_i = exp\left(-a\phi_2^{\,b}\right)$ with a and b established from the simulations. To account for obstruction, Philips[33] adopted the stochastic simulations of Johansson and Löfroth[49] represented by $S_i = exp(-0.84\alpha^{1.09})$. In Brinkman-effective-medium theory,[69,70] entry 3 in Table 2.5, hydrodynamic drag is given by

$$F_i = \left[1+(a_{iS}/\sqrt{\kappa})+\frac{1}{9}(a_{iS}/\sqrt{\kappa})^2\right]^{-1} \tag{6}$$

where κ is the absolute hydrodynamic (Darcy) permeability of aqueous solvent in the gel. The accompanying steric factor in Table 2.5 originates from the analytical cylindrical-cell theory of Johansson et al.[34] that well represents the hard-sphere steric simulations of Johansson and Löfroth.[49]

To implement Brinkman-effective-medium theory, we invoke the Carman-Kozeny expression for hydrodynamic permeability: $\kappa = (1-\phi_2)\left\langle r_H^2\right\rangle / 2\tau_H^2$ where $\left\langle r_H^2\right\rangle$ is the mean square hydraulic radius and τ_H is the gel hydrodynamic tortuosity.[32,59] For a random array of fibers with negligible overlap,[30] the mean hydraulic radius is $a_f(1-\phi_2)/2\phi_2$ revealing that κ scales as the square of the polymer-strand radius with the familiar Carman-Kozeny porosity dependence

$$\kappa = \frac{(1-\phi_2)^3}{8\phi_2^{\,2}\tau_H^2}a_f^2 \tag{7}$$

Tortuosity is included in Eq. 7 to account for increased path length, for channel shape, and for error in employing a hydraulic radius in creeping flow and in approximating the mean-square hydraulic radius by the square mean. To establish τ_H, Figure 2.5 displays measured hydrodynamic permeability for gels similar to our HEMA/MAA copolymer[71-73] as a function of $(1-\phi_2)^3/\phi_2^{\,2}$ on logarithmic scales. Hydraulic permeabilities of the hydrogels are extremely low, in the nDarcy range, due to the molecular size of the polymer strands and to the relatively low water contents of the gels (i.e., due to the small mesh sizes). The unity-slope solid line in Figure 2.5 is best fit to Eq. 7. With a_f fixed at 2 nm, we establish a tortuosity of $\tau_H \sim 4.7$.for our HEMA/MAA gels.

Figures 2.6 – 2.8 compare the *a priori* theories listed in Table 2.5 to our measured dextran solute diffusivities in the 70-wt % HEMA/ 30-wt% MAA gels as a function of polymer volume fraction. Obstruction alone in Ogston's model[35] (small dashed lines) significantly over predicts the data. The combined theory of Phillips[33] (long dashed lines) also does not reduce diffusivity enough, especially for the smaller dextrans. Effective-medium theory (dash-dot lines) demonstrates a larger solute-size dependence than that from experiment especially for the largest solute. Although the range of polymer volume fractions is limited in Figures 2.3 and 2.6-2.8 (i.e., a narrow range of cross-link densities) and data are

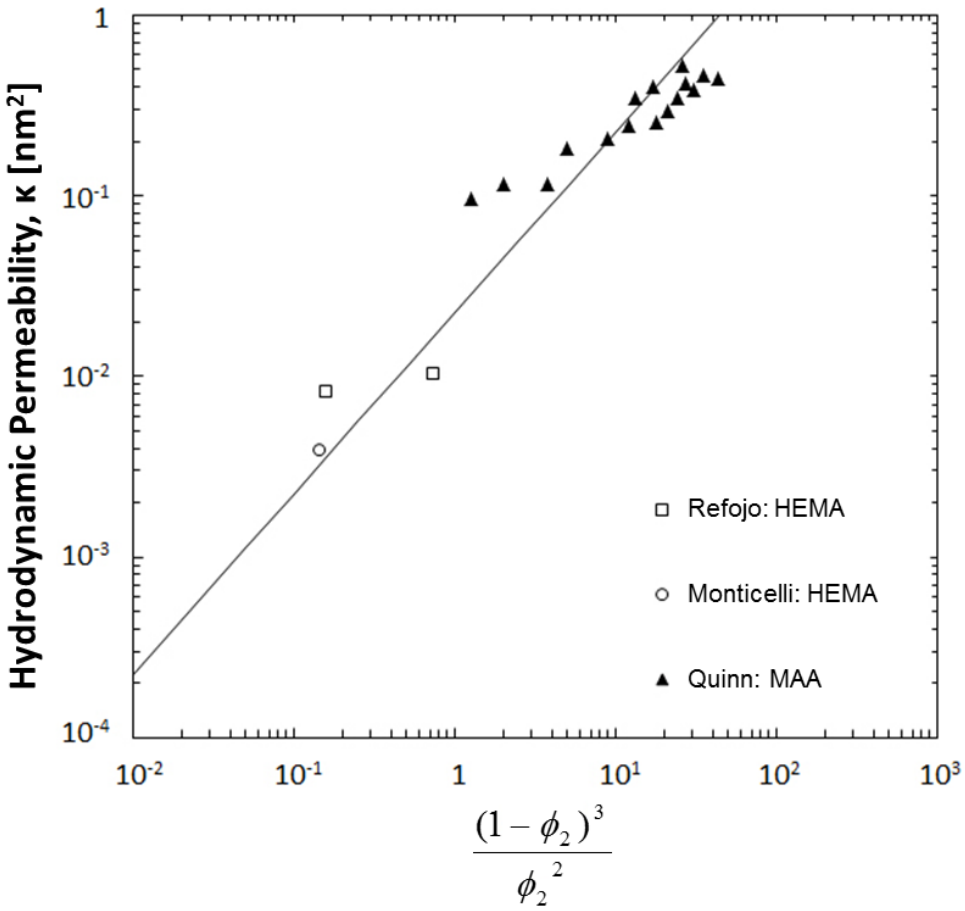

Figure 2.5: Hydrodynamic permeability, κ, as a function of water content expressed as $(1-\phi_2)^3/\phi_2^2$ for hydrogels similar to 70-wt% HEMA/ 30-wt% MAA: Refojo[73] (□); Quinn and Grodzinsky[72] (▲); Monticelli et al.[71] (○). With a_f = 2 nm, the best-fit unity-slope straight line gives a hydrodynamic tortuosity of τ_H = 4.7.

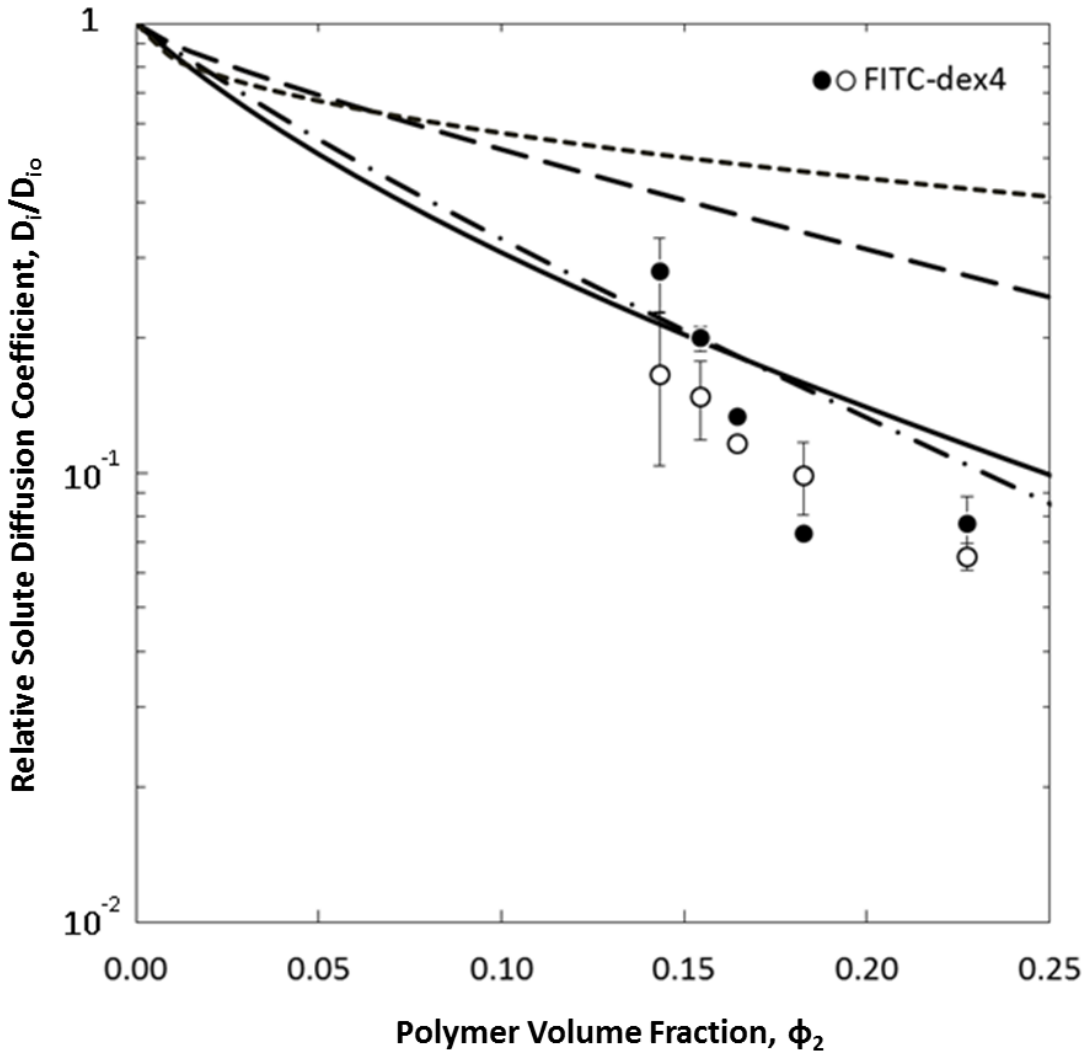

Figure 2.6: Relative diffusion coefficients of FITC-dextran4 (●○) in 70-wt % HEMA/ 30-wt % MAA hydrogels as a function of polymer volume fraction. Filled symbols correspond to the loading direction while open symbols correspond to the release direction. Lines reflect the predictions of Ogston[35] (– – –), Phillips[33] (— —), effective-medium theory[34,69] (— . —) and LPEM theory (——).

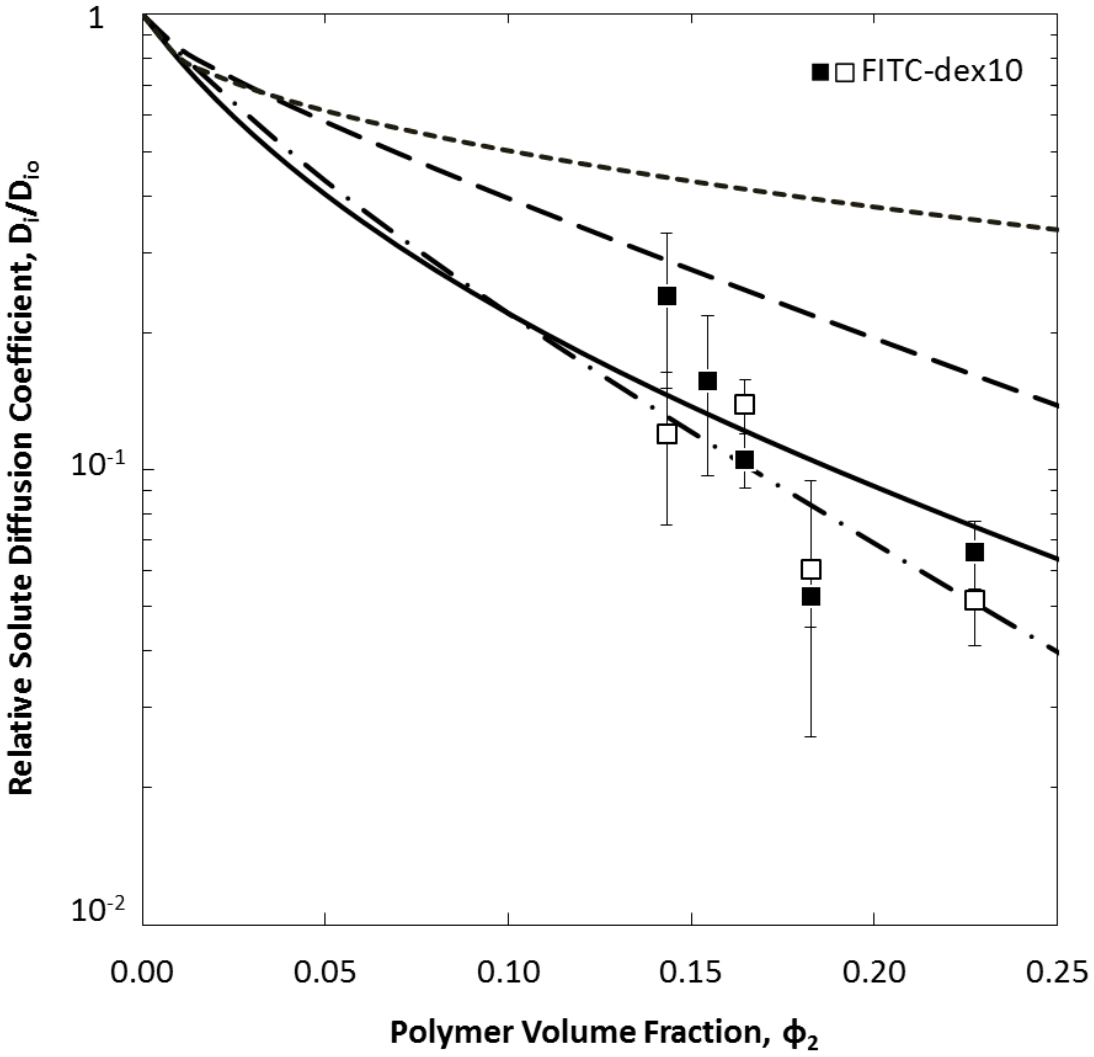

Figure 2.7: Relative diffusion coefficients FITC-dextran10 (■□) in 70-wt % HEMA/ 30-wt % MAA hydrogels as a function of polymer volume fraction. Filled symbols correspond to the loading direction while open symbols correspond to the release direction. Lines reflect the predictions of Ogston[35] (– – –), Phillips[33] (— —), effective-medium theory[34,69] (— . —) and LPEM theory (——).

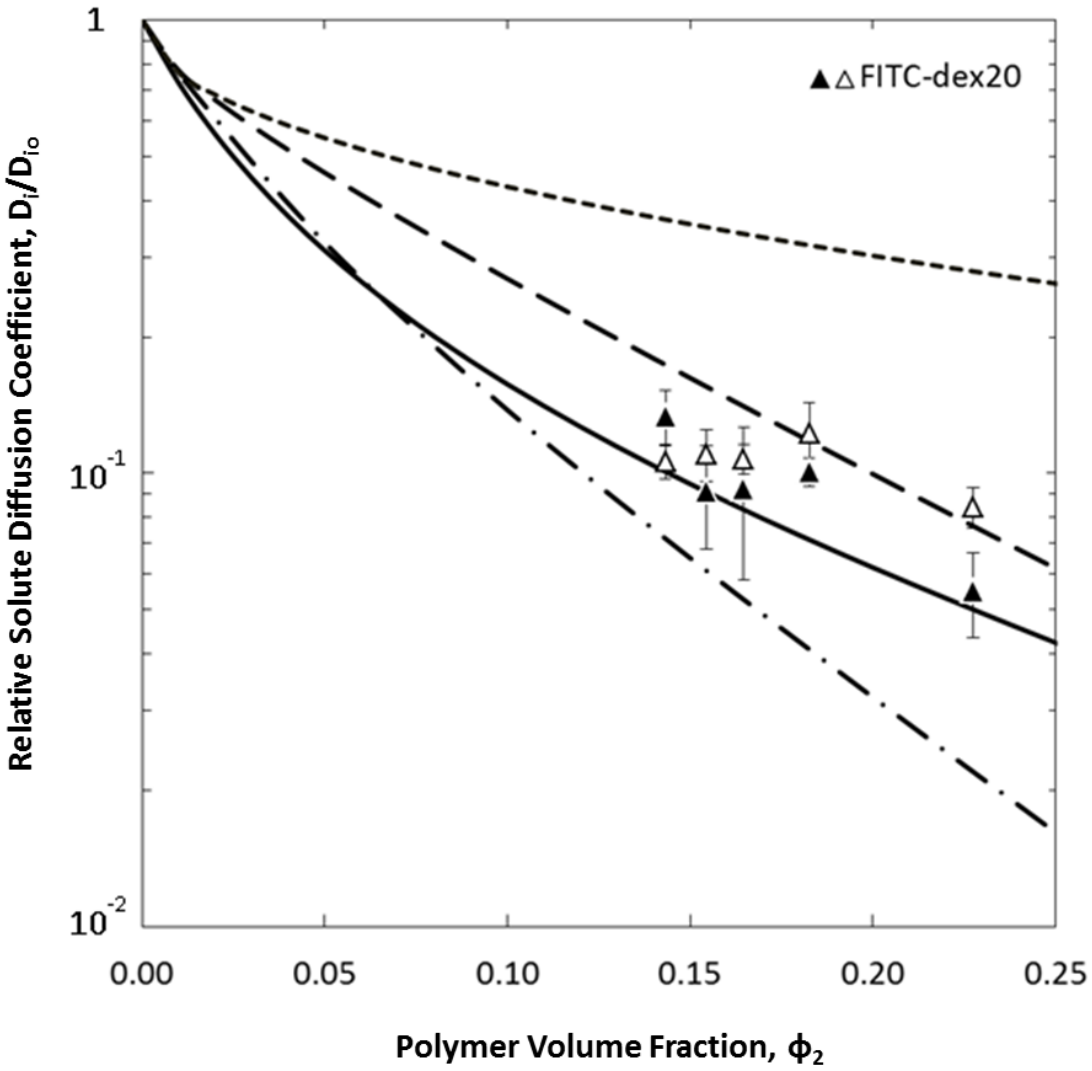

Figure 2.8: Relative diffusion coefficients of FITC-dextran20 (▲ △**)** in 70-wt % HEMA/ 30-wt % MAA hydrogels as a function of polymer volume fraction. Filled symbols correspond to the loading direction while open symbols correspond to the release direction. Lines reflect the predictions of Ogston[35] (– – –), Phillips[33] (— —), effective-medium theory[34,69] (— . —) and LPEM theory (——).

scattered, the measured solute-size dependence of D_i/D_{io} is, in all cases, weaker than that predicted. No simple scaling factor(s) overcomes this disagreement.

A likely explanation for both minimal penetration and faster measured diffusion rates of solutes with sizes larger than the average gel mesh size is that only a fraction of the liquid-filled voids are solute occupied. Hydrogels clearly exhibit a distribution of mesh sizes. Large solutes in high-polymer-content gels penetrate and permeate through the larger interconnected mesh-size spaces.[31] This framework successfully predicts measured equilibrium partition coefficients of the labeled dextrans in our HEMA/MAA gels.[31] The larger is the solute, the larger are the mesh sizes necessary to permit diffusion and the smaller is the fraction of liquid-filled space available for transport.

Current estimates of F_i and S_i in Table 2.5 apply to solutes that are small relative to the gel mesh sizes and do not account for solute-size exclusion from the smaller liquid-filled spaces. Apparently, small solutes experience relatively more hydrodynamic drag and obstruction compared to larger ones because of transport through the larger mesh-size spaces. This effect partially offsets the larger drag and obstruction attributed to solute size in current effective-medium theory.

2.5.2 Large Pore Effective Medium Theory

To account for solute transport only in the occupied portion of the gel voids, we create a hypothetical large-pore effective medium (LPEM) consisting of the distribution of mesh sizes available for solute transport. Hydrodynamic and obstruction factors, F_i[69,70] and S_i,[34] are modified to describe solute access only to mesh sizes larger than their size and, thus, to account for drag and obstruction only within accessible liquid-filled voids. All liquid-filled pores sizes in the LPEM are assumed to percolate.

The hydrodynamic factor of the large-pore gel is estimated from Eqs. 6 and 7 but at a larger liquid volume fraction, $1-\phi_{2L}$, characteristic of the LPEM. To determine ϕ_{2L}, we assume that the average hydraulic radius in the large-pore medium, $< r_H >_L$, relative to that of original medium from Carman-Kozeny, i.e., $a_f(1-\phi_2)/2\phi_2$, scales linearly with the average mesh radius

$$< r_H >_L = [\, a_f(1-\phi_2)/2\phi_2 \,] \langle r \rangle_L / \langle r \rangle \tag{8}$$

where r is the mesh radius or one-half of the mesh size and subscript L indicates the large-pore pseudo-medium. Average mesh radius is obtained from the Ogston distribution.[30]

$$a_f g_o(r) = 2\phi_2(1+r/a_f)exp[-\phi_2(1+r/a_f)^2] \tag{9}$$

where $g_o(r;a_f)dr$ is the volume fraction of water-filled spaces with radii between r and $r + dr$. The average mesh radius of the original distribution and that of the LPEM follow by definition

$$< r >= \frac{\int_0^\infty r g_o(r)dr}{\int_0^\infty g_o(r)dr} = \frac{a_f}{2}\sqrt{\frac{\pi}{\phi_2}}\, exp(\phi_2) erfc(\sqrt{\phi_2}) \tag{10}$$

and

$$< r >_L = \frac{\int_{a_{iS}}^\infty r g_o(r)dr}{\int_{a_{iS}}^\infty g_o(r)dr} = a_{iS} + \frac{a_f}{2}\sqrt{\frac{\pi}{\phi_2}}\, exp\left(\phi_2(1+a_{iS}/a_f)^2\right) erfc\left[\sqrt{\phi_2}(1+a_{iS}/a_f)\right] \tag{11}$$

respectively. Eqs. 8-11 give the polymer fraction of the LPEM since $< r_H >_L \equiv a_f(1-\phi_{2L})/2\phi_{2L}$. Darcy permeability of the accessible voids, κ_L, is then available from Eq. 7 with ϕ_2 replaced by ϕ_{2L}. The hydrodynamic factor follows from Eq. 6. We do not adjust the hydraulic tortuosity of the LPEM in Eq. 7.

The LPEM-modified obstruction factor emerges from two extensions of the cylindrical-cell model of Johansson et al.[34] First, we correct the original expression of Johansson et al.[34] for the diffusion coefficient, $D_{i\perp}(R)$, of solute transporting across a single cylindrical cell of radius R[74,75] to read

$$\frac{D_{i\perp}(R)}{D_{io}} = \frac{[1-a^2/R^2]}{[1+a^2/R^2]} \tag{12}$$

where $a = a_{iS} + a_f$. Adoption of Eq. 12 gives a slightly modified expression for the obstruction factor: $S_i = (1-\alpha)e^{-\alpha} + 2\alpha^2 e^{\alpha} E_1(2\alpha)$ where $\alpha \equiv \phi_2(1+a_{iS}/a_f)^2$ and E_1 is the exponential integral, $E_1(x) = \int_x^\infty \frac{e^{-u}}{u} du$. Second, we replace the original-medium polymer volume fraction by that of the hypothetical large-pore medium

$$S_i = (1-\alpha_L)e^{-\alpha_L} + 2\alpha_L^2 e^{\alpha_L} E_1(2\alpha_L) \tag{13}$$

where $\alpha_L = \phi_{2L}(1+a_{iS}/a_f)^2$. Eq. 13 explicitly accounts for occupancy of solute only in the large liquid-filled voids and for excluded volume within those larger pores. The LPEM-modified obstruction factor also agrees with the hard-sphere steric simulations of Johansson and Loforoth.[49] With F_i and S_i now specified in Eqs. 6 and 13, solute diffusivity in the gel follows from Eq. 5

Solid lines in Figures 2.6-2.8 display predictions of the proposed LPEM theory for the relative diffusivities of FITC-dextran 4, 10, and 20 in the 70-wt % HEMA/ 30-wt% MAA gels measured as a function of polymer volume fraction using no adjustable parameters. Agreement for all non-interacting solutes is acceptable to within, at most, a factor of 2. Thus, LPEM theory well predicts diffusion coefficients of large solutes (relative to mesh size) in high-polymer content gels with no adjustable constants.

2.5.3 Specific Interacting Counterion Solute

The slow loading and release of cationic Fl-avidin shown in Figure 2.4 coupled with the large measured partition coefficient[31] of 23.9 and the small loading diffusion coefficient of 7.2 x 10^{-10} cm^2/s indicates strong specific adsorption to the HEMA/MAA polymer chains. To understand the transport kinetics, we first extend Eq. 1 to account for the amount of protein specifically adsorbed to the polymer as distinct from that occupying the liquid-filled spaces

$$\frac{\partial C_i^L(t,x)}{\partial t} + \left(\frac{\phi_2}{1-\phi_2}\right)\frac{\partial n_i(t,x)}{\partial t} = D_i \frac{\partial^2 C_i^L(t,x)}{\partial x^2} \tag{14}$$

where C_i^L is the moles of nonadsorbed solute *i* in the liquid-filled voids per liquid volume and n_i is the moles of specifically adsorbed solute *i* per unit polymer volume in the gel.[31] Eq. 14 assumes that the dilute solute does not influence swelling, that diffusion occurs only in the liquid phase of the gel, and that surface diffusion along the polymer backbone is negligible. This approach contrasts with that of Russell et al.[29] who make no distinction between liquid-phase and chain- surface transport in a gel.

To describe the rate of adsorption, the simplest approach is to assume local equilibrium with a linear isotherm: $n_i = K_i C_i^L$ where K_i is Henry's adsorption constant (dimensionless).[31] Substitution of Henry's law into Eq. 14 yields an effective diffusion coefficient governing transport in the gel: $D_{i\pi} = D_i / [1+\phi_2 K_i / (1-\phi_2)]$. Accordingly, specific adsorption of solute onto the polymer chains with a large Henry's constant drastically retards diffusion rates. The measured Henry's adsorption constant for Fl-avidin[31] is 5500 giving an effective diffusion coefficient 3 orders of magnitude smaller than that for a nonadsorbing solute of the same size, qualitatively consistent with the observed loading diffusion coefficient of Fl-avidin. Quantitative agreement between the calculated D_{ie} and the measured loading diffusion coefficient from Figure 2.4b, however, is lacking.

The lower dashed line in Figure 2.4b reflects the predicted release profile after $t^* = 16$ d of leaching using the expression $C_i^L(t,x)/C_{i\infty}^L = \sum_{n=0}^{\infty} A_n(t,x;t^*)$ and the measured loading diffusion coefficient of 7.2 x 10^{-10} cm^2/s. Because the amount of solute adsorbed is linearly proportional to the liquid-phase concentration, separate accounting for $n_i(t,x)$ is not requisite. In Figure 2.4b, theory predicts that 75 % of the initially loaded solute is released over the 16-d extraction period, much more than the measured 20 %.

The large discrepancy between observed and predicted Fl-avidin release kinetics in Figure 2.4b and the quantitative disagreement between calculated and measured D_{ie} values

suggest that local sorption equilibrium is not attained within the gel. To relieve the local-equilibrium restriction, we invoke simple linear adsorption/desorption kinetics for the solute in the gel

$$\frac{\partial n_i(t,x)}{\partial t} = k_{-1}\left[K_i C_i^L - n_i\right] \tag{15}$$

so that

$$\frac{\partial C_i^L(t,x)}{\partial t} = D_i \frac{\partial^2 C_i^L(t,x)}{\partial x^2} - \left(\frac{\phi_2}{1-\phi_2}\right) k_{-1}\left[K_i C_i^L - n_i\right] \tag{16}$$

where k_{-1} is the first-order desorption rate constant and $k_{-1}K_i$ is the first-order adsorption rate constant. Solution to Eqs. 15 and 16 is given in Appendix 2A. As with loading of the nonadsorbing solutes because of surface blotting, we first estimate the surface concentration $C_i^L(t,-L) = C_{i\infty}^L$ in Eq. 2A.3 from the Fl-avidin loading profile in Figure 2.4b near the top face of the gel. The remainder of the loading profile at 6 d is then fit to obtain desorption rate constant and the diffusion coefficient of Fl-avidin in the 70-wt % HEMA/ 30-wt % MAA gel.

The upper dashed line in Figure 2.9 shows the resulting model fit to the measured loading profile with $D_i/D_{io} = 0.5$ and $k_{-1} = 6 \times 10^{-7}$ s^{-1} giving a characteristic desorption time of 19 d. Shown in the lower dashed line is the corresponding release profile of Fl-avidin predicted with no adjustable parameters. Although not quantitative, agreement of the measured profiles with the linear-kinetic model is much improved over that based on the local-equilibrium assumption shown in Figure 2.3b. The observed small desorption rate constant suggests that Fl-avidin is tightly bound to the polymer strands, approaching irreversible attachment, typical for proteins at long exposure times.[76-80] Strict conformance to linear sorption kinetics is, therefore, unlikely. Additional transient-profile data at differing Fl-avidin concentrations are necessary to establish more realistic sorption kinetics.

Considerable size-exclusion is expected for the 7.1-nm avidin molecule in the 8.3-nm mesh-size gel. Accordingly, Fl-avidin penetrates only a small fraction of the aqueous-occupied voids.[31] In view of the small voidage occupancy, the large measured Henry's adsorption constant and the concomitant small desorption rate constant indicate strong specific adsorption on the polymer matrix. Donnan electrostatic attraction[81] is an unlikely explanation because of extensive screening by the background aqueous electrolyte at a Debye length of 0.5 nm. Rather, the experimental evidence strongly supports specific ion binding between cationic Fl-avidin and anionic MAA groups along the polymer strands.

2.6 Conclusions

Using two-photon confocal fluorescence microscopy, we measured transient loading and release concentration profiles of 4 labeled aqueous solutes: FITC dextran of 4, 10, and 20 kDa molecular weights, and fluorescein conjugate avidin, at pH = 7.4 in negatively charged 70-wt% HEMA/ 30-wt% MAA hydrogels having 0 to 1-wt % cross-link density. A unique feature of our measurements is that solute size is comparable to or larger than the average

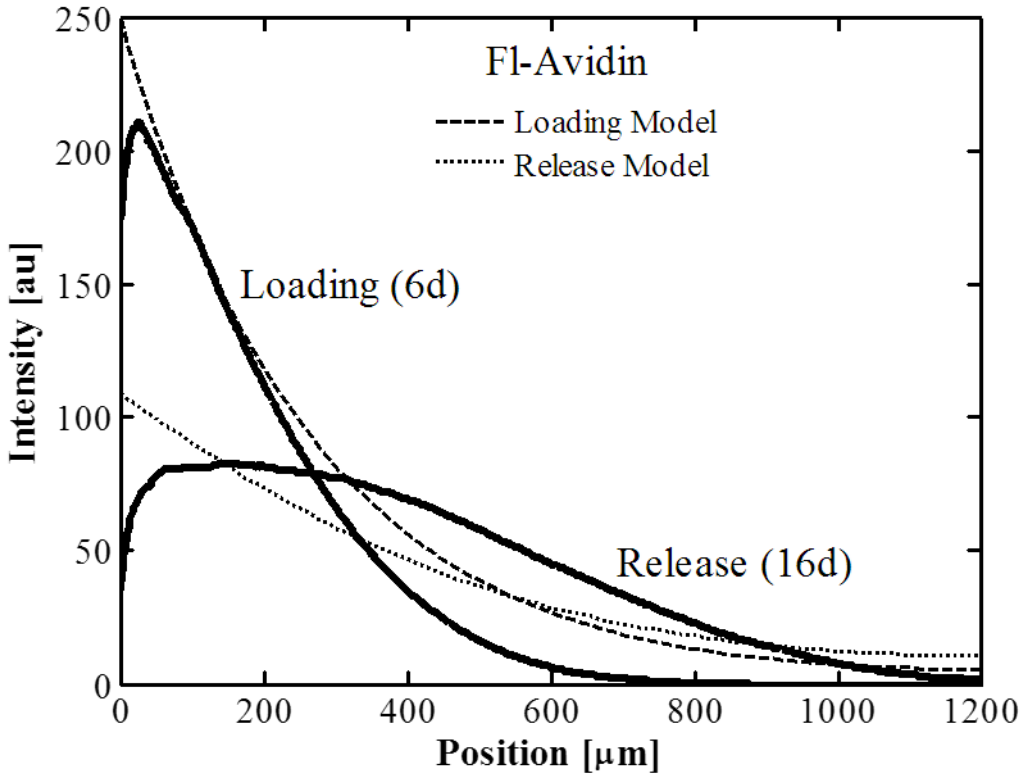

Figure 2.9: Transient loading and release profiles (dark lines) of Fl-avidin in a 70-wt% HEMA/ 30-wt% MAA hydrogel with 0.05-wt % cross-link density. Desorption begins after 6 d of loading. Dashed and dotted lines are predicted from linear sorption kinetics with D_i/D_{io} = 0.5, K_i = 5500, and k_{-1} = 6 x 10^{-7} s^{-1}.

mesh size of the gels and the polymer volume fraction range is higher than those typically studied. Although all solutes are significantly size-excluded from major portions of the gel voids, they all permeate through the available gel network by liquid-phase diffusion. Except for cationic Fl-avidin, all solutes exhibit reversible absorption and desorption with diffusion coefficients approximately equal in both directions in obedience to Fick's second law. For these non-adsorbing solutes, gel diffusivities decrease strongly with increasing polymer content and less so with increasing solute size. LPEM theory gives D_i / D_{io} as a product of a hydrodynamic factor, F_i, and an obstruction factor, S_i, taking into account only gel mesh sizes available for transport. When all parameters are independently determined, LPEM theory agrees quantitatively with measured solute diffusion coefficients. Accordingly, an estimate of nonadsorbing aqueous-solute transport rates in hydrogels is available without need to adjust parameters. Although LPEM is physically grounded, it does not account for dynamic fluctuations in the mesh-size distribution.

For the positively charged counterion Fl-avidin solute, diffusion is significantly slowed by strong specific adsorption on the anionic polymer strands. When compared to a dextran molecule of the same hydrodynamic size, avidin absorbs more slowly into the gel by over 3 orders of magnitude. Desorption is even slower, approaching irreversible uptake. An effective local-equilibrium diffusion coefficient does not predict uptake and release kinetics. Simple linear adsorption/desorption kinetics more successfully fits the measured concentration profiles, giving a desorption time constant of about 20 d. The large measured Henry's adsorption constant and the small desorption rate constant highlight strong ion-binding of the cationic avidin onto the anionic MAA moieties of the gel polymer. The difference between diffusion rates of non-adsorbing and specific adsorbing solutes in hydrogels is striking and must be accounted for.

2.7 Acknowledgements

Alcon Laboratories is acknowledged for financial support. We thank Joshua Tan and Kevin Yeh for performing the restricted-diffusion measurements.

2.8 References

1. Boschetti, E. Advanced sorbents for preparative protein separation purposes. *Journal of Chromatography A* **1994,** 658, (2), 207-236.
2. Farnan, D.; Frey, D. D.; Horváth, C. Surface and pore diffusion in macroporous and gel-filled gigaporous stationary phases for protein chromatography. *Journal of Chromatography A* **2002,** 959, (1–2), 65-73.
3. Fernandez, M. A.; Carta, G. Characterization of protein adsorption by composite silica-polyacrylamide gel anion exchangers I. Equilibrium and mass transfer in agitated contactors. *Journal of Chromatography A* **1996,** 746, (2), 169-183.
4. Farnan, D.; Frey, D. D.; Horvath, C. Intraparticle mass transfer in high-speed chromatography of proteins. *Biotechnology Progress* **1997,** 13, (4), 429-439.

5. Peppas, N. A.; Bures, P.; Leobandung, W.; Ichikawa, H. Hydrogels in pharmaceutical formulations. *European Journal of Pharmaceutics and Biopharmaceutics* **2000,** 50, (1), 27-46.

6. Jen, A. C.; Wake, M. C.; Mikos, A. G. Review: Hydrogels for cell immobilization. *Biotechnology and Bioengineering* **1996,** 50, (4), 357-364.

7. Drury, J. L.; Mooney, D. J. Hydrogels for tissue engineering: scaffold design variables and applications. *Biomaterials* **2003,** 24, (24), 4337-4351.

8. Kretsinger, J. K.; Haines, L. A.; Ozbas, B.; Pochan, D. J.; Schneider, J. P. Cytocompatibility of self-assembled β-hairpin peptide hydrogel surfaces. *Biomaterials* **2005,** 26, (25), 5177-5186.

9. Amsden, B. Solute diffusion in hydrogels: An examination of the retardation effect. *Polymer Gels and Networks* **1998,** 6, (1), 13-43.

10. Jones, D. S.; Lorimer, C. J.; Andrews, G. P.; McCoy, C. P.; Gorman, S. P. An examination of the thermorheological and drug release properties of zinc tetraphenylporphyrin-containing thermoresponsive hydrogels, designed as light activated antimicrobial implants. *Chemical Engineering Science* **2007,** 62, (4), 990-999.

11. Peppas, N. A.; Langer, R. New challenges in biomaterials. *Science* **1994,** 263, (5154), 1715-1720.

12. Castillo, E. J.; Koenig, J. L.; Anderson, J. M.; Lo, J. Protein adsorption on hydrogels: II. Reversible and irreversible interactions between lysozyme and soft contact lens surfaces. *Biomaterials* **1985,** 6, (5), 338-345.

13. Luensmann, D.; Zhang, F.; Subbaraman, L.; Sheardown, H.; Jones, L. Localization of lysozyme sorption to conventional and silicone hydrogel contact lenses using confocal microscopy. *Current Eye Research* **2009,** 34, (8), 683-697.

14. Nicolson, P. C.; Vogt, J. Soft contact lens polymers: An evolution. *Biomaterials* **2001,** 22, (24), 3273-3283.

15. Alvarez-Lorenzo, C.; Hiratani, H.; Concheiro, A. Contact lenses for drug delivery: achieving sustained release with novel systems. *American Journal of Drug Delivery* **2006** 4, (3), 131-151.

16. Venkatesh, S.; Sizemore, S. P.; Byrne, M. E. Biomimetic hydrogels for enhanced loading and extended release of ocular therapeutics. *Biomaterials* **2007,** 28, (4), 717-724.

17. Peng, C.-C.; Kim, J.; Chauhan, A. Extended delivery of hydrophilic drugs from silicone-hydrogel contact lenses containing Vitamin E diffusion barriers. *Biomaterials* **2010,** 31, (14), 4032-4047.

18. Xinming, L.; Yingde, C.; Lloyd, A. W.; Mikhalovsky, S. V.; Sandeman, S. R.; Howel, C. A.; Liewen, L. Polymeric hydrogels for novel contact lens-based ophthalmic drug delivery systems: A review. *Contact Lens and Anterior Eye* **2008,** 31, (2), 57-64.

19. White, C. J.; Tieppo, A.; Byrne, M. E. Controlled drug release from contact lenses: A comprehensive review from 1965-present. *Journal of Drug Delivery Science and Technology* **2011,** 21, (5), 369-384.

20. Ketelson, H. A.; Meadows, D. L.; Stone, R. P. Dynamic wettability properties of a soft contact lens hydrogel. *Colloids and Surfaces B: Biointerfaces* **2005,** 40, (1), 1-9.

21. Tran, V. B.; Sung, Y. S.; Copley, K.; Radke, C. J. Effects of aqueous polymeric surfactants on silicone-hydrogel soft- contact-lens wettability and bacterial adhesion of Pseudomonas aeruginosa. *Contact Lens and Anterior Eye* **2012,** 35, (4), 155-162.

22. Peppas, N. A.; Moynihan, H. J.; Lucht, L. M. The structure of highly crosslinked poly(2-hydroxyethyl methacrylate) hydrogels. *Journal of Biomedical Materials Research* **1985,** 19, (4), 397-411.

23. Anseth, K. S.; Bowman, C. N.; Brannon-Peppas, L. Mechanical properties of hydrogels and their experimental determination. *Biomaterials* **1996,** 17, (17), 1647-1657.

24. D'Errico, G.; De Lellis, M.; Mangiapia, G.; Tedeschi, A.; Ortona, O.; Fusco, S.; Borzacchiello, A.; Ambrosio, L. Structural and mechanical properties of UV-photo-cross-linked poly(N-vinyl-2-pyrrolidone) hydrogels. *Biomacromolecules* **2008,** 9, (1), 231-240.

25. De Gennes, P. G. *Scaling concepts in polymer physics*. Cornell university press: Ithaca, 1979.

26. Lewus, R. K.; Carta, G. Protein diffusion in charged polyacrylamide gels: visualization and analysis. *Journal of Chromatography A* **1999,** 865, (1), 155-168.

27. Lewus, R. K.; Carta, G. Protein transport in constrained anionic hydrogels: Diffusion and boundary-layer mass transfer. *Industrial & Engineering Chemistry Research* **2001,** 40, (6), 1548-1558.

28. Russell, S. M.; Belcher, E. B.; Carta, G. Protein partitioning and transport in supported cationic acrylamide-based hydrogels. *AIChE Journal* **2003,** 49, (5), 1168-1177.

29. Russell, S. M.; Carta, G. Multicomponent protein adsorption in supported cationic polyacrylamide hydrogels. *AIChE Journal* **2005,** 51, (9), 2469-2480.

30. Ogston, A. G. The spaces in a uniform random suspension of fibres. *Transactions of the Faraday Society* **1958,** 54, (0), 1754-1757.

31. Kotsmar, C.; Sells, T.; Taylor, N.; Liu, D. E.; Prausnitz, J. M.; Radke, C. J. Aqueous Solute Partitioning and Mesh Size in HEMA/MAA Hydrogels. *Macromolecules* **2012,** 45, (22), 9177-9187.

32. Pluen, A.; Netti, P. A.; Jain, R. K.; Berk, D. A. Diffusion of macromolecules in agarose gels: Comparison of linear and globular configurations. *Biophysical Journal* **1999,** 77, (1), 542-552.

33. Phillips, R. J. A hydrodynamic model for hindered diffusion of proteins and micelles in hydrogels. *Biophysical Journal* **2000,** 79, (6), 3350.

34. Johansson, L.; Elvingson, C.; Löfroth, J. E. Diffusion and interaction in gels and solutions. 3. Theoretical results on the obstruction effect. *Macromolecules* **1991,** 24, (22), 6024-6029.

35. Ogston, A. G.; Preston, B. N.; Wells, J. D. On the transport of compact particles through solutions of chain-polymers. *Proceedings of the Royal Society of London. A. Mathematical and Physical Sciences* **1973,** 333, (1594), 297-316.

36. Johnson, E. M.; Berk, D. A.; Jain, R. K.; Deen, W. M. Hindered diffusion in agarose gels: test of effective medium model. *Biophysical Journal* **1996,** 70, (2), 1017-1023.

37. Tong, J.; Anderson, J. L. Partitioning and diffusion of proteins and linear polymers in polyacrylamide gels. *Biophysical Journal* **1996,** 70, (3), 1505-1513.

38. Lustig, S. R.; Peppas, N. A. Solute diffusion in swollen membranes. IX. Scaling laws for solute diffusion in gels. *Journal of Applied Polymer Science* **1988,** 36, (4), 735-747.

39. Peppas, N. A.; Reinhart, C. T. Solute diffusion in swollen membranes: Part I. A new theory. *Journal of Membrane Science* **1983,** 15, (3), 275-287.

40. Phillips, R. J.; Deen, W. M.; Brady, J. F. Hindered transport in fibrous membranes and gels: Effect of solute size and fiber configuration. *Journal of Colloid and Interface Science* **1990,** 139, (2), 363-373.

41. Brady, J. In *Hindered diffusion*, Extended Abstracts, AIChE Annual Meeting, San Fransisco, CA, 1994; 1994; p 320.

42. Grassi, M.; Lapasin, R.; Coviello, T.; Matricardi, P.; Di Meo, C.; Alhaique, F. Scleroglucan/borax/drug hydrogels: Structure characterisation by means of rheological and diffusion experiments. *Carbohydrate Polymers* **2009,** 78, (3), 377-383.

43. Waters, D. J.; Frank, C. W. Hindered diffusion of oligosaccharides in high strength poly(ethylene glycol)/poly(acrylic acid) interpenetrating network hydrogels: Hydrodynamic vs. obstruction models. *Polymer* **2009,** 50, (26), 6331-6339.

44. Masaro, L.; Zhu, X. X. Physical models of diffusion for polymer solutions, gels and solids. *Progress in Polymer Science* **1999,** 24, (5), 731-775.

45. Guan, L.; Jiménez, M. E. G.; Walowski, C.; Boushehri, A.; Prausnitz, J. M.; Radke, C. J. Permeability and partition coefficient of aqueous sodium chloride in soft contact lenses. *Journal of Applied Polymer Science* **2011,** 122, (3), 1457-1471.

46. am Ende, M. T.; Peppas, N. A. Transport of ionizable drugs and proteins in crosslinked poly(acrylic acid) and poly(acrylic acid-co-2-hydroxyethyl methacrylate) hydrogels. II. Diffusion and release studies. *Journal of Controlled Release* **1997,** 48, (1), 47-56.

47. Kong, D. D.; Kosar, T. F.; Dungan, S. R.; Phillips, R. J. Diffusion of proteins and nonionic micelles in agarose gels by holographic interferometry. *AIChE Journal* **1997,** 43, (1), 25-32.

48. Clague, D. S.; Phillips, R. J. Hindered diffusion of spherical macromolecules through dilute fibrous media. *Physics of Fluids* **1996,** 8, 1720.

49. Johansson, L.; Löfroth, J. E. Diffusion and interaction in gels and solutions. 4. Hard sphere Brownian dynamics simulations. *The Journal of chemical physics* **1993,** 98, 7471.

50. Johnson, E. M.; Berk, D. A.; Jain, R. K.; Deen, W. M. Diffusion and partitioning of proteins in charged agarose gels. *Biophysical Journal* **1995,** 68, (4), 1561-1568.

51. Amsden, B. An obstruction-scaling model for diffusion in homogeneous hydrogels. *Macromolecules* **1999,** 32, (3), 874-879.

52. Bosma, J. C.; Wesselingh, J. A. Partitioning and diffusion of large molecules in fibrous structures. *Journal of Chromatography B: Biomedical Sciences and Applications* **2000,** 743, (1), 169-180.

53. Phillips, R. J.; Deen, W. M.; Brady, J. F. Hindered transport of spherical macromolecules in fibrous membranes and gels. *AIChE Journal* **1989,** 35, (11), 1761-1769.

54. Lazzara, M. J.; Blankschtein, D.; Deen, W. M. Effects of multisolute steric interactions on membrane partition coefficients. *Journal of Colloid and Interface Science* **2000,** 226, (1), 112-122.

55. Shalviri, A.; Liu, Q.; Abdekhodaie, M. J.; Wu, X. Y. Novel modified starch–xanthan gum hydrogels for controlled drug delivery: Synthesis and characterization. *Carbohydrate Polymers* **2010,** 79, (4), 898-907.

56. Fatin-Rouge, N.; Wilkinson, K. J.; Buffle, J. Combining small angle neutron scattering (SANS) and fluorescence correlation spectroscopy (FCS) measurements to relate diffusion in agarose gels to structure. *The Journal of Physical Chemistry B* **2006,** 110, (41), 20133-20142.

57. Newman, J.; Chapman, T. W. Restricted diffusion in binary solutions. *AIChE Journal* **1973,** 19, (2), 343-348.

58. Stewart, S. G.; Newman, J. The use of UV/vis absorption to measure diffusion coefficients in LiPF6 electrolytic solutions. *Journal of the Electrochemical Society* **2008,** 155, (1), F13-F16.

59. Bird, R. B.; Stewart, W. E.; Lightfoot, E. N. *Transport phenomena*. 2nd ed.; Wiley: New York, 2006.

60. Kopeček, J.; Lím, D. Mechanism of the three-dimensional polymerization of glycol methacrylates. II. The system glycol monomethacrylate–glycol dimethacrylates–solvents. *Journal of Polymer Science Part A-1: Polymer Chemistry* **1971,** 9, (1), 147-154.

61. Erman, B.; Mark, J. E. *Structures and properties of rubberlike networks*. Oxford University Press New York: 1997.

62. Hasa, J.; Ilavský, M. Deformational, swelling, and potentiometric behavior of ionized poly(methacrylic acid) gels. II. Experimental results. *Journal of Polymer Science: Polymer Physics Edition* **1975,** 13, (2), 263-274.

63. Göppert-Mayer, M. Über elementarakte mit zwei quantensprüngen. *Annalen der Physik* **1931,** 401, (3), 273-294.

64. Denk, W.; Strickler, J. P.; Webb, W. W. Two-photon laser microscopy. USA Patent 5034613, 1991.

65. Song, Y.; Srinivasarao, M.; Tonelli, A.; Balik, C.; McGregor, R. Laser scanning confocal microscopy study of dye diffusion in fibers. *Macromolecules* **2000,** 33, (12), 4478-4485.

66. Michielsen, S. Aberrations in confocal spectroscopy of polymeric materials: Erroneous thicknesses and intensities, and loss of resolution. *Journal of Applied Polymer Science* **2001,** 81, (7), 1662-1669.

67. Russell, S. M.; Carta, G. Mesh size of charged polyacrylamide hydrogels from partitioning measurements. *Industrial & Engineering Chemistry Research* **2005,** 44, (22), 8213-8217.

68. Press, W. H.; Teukolsky, S. A.; Vetterling, W. T.; Flannery, B. P. *Numerical Recipes*. Cambridge Univ. Press: 1992.

69. Solomentsev, Y. E.; Anderson, J. L. Rotation of a sphere in Brinkman fluids. *Physics of Fluids* **1996,** 8, 1119.

70. Brinkman, H. C. A calculation of the viscous force exerted by a flowing fluid on a dense swarm of particles. *Applied Scientific Research* **1949,** 1, (1), 27-34.

71. Monticelli, M. V.; Chauhan, A.; Radke, C. J. The effect of water hydraulic permeability on the settling of a soft contact lens on the eye. *Current Eye Research* **2005,** 30, (5), 329-336.

72. Quinn, T. M.; Grodzinsky, A. J. Longitudinal modulus and hydraulic permeability of poly (methacrylic acid) gels: Effects of charge density and solvent content. *Macromolecules* **1993,** 26, (16), 4332-4338.

73. Refojo, M. F. Permeation of water through some hydrogels. *Journal of Applied Polymer Science* **1965,** 9, (10), 3417-3426.

74. Belloni, L.; Drifford, M.; Turq, P. Counterion diffusion in polyelectrolyte solutions. *Chemical Physics* **1984,** 83, (1), 147-154.

75. Nilsson, L. G.; Nordenskioeld, L.; Stilbs, P.; Braunlin, W. H. Macroscopic counterion diffusion in solutions of cylindrical polyelectrolytes. *The Journal of Physical Chemistry* **1985,** 89, (15), 3385-3391.

76. Kim, J.-H.; Yoon, J.-Y. Protein adsorption on polymer particles. In *Encyclopedia of surface and colloid science*, Soma Sundaran, P., Ed. Marcel Dekker: 2002; Vol. 4, pp 4373-4381.

77. Kim, D. T.; Blanch, H. W.; Radke, C. J. Direct imaging of lysozyme adsorption onto mica by atomic force microscopy. *Langmuir* **2002,** 18, (15), 5841-5850.

78. Cascão Pereira, L. G.; Hickel, A.; Radke, C. J.; Blanch, H. W. A kinetic model for enzyme interfacial activity and stability: pa-hydroxynitrile lyase at the diisopropyl ether/water interface. *Biotechnology and Bioengineering* **2002,** 78, (6), 595-605.

79. Tie, Y.; Calonder, C.; Van Tassel, P. R. Protein adsorption: Kinetics and history dependence. *Journal of Colloid and Interface Science* **2003,** 268, (1), 1-11.

80. Karlsson, M.; Ekeroth, J.; Elwing, H.; Carlsson, U. Reduction of irreversible protein adsorption on solid surfaces by protein engineering for increased stability. *Journal of Biological Chemistry* **2005,** 280, (27), 25558-25564.

81. Overbeek, J. T. G. Electrochemistry of the double layer. In *Colloid Science. I Irreversible Systems*, Kruyt, H. R., Ed. Elsevier: Amsterdam, 1952.

82. Carslaw, H.; Jaeger, J. *Conduction of Heat in Solids*. 1959.

Appendix 2A: Solution To Linear-Adsorption Kinetics Model

Boundary conditions for Eqs. 14 and 15 are described in Section 2.5.3 for loading and release after a time t^*. Convenient solution of these equations is by Laplace transform with inversion by residues and convolution.[82] The measured concentration per unit volume of gel is the sum of that in the liquid pores and that on the gel strands: $C_i^{gel} = (1-\phi_2)C_i^L + \phi_2 n_i$. Let $B_n(x;t^*)$ be defined as

$$B_n(x;t^*) \equiv 2\frac{(-1)^n}{\lambda_n}\frac{(1+S_n)}{S_n[1+\Phi^2(1+rK+2S_n)/\lambda_n^2]}\cos[\lambda_n x/L]\{\exp[S_n k_{-1} t^*]-1\} \qquad (2A.1)$$

where $\lambda_n \equiv (2n+1)\pi/2$, $r \equiv \phi_2/(1-\phi_2)$, $\Phi^2 \equiv k_{-1}L^2/D_i$ is the Thiele parameter, and

$$2S_n\Phi^2\lambda_n^{-2} = -[1+(1+rK)\Phi^2/\lambda_n^2] \pm \sqrt{[1+(1+rK)\Phi^2/\lambda_n^2]^2 - 4\Phi^2/\lambda_n^2} \qquad (2A.2)$$

Accordingly, for loading into a gel initially devoid of solute, the measured concentration profile obeys the expression

$$\begin{aligned}\frac{C_i^{gel}(t,x;\infty)}{(1-\phi_2)C_{i\infty}^L} &= 1-\sum_{n=0}^{\infty} B_n(x;\infty)\exp[S_n k_{-1} t] \\ &+ rK\left[1-\exp[-k_{-1}t]-\sum_{n=0}^{\infty}(1+S_n)^{-1}B_n(x;\infty)\{\exp[S_n k_{-1}t]-\exp[-k_{-1}t]\}\right]\end{aligned} \qquad (2A.3)$$

The first two terms on the right of Eq. 2A.3 correspond to the solute concentration in the liquid-filled voids per unit gel volume while the last term on the right corresponds to solute adsorbed on the polymer matrix per unit gel volume. Because adsorption is not instantaneous, the amount adsorbed at $x=-L$ rises while solute concentration in the gel pores remains at $C_{i\infty}^L$.

The case of desorption from a partially saturated gel is more complicated. We find for extraction from an initial solute concentration profile at t^* that

$$\begin{aligned}\frac{C_i^{gel}(t,x;t^*)}{(1-\phi_2)C_{i\infty}^L} &= \left[\sum_{n=0}^{\infty} B_n(x;t^*)\exp[S_n k_{-1} t]\right] \\ &+ rK_i\left[\sum_{n=0}^{\infty}(1+S_n)^{-1}B_n(x;t^*)\{\exp[S_n k_{-1}t]-\exp[-k_{-1}t]\}\right] \\ &+ rK_i\exp[-k_{-1}t]\left[1-\exp[-k_{-1}t^*]-\sum_{n=0}^{\infty}(1+S_n)^{-1}B_n(x;\infty)\{\exp[S_n k_{-1}t^*]-\exp[-k_{-1}t^*]\}\right]\end{aligned} \qquad (2A.4)$$

Again, the first term on the right of Eq. 2A.4 reflects the solute profile in the liquid-filled voids of the gel while the second two terms on the right correspond to the adsorption profile. Factors in which t^* appears reflect the initial partially-saturated solute profile. Both roots in Eq. 2A.2 are used as are over 100 terms in the indicated summations.

Chapter 3

Water-Soluble Drug Partitioning and Adsorption in HEMA/MAA Hydrogels

3.1 Abstract

Using two-photon confocal microscopy and back extraction with UV/Vis-absorption spectrophotometry, we measure equilibrium partition coefficients, k_i, for six prototypical drugs in five soft-contact-lens-material hydrogels over a range of water contents from 40 to 92 %. Partition coefficients were obtained for acetazolamide, caffeine, hydrocortisone, Oregon Green 488, sodium fluorescein, and theophylline in 2-hydroxyethyl methacrylate/methacrylic acid (HEMA/MAA, $pK_a \approx 5.2$) copolymer hydrogels as functions of composition, aqueous pH (2 and 7.4), and salinity. At pH 2, the hydrogels are nonionic, whereas at pH 7.4 the hydrogels are anionic due to MAA ionization. Solute adsorption on and electrostatic interaction with the polymer matrix are pronounced. To express deviation from ideal partitioning, we define an enhancement or exclusion factor, $E_i \equiv k_i / \phi_1$, where ϕ_1 is hydrogel water volume fraction. At pH 7.4, all solutes exhibit $E_i > 1$ in 100 wt % HEMA hydrogels owing to strong specific adsorption to HEMA strands. For all solutes, E_i significantly decreases upon incorporation of anionic MAA into the hydrogel due to lack of adsorption onto charged MAA moieties. For dianionic sodium fluorescein and Oregon Green 488, and partially ionized monoanionic acetazolamide at pH 7.4, however, the decrease in E_i is more severe than that for similar-sized nonionic solutes. Conversely, at pH 2, E_i generally increases with addition of the nonionic MAA copolymer due to strong preferential adsorption to the uncharged carboxylic-acid group of MAA. For all cases, we quantitatively predict enhancement factors for the six drugs using only independently obtained parameters. In dilute solution for solute i, E_i is conveniently expressed as a product of individual enhancement factors for size exclusion (E_i^{ex}), electrostatic interaction (E_i^{el}), and specific adsorption (E_i^{ad}): $E_i \equiv E_i^{ex} E_i^{el} E_i^{ad}$. To obtain the individual enhancement factors, we employ an extended Ogston mesh-size distribution for E_i^{ex}; Donnan equilibrium for E_i^{el}; and Henry's law characterizing specific adsorption to the polymer chains for E_i^{ad}. Predicted enhancement factors are in excellent agreement with experiment.

Reprint of Dursch, T. J.; Taylor, N. O.; Liu, D. E.; Wu, R. Y.; Prausnitz, J. M.; Radke, C. J. *Biomaterials* **2014,** 35, (2), 620-629.

3.2 Introduction

Hydrogels are cross-linked polymeric networks that readily imbibe water and swell without dissolving.[1-7] Because of their soft consistency, high water content, and biocompatibility, hydrogels are used in numerous biomedical and pharmaceutical applications, including: drug delivery,[8,9] bioseparations,[10,11] and soft-contact lenses.[12-14] The effectiveness of these applications is dictated, in large part, by the solubilities of aqueous solutes in hydrogels. Accordingly, a key hydrogel characteristic is the equilibrium partition coefficient, k_i, of a dilute solute i defined by[1,12,15]

$$k_i \equiv C_i^{gel} / C_i^{bulk} \tag{1}$$

where C_i^{gel} is the concentration of solute in the hydrogel per unit volume of swollen hydrogel and C_i^{bulk} is the corresponding solute concentration in the external aqueous solution equilibrated with the hydrogel. Eq. 1 strictly applies for reversible equilibrium solute partitioning. Further, the partition coefficient is independent of bulk aqueous solute concentration only in dilute solution where solute molecules do not interact with each other.[1,2]

For point solutes that do not interact with the polymer network, k_i equals the hydrogel water volume fraction, ϕ_1. It is, therefore, useful to define an enhancement (or exclusion) factor E_i by[1]

$$E_i \equiv k_i / \phi_1 . \tag{2}$$

For solutes that are partially rejected from the hydrogel, $E_i < 1$, whereas $E_i > 1$ occurs only for favorable solute interaction with the internal polymer network (e.g., through specific adsorption or ion binding). $E_i = 1$ corresponds either to ideal partitioning or to apparent ideal partitioning arising from compensation between exclusion and enhancement. $E_i = 0$ indicates a solute too large to penetrate the water-filled pockets of the hydrogel network.

When the aqueous solution is dilute, it is reasonable to assume additivity of the separate free energies arising from different molecular contributions. Appendix 3A demonstrates that the resulting enhancement factor for solute i is the product of individual enhancement factors

$$E_i \equiv E_i^{ex} E_i^{el} E_i^{ad} \tag{3}$$

where E_i^{ex} designates hard-sphere size exclusion, E_i^{el} denotes electrostatic interaction, and E_i^{ad} indicates specific solute adsorption on polymer strands. Thus, whether E_i is greater or less than unity depends on combinations of the various solute/hydrogel enhancement factors. $E_i < 1$ reflects partial rejection due to size exclusion ($E_i^{ex} < 1$) and/or repulsive electrostatic interaction ($E_i^{el} < 1$). For nonionic ($E_i^{el} = 1$) or counterion ($E_i^{el} > 1$) solutes, $E_i < 1$ arises

solely due to size exclusion. Because larger solutes access only a fraction of the water-filled space, E_i approaches zero as solute size increases.[1] If solutes complex specifically with the polymer chains ($E_i^{ad} > 1$), $E_i < 1$ results from competition between severe size exclusion and favorable adsorption. For non-adsorbing solutes, however, $E_i^{ad} = 1$. Coion solutes ($E_i^{el} < 1$), exhibit $E_i < 1$ because of both size exclusion and electrostatic repulsion. In this case, as solute charge or hydrogel charge density increases, electrostatic repulsion increases ($E_i^{el} << 1$), and E_i tends towards zero.

For counterion solutes, $E_i > 1$ diagnoses favorable electrostatic interaction and possibly specific adsorption offsetting partial rejection from size exclusion. Similarly, for nonionic and coion solutes, $E_i > 1$ arises only when adsorption overcomes size exclusion and/or electrostatic repulsion. When solutes are large (relative to the average mesh size) or for strong electrostatic repulsion, $E_i > 1$ results only from strong complexation with polymer strands. Solutes may adsorb reversibly ($E_i^{ad} > 1$) or irreversibly ($E_i^{ad} >> 1$) on the interior hydrogel network, and in some cases, also adsorb to the hydrogel exterior surface.[13] Because of the wide variety of applications and because observed enhancement factors vary widely,[1,5,7,12-30] significant effort has been expended toward obtaining solute equilibrium partition coefficients, often by back extraction[12,15,16,24,27] using UV/Vis-absorption spectrophotometry.[18,22,24,25]

Published work falls primarily into three classes: (1) $E_i < 1$ solely due to size exclusion;[1,5,7,12,13,20,21,23,28,30] (2) $E_i < 1$ resulting from size exclusion and electrostatic repulsion;[12,17-19] and (3) $E_i > 1$ where solutes interact specifically with the polymer chains.[2,13-18,22,24-27,29] The first class consists of small nonionic solutes, such as small sugars and non-adsorbing drugs, and larger nonionic solutes, including polymers and proteins. Solutes in the second class are typically coions, both small (e.g., salts and fluorescent dyes) and large (e.g., proteins and polymeric surfactants). The third class includes counterion solutes (e.g., polymeric surfactants and proteins) and specifically adsorbing nonionic solutes, such as drugs and polymers. Most systems studied[1,2,5,7,12-18,20-30] fall into the first or third class. For systems where prediction of k_i is attempted, however, nearly all fall into the first class (i.e., $E_i < 1$).[1,5,7,17,19-21,23] $E_i > 1$ is often exhibited by polymers, polymeric surfactants, and proteins in soft-contact-lens materials[1,2,13,16-20] and by ionic/nonionic drugs and vitamins in drug-delivery hydrogels.[14,15,21-30] Quantifying the effects of specific adsorption and electrostatic interaction on equilibrium solute partitioning is critical for data interpretation.

This work reports experimental and theoretically predicted solute enhancement factors in hydrogels where specific adsorption is pronounced. Attention is given to hydrogels representative of soft-contact-lens materials that have relatively high polymer content and are sometimes partially ionic.[1,2,12-14] The hydrogels studied are copolymers of 2-hydroxyethyl methacrylate (HEMA) and anionic methacrylic acid (MAA) (for pH > 5.2) over a large range of water content. We employ two-photon confocal microscopy and back extraction with UV/Vis spectrophotometry. Partition coefficients are obtained for small ionic and nonionic water-soluble drugs as functions of pH, hydrogel composition, and aqueous salinity. Solute sizes are determined from independent measurement of bulk aqueous diffusion coefficients in a restricted diffusion cell and Stokes-Einstein theory. Enhancement factors are predicted

for six solutes (acetazolamide, caffeine, hydrocortisone, Oregon Green 488, sodium fluorescein, and theophylline) in five different water-content hydrogels accounting for hard-sphere size exclusion, Donnan electrostatic repulsion, and specific adsorption. Predictions are based on independently measured parameters, and not on correlation of the experimental partition coefficients.

3.3 Materials and Methods

3.3.1. Chemicals

Sigma Aldrich (St. Louis, MO) provided all monomers and chemicals used in hydrogel synthesis: 2-hydroxyethyl methacrylate (97 %, HEMA, Cat. No. 128635-500G), methacrylic acid (99 %, MAA, Cat. No. 155721-500G), ethylene glycol dimethacrylate (98 %, EGDMA, Cat. No. 335681-100ML), 4,4'-azobis (4-cyanovaleric acid) (98+ %, 11590-100G), and Sigmacote (SL2-100ML), the latter used to hydrophobize glass-mold surfaces prior to polymerization. Following free radical polymerization, hydrogels were swollen or deswollen in pH 7.4 or 2, respectively. To prepare a pH = 7.4 phosphate buffer saline solution (PBS: 0.15 M NaCl, 0.017 M $Na_2HPO_4{\cdot}7H_2O$, and 0.003 M $NaH_2PO_4{\cdot}H_2O$), sodium phosphate dibasic heptahydrate ($Na_2HPO_4{\cdot}7H_2O$, 99+ %, SX0715-1), sodium phosphate monobasic monohydrate ($NaH_2PO_4{\cdot}H_2O$, 98 %, SX0710-1), and sodium chloride (NaCl, 99.8+ %, SX0425-1), purchased from EMD Chemicals Inc. (Darmstadt, Germany), were dissolved in distilled/deionized (DI) water. To prepare a pH = 2 hydrochloric acid solution (HCl: 0.15 M NaCl and 0.02 M HCl), hydrochloric acid (HCl, 0.1 N, Cat. No. 38280-1EA), purchased from Sigma Aldrich, and NaCl were mixed with DI water.

Solutes purchased from Sigma Aldrich include: theophylline (99+ %, Cat. No. T1633-50G), caffeine (99+ %, Cat. No. C0750-5G), acetazolamide (99+ %, Cat. No. A6011-10G), hydrocortisone (98+ %, Cat. No. H4001-5G), and fluorescein sodium salt (99+ %, Cat. No. F-6377-100G). 2'7'-Difluorofluorescein (Oregon Green 488, 97 %, Cat. No. D-6145-10MG) was purchased from Life Technologies (Grand Island, NY, USA). Aqueous theophylline, caffeine, and hydrocortisone are nonionic over the studied pH range. At pH 7.4, sodium fluorescein and Oregon Green 488 are dianionic,[31] and acetazolamide is monoanionic and partially ionized.[32] At pH 2, all solutes are neutral. All chemicals were used without further purification. Partitioning and diffusion experiments were performed at ambient temperature.

3.3.2. Hydrogel Synthesis

Following Kotsmar et al.,[1] HEMA/MAA hydrogels were synthesized by simultaneous copolymerization and cross-linking of monomers in aqueous solution with EGDMA as the cross-linking agent.[1,2,25] Solutions consisted of varying HEMA:MAA ratio (100:0, 99:1, 90:10, 70:30, and 0:100), 0.25 wt % EGDMA, 0.5 wt % 4,4'-azobis(4-cyanovaleric acid), and 30 wt % DI water. Hydrogels are referred to by their corresponding wt % MAA, where wt % MAA and wt % HEMA sum to 100. All percentages are of total monomer. The reaction mixture was magnetically stirred until complete dissolution of the thermoinitiator. Nitrogen gas was bubbled through the reaction mixture for 15 min to remove dissolved oxygen, resulting in less than 1 % change in HEMA:MAA composition. The bubbled reaction mixture was injected between two upright glass plates previously hydrophobized with Sigmacote and separated by a 100 or 250-µm spacer. Free-radical

thermally initiated polymerization took place in an oven whose temperature was raised from 60 to 90 °C over a 60-min period and then maintained at 90 °C for 60 min. When cooled, hydrogels were boiled in DI water for 45 min to remove unreacted monomer.

3.3.3. Equilibrium Water Content

Hydrogel equilibrium water content, or water volume fraction, ϕ_1, was determined gravimetrically following Guan et al.[12] 9-mm-diameter discs were bored into synthesized hydrogel slabs and placed into either PBS buffer or HCl solutions. Solutions were changed daily for a minimum of 3 d to ensure equilibrium with the surrounding solution. To determine water content, equilibrated hydrogels were removed from solution, lightly blotted with Fisherbrand® weighing paper (Fisher Scientific, Pittsburgh, PA), and weighed (m_{wet}). Hydrogels were then placed in an oven at 70 °C overnight and ambient-temperature dry-hydrogel mass (m_{dry}) was used to calculate water content by

$$\phi_1 = \frac{\rho_{wet}}{\rho_1}\left[\frac{m_{wet} - m_{dry}}{m_{wet}}\right], \tag{4}$$

where ρ is mass density and subscripts *1*, *wet*, and *dry* denote water, swollen hydrogel, and dry hydrogel, respectively. Since $\rho_1 \approx \rho_{wet}$ (to within 5 %), ϕ_1 in Eq. 4 is approximately weight fraction. Table 3.1 reports measured ϕ_1 for the HEMA/MAA hydrogels equilibrated in either PBS (pH 7.4) or HCl (pH 2), where hydrogel composition varied from 0 to 100 wt % MAA. Each water-content measurement was repeated at least three times. At pH 7.4 (PBS), hydration of charged carboxylic groups swells the MAA-containing hydrogels from 55 to 90 % water, for gels containing 1 and 100 wt % MAA, respectively. At pH 2 (HCl), addition of MAA initially (1-50 wt %) results in hydrogel deswelling likely due to interstrand hydrogen bonding between uncharged MAA and HEMA monomers.[33] Further addition of MAA (beyond 50 wt %), however, significantly increases hydrogel water content, because hydration of hydrophilic uncharged MAA moieties overcomes interchain hydrogen bonding.

Table 3.1: Hydrogel Water Volume Fractions with Varying HEMA:MAA Weight Ratios

Hydrogel Composition (HEMA:MAA)	ϕ_1 (in PBS)	ϕ_1 (in HCl)
100:0	0.43 ± 0.02	0.40 ± 0.01
99:1	0.54 ± 0.02	0.39 ± 0.01
90:10	0.77 ± 0.04	0.29 ± 0.01
70:30	0.83 ± 0.02	0.31 ± 0.02
0:100	0.92 ± 0.01	0.71 ± 0.07

3.3.4. Solute Loading

Swollen hydrogels were soaked for a minimum of 2 d in 50 and 20-mL solute solutions (i.e., volume ratio of solution to hydrogel was 250) at pH 7.4 and 2, respectively. Initial loading concentrations for sodium fluorescein and Oregon Green 488 were 1×10^{-5} M and 1×10^{-7} M in PBS and HCl solutions, respectively. Initial loading concentrations for theophylline and caffeine, acetazolamide, and hydrocortisone were 6×10^{-3} M, 2×10^{-3} M, and 2×10^{-4} M, respectively, in both PBS and HCl. In this concentration range, ϕ_1 was unaffected by solute loading. To confirm that the hydrogels were fully saturated, solute uptake time was varied from 2 to 7 d, resulting in less than 4 % change in solute partition coefficients.

3.3.5. Fluorescence Confocal Microscopy

To complement back-extraction data, sodium fluorescein and Oregon Green 488 equilibrium partition coefficients were also obtained using two-photon fluorescence confocal microscopy following Kotsmar et al.[1] A Carl Zeiss 510 LSM META NLO AxioImager confocal microscope (Jena, Germany) equipped with a Spectra-Physics MaiTai HP DeepSee Laser (Santa Clara, CA) was used for imaging at 780 nm. Fluorescence emission was detected through a Plan-Neofluar 10x/0.30 NA objective (Carl Zeiss GmbH) using a 500-550 nm emission filter.

Prior to the partition-coefficient measurement, swollen hydrogels were soaked in the pertinent aqueous solute-containing solution under magnetic stirring for at least 2 d at 400 rpm. Subsequently, a 1-mm thick layer of the aqueous solution in a small Petri dish was placed on the microscope platform and scanned in the vertical (z) direction at 5-μm intervals to a depth of at least 250 μm. Afterward, a solute-equilibrated 4 mm × 4 mm, 250-μm thick hydrogel was placed on a microscope slide (48300-047, VWR International, West Chester, PA, USA), covered (coverslip, 12-541-B, Fisher Scientific, Fair Lawn, New Jersey, USA), and placed on the microscope for scanning in the z-direction at the same laser power and detector setting as those during scanning of the bulk-aqueous solute solution. During each experiment, background fluorescence intensity was recorded and subtracted from solution and hydrogel signals. To test for reversibility, hydrogel samples were placed in solute-free solvent following equilibration. Loading concentration was varied over a factor of 10 with no change in the measured partition coefficient.

Figure 3.1 displays typical fluorescence-confocal-microscopy images of sodium fluorescein in 0, 1, 10, 30, and 100 wt % MAA hydrogels at pH 7.4. The top half of each micrograph corresponds to the equilibrated aqueous solution, whereas the bottom half corresponds to the first 50 μm of the hydrogel, where measured fluorescence intensity is independent of sample depth (i.e., there is minimal signal attenuation over this depth[1,2]). In the concentration range studied, detected solute intensities inside the hydrogel and in the surrounding aqueous solution were proportional to dye concentration in all cases.[1,2] Thus, the partition coefficient is the ratio of solute intensity in the hydrogel to that in the aqueous-loading solution. Figure 3.1 reveals that the partition coefficient of sodium fluorescein at pH 7.4 diminishes as the anionic MAA content of the copolymer hydrogel increases. At this pH, both sodium fluorescein and Oregon Green 488 completely desorb confirming reversible uptake. Accordingly, partition coefficients for sodium fluorescein and Oregon Green 488

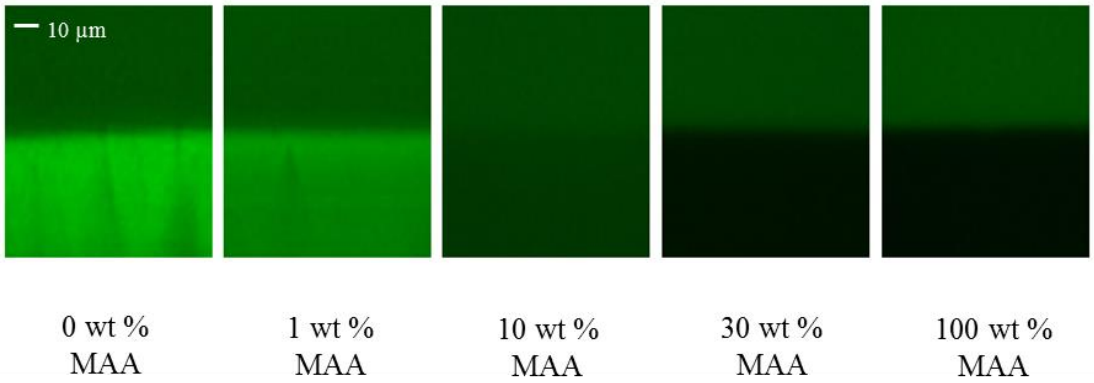

Figure 3.1: Fluorescence-confocal-microscopy images of sodium fluorescein in 0, 1, 10, 30, and 100 wt % MAA hydrogels at pH 7.4. The top half of each micrograph corresponds to the equilibrated aqueous solution, whereas the bottom half corresponds to the first 50 µm of the hydrogel. The scale bar represents 10 µm in the vertical direction.

from fluorescence confocal microscopy agree well with those obtained separately from back extraction at pH 7.4.

At pH 2, however, sodium fluorescein and Oregon Green 488 do not completely desorb even after 1 mo of release. To quantify the amount of irreversibly adsorbed sodium fluorescein and Oregon Green 488 at pH 2, partition coefficients measured by fluorescence confocal microscopy in the loading direction were compared to those measured in release direction by back extraction. For 30 wt % MAA copolymer, where irreversible adsorption is most prevalent, k_i measured by back extraction was 35 % lower, suggesting a maximum of 35 % irreversible adsorption after 1 d of continued extraction. Partition coefficients reported here for sodium fluorescein and Oregon Green 488 are those obtained in the uptake direction.

3.3.6. Back Extraction with UV/Vis-Absorption Spectrophotometry

Theophylline, caffeine, acetazolamide, and hydrocortisone equilibrium partition coefficients were obtained using back extraction or desorption[12,15,16,24,27] with UV/Vis-absorption spectrophotometry.[18,22,24,25] Solute-equilibrated hydrogels were removed from the loading solution, lightly blotted with Fisherbrand® weighing paper, and immediately placed into stirred aqueous solutions (400 rpm) of either PBS or HCl. Solute concentration was obtained as a function of time by periodically pipetting 1 mL of solvent into a 4-mm wide UV quartz cuvette (path length 10 mm), and measuring previously calibrated solution absorbance at 220-250 nm with an Ocean Optics spectrophotometer (Model ADC-1000, Dunedin, FL) and a deuterium UV/Vis DH-2000 light source. To maintain constant solution volume, the 1-mL samples were returned to the back-extraction solution following each concentration measurement.

The equilibrium partition coefficient, k_i, is calculated using the equilibrium back-extraction-solution concentration, C_i^S, by[12]

$$k_i = \frac{C_i^S \; V^S}{C_i^{load} \; V^{gel}}, \tag{5}$$

where V^S is back-extraction-solution volume, V^{gel} is swollen-hydrogel volume, and C_i^{load} is equilibrium loading-solution concentration. Typical ratios of back-extraction-to-hydrogel volume (V^S/V^{gel}) ranged from 20 to 2000, and were adjusted to provide precise calculation of k_i. Further increase of V^S/V^{gel} resulted in no significant change in k_i. To confirm constant dilute-solution partition coefficients, k_i, initial-solute-loading concentrations were increased and decreased by a factor of 4 resulting in less than a 10 % difference.

To evaluate reversible adsorption for these four solutes, each hydrogel was loaded in aqueous HCl (pH 2) where solute adsorption is significant. The gels were then back extracted into aqueous PBS (pH 7.4) where solute adsorption is minimal. In all cases, k_i obtained by release into aqueous PBS agreed to within 5 % of those obtained by back extraction into aqueous HCl (pH 2). It is thus reasonable to assert that theophylline, caffeine, acetazolamide, and hydrocortisone exhibit reversible uptake in all hydrogels and solution pH values studied here.

3.3.7. Solute Size

To obtain the hydrodynamic radius of solute i, a_{is}, we first determined the corresponding dilute-aqueous bulk diffusion coefficient in a restricted diffusion cell[34] using UV/Vis absorption following Kotsmar et al.[1] From the measured bulk diffusion coefficients, a_{is} was calculated from the Stokes-Einstein equation.[1,2,34] Solute concentrations were 4×10^{-4} M, in the range where light absorbance is linear with concentration. Bulk diffusion coefficients, D_{io}, were obtained from the constant slope of absorptivity versus time at later times.[1,2,34] Table 3.2 reports measured bulk aqueous diffusion coefficients and calculated Stokes-Einstein hydrodynamic radii, compared to available literature values. Agreement between literature and measurement is excellent.

Table 3.2: Solute Properties in Aqueous PBS /HCl [a]

Solute	Structure	pK$_a$	D$_{io}$ x 10^6 (cm^2/s)	a_{is} (nm) [b]	a_{is} (nm) lit.
Acetazolamide	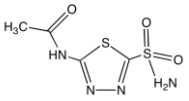	7.2, 8.8[32]	6.1 / 4.8	0.41 / 0.50	0.40[35,36]
Caffeine	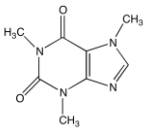	14.0[37]	6.7 / 6.7	0.36 / 0.36	0.46[36]
Hydrocortisone	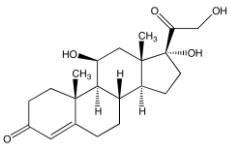	12.8[38]	4.7 / 4.7	0.52 / 0.52	0.51[36,39]
Oregon Green 488	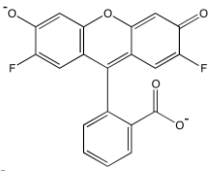	4.5, 4.8[31]	4.0 / 3.9	0.62 / 0.54	0.60[40]
Sodium Fluorescein	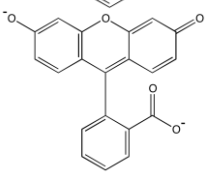	4.5, 6.5[31]	4.0 / 3.9	0.62 / 0.56	0.58[40]
Theophylline	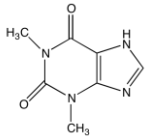	8.6[41]	6.7 / 6.7	0.37 / 0.37	0.38[24]

[a] table entries separated by a diagonal correspond to measurement in aqueous PBS (pH 7.4) or in aqueous HCl (pH 2)

[b] calculated from the Stokes-Einstein equation and measured diffusion coefficients

3.4 Experimental Results

Table 3.3 reports measured enhancement factors, $E_i \equiv k_i / \phi_1$, for acetazolamide, caffeine, hydrocortisone, Oregon Green 488, sodium fluorescein, and theophylline in HEMA/MAA hydrogels equilibrated in either PBS (pH 7.4) or HCl (pH 2) solutions. Hydrogel composition varies from 0 to 100 wt % MAA. At pH 7.4, all solutes exhibit $E_i > 1$ in 0 wt % MAA hydrogels (i.e., 100 wt % HEMA) owing to strong specific adsorption to the HEMA matrix, most significantly hydrocortisone. Conversely, for the nonionic solutes at pH 7.4 in 100 wt % polyelectrolyte MAA, near-unity enhancement factors suggest no specific adsorption to anionic MAA. As a result, E_i significantly decreases with addition of solute-non-interacting anionic MAA and with a corresponding decrease in the amount of specifically interacting HEMA copolymer.

Table 3.3: Enhancement Factors [a] with Varying HEMA:MAA Weight Ratios in Aqueous PBS / HCl [b]

Hydrogel Composition (HEMA:MAA)	**Acetazolamide**	**Caffeine**	**Theophylline**	**Hydrocortisone**	**Oregon Green 488 & Sodium fluorescein**
100:0	5.8 / 11.0	6.5 / 6.5	6.5 / 7.0	53.5 / 53.5	5.5 / 258.0
99:1	3.8 / 11.1	4.3 / 7.2	4.5 / 7.4	33.6 / 87.2	3.2 / 350.0
90:10	1.7 / 13.1	2.1 / 10.7	2.4 / 11.0	12.9 / 103.5	0.9 / 385.6
70:30	1.2 / 10.4	1.6 / 12.6	1.5 / 11.3	9.5 / 97.9	0.3 / 381.3
0:100	0.6 / 2.5	0.7 / 9.7	0.8 / 8.2	1.0 / 108.5	0.1 /187.3

[a] partition coefficients may be obtained by multiplying table entries by the corresponding water volume fractions listed in Table 3.1

[b] table entries separated by a diagonal correspond to solute enhancement factors measured in aqueous PBS (pH 7.4) or aqueous HCl (pH 2)

Table 3.3 likewise reports solute enhancement factors in the HEMA/MAA hydrogels equilibrated in HCl (pH 2) solutions. All solutes and all hydrogels are neutral at pH 2; E_i is significantly greater than unity revealing strong specific adsorption to both HEMA and uncharged MAA polymers. The increase in E_i with addition of neutral MAA to the hydrogel (despite similar water contents from 0 to 30 wt % MAA) indicates preferential adsorption on the uncharged MAA copolymer compared to that on the HEMA copolymer for all solutes. Accordingly, solute enhancement factors are greater in MAA-containing hydrogels equilibrated at pH 2 relative to those equilibrated at pH 7.4. At pH 2, all enhancement factors for 100 wt % MAA decline significantly compared to those for lower MAA-content hydrogels. This result discloses that the individual contributions to E_i are functions of water content. The large enhancement factors for neutral sodium fluorescein and Oregon Green 488 in Table 3.3 at pH 2 are commensurate with observed partial irreversibility.

Enhancement factors in Table 3.3 for dianionic sodium fluorescein ($pK_a \approx 4.5, 6.5$[31]) and Oregon Green 488 ($pK_a \approx 4.5, 4.8$[31]) in 100 wt % MAA ($pK_a \approx 5.2$[30,42]) at pH 7.4 are a factor of six lower than those of the similar-sized neutral solutes. Thus, in addition to diminished specific solute interaction with the ionized MAA copolymer compared to neutral MAA groups, polymer-matrix charge density apparently plays a significant role in determining uptake of ionized solutes.[42] To investigate the possible effect of electrostatic interaction on E_i, the ionic strength of the phosphate buffer solution (pH 7.4) was varied by adding NaCl to yield concentrations ranging from 0.02 to 1 M. Figure 3.2 shows E_i versus ϕ_1 on a semi-logarithmic scale for sodium fluorescein in the HEMA/MAA hydrogels with 0.02 M (open triangles), 0.15 M (filled circles), and 1 M added aqueous NaCl (open squares). Lines in this figure correspond to theory described later. Despite a background-electrolyte Debye length of approximately 0.5 nm in PBS solution,[1,2] we conclude that the significant rejection of dianionic sodium fluorescein reported in Table 3.3 for pH 7.4 results from electrostatic repulsion from anionic MAA groups. Added NaCl in Figure 3.2 increases the enhancement factor of anionic sodium fluorescein because of increased screening of the negatively charged MAA copolymer.

3.5 Theory

Table 3.3 reports enhancement factors ranging from 0.1 to over 400 with substantial contributions from size exclusion, electrostatic repulsion, and specific adsorption. At the dilute solute concentrations studied here, the adsorbing solutes follow Henry's law for uptake on the polymer chains.[1] Because solute concentrations are orders-of-magnitude smaller than that of the background electrolyte, there is no need to account for adsorption of the ionized-solute counterions.

Appendix 3A demonstrates that

$$E_i \equiv \frac{k_i}{\phi_1} = E_i^{ex} E_i^{el} \left(1 + \sum_j K_{ij}\ \phi_{2j} / \phi_1 \right) = E_i^{ex} E_i^{el} E_i^{ad}\ , \qquad (6)$$

where ϕ_{2j} is the volume fraction of polymer component j, i.e., $\phi_2 \equiv 1 - \phi_1 = \sum_j \phi_{2j}$. The bracketed term in Eq. 6 represents the adsorption enhancement factor, $E_i^{ad} \equiv 1 + \sum_j K_{ij}\ \phi_{2j} / \phi_1$. Eq. 6 assumes that, at large dilution, each adsorbing solute does so independently on each copolymer of the hydrogel. With no specific adsorption ($K_{ij} = 0$), E_i reduces to that of size exclusion and electrostatic interaction. K_{ij} in Eq. 6 are unknown constants that are obtained here from independent experiment. Adsorption on the external surface of the hydrogel is not included because the area of external-surface polymer strands is miniscule compared to that of the internal chains.

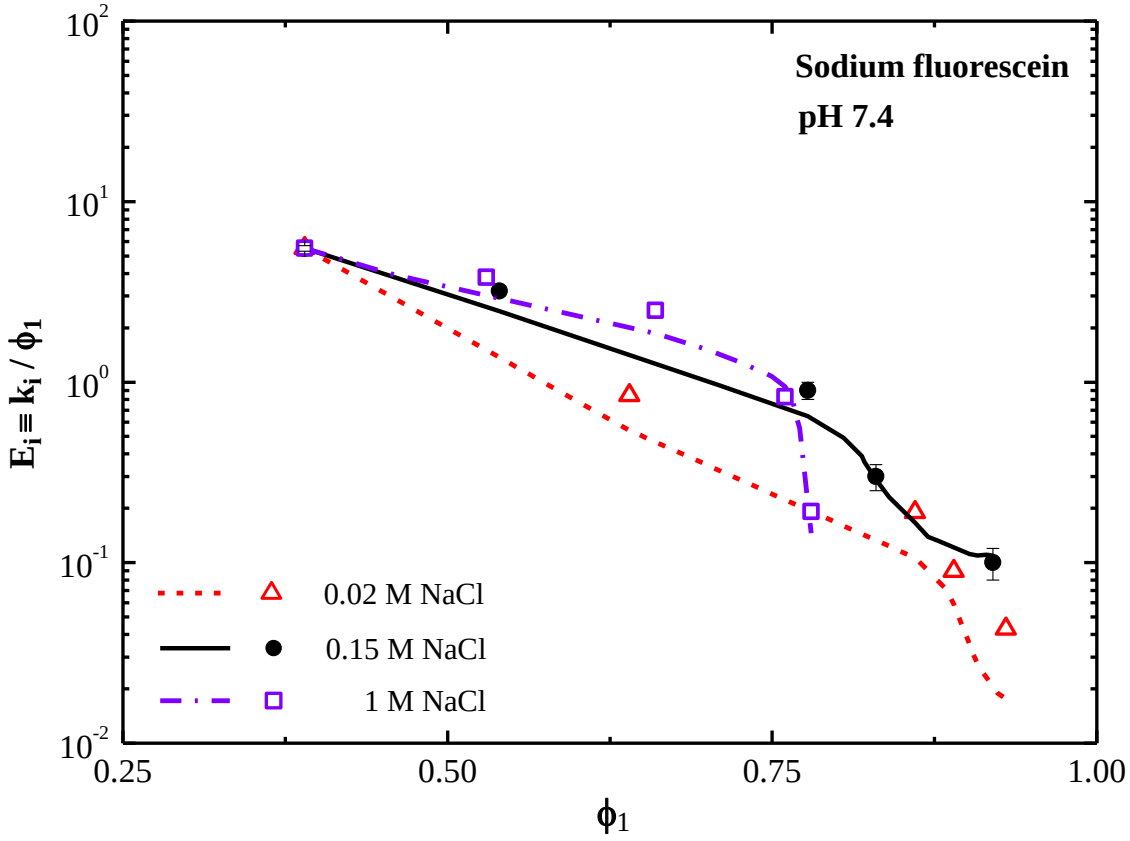

Figure 3.2: Sodium-fluorescein enhancement factor, $E_i \equiv k_i / \phi_1$, as a function of water volume fraction, ϕ_1, in HEMA/MAA hydrogels equilibrated in phosphate buffer (pH 7.4) with 0.02 (open triangles), 0.15 (filled circles), and 1 M NaCl (open squares). Typical error bars are shown. Semi-logarithmic lines are drawn according to theory. Solid and dashed lines correspond to filled and open symbols, respectively.

The size-exclusion enhancement factor in Eq. 6, E_i^{ex}, follows from an extended Ogston mesh-size distribution[1,2,23,43]

$$E_i^{ex} = \exp\left\{-4(1-\phi_1)[(a_{is}/a_f)(1+a_{is}/a_f)]\right\}, \tag{7}$$

where a_{is} and a_f are solute and strand-fiber radii, respectively. Table 3.2 reports measured a_{is} for the six solutes studied. Following Kotsmar et al.,[1] we take $a_f = 2$ nm, typical for HEMA/MAA hydrogels. For non-adsorbing, uncharged point solutes, Eqs. 6 and 7 correctly reduce to ideal partitioning (i.e., to $k_i = \phi_1$). As a_{is} increases, however, E_i^{ex} tends towards zero, because large solutes can access only a portion of the water-filled spaces in the hydrogel.[1,2]

As outlined in Appendix 3A, the electrostatic enhancement factor for ionized solutes in Eq. 6, E_i^{el}, follows from equality of solute chemical potential in the hydrogel liquid-filled voids and that in the bulk aqueous solution including the electrostatic potentials of the two phases (i.e., Donnan theory[44])

$$E_i^{el} = \exp\left(-\frac{z_i F\psi}{RT}\right), \tag{8}$$

where z_i is the valence of solute i, F is Faraday's constant, and ψ is the Donnan electric potential difference between the hydrogel and the bulk aqueous solution.[44] Eq. 8 predicts E_i^{el} once the unknown parameter ψ is specified.

Because the concentration of solutes is dilute compared to that of the background electrolyte, ψ is set by the aqueous electrolyte ionic strength and pH, and the polyelectrolyte charge density. The indifferent electrolyte is assumed to be completely dissociated NaCl. As outlined in Appendix 3B, electroneutrality and phase equilibria for Na^+ and Cl^- ions provide an analytical expression for ψ

$$F\psi / RT = \ln\left[\sqrt{E_{Na^+}^{ex} / E_{Cl^-}^{ex} + \alpha_{el}^{\,2}} - \alpha_{el}\right], \tag{9}$$

where $\alpha_{el} \equiv C_{MAA^-}^{gel} / (2C_{NaCl}^{bulk}\ E_{Cl^-}^{ex}\ \phi_1)$, $C_{MAA^-}^{gel}$ is the molar concentration of charged MAA per total swollen hydrogel volume, F is Faraday's constant, R is the gas constant, and T is absolute temperature. In Eq. 9, C_{NaCl}^{bulk} is taken as the sum of the buffer (assumed a 1:1 electrolyte) and added NaCl concentrations in the bulk aqueous solution. $C_{MAA^-}^{gel}$ is related to the MAA copolymer weight fraction during synthesis, w_{MAA}, by $C_{MAA^-}^{gel} = w_{MAA}\ f_{[-]}\ (1-\phi_1)\ \rho_{dry} / M_{MAA}$, where M_{MAA} is MAA monomer molecular weight (86.1 g/mol[1]), ρ_{dry} is the mass density of dry polymer, and $f_{[-]}$ is the degree of ionization

given by $f_{[-]} = 10^{-pK_a}/(10^{-pH} + 10^{-pK_a})$.[30] We do not account for ion binding of the background electrolyte to the polymer strands.

Henry's adsorption constant for specifically adsorbed solute i on polymer component j, K_{ij} in Eqs. 6-9, is undetermined. Here subscript j denotes HEMA, anionic MAA (MAA- at pH 7.4), or nonionic MAA (MAA at pH 2). To obtain $K_{i\,HEMA}$, $K_{i\,MAA-}$, and $K_{i\,MAA}$, Eqs. 6-9 are fit to measured solute partition coefficients in 100 wt % HEMA, 100 wt % ionized MAA-, and 100 wt % unionized MAA hydrogels. Obtained values are listed in Table 3.4. As expected, none of the studied solutes adsorb onto the charged MAA polymer while adsorption on neutral MAA groups is larger than that on HEMA groups. Additionally, adsorption of the ionized forms of the solutes (pH 7.4) on HEMA is less than that of the corresponding neutral forms (pH 2).

Table 3.4: Henry's Adsorption Constant (dimensionless)

Solute	$K_{i\,HEMA}$ [a]	$K_{i\,MAA-}$	$K_{i\,MAA}$ [b]
Acetazolamide	6.5 / 13	0	5
Caffeine	9.2 / 9.2	0	30
Hydrocortisone	83 / 83	0	380
Oregon Green 488	8.6 / ~ 455	0	~ 730
Sodium fluorescein	8.5 / ~ 455	0	~ 730
Theophylline	7.5 / 7.5	0	21

[a] table entries separated by a diagonal correspond to Henry's constant measured in aqueous PBS (pH 7.4) or in aqueous HCl (pH 2)

[b] in aqueous HCl (pH 2)

3.6 Discussion

At pH 7.4, all solutes in Table 3.3 exhibit $E_i > 1$ for 0 wt % MAA hydrogels (i.e., 100 wt % HEMA) arising from strong specific adsorption to aqueous HEMA strands ($K_{i\,HEMA} > 0$ in Table 3.4). Except for hydrocortisone, Henry's adsorption constants for all solutes in Table 3.4 are similar in value (i.e., $6.5 < K_{i\,HEMA} < 9.2$) due to analogous hydrogen bonding between the solutes and the HEMA hydroxyl groups. For hydrocortisone, however, stronger adsorption to HEMA ($K_{i\,HEMA} = 83$) originates from a larger number of hydrogen-bond donors compared to the five other solutes. Conversely, at pH 7.4, the solutes display $E_i \sim 1$ in 100 wt % MAA- resulting from lack of solute adsorption to anionic MAA moieties (i.e., $K_{i\,MAA-} = 0$).

At pH 2, however, all solutes exhibit $E_i > 1$ indicating strong specific adsorption to both HEMA and uncharged MAA copolymers ($K_{i\,HEMA} > 0$ and $K_{i\,MAA} > 0$ in Table 3.4). For

nearly all solutes, $K_{i\,MAA} > K_{i\,HEMA}$ consistent with the lower pK_a of a carboxylic acid (MAA) compared to that of an alcohol (HEMA).[30] For those solutes in Table 3.2 with $pK_a < 7.4$ (acetazolamide, sodium fluorescein, and Oregon Green 488), $K_{i\,HEMA}$ is larger when the solutes are neutral compared to their ionized states. $K_{i\,HEMA}$ and $K_{i\,MAA}$ for uncharged sodium fluorescein and Oregon Green 488 are an order of magnitude larger than those for the other solutes, commensurate with the observation of partial irreversibility.

With Henry's adsorption constants specified, Eqs. 6-9 predict E_i as a function of hydrogel composition, aqueous pH, and salinity. Solid and dashed lines in Figure 3.3 compare predicted to measured (symbols) enhancement factors, E_i, as functions of water content, ϕ_1, for the six prototypical drugs in aqueous PBS buffer (pH 7.4). Lines are drawn using theory with no adjustable parameters. HEMA and charged MAA copolymer volume fractions follow from definition: $\phi_{2\,HEMA} = (1-w_{MAA})(1-\phi_1)$ and $\phi_{2\,MAA-} = w_{MAA}\, f_{[-]}(1-\phi_1)$. In all cases, agreement between theory and experiment is excellent. For all solutes, E_i significantly decreases with incorporation of anionic MAA into the hydrogel, due to non-adsorption onto the charged MAA copolymer (i.e., $K_{i\,MAA-} = 0$). This lack of adsorption explains the general trend of decreasing E_i with increasing ϕ_1 seen in Figure 3.3 and Table 3.3 for pH 7.4.

The magnitude of the enhancement factor is determined by the various contributions in Eq. 6. To illustrate, semi-logarithmic lines in Figure 3.4 predict E_i^{ad} (dashed), E_i^{ex} (dotted), E_i^{el} (dash-dotted), and E_i (solid) for sodium fluorescein as a function of ϕ_1 in HEMA/MAA hydrogels equilibrated in aqueous PBS (pH 7.4). Filled circles denote measured enhancement factors. In 100 wt % HEMA (i.e., 0 wt % MAA) at pH 7.4, $E_i \sim 10$ arises from specific adsorption of 1:2 valence sodium fluorescein offsetting partial rejection due to size exclusion (i.e., $E_i^{ad} >> E_i^{ex}$ in Figure 3.4). At pH 7.4, addition of anionic MAA copolymer increases ϕ_1 (see Table 3.1), gradually increasing E_i^{ex}, since sodium fluorescein accesses a larger fraction of the water-filled spaces.[1] Since E_i^{ad} decreases drastically compared to the slight increase in E_i^{ex} (typical for small solutes), E_i diminishes with addition of charged MAA. Sodium dianionic fluorescein (at pH 7.4) experiences additional rejection through Donnan electrostatic repulsion ($E_i^{el} < 1$) originating from the anionic MAA copolymer. Consequently, E_i decreases more dramatically with added MAA- compared to E_i for similar-adsorbing nonionic solutes (e.g., theophylline in Table 3.3).

Figure 3.2 also emphasizes the importance of E_i^{el} for determining enhancement factors of dilute, charged solutes. Lines in this figure correspond to Eqs. 6-9 for sodium fluorescein, as in Figures 3.3 and 3.4. Increasing solution ionic strength increases the enhancement factor. The dependence of the enhancement factor on background ionic strength arises from the Donnan electrostatic potential, which is negative when the hydrogel is charged. Figure 3.5 shows the calculated Donnan electric potential, expressed as $-F\psi/RT$, versus water content, ϕ_1, on a semi-logarithmic scale, corresponding to the enhancement factors predicted in Figure 3.2. Lines are drawn using Eq. 9. As added NaCl

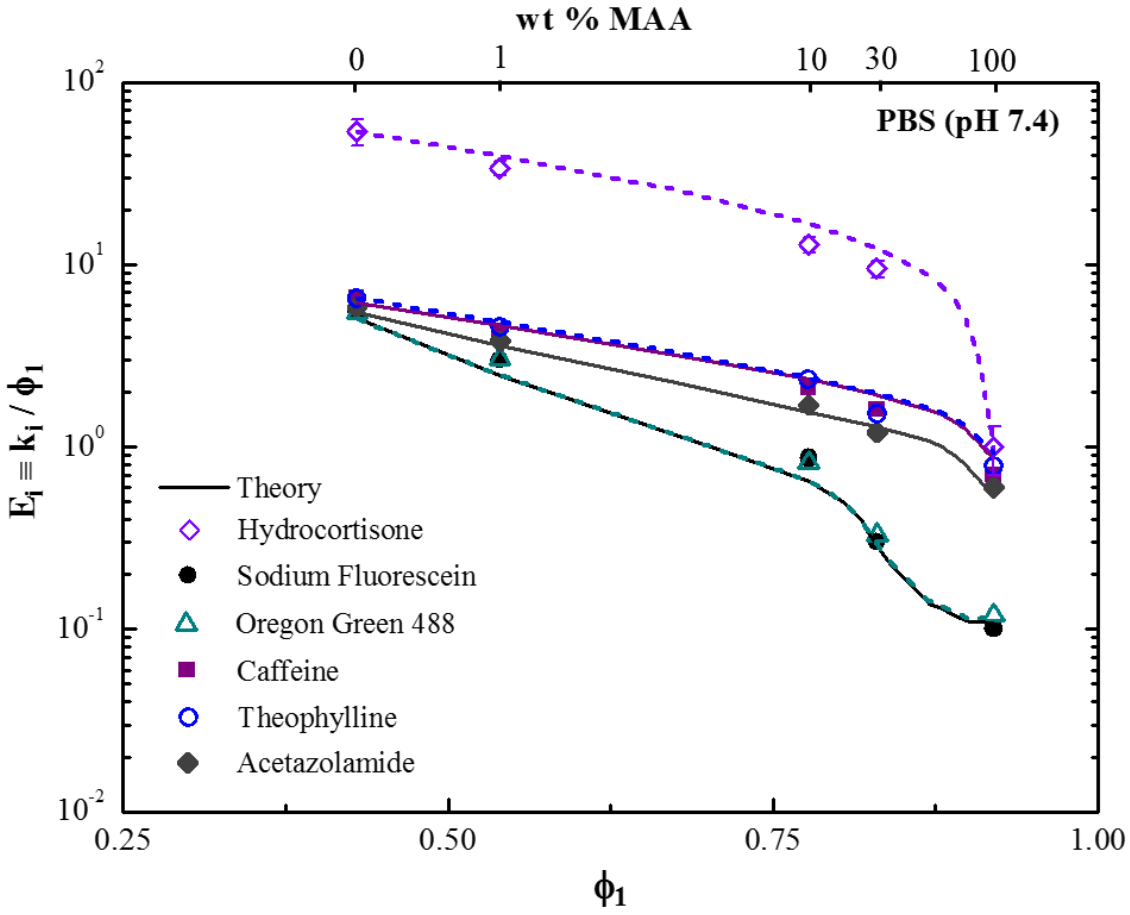

Figure 3.3: Measured solute enhancement factors, $E_i \equiv k_i / \phi_1$, as functions of water volume fraction, ϕ_1, for hydrocortisone (open diamonds), sodium fluorescein (filled circles), Oregon Green 488 (open triangles), caffeine (filled squares), theophylline (open circles), and acetazolamide (filled diamonds) in HEMA/MAA hydrogels with varying wt % MAA in PBS (pH 7.4). Typical error bars are shown. Semi-logarithmic lines are drawn according to theory. Solid and dashed lines correspond to filled and open symbols, respectively.

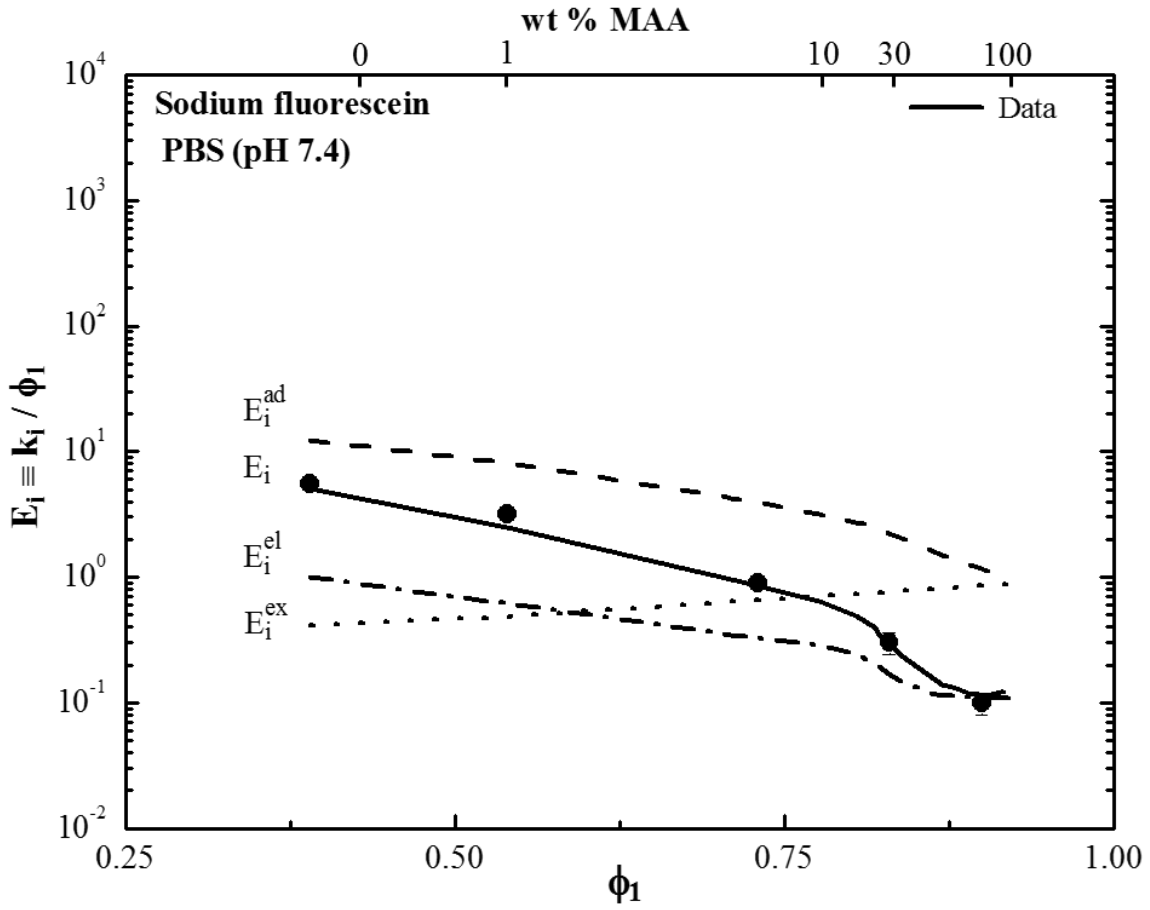

Figure 3.4: Sodium-fluorescein enhancement factor versus water volume fraction, ϕ_1, in HEMA/MAA hydrogels equilibrated in PBS (pH 7.4). Semi-logarithmic lines are drawn according to theory. Solid, dashed, dotted, and dash-dotted lines correspond to E_i, E_i^{ad}, E_i^{ex}, and E_i^{el}. Symbols denote measured E_i in Table 3.

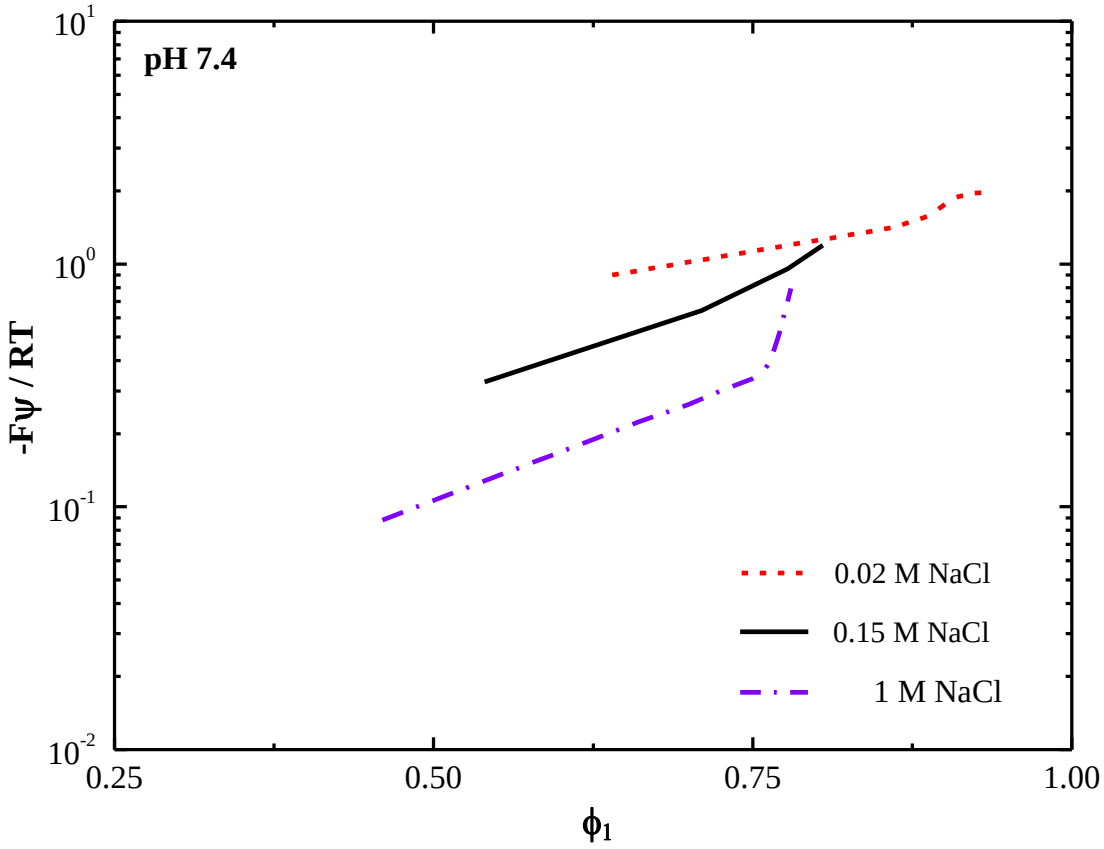

Figure 3.5: Calculated dimensionless Donnan electric potential, $-F\psi / RT$, as a function of water volume fraction, ϕ_1, for MAA-containing HEMA/MAA hydrogels equilibrated in phosphate buffer (pH 7.4) with 0.02 (dashed line), 0.15 (solid line), and 1 M NaCl (dash-dotted line). Semi-logarithmic lines are drawn according to theory.

concentration increases from 0.02 to 1 M, the magnitude of ψ decreases due to enhanced screening of the negative polyelectrolyte charge density by aqueous sodium chloride. As a result, E_i^{el} increases with addition of NaCl for a fixed polyelectrolyte charge density, giving rise to the increase in E_i seen in Figure 3.2. Reduction in Donnan-potential magnitude confirms that ϕ_1 decreases with addition of NaCl for MAA-containing hydrogels at pH values above the pK_a.[34]

Similar to Figure 3.3, solid and dashed theory lines in Figure 3.6 compare predicted to measured (symbols) enhancement factors, E_i, as a function of MAA copolymer content for the six prototypical drugs now in aqueous HCl (pH 2). Here, E_i is plotted against wt % MAA rather than ϕ_1, because addition of MAA at pH 2 yields a non-monotonic increase in ϕ_1 (see Table 3.1). Lines are drawn from Eqs. 6-9 with no adjustable parameters. The uncharged-MAA volume fraction is $\phi_{2\,MAA} = w_{MAA}(1-\phi_1)$. All solutes exhibit moderate Henry's adsorption constants in both 100 wt % HEMA and 100 wt % MAA at pH 2 (Table 3.4). Consequently, $E_i > 1$. Despite the very large loading partition coefficients of neutral sodium fluorescein and Oregon Green 488 and their partial irreversible adsorption, agreement between theory and experiment is excellent for all solutes.

The six studied solutes are neutral at pH 2; therefore, E_i is determined by a balance between size exclusion ($E_i^{ex} < 1$) and specific adsorption ($E_i^{ad} > 1$). Lines in Figure 3.7 predict E_i^{ad} (dashed), E_i^{ex} (dotted), E_i^{el} (dash-dotted), and E_i (solid) for neutral sodium fluorescein as a function of MAA-copolymer content for HEMA/MAA hydrogels equilibrated in aqueous HCl (pH 2). In 100 wt % HEMA (i.e., 0 wt % MAA) at pH 2, $E_i > 1$ arises from significant specific adsorption offsetting rejection due to size exclusion (i.e., $E_i^{ad} >> E_i^{ex}$ in Figure 3.7). Thus in Figure 3.7 (and Figure 3.6), E_i initially rises with incorporation of uncharged MAA into the hydrogel (corresponding to decreasing ϕ_1 in Table 3.1) due to an increase in E_i^{ad} that follows from an increase in the total polymer volume fraction $(1-\phi_1)$. E_i decreases with further addition of uncharged MAA (corresponding to increasing ϕ_1) due to a substantial decrease in the total polymer volume fraction, similar to the decrease seen with MAA addition at pH 7.4. A slight maximum appears near 30 wt % MAA content.

The proposed model well predicts partitioning of drugs in copolymer hydrogels as a function of hydrogel composition, and aqueous pH and salinity. Theory assumes that in dilute solution the free energy of a dilute-solute-equilibrated hydrogel is additive in potential-of-mean-force molecular contributions or equivalently: $E_i \equiv E_i^{ex} E_i^{el} E_i^{ad}$. Several physical parameters are necessary to quantify the various individual enhancement factors. To establish E_i^{ex} in Eq. 7, required parameters are the hydrogel water content, ϕ_1, solute hydrodynamic radius, a_{is}, and fiber radius, a_f. As discussed elsewhere,[1,2] ϕ_1, a_{is}, and a_f are conveniently obtained gravimetrically, from dilute bulk diffusion coefficients, and from oscillatory linear shear rheology, respectively. To obtain the Donnan electric potential needed in Eq. 9, and, therefore, E_i^{el} in Eq. 8, required hydrogel properties are the concentration of charged MAA

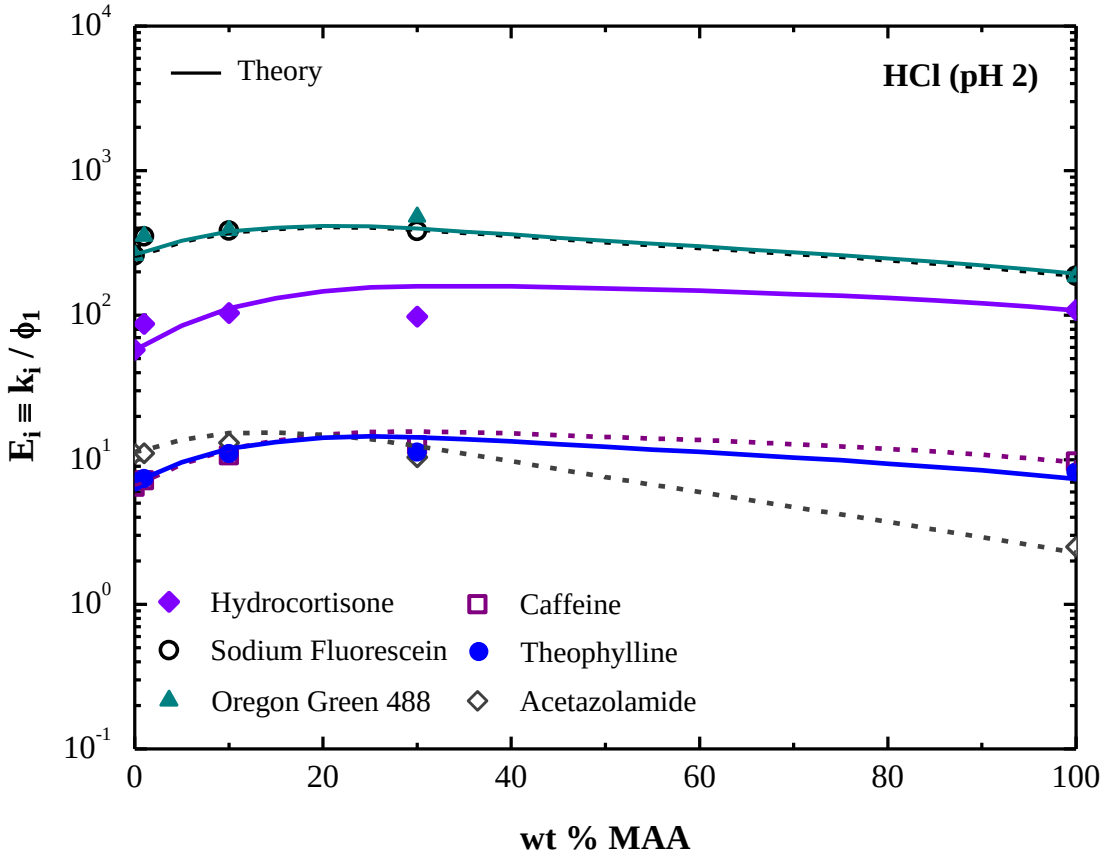

Figure 3.6: Measured solute enhancement factors as functions of MAA copolymer content for hydrocortisone (filled diamonds), sodium fluorescein (open circles), Oregon Green 488 (filled triangles), caffeine (open squares), theophylline (filled circles), and acetazolamide (open diamonds) in HEMA/MAA hydrogels equilibrated in aqueous HCl (pH 2). Semi-logarithmic lines are drawn according to theory. Solid and dashed theory lines correspond to filled and open symbols, respectively.

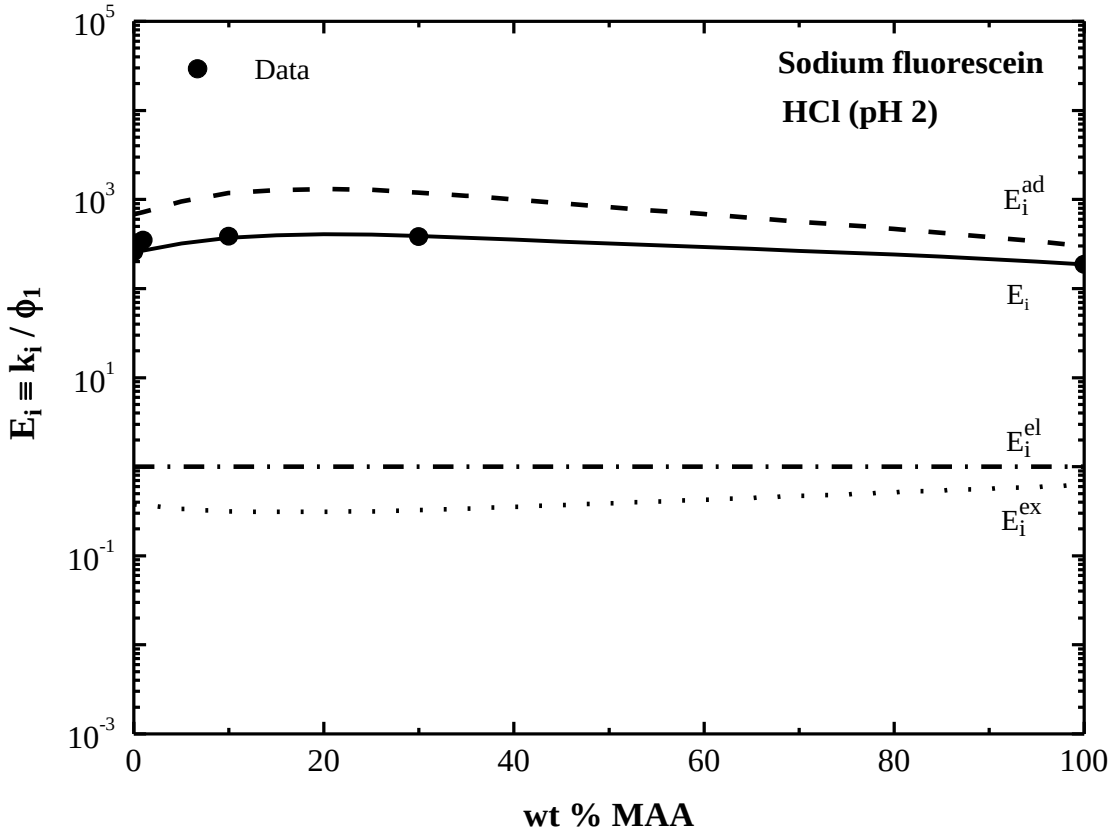

Figure 3.7: Sodium-fluorescein enhancement factor as a function of MAA copolymer content in HEMA/MAA hydrogels equilibrated in aqueous HCl (pH 2). Semi-logarithmic lines are drawn according to theory. Solid, dashed, dotted, and dash-dotted lines correspond to E_i, E_i^{ad}, E_i^{ex}, and E_i^{el}. Symbols denote measured E_i in Table 3.

carboxylate groups, $C_{MAA^-}^{gel}$, calculated from the MAA-copolymer weight fraction during synthesis and the degree of ionization, $f_{[-]}$. Finally, E_i^{ad} in Eq. 6 is established from ϕ_1, w_{MAA}, and the Henry's adsorption constants, K_{ij}. K_{ij} is obtained from fits of Eqs. 6-9 to measured solute partition coefficients in the corresponding homopolymer hydrogels. A more complete predictive theory demands *a priori* prediction of K_{ij} and ϕ_1.

3.7 Conclusions

We report measured and predicted equilibrium partition coefficients for six prototypical drugs in five soft-contact-lens-material hydrogels over a range of water contents. Partition coefficients were obtained using two-photon confocal microscopy and back extraction with UV/Vis-absorption spectrophotometry for acetazolamide, caffeine, hydrocortisone, Oregon Green 488, sodium fluorescein, and theophylline in 2-hydroxyethyl methacrylate/methacrylic acid (HEMA/MAA, $pK_a \approx 5.2$) copolymer hydrogels as functions of composition, aqueous pH (2 and 7.4), and salinity. Size exclusion, specific adsorption, and electrostatic interaction control solute partitioning. To express deviation from ideal partitioning, we define an enhancement (or exclusion) factor, $E_i \equiv k_i / \phi_1$, where ϕ_1 is hydrogel water volume fraction.[1] At pH 7.4, all solutes exhibit $E_i > 1$ in 100 wt % HEMA hydrogels owing to strong specific adsorption to HEMA strands. As a result, E_i significantly decreases with addition of anionic MAA to the hydrogel due to non-interaction with the charged MAA. E_i for anionic sodium fluorescein, Oregon Green 488, and acetazolamide at pH 7.4, however, decreases more than those for similar-sized nonionic solutes. For divalent anionic sodium fluorescein, E_i increases significantly with rising NaCl concentration in phosphate buffer (from 0.15 to 1 M) due to screening of the dissociated carboxylate groups on the MAA copolymer. For all cases, theory predicts enhancement factors for the six ionic and nonionic solutes. By assuming that the free energy of a solute-equilibrated hydrogel is additive in molecular contributions, we express the enhancement factor as a product of individual enhancement factors for size-exclusion (E_i^{ex}), electrostatic interaction (E_i^{el}), and specific adsorption (E_i^{ad}) leading to $E_i \equiv E_i^{ex} E_i^{el} E_i^{ad}$. To obtain the individual enhancement factors, we employ an extended Ogston mesh-size distribution for E_i^{ex}, Donnan equilibrium for E_i^{el}, and Henry's law characterizing specific adsorption to the polymer chains for E_i^{ad}. In all cases, predicted enhancement factors demonstrate excellent agreement with experiment.

3.8 References

1. Kotsmar, C.; Sells, T.; Taylor, N.; Liu, D. E.; Prausnitz, J. M.; Radke, C. J. Aqueous solute partitioning and mesh size in HEMA/MAA hydrogels. *Macromolecules* **2012,** 45, (22), 9177-9187.
2. Liu, D. E.; Kotsmar, C.; Nguyen, F.; Sells, T.; Taylor, N. O.; Prausnitz, J. M.; Radke, C. J. Macromolecule sorption and diffusion in HEMA/MAA hydrogels. *Industrial & Engineering Chemistry Research* **2013,** 52, (50), 18109-18120.

3. Peppas, N. A.; Bures, P.; Leobandung, W.; Ichikawa, H. Hydrogels in pharmaceutical formulations. *European Journal of Pharmaceutics and Biopharmaceutics* **2000,** 50, (1), 27-46.

4. D'Errico, G.; De Lellis, M.; Mangiapia, G.; Tedeschi, A.; Ortona, O.; Fusco, S.; Borzacchiello, A.; Ambrosio, L. Structural and mechanical properties of UV-photo-cross-linked poly(N-vinyl-2-pyrrolidone) hydrogels. *Biomacromolecules* **2008,** 9, (1), 231-240.

5. Lazzara, M. J.; Deen, W. M. Effects of concentration on the partitioning of macromolecule mixtures in agarose gels. *Journal of Colloid and Interface Science* **2004,** 272, (2), 288-297.

6. Mathur, A. M.; Moorjani, S. K.; Scranton, A. B. Methods for synthesis of hydrogel networks: A review. *Journal of Macromolecular Science, Part C* **1996,** 36, (2), 405-430.

7. Kosto, K. B.; Panuganti, S.; Deen, W. M. Equilibrium partitioning of Ficoll in composite hydrogels. *Journal of Colloid and Interface Science* **2004,** 277, (2), 404-409.

8. Peppas, N. A. Hydrogels and drug delivery. *Current Opinion in Colloid & Interface Science* **1997,** 2, (5), 531-537.

9. Gupta, P.; Vermani, K.; Garg, S. Hydrogels: From controlled release to pH-responsive drug delivery. *Drug Discovery Today* **2002,** 7, (10), 569-579.

10. Güven, O.; Şen, M.; Karadağ, E.; Saraydın, D. A review on the radiation synthesis of copolymeric hydrogels for adsorption and separation purposes. *Radiation Physics and Chemistry* **1999,** 56, (4), 381-386.

11. Kim, J. J.; Park, K. Smart hydrogels for bioseparation. *Bioseparation* **1998,** 7, (4-5), 177-184.

12. Guan, L.; Jiménez, M. E. G.; Walowski, C.; Boushehri, A.; Prausnitz, J. M.; Radke, C. J. Permeability and partition coefficient of aqueous sodium chloride in soft contact lenses. *Journal of Applied Polymer Science* **2011,** 122, (3), 1457-1471.

13. Luensmann, D.; Zhang, F.; Subbaraman, L.; Sheardown, H.; Jones, L. Localization of lysozyme sorption to conventional and silicone hydrogel contact lenses using confocal microscopy. *Current Eye Research* **2009,** 34, (8), 683-697.

14. Peng, C.-C.; Burke, M. T.; Chauhan, A. Transport of topical anesthetics in vitamin E loaded silicone hydrogel contact lenses. *Langmuir* **2011,** 28, (2), 1478-1487.

15. Kim, J.; Chauhan, A. Dexamethasone transport and ocular delivery from poly (hydroxyethyl methacrylate) gels. *International Journal of Pharmaceutics* **2008,** 353, (1), 205-222.

16. Bengani, L. C.; Leclerc, J.; Chauhan, A. Lysozyme transport in p-HEMA hydrogel contact lenses. *Journal of Colloid and Interface Science* **2012,** 386, (1), 441-450.

17. Wu, J.; Sassi, A. P.; Blanch, H. W.; Prausnitz, J. M. Partitioning of proteins between an aqueous solution and a weakly-ionizable polyelectrolyte hydrogel. *Polymer* **1996,** 37, (21), 4803-4808.

18. Hirota, N.; Kumaki, Y.; Narita, T.; Gong, J. P.; Osada, Y. Effect of charge on protein diffusion in hydrogels. *The Journal of Physical Chemistry B* **2000,** 104, (42), 9898-9903.

19. Johnson, E. M.; Berk, D. A.; Jain, R. K.; Deen, W. M. Diffusion and partitioning of proteins in charged agarose gels. *Biophysical Journal* **1995,** 68, (4), 1561-1568.

20. Abbott, N. L.; Blankschtein, D.; Hatton, T. A. Protein partitioning in two-phase aqueous polymer systems. 1. Novel physical pictures and a scaling thermodynamic formulation. *Macromolecules* **1991,** 24, (15), 4334-4348.

21. Sassi, A. P.; Blanch, H. W.; Prausnitz, J. M. Characterization of size-exclusion effects in highly swollen hydrogels: Correlation and prediction. *Journal of Applied Polymer Science* **1996,** 59, (8), 1337-1346.

22. Stringer, J. L.; Peppas, N. A. Diffusion of small molecular weight drugs in radiation-crosslinked poly (ethylene oxide) hydrogels. *Journal of Controlled Release* **1996,** 42, (2), 195-202.

23. Tong, J.; Anderson, J. L. Partitioning and diffusion of proteins and linear polymers in polyacrylamide gels. *Biophysical Journal* **1996,** 70, (3), 1505-1513.

24. Bettini, R.; Colombo, P.; Peppas, N. A. Solubility effects on drug transport through pH-sensitive, swelling-controlled release systems: Transport of theophylline and metoclopramide monohydrochloride. *Journal of Controlled Release* **1995,** 37, (1–2), 105-111.

25. Merrill, E. W.; Dennison, K. A.; Sung, C. Partitioning and diffusion of solutes in hydrogels of poly(ethylene oxide). *Biomaterials* **1993,** 14, (15), 1117-1126.

26. Am Ende, M. T.; Peppas, N. A. Transport of ionizable drugs and proteins in crosslinked poly (acrylic acid) and poly (acrylic acid-co-2-hydroxyethyl methacrylate) hydrogels. II. Diffusion and release studies. *Journal of Controlled Release* **1997,** 48, (1), 47-56.

27. Kapoor, Y.; Thomas, J. C.; Tan, G.; John, V. T.; Chauhan, A. Surfactant-laden soft contact lenses for extended delivery of ophthalmic drugs. *Biomaterials* **2009,** 30, (5), 867-878.

28. Ratner, B. D.; Miller, I. F. Transport through crosslinked poly(2-hydroxyethyl methacrylate) hydrogel membranes. *Journal of Biomedical Materials Research* **1973,** 7, (4), 353-367.

29. Fatin-Rouge, N.; Milon, A.; Buffle, J.; Goulet, R. R.; Tessier, A. Diffusion and partitioning of solutes in agarose hydrogels: The relative influence of electrostatic and specific interactions. *The Journal of Physical Chemistry B* **2003,** 107, (44), 12126-12137.

30. Chan, A. W.; Neufeld, R. J. Modeling the controllable pH-responsive swelling and pore size of networked alginate based biomaterials. *Biomaterials* **2009,** 30, (30), 6119-6129.

31. Mottram, L. F.; Boonyarattanakalin, S.; Kovel, R. E.; Peterson, B. R. The pennsylvania green fluorophore: A hybrid of oregon green and tokyo green for the construction of hydrophobic and pH-insensitive molecular probes. *Organic Letters* **2006,** 8, (4), 581-584.

32. Ribeiro, A.; Veiga, F.; Santos, D.; Torres-Labandeira, J. J.; Concheiro, A.; Alvarez-Lorenzo, C. Bioinspired imprinted pHEMA-hydrogels for ocular delivery of carbonic anhydrase inhibitor drugs. *Biomacromolecules* **2011,** 12, (3), 701-709.

33. Çaykara, T.; Doğmuş, M.; Kantoğlu, Ö. Network structure and swelling–shrinking behaviors of pH-sensitive poly(acrylamide-co-itaconic acid) hydrogels. *Journal of Polymer Science Part B: Polymer Physics* **2004,** 42, (13), 2586-2594.

34. Newman, J.; Chapman, T. W. Restricted diffusion in binary solutions. *AIChE Journal* **1973,** 19, (2), 343-348.

35. Edwards, A.; Prausnitz, M. R. Fiber matrix model of sclera and corneal stroma for drug delivery to the eye. *AIChE Journal* **1998,** 44, (1), 214-225.

36. Prausnitz, M. R.; Noonan, J. S. Permeability of cornea, sclera, and conjunctiva: A literature analysis for drug delivery to the eye. *Journal of Pharmaceutical Sciences* **1998,** 87, (12), 1479-1488.

37. Järvinen, K.; Åkerman, S.; Svarfvar, B.; Tarvainen, T.; Viinikka, P.; Paronen, P. Drug release from pH and ionic strength responsive poly(acrylic acid) grafted poly(vinylidenefluoride) membrane bags in vitro. *Pharmaceutical Research* 15, (5), 802-805.

38. Ghafourian, T.; Zandasrar, P.; Hamishekar, H.; Nokhodchi, A. The effect of penetration enhancers on drug delivery through skin: a QSAR study. *Journal of Controlled Release* **2004,** 99, (1), 113-125.

39. Johnson, K. A.; Westermann-Clark, G. B.; Shah, D. O. Diffusion of charged micelles through charged microporous membranes. *Langmuir* **1989,** 5, (4), 932-938.

40. Müller, C. B.; Loman, A.; Pacheco, V.; Koberling, F.; Willbold, D.; Richtering, W.; Enderlein, J. Precise measurement of diffusion by multi-color dual-focus fluorescence correlation spectroscopy. *EPL (Europhysics Letters)* **2008,** 83, (4), 46001.

41. Spãtaru, N.; Sarada, B. V.; Tryk, D. A.; Fujishima, A. Anodic voltammetry of xanthine, theophylline, theobromine and caffeine at conductive diamond electrodes and its analytical application. *Electroanalysis* **2002,** 14, (11), 721-728.

42. Khare, A. R.; Peppas, N. A. Swelling/deswelling of anionic copolymer gels. *Biomaterials* **1995,** 16, (7), 559-567.

43. Ogston, A. G. The spaces in a uniform random suspension of fibres. *Transactions of the Faraday Society* **1958,** 54, 1754-1757.

44. Overbeek, J. T. G. *Colloid Science I*. Elsevier Pub. Co.: New York, 1969.

45. Newman, J.; Thomas-Alyea, K. E. *Electrochemical systems*. John Wiley & Sons: New Jersey, 2004.

46. Victorov, A. I. Effect of morphology of a swollen ionomer gel on its salt uptake. *Fluid Phase Equilibria* **2006,** 241, (1–2), 334-343.

Appendix 3A: Thermodynamics of Partitioning

Consider a dilute aqueous weak-electrolyte solute of molar concentration, C_i^{bulk}, equilibrated with a copolymer hydrogel at solute concentration, C_i^{gel}, giving a partition coefficient $k_i \equiv C_i^{gel} / C_i^{bulk}$. Solute i resides in the liquid-filled spaces of the hydrogel and adsorbs onto the internal polymer strands so that[1,2]

$$C_i^{gel} \equiv \phi_1 C_i^L + \phi_2 n_i \,, \tag{3A.1}$$

where ϕ_1 and $\phi_2 \equiv 1 - \phi_1$ are the volume fractions of the liquid and polymer in the hydrogel, respectively, C_i^L is the liquid-space molar concentration (moles per liquid volume), and n_i is the total solute adsorption density on the polymer matrix (moles per polymer volume). Phase equilibrium demands that the solute chemical potential in the bulk aqueous phase equals that in the liquid interstices of the hydrogel which, in turn, equals that of the solute adsorbed on the polymer matrix

$$\mu_i^{bulk} = \mu_i^L = \mu_i^{ad} \,. \tag{3A.2}$$

When the weak-electrolyte solute is charged, chemical potentials in Eq. 3A.2 are replaced by electrochemical potentials.[45]

The second expression in Eq. 3A.2 is evaluated by Henry's law for dilute-solute adsorption

$$\mu_i^o + RT \ln C_i^L = \mu_{ij}^{oad} + RT \ln n_{ij} \,, \tag{3A.3}$$

where n_{ij} is the adsorption density of solute i on copolymer j (i.e., moles of i per swollen volume of copolymer j), μ_i^o is the ideal dilute-solution standard-state chemical potential for uncharged, point particles i at unit concentration, and μ_{ij}^{oad} is the standard-state chemical potential for ideal adsorbed solute i at unit adsorption density on copolymer strands j. Henry's law for solute adsorption is rewritten from Eq. 3A.3 as

$$\phi_2 n_i \equiv \sum_j n_{ij} \phi_{2\,j} = C_i^L \sum_j K_{ij} \phi_{2\,j} \,, \tag{3A.4}$$

where $\phi_{2\,j}$ is the volume fraction of copolymer j. Individual copolymer Henry's adsorption constants for solute i are defined by $K_{ij} \equiv \exp[-(\mu_{ij}^{oad} - \mu_i^o) / RT]$.

The concentration of equilibrated solute in the liquid-filled spaces of the hydrogel, C_i^L, follows from the first part of Eq. 3A.3

$$\mu_i^o + RT \ln C_i^{bulk} = \mu_i^o + \Delta\mu_i^{ex} + \Delta\mu_i^{el} + RT \ln C_i^L \,, \tag{3A.5}$$

where $\Delta\mu_i^{ex}$ is the increment of ideal-dilute solute chemical potential in the hydrogel due to finite size, and $\Delta\mu_i^{el}$ is the increment of ideal-dilute solute chemical potential in a polyelectrolyte hydrogel due to solute charge. Similar to Eq. 3A.3, Eq. 3A.5 is rewritten as

$$C_i^L = E_i^{ex} E_i^{el} C_i^{bulk}, \tag{3A.6}$$

where $E_i^{ex} \equiv \exp(-\Delta\mu_i^{ex} / RT)$ is the finite-sized solute exclusion factor and $E_i^{el} \equiv \exp(-\Delta\mu_i^{el} / RT)$ is the finite-charge solute exclusion/enhancement factor. From Eq. 3A.5, the solute enhancement factors may be considered also as inverse activity coefficients in the gel.

Eqs. 1, 3A.1, 3A.4, and 3A.6 lead to Eq. 6 of the text. The size-exclusion enhancement factor E_i^{ex} is estimated from Eq. 7 while the electrical enhancement/exclusion factor E_i^{el} is obtained from Donnan exclusion in Eq. 8.[44] Calculation of the Donnan potential is outlined in Appendix 3B.

Appendix 3B: Donnan Potential

Since the aqueous solute concentration is much lower than that of the background electrolyte, the Donnan potential of the gel relative to the bulk solution, ψ, is set by the aqueous electrolyte ionic strength and pH, and the polyelectrolyte charge density. We approximate the buffer and acid electrolyte as completely dissociated, indifferent NaCl with bulk aqueous molar concentration C_{NaCl}^{bulk}.

Phase equilibrium demands that chloride (Cl^-) and sodium (Na^+) ion chemical potentials in the bulk aqueous phase equal those in the liquid-filled domains of the hydrogel. Because Donnan theory gives $\Delta\mu_i^{el} = z_i F\psi$,[44] Eqs. 3A.5 and 3A.6 for Cl^- reveal that

$$-\frac{F\psi}{RT} = \ln \frac{C_{NaCl}^{bulk} E_{Cl^-}^{ex}}{C_{Cl^-}^{L}}, \tag{3B.1}$$

where $C_{Cl^-}^{L}$ is the liquid-region chloride-ion molar concentration (moles of Cl^- per liquid volume) and ψ is the electric potential difference between the hydrogel and the bulk aqueous solution.[44] Eq. 3B.1 neglects specific adsorption of the background electrolyte to the polymer matrix. Consequently, addition of Eq. 3A.5 for Cl^- and Na^+ ions gives[44]

$$C_{Na^+}^{L} C_{Cl^-}^{L} = E_{Na^+}^{ex} E_{Cl^-}^{ex} \left(C_{NaCl}^{bulk}\right)^2, \tag{3B.2}$$

where $C_{NaCl}^{bulk} = C_{Cl^-}^{bulk} = C_{Na^+}^{bulk}$.

The hydrogel water phase contains mobile Na^+ and Cl^- ions and immobile charges MAA^- (dissociated MAA at pH 7.4). Electroneutrality requires that

$$C_{MAA^-}^{gel} / \phi_1 + C_{Cl^-}^{L} - C_{Na^+}^{L} = 0 . \qquad \text{(3B.3)}$$

Due to their very low concentrations compared to that of the background electrolyte, Eq. 3B.3 neglects the presence of H^+, OH^-, and dissociated solute i. Upon solving Eqs. 3B.2 and 3B.3 for $C_{Cl^-}^{L}$ and dividing by C_{NaCl}^{bulk}, we establish that

$$\frac{C_{Cl^-}^{L}}{C_{NaCl}^{bulk}} = \sqrt{(E_{Cl^-}^{ex} E_{Na^+}^{ex})^2 + (\alpha_{el} E_{Cl^-}^{ex})^2} - \alpha_{el} E_{Cl^-}^{ex} , \qquad \text{(3B.4)}$$

where $\alpha_{el} \equiv C_{MAA^-}^{gel} / (2 C_{NaCl}^{bulk} \; E_{Cl^-}^{ex} \; \varphi_1)$. Finally, Eq. 9 of the text follows using Eq. 3B.1 to eliminate $C_{Cl^-}^{L}$ from Eq. 3B.4. Possible spatial non-uniformity of the electrostatic potential in the hydrogel is negligible at the background ionic strengths pertinent to this work.[46]

Chapter 4

Diffusion of Water-Soluble Sorptive Drugs in HEMA/MAA Hydrogels

4.1 Abstract

We measure and theoretically predict four prototypical aqueous-drug diffusion coefficients in five soft-contact-lens material hydrogels where solute-specific adsorption is pronounced. Two-photon fluorescence confocal microscopy and UV/Vis-absorption spectrophotometry assess transient solute concentration profiles and concentration histories, respectively. Diffusion coefficients are obtained for acetazolamide, riboflavin, sodium fluorescein, and theophylline in 2-hydroxyethyl methacrylate/methacrylic acid (HEMA/MAA) copolymer hydrogels as functions of composition, equilibrium water content (30-90%), and aqueous pH (2 and 7.4). At pH 2, MAA chains are nonionic, whereas at pH 7.4, MAA chains are anionic ($pK_a \approx 5.2$). All studied prototypical drugs specifically interact with HEMA and nonionic MAA (at pH 2) moieties. Conversely, none of the prototypical drugs adsorb specifically to anionic MAA (at pH 7.4) chains. As expected, diffusivities of adsorbing solutes are significantly diminished by specific interactions with hydrogel strands. Despite similar solute size, relative diffusion coefficients in the hydrogels span several orders of magnitude because of varying degrees of solute interactions with hydrogel-polymer chains. To provide a theoretical framework for the new diffusion data, we apply an effective-medium model extended for solute-specific interactions with hydrogel copolymer strands. Sorptive-diffusion kinetics is successfully described by local equilibrium and Henry's law. All necessary parameters are determined independently. All predicted diffusivities are in good agreement with experiment.

Reprint of Liu, D.E.*; Dursch, T. J.*; Taylor, N. O.; Chan, S.Y.; Bregante, D.T.; Radke, C. J. Submitted. *authors contributed equally

4.2 Body

Hydrogels are cross-linked polymeric networks that readily imbibe water and typically swell without dissolving.[1-7] The ability of hydrogels to uptake aqueous solutes and later release them in a controlled manner has led to their extensive use in drug delivery,[1,4-6,8-15] tissue engineering,[16-18] bioseparations,[19,20] and biosensing.[21-24] For example, hydrogels have been recently introduced as soft contact lenses (SCLs) capable of detecting tear-film components and administering drugs and bioactive agents to the eye, allowing for early disease diagnosis and treatment.[25,26] Because solute and hydrogel properties (e.g., hydrophilicity, charge, and chemistry) vary significantly with application, solute release rates are highly system dependent. Accordingly, designing optimal solute-hydrogel combinations for controlled and targeted solute delivery remains a challenge.

Diffusion of aqueous solutes occurs primarily through the water-filled meshes of the hydrogel-polymer network.[2,7,11,14,27-36] Aqueous-solute diffusivities in hydrogels, D_i, are diminished relative to those in bulk solution, $D_{io,}$ by nonspecific interaction with the hydrogel-polymer chains including steric obstruction and hydrodynamic resistance.[2,7,11,14,27-36] In many cases, overall aqueous-solute diffusivities are further diminished by specific complexation of solutes to hydrogel-polymer chains that arises when specific solute-hydrogel binding overcomes their competing interactions with water.[1-4,7,9,10,12,14,29,37-39] Aqueous solutes may adsorb reversibly or irreversibly to the interior hydrogel network, hindering solute release rates by orders of magnitude. Consequently, solute-specific interactions with the hydrogel-polymer network often dictate the efficacy of hydrogels in applications requiring controlled and targeted release.

Because of the wide variety of applications, significant effort has been expended toward obtaining aqueous-solute diffusivities both experimentally[2,10-12,14,27-36,38-41] and theoretically.[2,11,27-36,38,42-44] Most published experimental work, however, focuses on diffusion of nonspecific-interacting aqueous solutes in high water-content hydrogels (i.e., >90%).[2,11,12,14,27-36,38,40,44] As a result, theoretical models typically exploit dilute hydrogel-polymer fractions and consider almost exclusively hydrodynamic drag, available free-volume, and/or steric obstruction by hydrogel-polymer chains. Solute-specific interaction is often exhibited by polymers, polymeric surfactants, and proteins in SCL-material hydrogels and by ionic/nonionic drugs and vitamins in drug-delivery hydrogels.[1,2,4,7,10,12,14,37-39,41] To date, however, relatively little attention has been given to aqueous-solute diffusion in hydrogels where solute/polymer-chain interactions are significant.

We report experimental and theoretically predicted diffusion coefficients of four prototypical water-soluble drugs (i.e., acetazolamide, riboflavin, sodium fluorescein, and theophylline) in hydrogels where solute-specific binding is pronounced.[1] The hydrogels studied are representative of SCL materials and are copolymers of 2-hydroxyethyl methacrylate (HEMA) and methacrylic acid (MAA). To vary the extent of solute adsorption, hydrogel copolymer composition was varied in HEMA:MAA weight ratios of 100:0, 99:1, 90:10, 70:30, and 0:100. Hydrogel-synthesis and water-content-measurement procedures are provided in Appendix 4A: Supporting Information (SI) Section S1. All hydrogels are referred to by their corresponding wt % MAA, where wt % MAA and wt % HEMA sum to 100.

To assess the extent of solute-specific binding to hydrogel-polymer chains, equilibrium partition coefficients of dilute solute i, k_i, were obtained following Dursch et al.[1] Table 4.1

displays k_i for theophylline, acetazolamide, sodium fluorescein, and riboflavin in HEMA/MAA hydrogels equilibrated in phosphate-buffered saline (pH 7.4, PBS[1-3]) and equal ionic strength hydrochloric-acid saline (pH 2, HCl[2-4]). Also shown are hydrogel equilibrium water volume fractions, ϕ_1. At pH 7.4, sodium fluorescein (pK_a = 4.5, 6.5) is dianionic and acetazolamide (pK_a = 7.2) is partially anionic, whereas all other solutes are neutral. As discussed elsewhere[1], $k_i > \phi_1$ for all solutes in 0 wt % MAA hydrogels (i.e., 100 wt % HEMA) reveals specific adsorption to HEMA copolymer chains, most significant for riboflavin. Conversely, similar k_i (~ 0.7) for nearly all solutes in 100 wt % MAA hydrogels is due to similar solute Stoke's radii (0.37-0.62 nm[1,45]) and nonspecific-interaction with ionized MAA.[1] Table 4.1 also displays k_i in HEMA/MAA hydrogels equilibrated in HCl (pH 2) where all solutes and hydrogels are uncharged. At this lower pH, all solutes exhibit $k_i > \phi_1$ in all hydrogels, most significant by uncharged sodium fluorescein. Measured k_i clearly demonstrate specific solute/polymer-chain interactions in the HEMA/MAA hydrogels.

Table 4.1: Hydrogel Water Contents and Solute Partition Coefficients with Varying HEMA:MAA Weight Ratios in Aqueous PBS/HCl[c]

Hydrogel Composition (HEMA:MAA)	Water Content[a] ϕ_1	Theophyline[a]	Acetazolamide[a]	Sodium Fluorescein[a]	Riboflavin[b]
100:0	0.43 / 0.40	2.8 / 2.8	2.5 / 4.4	2.4 / 103.2	5.4 / 5.4
99:1	0.54 / 0.39	2.4 / 2.9	2.1 / 4.3	1.7 / 136.5	5.3 / 4.6
90:10	0.77 / 0.29	1.8 / 3.2	1.3 / 3.8	0.7 / 111.8	2.5 / 5.8
70:30	0.83 / 0.31	1.2 / 3.5	1.0 / 3.2	0.2 / 118.2	1.4 / 5.2
0:100	0.92 / 0.71	0.7 / 5.8	0.6 / 1.8	0.1 / 133.0	0.7 / 5.4

[a]from Dursch et al.[1]

[b]measured by two-photon fluorescence confocal microscopy with 780-nm excitation according to Dursch et al.[1]

[c]Table entries separated by a diagonal represent partition coefficients measured in PBS (pH 7.4) or HCl (pH 2)

Aqueous-solute diffusion coefficients were obtained for all solute-hydrogel systems reported in Table 4.1. Two-photon fluorescence confocal microscopy detected transient sodium-fluorescein and riboflavin concentration release profiles and classical back extraction and UV/Vis-absorption spectrophotometry assessed theophylline and acetazolamide concentration desorption histories (see SI Section S2 for detailed procedures). Constant overall

diffusion coefficients of dilute solute i in the hydrogels, $D_{i\pi}$, were fit to resulting transient concentration profiles and concentration histories using Fick's law.[2,46] Figure 4.1 graphs measured solute diffusion coefficients as relative values, $D_{i\pi}/D_{io}$, as a function of equilibrium polymer volume fraction, ϕ_2, in the HEMA/MAA hydrogels equilibrated in PBS (pH 7.4). For reference, all bulk-aqueous drug diffusion coefficients, D_{io}, are provided in Table 4.2. Lines in Figure 4.1 are drawn according to theory discussed below (i.e., Eq. 1). As expected, $D_{i\pi}/D_{io}$ for all solutes decreases with rising ϕ_2 (i.e., increasing HEMA copolymer fraction), corresponding to fewer available meshes for solute diffusion, increased hydrodynamic drag, and increased tortuosity. In MAA homopolymer hydrogels (i.e., ϕ_2 = 0.08), where copolymer-chains are anionic and non-specifically-interacting, relative diffusion coefficients are similar for all solutes. However, despite all solutes being of similar size, relative diffusion coefficients vary by orders of magnitude in HEMA-containing hydrogels of the same composition (and, accordingly, identical ϕ_2). Notably, riboflavin, which displays the strongest interaction with HEMA-copolymer strands (i.e., the largest k_i in Table 4.1 for 0% MAA hydrogels), also exhibits the smallest relative diffusion coefficient for all HEMA-containing hydrogels. Clearly, diffusion rates are significantly reduced by solute adsorption to HEMA-copolymer strands.

Table 4.2: Solute Bulk-Aqueous Diffusion Coefficients and Hydrodynamic Radii

Solute	$D_{io} \times 10^6$	Hydrodynamic radius [nm]
Theophylline [a]	6.7	0.37
Acetazolamide [a]	6.1	0.41
Riboflavin [b]	4.2	0.58
Sodium fluorescein [a]	4.0	0.62

[a]from Dursch et al.[1]

[b]Hydrodrodynamic radius from Shin et al.[45] D_{io} is back-calculated using the Stokes-Einstein equation at 25 ^{o}C

At pH 2, all solutes are neutral and specifically adsorb to both HEMA and nonionic MAA moieties. Figure 4.2 again displays relative solute-hydrogel diffusion coefficients for the four prototypical drugs, but now as a function of the MAA-copolymer content for hydrogels equilibrated in HCl (pH 2). Here, $D_{i\pi}/D_{io}$ is plotted against wt % MAA rather than against ϕ_2 because addition of MAA copolymer at pH 2 results in a non-monotonic change in ϕ_2 (see Table 4.1). Similar to Figure 4.1, lines in Figure 4.2 correspond to predicted relative diffusion coefficients from theory discussed below. $D_{i\pi}/D_{io}$ initially declines with addition of uncharged MAA (0% to 10%) and a consequent rise in ϕ_2 (0.60 to 0.71). However, with further addition

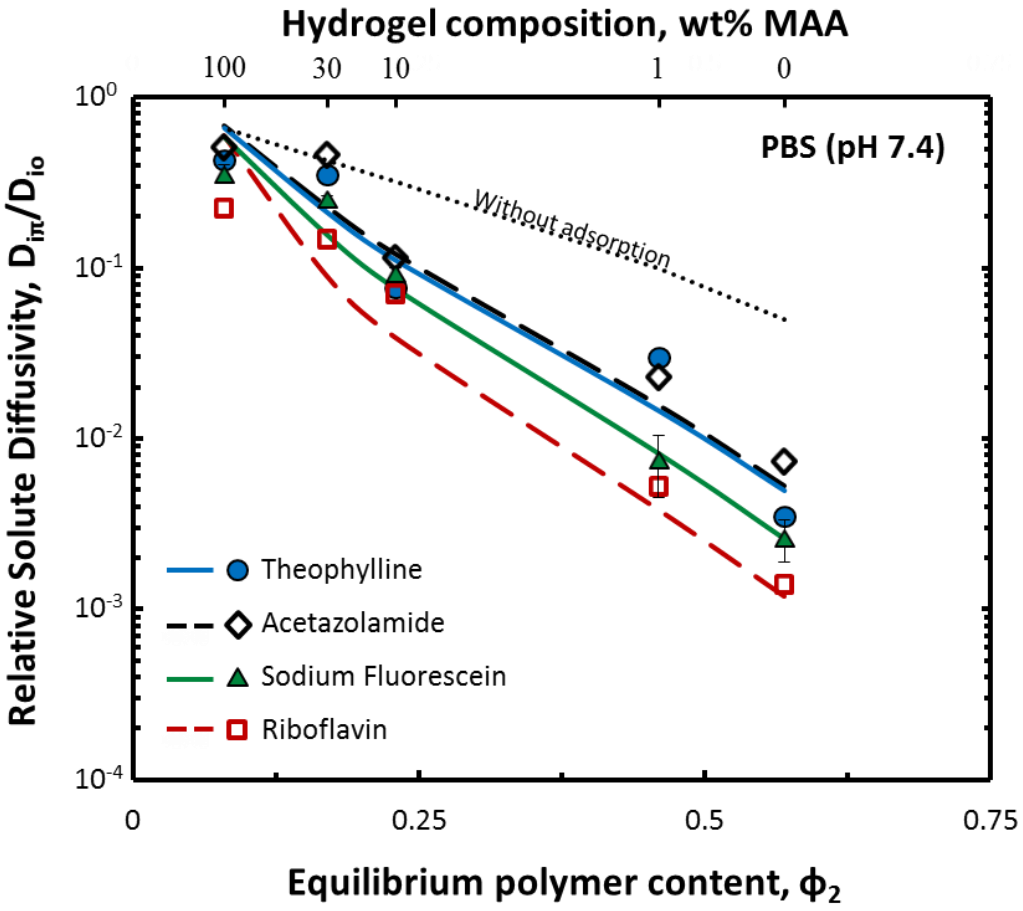

Figure 4.1: Relative solute diffusion coefficients, $D_{i\pi} / D_{io}$, as functions of polymer volume fraction, ϕ_2, for theophylline (closed circles), acetazolamide (open diamonds), sodium fluorescein (closed triangles), and riboflavin (open squares), in HEMA/MAA hydrogels equilibrated in PBS (pH 7.4). Typical error bars are shown. Solid and dashed lines are drawn according to theory with adsorption (i.e., Eq. 1 with K_{ij} specified by EFPT). Solid and dashed lines correspond to filled and open symbols, respectively. The dotted line is drawn for acetazolamide according to theory without adsorption (i.e., Eq. 1 with $K_{ij} = 0$ for all j).

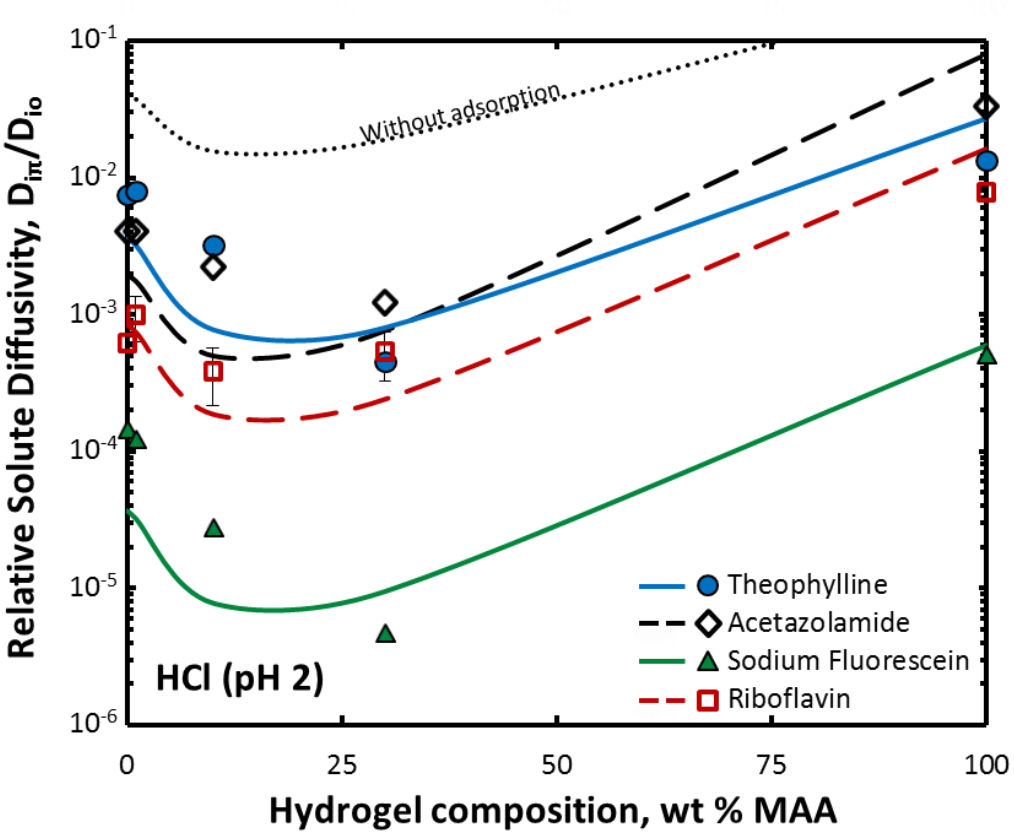

Figure 4.2: Relative solute diffusion coefficients, $D_{i\pi} / D_{io}$, as functions of MAA copolymer content for theophylline (closed circles), acetazolamide (open diamonds), sodium fluorescein (closed triangles), and riboflavin (open squares) in HEMA/MAA hydrogels equilibrated in HCl (pH 2). Typical error bars are shown. Solid and dashed lines are drawn according to theory with adsorption (i.e., Eq. 1 with K_{ij} specified by EFPT). Solid and dashed lines correspond to filled and open symbols, respectively. The dotted line is drawn for acetazolamide according to theory without adsorption (Eq. 1 with $K_{ij} = 0$ for all j).

of MAA (10% to 100%), $D_{i\pi}/D_{io}$ rises for all solutes due to the sharp decline in ϕ_2 (0.71 to 0.29). Again, despite similar solute size, relative diffusion coefficients vary by orders of magnitude in HEMA-containing hydrogels of identical water content. This observation is again attributed to reduced diffusion rates arising from specific interactions with HEMA-copolymer chains. Here, however, relative diffusion coefficients also vary by orders of magnitude in 100% MAA hydrogels, suggesting solute-specific interactions with electrically neutral MAA-copolymer strands. These interactions significantly slow diffusion rates in all MAA-containing hydrogels. Notably, acetazolamide exhibits both the greatest $D_{i\pi}/D_{io}$ value and the smallest k_i (1.8 in Table 4.1) of the five solutes in 100% MAA hydrogels at pH 2. In comparison to those of acetazolamide, the lesser $D_{i\pi}/D_{io}$ values for theophylline and riboflavin in 100% MAA hydrogels are complemented by larger k_i (5.8 and 5.4 in Table 4.1, respectively). A greater reduction of $D_{i\pi}/D_{io}$ is exhibited by solutes of stronger specific interactions with MAA-copolymer. For all hydrogels, the smallest relative diffusion coefficients are exhibited by uncharged sodium fluorescein that displays the highest adsorption to both HEMA- and neutral MAA-copolymer chains. Evidently, solute-specific interactions with both HEMA- and neutral MAA-copolymer chains account for the reduced diffusion rates seen at pH 2.

We predict diffusion coefficients for specifically interacting solutes in polyelectrolyte hydrogels using an extended version of Large-Pore-Effective-Medium (LPEM) Theory.[2] LPEM theory accounts for hydrodynamic drag, steric obstruction, and the accessible meshes available to diffusing solutes. To describe reversible specific adsorption to the hydrogel-polymer chains, we employ local equilibrium with dilute-solution Henry adsorption[1] to each monomer type (i.e., HEMA, anionic MAA, or nonionic MAA). Resulting diffusivity is that predicted by LPEM theory for nonspecifically interacting solutes divided by a retardation term accounting for specific adsorption (see SI Section S3 for detailed derivation),

$$\frac{D_{i\pi}}{D_{io}} = \frac{F_i S_i}{1+\sum_j K_{ij}\varphi_{2j}/\varphi_1} \tag{1}$$

where $D_{i\pi}$ is the overall effective solute diffusivity of solute i in the gel (see SI Section S3), F_i and S_i are hydrodynamic and steric resistance factors, respectively, K_{ij} is the Henry's adsorption constant for specifically adsorbed solute i on polymer component j, ϕ_{2j} is the volume fraction of polymer component j, and ϕ_1 is the water volume fraction. Here subscript j denotes HEMA, anionic MAA (at pH 7.4), or nonionic MAA (at pH 2). The retardation factor in the denominator of Eq. 1 is equivalent to the adsorption enhancement factor in Enhancement-Factor-Partitioning Theory[1] (EFPT). Without specific solute adsorption to the polymer chains (i.e., $K_{ij} = 0$ for all j), Eq. 1 reduces to the relative diffusion coefficient for nonspecifically interacting solutes compared to those directly from LPEM theory.[2] To describe specific solute-polymer chain interactions, values for K_{ij} were calculated directly from partitioning data using EFPT[1] and are provided in SI Table 4A.1. With K_{ij} specified, Eq. 1

permits *a priori* calculation of relative solute-hydrogel diffusion coefficients for all prototypical drugs as a function of hydrogel composition and aqueous pH.

Lines in Figure 4.1 compare predicted and measured $D_{i\pi}/D_{io}$ of the prototypical drugs as a function of ϕ_2 in aqueous PBS (pH 7.4). A dotted line in Figure 4.1 is drawn according to Eq. 1 without specific solute-polymer-chain interactions (i.e., $K_{ij} = 0$ for all j) for acetazolamide. Predictions without adsorption for the remaining prototypical drugs are similar due to similar solute size,[2] and are not shown for clarity. Predicted $D_{i\pi}/D_{io}$ values without adsorption decline with rising ϕ_2 because of increased hydrodynamic drag and steric obstruction. However, quantitative agreement is lacking. Without accounting for specific adsorption, theory consistently over predicts measured $D_{i\pi}/D_{io}$ by orders of magnitude.

As discussed above, all studied prototypical drugs specifically adsorb to HEMA chains reducing release rates in HEMA-containing hydrogels. Solid and dashed lines in Figure 4.1 are drawn according to Eq. 1 with specific adsorption (i.e., K_{ij} specified by EFPT). Predicted $D_{i\pi}/D_{io}$ now decline more drastically due to solute-specific adsorption to HEMA copolymer chains, in addition to the increased nonspecific interactions (i.e., F and S in Eq. 1). With increasing HEMA copolymer content, however, lines diverge between the various solutes due to varying degrees of specific interaction with HEMA copolymer. Because all Henry's adsorption constants are measured independently,[1] no adjustable parameters appear in the proposed theory. Nevertheless, agreement between theory and experiment is excellent.

Similar to Figure 4.1, lines in Figure 4.2 compare predicted and measured $D_{i\pi}/D_{io}$ for the aqueous drugs as a function of MAA copolymer content, now in dilute aqueous HCl (pH 2). Again a dotted line is drawn for acetazolamide neglecting specific solute-polymer-chain interactions (i.e., $K_{ij} = 0$ for all j). Predictions without adsorption (not shown) are similar for all studied prototypical drugs again due to similar solute size.[2] Agreement between theory without adsorption and experiment is poor. Without specific interactions, theory again over predicts measured $D_{i\pi}/D_{io}$ values.

In HCl (pH 2), all of the water-soluble drugs specifically interact with both HEMA and uncharged MAA chains, reducing diffusion rates in the hydrogels studied. Solid and dashed lines in Figure 4.2 are drawn according to theory with specific adsorption (i.e., K_{ij} specified by EFPT). Good agreement between theory with adsorption and experiment is also observed at pH 2. Consequently, specific adsorption is vital to quantify release rates from hydrogels when solute-specific binding is pronounced.

Slight discrepancies between theory and experiment in HCl (pH 2) may be explained by the low ϕ_1 of the studied hydrogels. Available theories predicting $D_{i\pi}/D_{io}$ from nonspecific interactions were derived for high-water-content hydrogels.[2,28-31,34,44] Extrapolation of those theories to lower ϕ_1 systems incurs increasing error in predicting hydrodynamic drag, steric obstruction, and the distribution of mesh sizes available for solute transport.[2] Additionally, with lower ϕ_1, fewer water-filled voids are accessible for solute diffusion and more polymer strands are available for solute-specific complexation. Consequently, accurate description of solute-specific interactions with hydrogel polymer chains is critical at lower ϕ_1.

We invoked local equilibrium to describe solute adsorption to the polymer strands. Local equilibrium requires that (1) solute adsorption is reversible (i.e., solutes desorb from

hydrogel polymer strands), and that (2) rates of solute adsorption and desorption are faster than the rate of diffusion through the water-filled meshes of the polymer network. If either assumption is violated, local equilibrium fails and a full description of adsorption kinetics is required.[2] Strong solute-hydrogel-polymer interactions suggest greater irreversibility with rates of solute adsorption much larger than those of desorption.

At pH 2, sodium fluorescein exhibits strong specific complexation with HEMA and MAA copolymer chains with k_i two orders of magnitude greater than ϕ_1 of HEMA/MAA hydrogels. Complete release from the lowest ϕ_1 hydrogels (30% and 10% MAA) is not observed even after one month of release, indicating substantial irreversibility.[1] Nevertheless, Eq. 1 provides a good first approximation to estimate solute release rates. In spite of no adjustable parameters, near quantitative prediction is achieved for all prototypical drugs in all hydrogels at both aqueous pH values.

The importance of specific adsorption in predicting solute release rates from hydrogels is readily apparent in a parity plot. Figure 4.3 displays $D_{i\pi}/D_{io}$ predicted by theory versus those measured by experiment on log-log scales for the prototypical drugs in the HEMA/MAA hydrogels at both aqueous pH 2 and pH 7.4. A linear unity-slope straight line is included for reference. Closed and open symbols denote predictions from Eq. 1 with adsorption (i.e., K_{ij} specified by EFPT) and without adsorption (i.e., $K_{ij} = 0$ for all j), respectively. Predictions without specific interactions consistently over predict the data by orders of magnitude, most significantly for those solutes with the strongest interactions with the hydrogel polymer chains (i.e., those with the largest k_i in Table 4.1). In contrast, predictions including specific interactions display excellent agreement with experiment. We note that the over prediction from neglect of specific adsorption is not an artifact of LPEM theory. Nonspecific interactions were also calculated *a priori* using other physical-based models;[28,30,31,43,44] identical trends were observed. Thus, solute-specific interactions with the hydrogel-polymer chains are critical to ascertain rates of solute release from hydrogels.

We obtained molecular diffusion coefficients of four prototypical drugs in soft-contact lens material hydrogels of varying copolymer composition and aqueous pH using two-photon fluorescence confocal microscopy and UV/Vis-absorption spectrophotometry. All prototypical drugs studied exhibited specific adsorption to nonionic MAA and HEMA moieties. Solute release rates were significantly diminished by specific interactions, most apparent at pH 2 where solute adsorption is strong. Measured relative diffusivities span several orders of magnitude, which is attributed to varying degrees of solute-specific interactions with hydrogel-polymer strands. By invoking local equilibrium and Henry-law adsorption, diffusion coefficients are quantitatively predicted using an LPEM model extended for solute-specific interactions with the hydrogel-polymer chains. Predicted diffusion coefficients are in good agreement with experiment using no adjustable parameters. Our new framework provides *a priori* quantitative prediction of specifically interacting solute uptake and release rates in hydrogels.

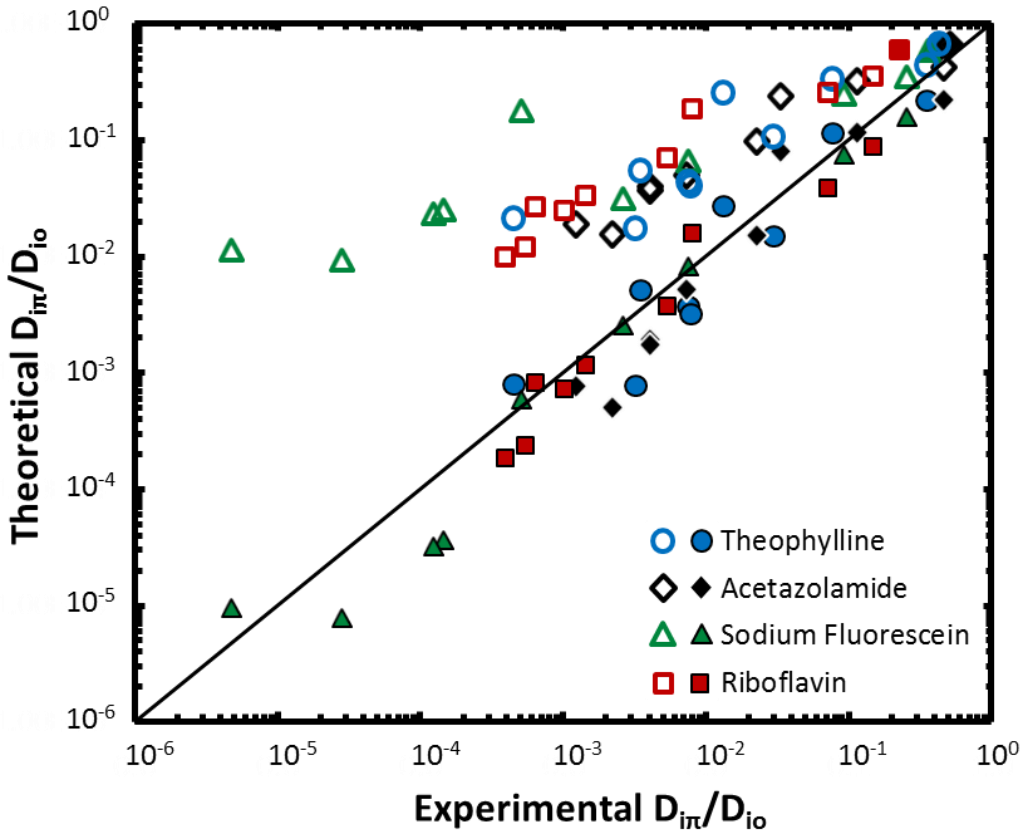

Figure 4.3: Parity plot of theoretical and experimental relative solute diffusion coefficients, $D_{i\pi} / D_{io}$ for acetazolamide (diamonds), sodium fluorescein (triangles), theophylline (circles), and riboflavin (squares), in HEMA/MAA hydrogels. Closed and open symbols denote predictions from Eq. 1 with adsorption (i.e., K_{ij} specified by EFPT) and without adsorption (i.e., $K_{ij} = 0$ for all j), respectively.

4.3 Acknowledgements

The authors thank the CRL Molecular Imaging Center and NIH grant number 3R01EY015514-01S1 for use of the fluorescence confocal microscope. The authors also thank Xiaoyi Li and Ryan Sawadichai for performing several of the UV/Vis-absorption spectrophotometry measurements.

4.4 References

1. Dursch, T. J.; Taylor, N. O.; Liu, D. E.; Wu, R. Y.; Prausnitz, J. M.; Radke, C. J. Water-soluble drug partitioning and adsorption in HEMA/MAA hydrogels. *Biomaterials* **2014,** 35, (2), 620-629.
2. Liu, D. E.; Kotsmar, C.; Nguyen, F.; Sells, T.; Taylor, N. O.; Prausnitz, J. M.; Radke, C. J. Macromolecule sorption and diffusion in HEMA/MAA hydrogels. *Industrial & Engineering Chemistry Research* **2013,** 52, (50), 18109-18120.
3. Kotsmar, C.; Sells, T.; Taylor, N.; Liu, D. E.; Prausnitz, J. M.; Radke, C. J. Aqueous solute partitioning and mesh size in HEMA/MAA hydrogels. *Macromolecules* **2012,** 45, (22), 9177-9187.
4. Liu, D. E.; Dursch, T. J.; Oh, Y.; Bregante, D. T.; Chan, S. Y.; Radke, C. J. Equilibrium water and solute uptake in silicone hydrogels. *Acta Biomaterialia* **2015,** 18, 112-117.
5. Peppas, N. A.; Bures, P.; Leobandung, W.; Ichikawa, H. Hydrogels in pharmaceutical formulations. *European Journal of Pharmaceutics and Biopharmaceutics* **2000,** 50, (1), 27-46.
6. Peppas, N. A. Hydrogels and drug delivery. *Current Opinion in Colloid & Interface Science* **1997,** 2, (5), 531-537.
7. Dursch, T. J.; Liu, D. E.; Oh, Y.; Radke, C. J. Fluorescent solute-partitioning characterization of layered soft contact lenses. *Acta Biomaterialia* **2015,** 15, 48-54.
8. Gupta, P.; Vermani, K.; Garg, S. Hydrogels: From controlled release to pH-responsive drug delivery. *Drug Discovery Today* **2002,** 7, (10), 569-579.
9. Peng, C.-C.; Burke, M. T.; Chauhan, A. Transport of topical anesthetics in vitamin E loaded silicone hydrogel contact lenses. *Langmuir* **2011,** 28, (2), 1478-1487.
10. Kim, J.; Chauhan, A. Dexamethasone transport and ocular delivery from poly (hydroxyethyl methacrylate) gels. *International Journal of Pharmaceutics* **2008,** 353, (1), 205-222.
11. Stringer, J. L.; Peppas, N. A. Diffusion of small molecular weight drugs in radiation-crosslinked poly (ethylene oxide) hydrogels. *Journal of Controlled Release* **1996,** 42, (2), 195-202.
12. Bettini, R.; Colombo, P.; Peppas, N. A. Solubility effects on drug transport through pH-sensitive, swelling-controlled release systems: Transport of theophylline and metoclopramide monohydrochloride. *Journal of Controlled Release* **1995,** 37, (1–2), 105-111.

13. Kapoor, Y.; Thomas, J. C.; Tan, G.; John, V. T.; Chauhan, A. Surfactant-laden soft contact lenses for extended delivery of ophthalmic drugs. *Biomaterials* **2009,** 30, (5), 867-878.

14. Am Ende, M. T.; Peppas, N. A. Transport of ionizable drugs and proteins in crosslinked poly (acrylic acid) and poly (acrylic acid-co-2-hydroxyethyl methacrylate) hydrogels. II. Diffusion and release studies. *Journal of Controlled Release* **1997,** 48, (1), 47-56.

15. Eckmann, D. M.; Composto, R. J.; Tsourkas, A.; Muzykantov, V. R. Nanogel carrier design for targeted drug delivery. *Journal of Materials Chemistry B* **2014,** 2, (46), 8085-8097.

16. Lee, K. Y.; Mooney, D. J. Hydrogels for tissue engineering. *Chemical Reviews* **2001,** 101, (7), 1869-1880.

17. Drury, J. L.; Mooney, D. J. Hydrogels for tissue engineering: scaffold design variables and applications. *Biomaterials* **2003,** 24, (24), 4337-4351.

18. Khademhosseini, A.; Langer, R. Microengineered hydrogels for tissue engineering. *Biomaterials* **2007,** 28, (34), 5087-5092.

19. Kim, J. J.; Park, K. Smart hydrogels for bioseparation. *Bioseparation* **1998,** 7, (4-5), 177-184.

20. Roy, I.; Gupta, M. N. Smart polymeric materials: Emerging biochemical applications. *Chemistry & Biology* **2003,** 10, (12), 1161-1171.

21. Brahim, S.; Narinesingh, D.; Guiseppi-Elie, A. Bio-smart hydrogels: co-joined molecular recognition and signal transduction in biosensor fabrication and drug delivery. *Biosensors and Bioelectronics* **2002,** 17, (11), 973-981.

22. Lin, G.; Chang, S.; Hao, H.; Tathireddy, P.; Orthner, M.; Magda, J.; Solzbacher, F. Osmotic swelling pressure response of smart hydrogels suitable for chronically implantable glucose sensors. *Sensors and Actuators B: Chemical* **2010,** 144, (1), 332-336.

23. Lin, G.; Chang, S.; Kuo, C.-H.; Magda, J.; Solzbacher, F. Free swelling and confined smart hydrogels for applications in chemomechanical sensors for physiological monitoring. *Sensors and Actuators B: Chemical* **2009,** 136, (1), 186-195.

24. Liu, J. Oligonucleotide-functionalized hydrogels as stimuli responsive materials and biosensors. *Soft Matter* **2011,** 7, (15), 6757-6767.

25. Yao, H.; Shum, A. J.; Cowan, M.; Lähdesmäki, I.; Parviz, B. A. A contact lens with embedded sensor for monitoring tear glucose level. *Biosensors and Bioelectronics* **2011,** 26, (7), 3290-3296.

26. Badugu, R.; Lakowicz, J. R.; Geddes, C. D. A glucose sensing contact lens: A non-invasive technique for continuous physiological glucose monitoring. *Journal of Fluorescence* **2003,** 13, (5), 371-374.

27. Amsden, B. Solute diffusion in hydrogels: An examination of the retardation effect. *Polymer Gels and Networks* **1998,** 6, (1), 13-43.

28. Phillips, R. J. A hydrodynamic model for hindered diffusion of proteins and micelles in hydrogels. *Biophysical Journal* **2000,** 79, (6), 3350-3353.

29. Johansson, L.; Elvingson, C.; Skantze, U.; Löfroth, J. E. Diffusion and interaction in gels and solutions. In *Trends in Colloid and Interface Science VI*, Helm, C.; Lösche, M.; Möhwald, H., Eds. Springer: New York, 1992; pp 25-29.

30. Ogston, A. G.; Preston, B. N.; Wells, J. D. On the transport of compact particles through solutions of chain-polymers. *Proceedings of the Royal Society of London. A. Mathematical and Physical Sciences* **1973,** 333, (1594), 297-316.

31. Johnson, E. M.; Berk, D. A.; Jain, R. K.; Deen, W. M. Hindered diffusion in agarose gels: test of effective medium model. *Biophysical Journal* **1996,** 70, (2), 1017-1023.

32. Tong, J.; Anderson, J. L. Partitioning and diffusion of proteins and linear polymers in polyacrylamide gels. *Biophysical Journal* **1996,** 70, (3), 1505-1513.

33. Peppas, N. A.; Reinhart, C. T. Solute diffusion in swollen membranes: Part I. A new theory. *Journal of Membrane Science* **1983,** 15, (3), 275-287.

34. Amsden, B. Solute diffusion within hydrogels: Mechanisms and models. *Macromolecules* **1998,** 31, (23), 8382-8395.

35. Phillips, R. J.; Deen, W. M.; Brady, J. F. Hindered transport in fibrous membranes and gels: Effect of solute size and fiber configuration. *Journal of Colloid and Interface Science* **1990,** 139, (2), 363-373.

36. Bosma, J. C.; Wesselingh, J. A. Partitioning and diffusion of large molecules in fibrous structures. *Journal of Chromatography B: Biomedical Sciences and Applications* **2000,** 743, (1), 169-180.

37. Wu, J.; Sassi, A. P.; Blanch, H. W.; Prausnitz, J. M. Partitioning of proteins between an aqueous solution and a weakly-ionizable polyelectrolyte hydrogel. *Polymer* **1996,** 37, (21), 4803-4808.

38. Merrill, E. W.; Dennison, K. A.; Sung, C. Partitioning and diffusion of solutes in hydrogels of poly(ethylene oxide). *Biomaterials* **1993,** 14, (15), 1117-1126.

39. Bengani, L. C.; Leclerc, J.; Chauhan, A. Lysozyme transport in p-HEMA hydrogel contact lenses. *Journal of Colloid and Interface Science* **2012,** 386, (1), 441-450.

40. Russell, S. M.; Belcher, E. B.; Carta, G. Protein partitioning and transport in supported cationic acrylamide-based hydrogels. *AIChE Journal* **2003,** 49, (5), 1168-1177.

41. Rossi, F.; Castiglione, F.; Ferro, M.; Marchini, P.; Mauri, E.; Moioli, M.; Mele, A.; Masi, M. Drug–polymer interactions in hydrogel-based drug-delivery systems: An experimental and theoretical study. *ChemPhysChem* **2015,** 16, (13), 2818-2825.

42. Hadjiev, N. A.; Amsden, B. G. An assessment of the ability of the obstruction-scaling model to estimate solute diffusion coefficients in hydrogels. *Journal of Controlled Release* **2015,** 199, 10-16.

43. Johansson, L.; Elvingson, C.; Löfroth, J. E. Diffusion and interaction in gels and solutions. 3. Theoretical results on the obstruction effect. *Macromolecules* **1991,** 24, (22), 6024-6029.

44. Clague, D. S.; Phillips, R. J. Hindered diffusion of spherical macromolecules through dilute fibrous media. *Physics of Fluids* **1996,** 8, 1720.

45. Shin, H. S.; Kim, S. Y.; Lee, Y. M.; Lee, K. H.; Kim, S. J.; Rogers, C. E. Permeation of solutes through interpenetrating polymer network hydrogels composed of poly(vinyl alcohol) and poly(acrylic acid). *Journal of Applied Polymer Science* **1998,** 69, (3), 479-486.

46. Bird, R. B.; Stewart, W. E.; Lightfoot, E. N. *Transport phenomena*. 2nd ed.; Wiley: New York, 2006.

Appendix 4A: Supporting Information

S1. Hydrogel Synthesis and Characterization

Hydrogel synthesis and equilibrium water contents. Detailed hydrogel-synthesis, and water-content-measurement are provided in Dursch et al.[1] Here, we briefly summarize. HEMA/MAA hydrogels were synthesized by simultaneous copolymerization and cross-linking of monomers in aqueous solution with EGDMA as the cross-linking agent.[1-3] Aqueous synthesis mixtures consisted of varying HEMA:MAA ratio (100:0, 99:1, 90:10, 70:30, and 0:100), 0.25 wt % EGDMA, 0.5 wt % 4,4'-azobis(4-cyanovaleric acid), and 30 wt % DI water. All percentages are of total monomer. Following free-radical polymerization, hydrogels were swollen or deswollen in excess aqueous buffered saline solutions of varying pH, but with equal ionic strength: phosphate-buffered saline solution (PBS; pH 7.4; 0.017 M $Na_2HPO_4 \cdot 7H_2O$, 0.003 M $NaH_2PO_4 \cdot H_2O$, 0.15 M NaCl,)[1-3] and dilute HCl (pH 2; 0.02 M HCl, 0.15 M NaCl). Solutions were changed daily for a minimum of 3 d to ensure equilibrium with the surrounding solution.

S2. Solute Diffusion-Coefficient Measurements

Solute loading. Equilibrium swollen hydrogels were soaked for a minimum of 2 d in solute solutions with a solution-to-hydrogel volume ratio of 250. Initial loading concentrations for sodium fluorescein were 1×10^{-5} M and 1×10^{-7} M in PBS and HCl solutions, respectively. Initial loading concentrations for riboflavin, theophylline, acetazolamide were 1×10^{-5} M, 6×10^{-3} M and 2×10^{-3} M, respectively, in both PBS and HCl. At these dilute concentrations, solute uptake had no measurable effect on hydrogel water content. To ensure equilibrium solute uptake, solute loading time was increased till no change was observed in solute partition coefficients measured according to Dursch et al[1].

Two-Photon Fluorescence Confocal Microscopy. Sodium fluorescein and riboflavin diffusion coefficients in the studied hydrogels were obtained by solute desorption measurements with two-photon laser-scanning confocal microscopy as described in Liu et al.[2] Transient concentration profiles were measured using a Carl Zeiss (Jena, Germany) 510 LSM META NLO AxioImager Confocal Microscope equipped with a Spectra-Physics (Santa Clara, CA) MaiTai HP DeepSee Laser set at 780 nm. In short, equilibrium solute-loaded hydrogel slabs (6 mm x 6 mm, 100-800 μm thick) were each placed in a large bath of pertinent solute-free aqueous solution (PBS or HCl) under magnetic stirring at 400 rpm. Hydrogel slab thicknesses (100-800 μm) were chosen to allow suitable time scales for measurement (between 10 min and 1 week). At selected times, a gel slab was removed from solution, set on a microscope slide, and covered with a cover slip to prevent evaporation. Scanning was performed in the center at 3-μm intervals through the entire gel thickness and resulting micrographs were converted into intensity profiles. At the dilute concentrations employed, fluorescence intensity is linearly proportional to dye concentration.[2] Figure 4A.1 displays typical fluorescence intensity as a function of position for sodium fluorescein desorbing from a 10 wt% MAA hydrogel at varying release times. The distance scale denotes top to bottom of the hydrogel slab. Profile shapes are characteristic of desorption. Intensity profiles are not perfectly symmetric due to signal attenuation.[2]

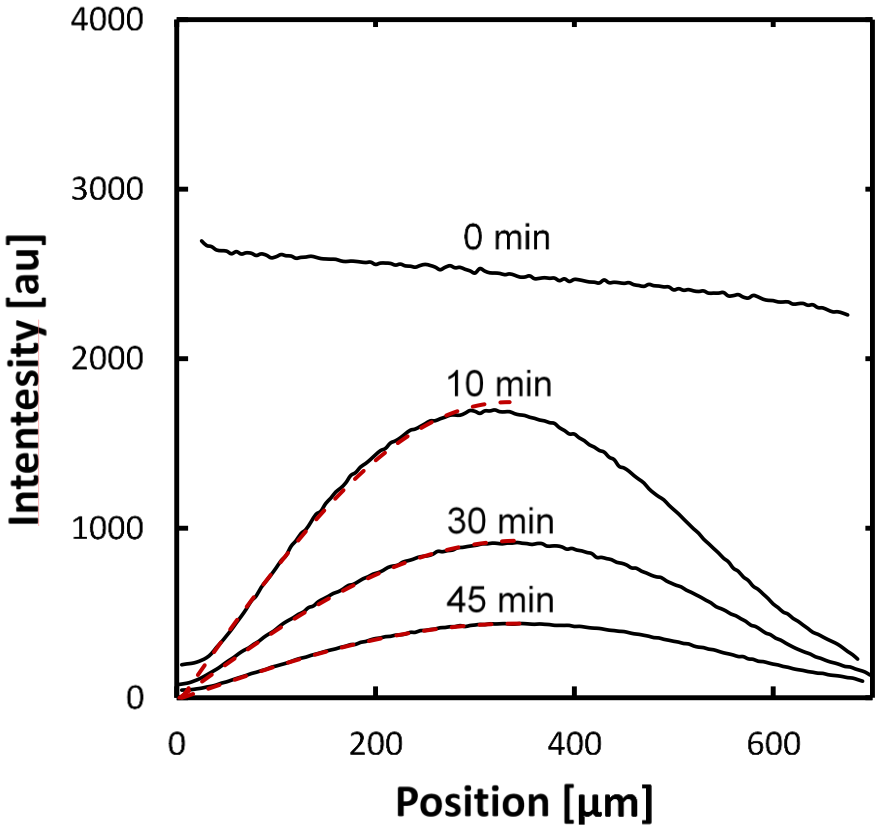

Figure 4A.1: Transient intensity profiles of sodium fluorescein desorption from a 10 wt% MAA hydrogel. Solid and dashed lines represent measured profiles and least-square fits to Fick's second law, respectively.

To describe the rates of solute release from hydrogels, we utilize Fick's second law

$$\frac{\partial C_i^{gel}}{\partial t} = D_{i\pi} \frac{\partial^2 C_i^{gel}}{\partial x^2} \qquad -L < x < L \qquad (4A.1)$$

where C_i^{gel} is the solute concentration of dilute solute *i* in the hydrogel, $D_{i\pi}$ is the overall solute diffusion coefficient through the gel, and *x* is the spatial coordinate for a hydrogel thickness of 2L with x = 0 at the center of the hydrogel slab. $C_i^{gel}(-L,t) = 0$, since we assume the concentration at the edge of the gel is in equilibrium with the surrounding aqueous release solution, and the latter is in excess and devoid of solute. $\frac{\partial C_i^{gel}(0,t)}{\partial x} = 0$, since profiles are symmetric about the center of the gel. Initially, $C_i^{gel}(t,0) = C_{i0}^{gel}$, where C_{i0}^{gel} is the final solute concentration in a hydrogel in equilibrium with aqueous solute loading solution (i.e., $C_{i0}^{gel} = k_i C_i^{load}$ where k_i is the solute partition coefficient in the hydrogel and C_i^{load} is the solute concentration of the aqueous loading solution). Integration of Eq. 4A.1 with the boundary and initial conditions specified gives

$$\frac{C_i^{gel}(t,x)}{C_{i0}^{gel}} = \sum_{n=0}^{\infty} A_n(t,x) \qquad (4A.2)$$

where $A_n(t,x) = 2\frac{(-1)^n}{\lambda_n}\exp[-\lambda_n^2 D_{i\pi} t / L^2]\cos[\lambda_n x / L]$ and $\lambda_n = (2n+1)\pi/2$.[2] Overall solute-hydrogel diffusion coefficients are obtained by fitting Eq. 4A.2 to fluorescent-solute intensity profiles by least squares error minimization as described in Liu et al.[2]

Back Extraction with UV/Vis-absorption Spectrophotometry. Theophylline and acetazolamide diffusion coefficients in the hydrogels were determined through desorption with back extraction. Back-extraction solution concentration histories were measured with UV/Vis-absorption spectrophotometry by a procedure adapted from Dursch et al.[1] An Ocean Optics spectrophotometer (Model ADC-1000, Dunedin, FL) equipped with a deuterium UV/Vis DH-2000 light source was employed for aqueous solution absorbance measurement. Equilibrium solute-loaded hydrogels (6 mm x 6 mm, 100-800 μm thick) were removed from their loading solution, lightly blotted on both sides, and immediately placed in a large volume of pertinent solute-free aqueous solution (PBS or HCl) under magnetic stirring at 400 rpm. Typical release-solution-to-hydrogel volume ratios ranged from 20 to 2000 and were set for accurate measurement of release solution concentration. Transient back-extraction solution concentrations were measured by periodically removing 2 mL of solvent and measuring previously calibrated solution absorbance at 220–250 nm in a 4-mm wide UV quartz cuvette (path length 10 mm). To account for minor fluctuations in the detected absorbance, multiple measurements (n = 3) were taken of each sample and averaged. Following measurement, each 2-mL samples was returned to the release solution to maintain constant solution volume.

Figure 4A.2 displays typical back-extraction-solution concentrations as a function of time for theophylline desorbing from a 10 wt% MAA hydrogel. Concentration history shape is typical for desorption. At early times, solute concentration in the back-extraction solution increases notably as theophylline is released from the hydrogel. At later times, solute concentration in the back-extraction solution plateaus to the equilibrium value as the hydrogel equilibrates with the surrounding solution.

To describe solute release rates from the hydrogel, Fick's second law is again applied under the same boundary and initial conditions as described above. The release-solution-to-hydrogel volume ratios employed were set large enough to impose the perfect-sink boundary condition. Mass balance dictates the accumulation of solute in the surrounding back-extraction solution is equal to the amount of solute released from the gel, or

$$V^S \frac{dC_i^S}{dt} = \frac{2V^{gel}}{L}\left[-D_{i\pi}\frac{\partial C_i^{gel}}{\partial x}\right]_{x=L}, \qquad (4A.3)$$

where C_i^S is the solute concentration of dilute solute *i* in the back extraction solution, V^S and V^{gel} are the volumes of the back extraction solution and of the hydrogel slab, respectively and $\left[-D_{i\pi}\frac{\partial C_i^{gel}}{\partial x}\right]_{x=L}$ is the flux of solute desorbing from a face of the hydrogel slab. Substituting Eq. 4A.2 into 4A.3 and integrating over time yields

$$\frac{C_i^S(t)}{C_i^S(t=\infty)} = \sum_{n=0}^{\infty}\frac{1-\exp\left[-\left(\frac{(2n+1)\pi}{2}\right)^2\frac{D_{i\pi}t}{L^2}\right]}{(2n+1)^2}, \qquad (4A.4)$$

where $C_i^S(t=\infty)$ is the equilibrium back-extraction-solution concentration. Overall solute-hydrogel diffusion coefficients are obtained by fitting Eq. 4A.4 to solute concentration histories utilizing least-squares error minimization.

To ensure that our results are independent of the experimental technique employed, select riboflavin and sodium fluorescein diffusion coefficients at both aqueous pH were obtained by both UV/Vis-absorption spectrophotometry and two-photon confocal microscopy. Consistency was confirmed as both UV/Vis-absorption spectrophotometry and two-photon confocal microscopy yielded nearly identical solute diffusion coefficients (i.e., within experimental error).

S3. Theory

Available models for aqueous solute diffusion in hydrogels almost exclusively consider nonspecific interactions and predict diffusion through the water filled meshes of the hydrogel network. However, specific-solute complexation with hydrogel copolymer strands further reduces diffusion rates. We desire a relation to extend existing models and predict overall diffusion coefficients in hydrogels where specific solute adsorption is pronounced. For this

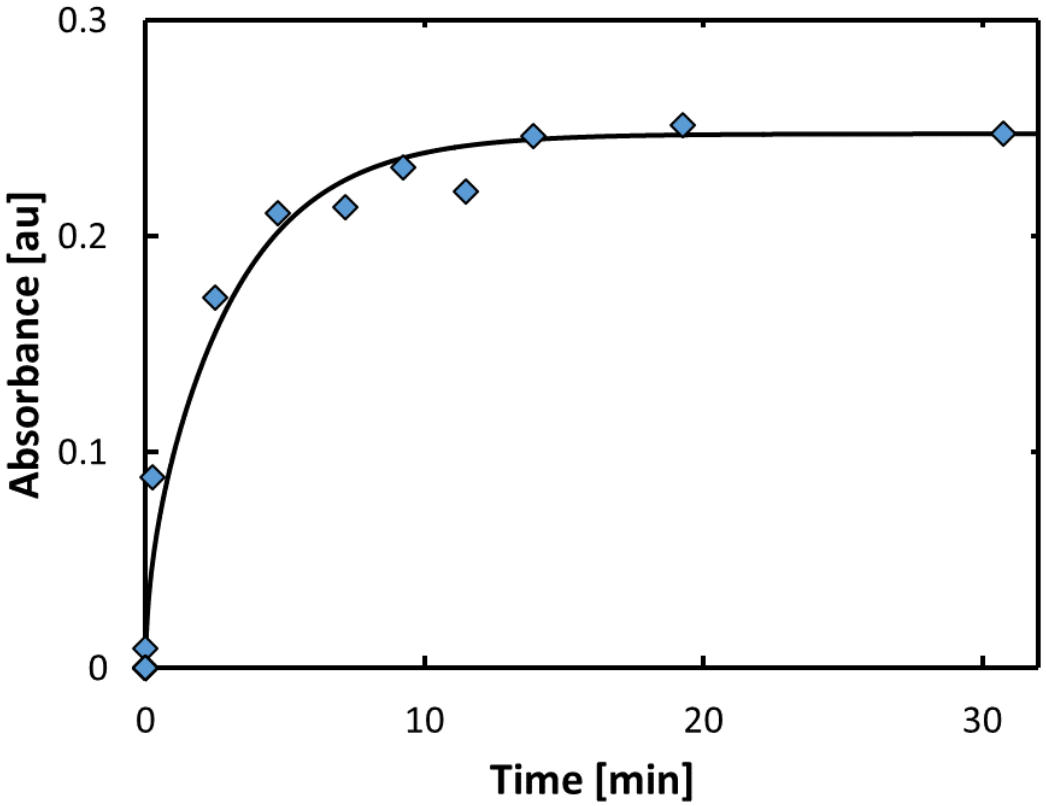

Figure 4A2: Release solution absorbance as a function of time for theophylline desorption from a 10 wt% MAA hydrogel. The solid line represents a least-squares fit to Fick's second law.

task, it proves useful to discriminate between solute diffusing in the water filled voids and solute adsorbed onto each hydrogel-copolymer component or,

$$C_i^{gel} = \sum_j \varphi_{2,j} n_{ij} + \varphi_1 C_i^L \tag{4A.5}$$

where ϕ_{2j} is the volume fraction of polymer component *j*, ϕ_1 is the water volume fraction, and n_{ij} and C_i^L are the concentrations of solute *i* specifically adsorbed to hydrogel polymer strands and diffusing through the water-filled meshes, respectively. Extending Fick's second law with this classification yields

$$\sum_j \varphi_{2,j} \frac{\partial n_{ij}}{\partial t} + \varphi_1 \frac{\partial C_i^L}{\partial t} = \varphi_1 D_i \frac{\partial^2 C_i^L}{\partial x^2} \tag{S6}$$

where D_i is the diffusion coefficient through the water-filled meshes of the hydrogel network. Here, we assume diffusion along the polymer strands is negligible. To describe the kinetics of solute adsorption to each hydrogel copolymer type, we impose local equilibrium with Henry's adsorption, or $n_{ij} = K_{ij} C_i^L$, where K_{ij} is the Henry's adsorption constant of the diffusing solute *i* to polymer component *j*. Upon substitution of Henry's law for each copolymer component into Eq. 4A.6, an overall effective diffusion coefficient arises, or

$$D_{i\pi} = \frac{D_i}{1 + \sum_j K_{ij} \varphi_{2j} / \varphi_1} \tag{S7}$$

Normalizing Eq. 4A.7 by the solute diffusion coefficient in bulk solution, D_{io}, and expressing D_i / D_{io} as a product of hydrodynamic and steric resistance factors yields Eq. 1 of the main text. Following Liu et al.,[2] D_i / D_{io} is calculated *a priori* using Large-Pore Effective Medium (LPEM) Theory with an average polymer fiber radius of, a_f = 2 nm, and hydrodynamic tortuosity of, τ_H = 4.7, both determined through independent measurement.[2,3] Following Dursch et al.,[1] K_{ij} are obtained for all *j* by applying Enhancement Factor Partitioning Theory (EFPT) to the partitioning data in Table 4.1. Table 4A.1 displays Henry's Adsorption constants calculated from EFPT. With D_i / D_{io} determined and K_{ij} specified for all *j*, overall solute diffusion coefficients may be predicted using no adjustable parameters.

Table 4A.1: Henry's Adsorption Constant (dimensionless)

Solute	$K_{i\,HEMA}$ [c]	$K_{i\,MAA-}$ [d]	$K_{i\,MAA}$ [e]
Theophylline [a]	7.5 / 7.5	0	21
Acetazolamide [a]	6.5 / 13	0	5
Riboflavin [b]	21 / 21	0	26
Sodium fluorescein [a]	8.5 / ~455	0	~730

[a]from Dursch et al.[1]

[b]measured by two-photon confocal microscopy with 780 nm excitation according to Dursch et al.[1]

[c]Table entries separated by a diagonal represent k_i measured in PBS (pH 7.4) or HCl (pH 2)

[d]In PBS (pH 7.4)

[e]In HCl (pH 2)

Chapter 5

Equilibrium Water and Solute Uptake in Silicone Hydrogels

5.1 Abstract

Equilibrium water content of and solute partitioning in silicone hydrogels (SiHys) are investigated using gravimetric analysis, fluorescence confocal laser-scanning microscopy (FCLSM), and back extraction with UV/Vis-absorption spectrophotometry. Synthesized silicone hydrogels consist of silicone monomer, hydrophilic monomer, cross-linking agent, and a triblock-copolymer macromer used as an amphiphilic compatibilizer to prevent macrophase separation. In all cases, immiscibility of the silicone and hydrophilic polymers results in microphase-separated morphologies. To investigate solute uptake in each of the SiHy microphases, equilibrium partition coefficients are obtained for two hydrophilic solutes (i.e., theophylline and caffeine dissolved in aqueous phosphate-buffered saline) and two oleophilic solutes (i.e., Nile Red and Bodipy Green dissolved in silicone oil), respectively. Measured water contents and aqueous-solute partition coefficients increase linearly with increasing solvent-free hydrophilic-polymer volume fraction. Conversely, oleophilic-solute partition coefficients decrease linearly with rising solvent-free hydrophilic-polymer volume fraction (i.e., decreasing hydrophobic silicone-polymer fraction). We quantitatively predict equilibrium SiHy water and solute uptake assuming that water and aqueous solutes reside only in hydrophilic microdomains, whereas oleophilic solutes partition predominately into silicone microdomains. Predicted water contents and solute partition coefficients are in excellent agreement with experiment. Our new procedure permits a priori estimation of SiHy water contents and solute partition coefficients based solely on properties of silicone and hydrophilic homopolymer hydrogels, eliminating the need for mixed-polymer-hydrogel experiments.

Reprint of Liu, D. E.*; Dursch, T. J.*; Oh, Y.; Bregante, D. T.; Chan, S. Y.; Radke, C. J. *Acta Biomaterialia* **2015,** 18, 112-117.
*authors contributed equally

5.2 Introduction

Silicone-hydrogel (SiHy) soft contact lenses (SCLs) are an important alternative to conventional hydrogel SCLs (i.e., lenses composed of only hydrophilic polymers, typically 2-hydroxyethyl methacrylate (HEMA)). Compared to conventional hydrogel SCLs, SiHy lenses allow six to ten times larger corneal oxygen supply, providing improved ocular health, especially for extended wear.[1-5] To date, SiHy SCLs have significantly reduced several serious hypoxia-related problems such as red eye, cornea swelling, and eye discomfort.[3-5] Accordingly, about two thirds of all contact lenses prescribed between 2011 and 2013 in the United States were silicone based.[6-8]

Despite the importance of SiHy SCLs, their phase structure and morphology are not well understood.[4] It is commonly accepted that distinct phases occur in various morphologies due to immiscibility of the silicone and hydrophilic polymers. Two typical examples include dispersions[4] (with microdomains isolated within a continuous phase) and co-continuous networks.[4,9] Conventional wisdom is that for SCL on-eye wear, the SiHy structure must contain interconnected silicone domains for sufficient oxygen permeability, as well as a co-continuous ion-conducting water phase localized within the hydrophilic-polymer domains.[1-4,10-13]

Hydrophilic-domain water uptake largely dictates mechanical and transport properties (e.g., lubricity, elasticity, aqueous solute uptake, and ion/water permeability) that contribute directly to lens performance.[1-4,10-18] For example, water content must be large enough to provide sufficient lubricity for comfortable wear and sufficient salt permeability for prevention of corneal lens-adherence.[13,17,19,20] However, if the lens water fraction is too large, mechanical stability may be compromised due to lack of polymer volume, rendering the material unsuitable as a SCL. Additionally, an increase in water content through an increase in hydrophilic-phase fraction must be accompanied by a decrease in silicone-phase fraction that may compromise oxygen permeability.[1-4,11]

Hydrophilic-domain water uptake also governs loading and release of water-soluble drugs, tear-film components, preservatives, and wetting agents.[11,13-15,18,21-24] When on eye, SCLs are continually exposed to and uptake tear-film components, such as proteins, lipids, mucins, and salts. During wear, SCLs release pre-impregnated drugs, preservatives, and wetting agents in the form of salts, polymers, and polymeric surfactants. In either case, absorbed solutes may result in beneficial effects, such as improved wettability and comfort, or harmful effects, such as contamination and loss of comfort. All else being equal, higher water content, reflective of larger water-filled hydrophilic domains, leads to greater partitioning of aqueous solutes into SCLs.[13-15,18,21-24] However, with higher water content, oleophilic solutes (with low water solubility) partition less, due to a decrease in the hydrophobic silicone-phase fraction.

Because of their importance, significant effort has been expended towards predicting SCL hydrogel water content[25-29] and solute partitioning.[11,13-15,18,21-24] Water-content predictions typically modify Flory-Rehner theory, where hydrogel swelling arises from a balance between the tendency of the polymer to dissolve in the aqueous phase and elasticity of the cross-linked network that opposes dissolution. With water content specified, solute-partition-coefficient models then account for solute/hydrogel-network interactions including: size exclusion, electrostatic interaction, and specific adsorption onto the polymer strands.[14] Currently, however, all systems where equilibrium water or solute uptake is predicted are

conventional hydrogels (i.e., those containing no silicone).[11,13-15,18,21-29] To our knowledge, no studies attempt prediction of water content or solute partitioning in SiHys.

This work reports experimental and theoretical equilibrium water content and solute uptake in thirty SiHys over a wide range of hydrogel compositions and water contents (3 to 82%). Silicone hydrogels are synthesized using thermally initiated free-radical polymerization, and consist of silicone monomer, hydrophilic monomer, cross-linking agent, and a triblock-copolymer macromer used as an amphiphilic compatibilizer to prevent macrophase separation. Equilibrium water contents and partition coefficients of four solutes are measured using gravimetric analysis, fluorescence confocal laser-scanning microscopy, and back extraction with UV/Vis-absorption spectrophotometry. SiHy equilibrium water contents are predicted assuming that water is localized within the hydrophilic-polymer domains. Therefore, aqueous solutes (with high water solubility) primarily partition into water-swollen hydrophilic microphases. Conversely, oleophilic solutes (with low water solubility) largely partition into hydrophobic silicone microdomains. To account for aqueous-solute size exclusion in the hydrophilic phase and oleophilic-solute specific adsorption in the silicone phase, enhancement-factor partitioning theory is adopted.[14] In all cases, predicted water contents and solute partition coefficients are in excellent agreement with experiment.

5.3 Materials and Methods

5.3.1 Chemicals

Synthesized silicone hydrogels (SiHys) consist of silicone monomer, amphiphilic macromer, hydrophilic monomer, cross-linking agent, thermoinitiator, and solvent. Silicone monomers, 3-methacryloxypropyltris(trimethylsiloxy)silane (97 %, TRIS, Cat. No. 1713, Lot 1713-020514), and methacryloxypropyl-terminated polydimethylsiloxane (97+ %, M-PDMS, 8-14 cSt, Cat. No. DMS-R11, Lot 3J-21494) were acquired from Silar Laboratories (Wilmington, NC) and Gelest Inc. (Morrisville, PA), respectively. The amphiphilic macromer acryloxy-terminated ethyleneoxide dimethylsiloxane-ethyleneoxide ABA triblock copolymer (95+ %, DBE-U12, 80-120 cSt, Cat. No. DBE-U12) was purchased from Gelest Inc., and used to prevent macrophase separation. Sigma Aldrich (St. Louis, MO) provided all other chemicals used in SiHy preparation: hydrophilic monomers: 2-hydroxyethyl methacrylate (97 %, HEMA, Cat. No. 128635-500G) and methacrylic acid (99 %, MAA, Cat. No. 155721-500G); cross-linking agent: ethylene glycol dimethacrylate (98 %, EGDMA, 335681-100ML); thermoinitiator: 4,4'-azobis (4-cyanovaleric acid) (98+ %, Cat. No. 11590-100G); and solvent: ethanol (99.5+ %, Cat. No. 459844-1L). Following free-radical polymerization, hydrogels were swollen for a minimum of 3 d in pH 7.4 phosphate-buffered saline solution (PBS) prepared as described previously.[14-16]

PBS was used as the solvent for the hydrophilic solutes: theophylline (99+ %, Sigma Aldrich, Cat. No. T1633-50G) and caffeine (99+ %, Sigma Aldrich, Cat. No. C0750-100G), whereas silicone oil (500 cSt, Fisher Scientific, Pittsburgh, PA, Cat. No. S159-500) was used as the solvent for the oleophilic fluorescent solutes: Nile Red (99 %, Life Technologies, Grand Island, NY, Cat. No. N-1142) and 4,4-Difluoro-1,3,5,7,8-Pentamethyl-4-Bora-3a,4a-Diaza-s-Indacene (99 %, Bodipy Green, Life Technologies, Cat. No. D-3922). Initial loading concentrations for the hydrophilic and oleophilic solutes were 6×10^{-3} and 1×10^{-5} M, respectively. Molecular weights and hydrodynamic radii of the four solutes are similar (i.e.,

190 to 315 Da and 0.3 to 0.58 nm).[14,18] All solutes are nonionic at pH 7.4. All chemicals were used as received. Water- and solute-uptake measurements were performed at ambient temperature.

5.3.2 Hydrogel Synthesis

SiHys were synthesized using thermally initiated free-radical polymerization and cross-linking of monomers and macromer in ethanol. Hydrogel composition was varied by altering the relative amounts of silicone monomer (i.e., TRIS or M-PDMS), macromer, and hydrophilic monomer (i.e., HEMA, MAA, or a mixture of 10 vol % MAA and 90 vol % HEMA denoted as 10%MAA/90%HEMA) in the volume ratios reported in Table 5.1. Typical reaction solutions consisted of monomer, macromer, 0.25 vol % EGDMA, 0.5 wt % 4,4'-azobis(4-cyanovaleric acid), and 50 vol % ethanol, where percentages are of total monomer plus macromer. Hydrogels are referred to by their corresponding solvent-free volume fraction of hydrophilic monomer, ν_{hyphil}, where the volume fraction of hydrophilic monomer, macromer ($\nu_{macromer}$), and hydrophobic monomer (ν_{hyphob}) sum to unity (i.e., $1 = \nu_{hyphil} + \nu_{macromer} + \nu_{hyphob}$). The reaction mixture was stirred magnetically until full dissolution of the thermoinitiator. Subsequently, nitrogen gas was bubbled through the solution for 15 min to remove dissolved oxygen. The stripped reaction mixture was injected between two upright glass plates separated by a 250-µm spacer, and previously hydrophobized with RainX® Original (Sopus Products, Houston, TX). Free-radical, thermally initiated polymerization took place in an oven whose temperature was raised from 65 to 75 °C over a 60-min period and then maintained at 75 °C for 60 min. When cooled, all hydrogels were boiled in DI water for at least 30 min to remove unreacted constituents. Experiments performed where ethanol was used as an extraction solvent yielded identical equilibrium water contents and solute partition coefficients as when boiling water was used indicating negligible unreacted silicone monomer. Following synthesis, all hydrogels were swollen for a minimum of 3 d in PBS (changing the solution daily). In PBS (pH 7.4), MAA moieties are fully ionized.[14-16]

Table 5.1: SiHy Composition and Hydrophilic-Monomer Volume Fraction, ν_{hyphil}

Constituent Volume Parts			ν_{hyphil}
[a] Silicone Monomer	Macromer	[b] Hydrophilic Monomer	
10	1	1	0.08
5	1	1	0.14
1	1	1	0.33
1	1	5	0.71
1	1	10	0.83

[a] TRIS or M-PDMS
[b] HEMA, MAA, or 10%MAA/90%HEMA

5.3.3 *Equilibrium Water Content*

Following others,[13-16,18,25] hydrogel equilibrium water content, approximately the water volume fraction, ϕ_1, was obtained gravimetrically. To determine water content, swollen 9-mm diameter SiHy discs were weighed in the PBS-equilibrated (m_{wet}) and ambient-temperature dry (m_{dry}) states. Let $\Delta m_1 \equiv m_{wet} - m_{dry}$. Equilibrium water volume fraction is given by

$$\phi_1 = \frac{\Delta m_1 / \rho_1}{\Delta m_1 / \rho_1 + m_{dry} / \rho_{dry}}, \tag{1}$$

where ρ is mass density, and subscripts *1, wet,* and *dry* denote water, swollen hydrogel, and dry hydrogel, respectively. In Eq. 1, ϕ_1 is approximately water content, since $\rho_1 \approx \rho_{dry}$. Equilibrium water-uptake measurements were performed in triplicate.

5.3.4 *Equilibrium Solute Partition Coefficients*

Aqueous-solute (i.e., theophylline and caffeine) partition coefficients in the SiHys were measured using back extraction with UV/Vis-absorption spectrophotometry, as described previously.[14] Equilibrium-swollen SiHys were soaked in aqueous-solute-containing PBS under magnetic stirring for at least 2 d. Following solute loading, solute-equilibrated hydrogels were removed from solution, blotted lightly with Fisherbrand® weighing paper, and immediately placed into PBS for solute release. Solute equilibrium supernatant concentration was obtained by pipetting 1 mL of solution into a 4-mm wide UV quartz cuvette (path length 10 mm), and measuring previously calibrated solution absorbance at 220-250 nm with an Ocean Optics spectrophotometer (Model ADC-1000, Dunedin, FL). The equilibrium partition coefficient, k_i, of solute i (i.e., the concentration of solute in the hydrogel phase divided by the concentration in bulk surrounding phase) is then calculated using the equilibrium-release PBS-solution concentration, C_i^S, by the expression[13]

$$k_i = C_i^S V^S / C_i^{load} V^{gel} \tag{2}$$

where V^S is back-extraction-solution volume, V^{gel} is water-swollen hydrogel volume, and C_i^{load} is equilibrium loading-solution concentration.

Oleophilic-solute (i.e., Nile Red and Bodipy Green) partition coefficients in the SiHys were obtained using two-photon fluorescence confocal laser-scanning microscopy (FCLSM), as described previously.[15,16,18] A Carl Zeiss 510 LSM META NLO AxioImager confocal microscope (Jena, Germany) equipped with a Spectra-Physics MaiTai HP DeepSee Laser (Santa Clara, CA) was used at 780-nm excitation. Nile-Red and Bodipy-Green fluorescence emissions were detected through a 685-nm short-pass emission filter and a 500-550-nm band-pass emission filter, respectively. Equilibrium aqueous-swollen SiHys were soaked in the solute-containing silicone oil under magnetic stirring for at least 2 wks at 400

rpm. Subsequently, an equilibrium-solute-loaded SiHy was placed on the microscope for scanning in the vertical *z*-direction at the same laser power and detector setting as those during scanning of the bulk-solute solution. Detected solute intensities inside the hydrogel and in the surrounding bulk solution were proportional to dye concentration in the concentration range studied.[15,16,18] Accordingly, the partition coefficient, k_i, is given by the ratio of solute intensity in the SiHy to that in the loading solution. Loading concentrations were varied over a factor of 10 with no change in measured partition coefficients. Additionally, gravimetric oil-uptake measurements of dry SiHys reveal little to no swelling when immersed in silicone oil.[18]

5.4 Experimental Results

Figure 5.1 plots SiHy equilibrium water volume fraction, ϕ_1, as a function of the solvent-free hydrophilic-monomer fraction, ν_{hyphil}. Again, the hydrophilic-monomer fraction consists of HEMA (triangles), MAA (squares), or a mixture of 10 vol % MAA and 90 vol % HEMA (circles), denoted as 10%MAA/90%HEMA. Filled and open symbols represent ϕ_1 for TRIS and M-PDMS-based SiHys, respectively. Water contents for conventional hydrogels that contain no silicone monomer or macromer (i.e., where $\nu_{hyphil}=1$) are also shown.[14] Solid lines are drawn according to theory discussed below. In all cases, ϕ_1 rises linearly with increasing ν_{hyphil}. For a given value of ν_{hyphil}, both TRIS- and M-PDMS-based SiHys have nearly identical ϕ_1 (compare open and filled symbols). As expected, the MAA-based hydrogels show consistently higher ϕ_1 than the HEMA-based and 10%MAA/90%HEMA-based hydrogels hydrogels because fully ionized MAA moieties (at pH 7.4) have higher affinity for water compared to uncharged HEMA moieties yielding greater equilibrium swelling.[14-16,26]

All else being equal, higher water contents, reflective of larger water-filled hydrophilic domains, allow for greater aqueous-solute partitioning in SiHys. Figures 5.2 and 5.3 display aqueous theophylline and caffeine partition coefficients, k_i, as a function of the solvent-free hydrophilic-monomer fraction, ν_{hyphil}. Also shown are theophylline and caffeine partition coefficients for conventional hydrogels that contain no hydrophobic polymer (i.e., $\nu_{hyphil}=1$).[14] Filled and open symbols correspond to TRIS- and M-PDMS-based SiHys, respectively. Solid lines are drawn according to theory discussed below. Identical to water content, aqueous-solute partition coefficients increase linearly with rising solvent-free hydrophilic-phase fraction in all cases. Again, the TRIS- and M-PDMS-based SiHys have similar values of k_i for a given value of ν_{hyphil} (compare open and filled symbols). In PBS (at pH 7.4), both nonionic caffeine and theophylline exhibit specific adsorption to HEMA strands, but not to anionic MAA chains. This result accentuates that, unlike HEMA strands, charged MAA strands have a higher affinity for water than for neutral caffeine and theophylline.[14] Consequently, k_i is largest for the HEMA-based SiHys, followed by the 10%MAA/90%HEMA-based SiHys, and finally by the MAA-based SiHys.

In contrast to the aqueous solutes that partition into the SiHy water-filled microphases (Figures 5.2 and 5.3), oleophilic solutes (with low water solubility) have higher affinity for the hydrophobic-silicone microdomains.[18] Figure 5.4 shows oleophilic partition

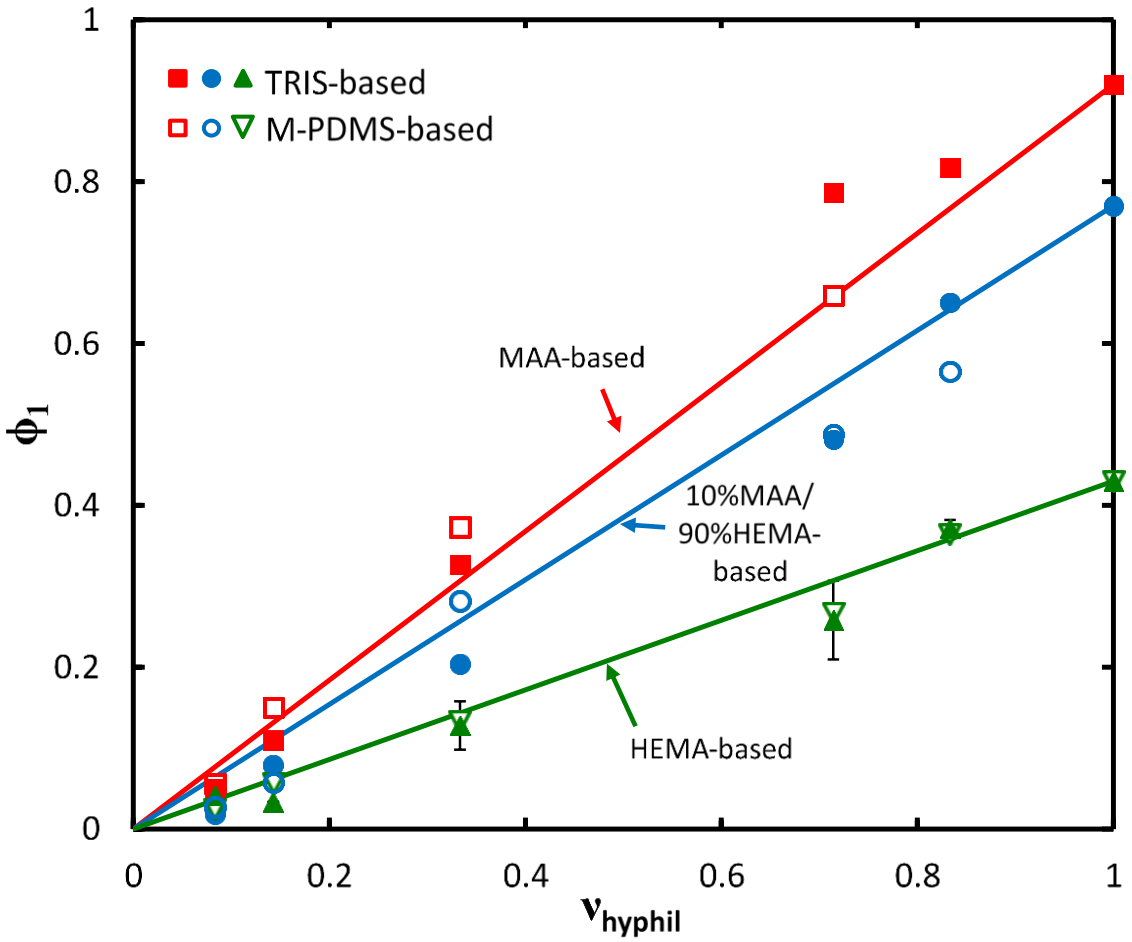

Figure 5.1: Equilibrium water volume fraction, ϕ_1, as a function of the solvent-free volume fraction of hydrophilic monomer, ν_{hyphil}, for HEMA- (triangles), MAA- (squares), and 10%MAA/90%HEMA-based (circles) SiHys. Filled and open symbols denote TRIS- or M-PDMS-based SiHys, respectively. Typical error bars are shown. Lines are drawn according to theory.

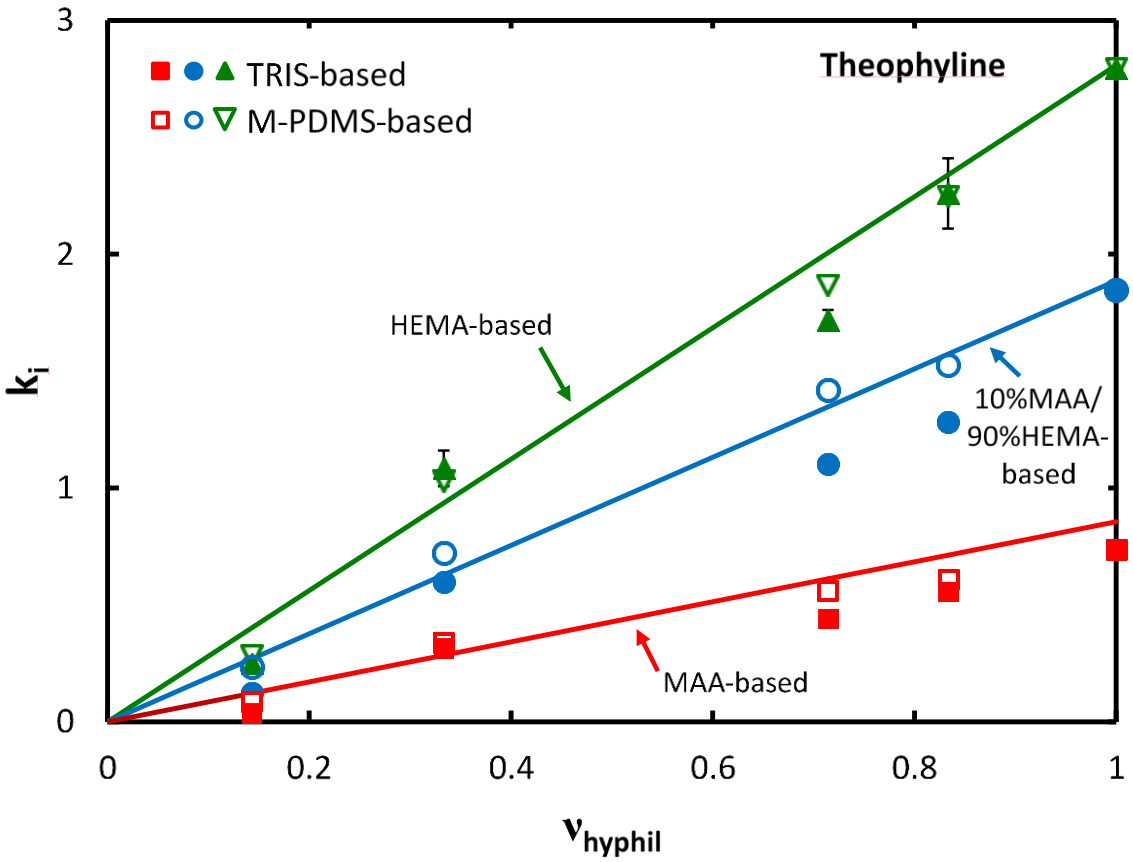

Figure 5.2: Theophylline partition coefficients, k_i, as a function of the solvent-free volume fraction of hydrophilic monomer, ν_{hyphil}, for HEMA- (triangles), MAA- (squares), and 10%MAA/90%HEMA-based (circles) SiHys. Filled and open symbols denote TRIS- or M-PDMS-based SiHys, respectively. Typical error bars are shown. Lines are drawn a priori according to theory.

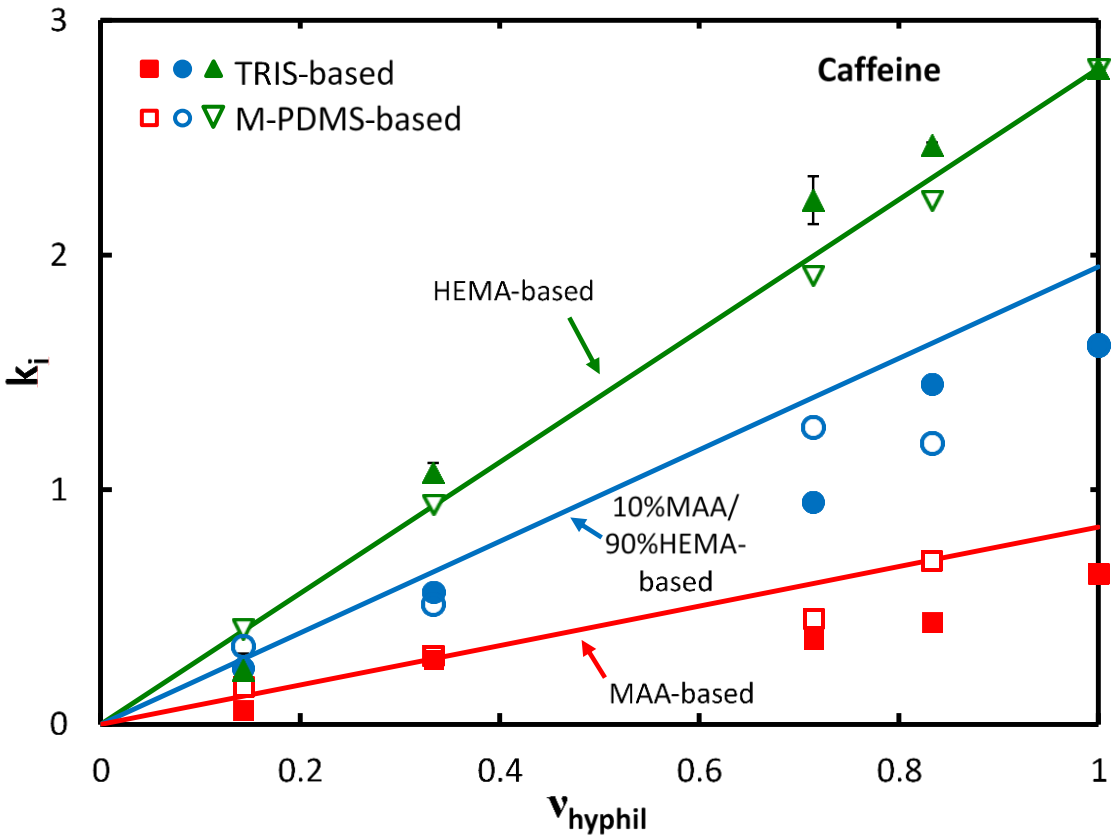

Figure 5.3: Caffeine partition coefficients, k_i, as a function of the solvent-free volume fraction of hydrophilic monomer, ν_{hyphil}, for HEMA- (triangles), MAA- (squares), and 10%MAA/90%HEMA-based (circles) SiHys. Filled and open symbols denote TRIS- or M-PDMS-based SiHys, respectively. Typical error bars are shown. Lines are drawn a priori according to theory.

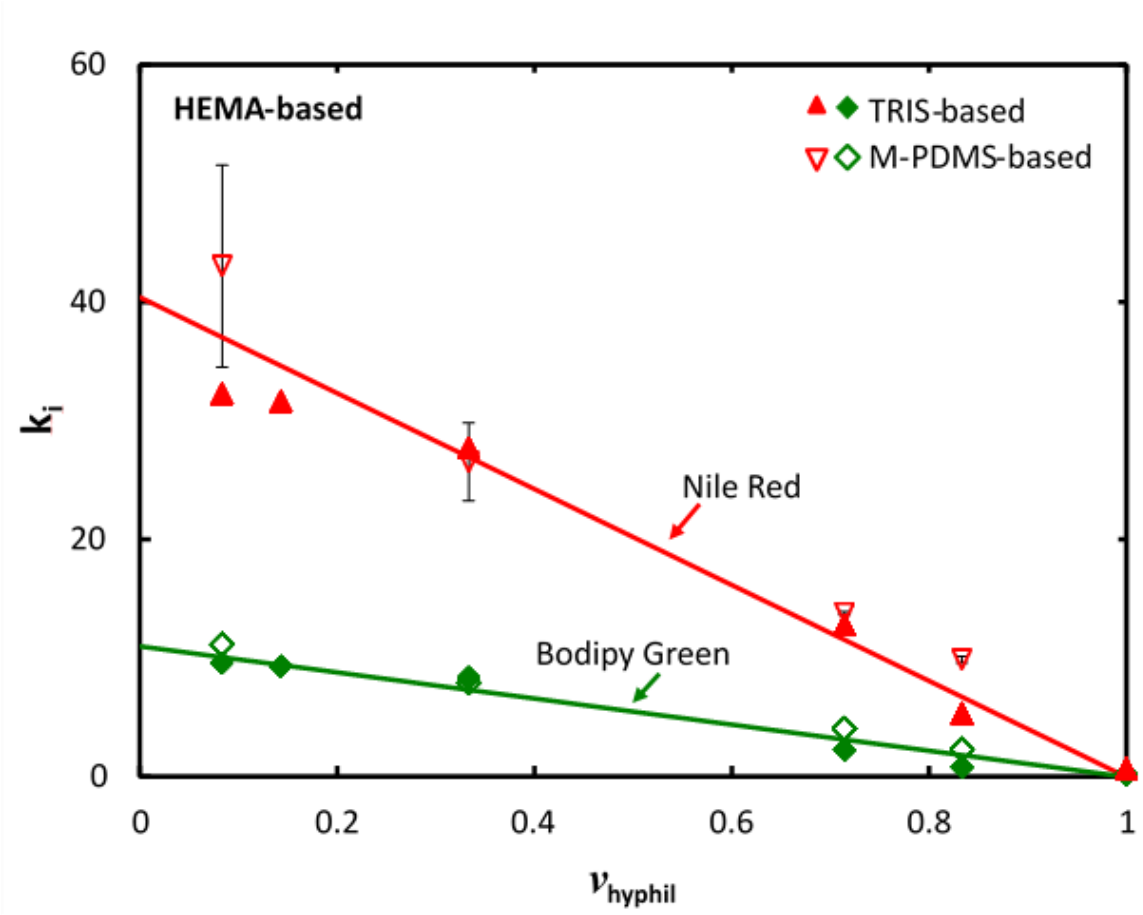

Figure 5.4: Oleophilic-solute partition coefficients, k_i, as a function of the solvent-free volume fraction of hydrophilic monomer, ν_{hyphil}, for Nile Red (triangles) and Bodipy Green (diamonds) in HEMA-based SiHys. Filled and open symbols denote TRIS- or M-PDMS-based SiHys, respectively. Typical error bars for Nile Red are shown. Error bars for Bodipy Green are the size of the data points. Lines are drawn according to theory.

coefficients (i.e., Nile Red and Bodipy Green), k_i, as a function of the solvent-free hydrophilic fraction, ν_{hyphil}, for the HEMA-based SiHys. Filled and open symbols denote TRIS- and M-PDMS-based SiHys, respectively. Oleophilic-solute partition coefficients were not obtained for 10%MAA/90%HEMA- and MAA-based SiHys because these hydrogels were translucent, preventing accurate FCLSM measurement. Solid lines are drawn according to theory discussed below. In this calculation, we classify the small amount of amphiphilic macromer as hydrophobic because the water content of a homopolymer macromer hydrogel is negligible (< 0.1). In all cases, k_i diminishes linearly with increasing ν_{hyphil} (i.e., decreasing silicone-phase fraction). Further, strong specific adsorption of the solutes to the silicone phase is observed (with k_i ranging from 3 to 43). Additionally, Nile Red exhibits a higher affinity for the silicone microphase than does Bodipy Green for both the TRIS- and M-PDMS-based SiHys.

5.5 Theory

Water contents in Figure 5.1 clearly increase linearly with increasing solvent-free hydrophilic-phase volume fraction. When $\nu_{hyphil} = 0$, water content is zero. When $\nu_{hyphil} = 1$, water content is simply the water content of the conventional hydrophilic hydrogel of the corresponding type (i.e., HEMA, MAA, or 10%MAA/90%HEMA). These findings suggest that overall SiHy water volume fraction is given by

$$\phi_1 = \nu_{hyphil}\, \phi_{1,hyphil}, \tag{3}$$

where $\phi_{1,hyphil}$ is the water content of the conventional hydrophilic hydrogel. Solid lines in Figure 5.1 are drawn according to Eq. 3 using no adjustable parameters. In all cases, agreement between theory and experiment is excellent. Eq. 3 reiterates that water primarily resides within the hydrophilic-polymer microdomains. In comparison, hydrophobic SiHy silicone-polymer microdomains uptake negligible water. Accordingly, SiHy water content can be directly controlled based on the relative monomer fractions added during synthesis.

Likewise, aqueous-solute partition coefficients in Figures 5.2 and 5.3 rise linearly with increasing solvent-free hydrophilic-phase fraction. When $\nu_{hyphil} = 0$, aqueous-solute partition coefficients are zero. When $\nu_{hyphil} = 1$, aqueous-solute partition coefficients are those of the conventional hydrogels of the same type (i.e., HEMA, MAA, or 10%MAA/90%HEMA). Thus, aqueous-solute partition coefficients are given by

$$k_i = \nu_{hyphil}\, \phi_{1,hyphil}\, E_{i,hyphil}, \tag{4}$$

where k_i is the solute partition coefficient of aqueous solute *i* and $E_{i,hyphil}$ is the overall hydrophilic-phase enhancement factor.[14] In Eq. 4, $E_{i,hyphil}$ accounts for specific solute adsorption to the polymer strands, electrostatic interaction, and solute hard-sphere size exclusion.[15] Table 5.2 reports values for $E_{i,hyphil}$ in the conventional hydrogels that contain no

silicone monomer or macromer (i.e., HEMA, MAA, or 10%MAA/90%HEMA). Details on the specific calculation are provided in Dursch et al.[14] Solid lines in Figures 5.2 and 5.3 are drawn using Eq. 4 with no adjustable constants. For all synthesized SiHys, agreement between theory and experiment is good. The slight discrepancies when $\nu_{hyphil} = 1$ are due to errors in accounting precisely for hard-sphere size exclusion, as discussed previously.[14] Eq. 4 re-emphasizes that aqueous solutes are confined to water-filled domains that localize in the SiHy hydrophilic-phase domains. Since silicone microdomains imbibe negligible water, aqueous-solute uptake is negligible. Thus, SiHy aqueous-solute partition coefficients are a volume-fraction weighted average of those in the conventional hydrogels of the same type. This result suggests that the structure of the SiHy hydrophilic-polymer microdomains is similar to that of the conventional hydrogel.

Table 5.2: Overall Solute Enhancement Factors, $E_{i,hyphil}$, for the Conventional Hydrogels

Hydrogel type	Theophylline[a]	Caffeine[a]
HEMA	6.5	6.5
10%MAA/90%HEMA	2.5	2.5
MAA	0.9	0.9

[a] From Dursch et al.[14]

Oleophilic-solute uptake in Figure 5.4 likewise shows a linear dependence on ν_{hyphil}. Contrary to water and aqueous-solute uptake, however, oleophilic-solute partition coefficients decrease linearly with ν_{hyphil} owing to strong solute affinity for the silicone-polymer microdomains. Since we find minimal uptake of silicone oil in the SiHys studied, theory for oleophilic-solute partition coefficients is slightly different than that for the hydrophilic solutes where significant amounts of water reside in the hydrophilic domains. We define the partition coefficient of an oleophilic solute distributed between a SiHy and bulk silicone oil by

$$k_i = (1-\nu_{hyphil})\phi_{2,hyphob} K_{i,hyphob}, \quad (5)$$

where k_i is the solute partition coefficient of oleophilic solute *i*, $\phi_{2,hyphob}$ is the silicone-polymer (i.e., monomer plus macromer) volume fraction of a hypothetical silicone-oil contacted TRIS or M-PDMS homopolymer network, and $K_{i,hyphob}$ is the Henry's adsorption constant of solute *i* between bulk silicone oil and the SiHy hydrophobic microdomains (e.g., TRIS or M-PDMS).[14] In Eq. 5, the amphiphilic macromer fraction is included in the hydrophobic-phase fraction, since water uptake of a homopolymer macromer hydrogel is minimal (i.e., the macromer hydrogel is primarily hydrophobic). Since our synthesized SiHys imbibe negligible silicone oil, $\phi_{2,hyphob}$ is unity.

$K_{i,hyphob}$ reflects the affinity of an oleophilic solute *i* for the polymer strands in the SiHy silicone microphases. In all cases, we assume $K_{i,hyphob}$ is identical for all hydrophobic-polymer strands because the hydrophobic groups of the macromer molecules are nearly identical to those of the silicone monomers. Following Dursch et al.,[14] $K_{i,hyphob}$ was taken as an adjustable constant from best least-squares fits to the partitioning data (with values of 40.4 and 11.4 for Nile Red and Bodipy Green, respectively). Large $K_{i,hyphob}$ values (i.e., >10) indicate strong interaction between the dye solutes and the silicone-domain polymer. In all cases, Nile Red exhibits stronger interaction with the silicone-domain polymer than does Bodipy Green. Lines in Figure 5.4 are drawn according to Eq. 5. Agreement between theory and experiment is excellent, confirming that oleophilic solutes partition primarily into the silicone-polymer microdomains. Consequently, oleophilic-solute partition coefficients can be directly controlled based on the relative amount of silicone monomer added during synthesis.

5.6 Discussion

Eqs. 3-5 describe SiHys as microphase separated with water and aqueous-solute uptake in the hydrophilic-polymer domains and oleophilic-solute uptake in the silicone-polymer domains. However, phase connectivity of these domains or the specific SiHy phase morphology present cannot be determined from our experiments. Several of the MAA SiHys were translucent, indicating possible macrophase separation. Conversely, all HEMA-based SiHys were transparent; FCLSM images revealed spatially homogeneous partitioning throughout each sample (data not shown), indicating microdomain sizes smaller than the resolution of the microscope (~1 μm).[18] Nevertheless, theory accurately predicts SiHy equilibrium water contents and solute partition coefficients over a wide range of hydrogel compositions and water contents (3 to 82%).

In determining SiHy equilibrium water contents and solute partition coefficients, the amphiphilic macromer is classified as: (1) hydrophobic (i.e., having negligible water and aqueous-solute uptake), (2) hydrophilic (i.e., having negligible oleophilic-solute uptake), or (3) amphiphilic (i.e., having non-negligible water, aqueous-solute, and oleophilic-solute uptake). Classification is done by measuring the water content and aqueous- and oleophilic-solute partition coefficients of a homopolymer macromer hydrogel. If the macromer is classified as hydrophobic, Eqs. 3-5 are used as above. However, when the hydrophobic groups of the macromer molecules are significantly different from those of the silicone monomer, Eq. 5 includes an additive term for oleophilic-solute adsorption to hydrophobic-macromer chains.[14] When the macromer is classified as hydrophilic, water contents of the hydrophilic-monomer/macromer copolymer hydrogel are measured and applied in Eq. 3. Aqueous-solute partition coefficients follow from Eq. 4, but with a second term for aqueous-solute adsorption to hydrophilic-macromer strands.[14] Because hydrophilic macromers uptake negligible oleophilic solutes, oleophilic-solute partitioning prediction uses Eq. 5 as above after replacing $(1-\nu_{hyphil})$ with $(1-\nu_{hyphil}-\nu_{macromer})$. When the macromer is classified as amphiphilic, water and aqueous-solute uptake follow that of a hydrophilic-designated macromer, whereas oleophilic-solute uptake follows that of a hydrophobic-designated macromer.

5.7 Conclusions

We report measured and predicted SiHy equilibrium water contents and solute partition coefficients. Fluorescence confocal laser-scanning microscopy and back extraction with UV/Vis-adsorption quantified partition coefficients of two aqueous solutes (i.e., theophylline and caffeine) and two oleophilic solutes (i.e., Nile Red and Bodipy Green) in thirty TRIS- and M-PDMS-based SiHys. Measured SiHy water contents and aqueous-solute partition coefficients increase linearly with the solvent-free hydrophilic-polymer fraction, ν_{hyphil}. Conversely, oleophilic-solute partition coefficients increase linearly with the solvent-free hydrophobic-polymer fraction, $(1-\nu_{hyphil})$. In all cases, predicted water contents and solute partition coefficients agree well with experiment. Importantly, our new procedure permits a priori estimation of SiHy water contents and solute partition coefficients based solely on properties of the silicone and hydrophilic homopolymer hydrogels, eliminating need for additional mixed-polymer-hydrogel experiments.

5.8 References

1. Alvord, L.; Davis, T.; Morgan, C. F.; Schindhelm, K.; Vogt, J.; Winterton, L. Oxygen permeability of a new type of high Dk soft contact lens material. *Optometry & Vision Science* **1998,** 75, (1), 30-36.
2. Chhabra, M.; Prausnitz, J. M.; Radke, C. J. A single-lens polarographic measurement of oxygen permeability (Dk) for hypertransmissible soft contact lenses. *Biomaterials* **2007,** 28, (30), 4331-4342.
3. Covey, M.; Sweeney, D. F.; Terry, R.; Sankaridurg, P. R.; Holden, B. A. Hypoxic effects on the anterior eye of high-Dk soft contact lens wearers are negligible. *Optometry & Vision Science* **2001,** 78, (2), 95-99.
4. Nicolson, P. C.; Vogt, J. Soft contact lens polymers: an evolution. *Biomaterials* **2001,** 22, (24), 3273-3283.
5. Sweeney, D. F. Clinical signs of hypoxia with high-Dk soft lens extended wear: is the cornea convinced? *Eye & contact lens* **2003,** 29, (1), S22-S25.
6. Nichols, J. J. Contact lenses 2011. *Contact Lens Spectrum* **2012,** 27, 20-25.
7. Nichols, J. J. Contact lenses 2012. *Contact Lens Spectrum* **2013,** 28, 24-29.
8. Nichols, J. J. Contact lenses 2013. *Contact Lens Spectrum* **2014,** 29, 22-28.
9. Erdodi, G.; Kennedy, J. P. Amphiphilic conetworks: definition, synthesis, applications. *Progress in Polymer Science* **2006,** 31, (1), 1-18.
10. Nicolson, P. C.; Carlton, R. B.; Chabrecek, P.; Court, J.; Domschke, A.; Griesser, H. J., et al. Extended wear ophthalmic lens. 1998.
11. Peng, C.-C.; Chauhan, A. Ion transport in silicone hydrogel contact lenses. *Journal of Membrane Science* **2012,** 399–400, (0), 95-105.
12. Willis, S. L.; Court, J. L.; Redman, R. P.; Wang, J.-H.; Leppard, S. W.; O'Byrne, V. J.; Small, S. A.; Lewis, A. L.; Jones, S. A.; Stratford, P. W. A novel phosphorylcholine-coated contact lens for extended wear use. *Biomaterials* **2001,** 22, (24), 3261-3272.

13. Guan, L.; Jiménez, M. E. G.; Walowski, C.; Boushehri, A.; Prausnitz, J. M.; Radke, C. J. Permeability and partition coefficient of aqueous sodium chloride in soft contact lenses. *Journal of Applied Polymer Science* **2011,** 122, (3), 1457-1471.

14. Dursch, T. J.; Taylor, N. O.; Liu, D. E.; Wu, R. Y.; Prausnitz, J. M.; Radke, C. J. Water-soluble drug partitioning and adsorption in HEMA/MAA hydrogels. *Biomaterials* **2014,** 35, (2), 620-629.

15. Kotsmar, C.; Sells, T.; Taylor, N.; Liu, D. E.; Prausnitz, J. M.; Radke, C. J. Aqueous solute partitioning and mesh size in HEMA/MAA hydrogels. *Macromolecules* **2012,** 45, (22), 9177-9187.

16. Liu, D. E.; Kotsmar, C.; Nguyen, F.; Sells, T.; Taylor, N. O.; Prausnitz, J. M.; Radke, C. J. Macromolecule sorption and diffusion in HEMA/MAA hydrogels. *Industrial & Engineering Chemistry Research* **2013,** 52, (50), 18109-18120.

17. Cerretani, C.; Peng, C.-C.; Chauhan, A.; Radke, C. J. Aqueous salt transport through soft contact lenses: An osmotic-withdrawal mechanism for prevention of adherence. *Contact Lens and Anterior Eye* **2012,** 35, (6), 260-265.

18. Dursch, T. J.; Liu, D. E.; Oh, Y.; Radke, C. J. Fluorescent solute-partitioning characterization of layered soft contact lenses. *Acta Biomaterialia* **2015,** 15, 48-54.

19. Jones, L.; Brennan, N. A.; González-Méijome, J.; Lally, J.; Maldonado-Codina, C.; Schmidt, T. A.; al., e. The TFOS international workshop on contact lens discomfort: Report of the contact lens materials, design, and care subcommittee. *Investigative Ophthalmology & Visual Science* **2013,** 54, (11), TFOS37-TFOS70.

20. Rennie, A. C.; Dickrell, P. L.; Sawyer, W. G. Friction coefficient of soft contact lenses: measurements and modeling. *Tribology Letters* **2005,** 18, (4), 499-504.

21. Jianzhong, W.; Sassi, A. P.; Blanch, H. W.; Prausnitz, J. M. Partitioning of proteins between an aqueous solution and a weakly-ionizable polyelectrolyte hydrogel. *Polymer* **1996,** 37, (21), 4803-4808.

22. Johnson, E. M.; Berk, D. A.; Jain, R. K.; Deen, W. M. Diffusion and partitioning of proteins in charged agarose gels. *Biophysical Journal* **1995,** 68, (4), 1561-1568.

23. Lazzara, M. J.; Deen, W. M. Effects of concentration on the partitioning of macromolecule mixtures in agarose gels. *Journal of Colloid and Interface Science* **2004,** 272, (2), 288-297.

24. Tong, J.; Anderson, J. L. Partitioning and diffusion of proteins and linear polymers in polyacrylamide gels. *Biophysical Journal* **1996,** 70, (3), 1505-1513.

25. Baker, J. P.; Blanch, H. W.; Prausnitz, J. M. Equilibrium swelling properties of weakly ionizable 2-hydroxyethyl methacrylate (HEMA)-based hydrogels. *Journal of Applied Polymer Science* **1994,** 52, (6), 783-788.

26. Brannon-Peppas, L.; Peppas, N. A. Equilibrium swelling behavior of pH-sensitive hydrogels. *Chemical Engineering Science* **1991,** 46, (3), 715-722.

27. English, A. E.; Mafé, S.; Manzanares, J. A.; Yu, X.; Grosberg, A. Y.; Tanaka, T. Equilibrium swelling properties of polyampholytic hydrogels. *Journal of Chemical Physics* **1996,** 104, (21), 8713-8720.

28. Hasa, J.; Ilavský, M.; Dušek, K. Deformational, swelling, and potentiometric behavior of ionized poly (methacrylic acid) gels. I. Theory. *Journal of Polymer Science: Polymer Physics Edition* **1975,** 13, (2), 253-262.

29. Horkay, F.; Tasaki, I.; Basser, P. J. Osmotic swelling of polyacrylate hydrogels in physiological salt solutions. *Biomacromolecules* **2000,** 1, (1), 84-90.

Chapter 6

Fluorescent Solute-Partitioning Characterization of Layered Soft Contact Lenses

6.1 Abstract

Partitioning of aqueous packaging, wetting, and care-solution agents into and out of soft contact lenses (SCLs) is important for improving wear comfort and also for characterizing lens physico-chemical properties. We illustrate both features of partitioning by application of fluorescent-solute partitioning into DAILIES TOTAL1® (delefilcon A) water-gradient SCLs, which exhibit a layered structure of a silicone-hydrogel (SiHy) core sandwiched between thin surface-gel layers. Two-photon fluorescence confocal laser-scanning microscopy (FCLSM) and attenuated total-reflectance Fourier-transform infrared spectroscopy (ATR-FTIR) characterize the lens and assess uptake profiles of six prototypical fluorescent solutes. To establish surface-layer charge, partition coefficients and water contents were obtained for aqueous pH values of 4 and 7.4. Solute fluorescence-intensity profiles clearly confirm a layered structure for the DAILIES TOTAL1® lenses. In all cases, aqueous solute partition coefficients are greater in the surface layers than in the SiHy core signifying higher water in the surface gels. ATR-FTIR confirmed surface-layer mass water contents of 82 ± 3%. Water uptake and hydrophilic-solute uptake at pH 4 compared to that at pH 7.4 reveal that the surface-gel layers are anionic at physiologic pH 7.4, whereas both the SiHy core and O_2OPTIX™ (lotrafilcon B) are nonionic. We successfully confirm the layered structure of DAILIES TOTAL1®, consisting of an 80-μm thick SiHy core surrounded by 10-μm thick polyelectrolyte surface-gel layers of significantly greater water content and aqueous solute uptake compared to that of the core. Accordingly, fluorescent-solute partitioning in SCLs provides information on gel structure and composition, in addition to quantifying uptake and release amounts and rates.

Reprint of Dursch, T. J.*; Liu, D. E.*; Oh, Y.; Radke, C. J. *Acta Biomaterialia* **2015,** 15, 48-54. *authors contributed equally

6.2 Introduction

Partitioning of packaging, wetting and care-solution agents in SCLs is a well-explored avenue to improve and maintain on-eye lens performance.[1-6] Likewise, partitioning of tear components in SCLs, such as proteins, salts, and lipids, can affect lens behavior during wear.[1,7-11] Further, solute partitioning is critical for possible use of SCLs as a drug delivery vehicle.[12-15] Thus, understanding how solutes partition and transport in hydrogels is an important challenge.[13,16-20]

While not as common, solute partitioning may be adopted to characterize hydrogel structure. Watkins et al.[21] utilized fluorescent-solute loading to visualize multi-laminated hydrogels. Furthermore, by employing non-interacting solutes of known shape and size, Walther et al.[22,23] ascertained the pore-size distribution (i.e., mesh-size distribution) of parent hydrogels. We apply this philosophy to understand the structure of DAILIES TOTAL1® lenses, which according to trade and patent literature, consist of a 33% water-content SiHy core that transitions through an interpenetrating anchor region to outer surface-gel layers with water contents greater than 80%.[24-28] As daily disposables, DAILIES TOTAL 1® lenses are designed for use without care solutions. Here we utilize solute partitioning to ascertain hydrogel structure. Because the reported surface-gel layers are of high water content, their mesh sizes are expected to be larger than those of the core region. Accordingly, larger aqueous solutes likely partition more favorably into the surface-gel region than into the core region.[13,16,17] Further, by comparing uptake of aqueous ionogenic solutes in their charged and neutral states, information can be obtained on the charge of the polymer strands in the surface and core gels. By comparing partitioning into a SiHy-core prototype lens (e.g., O_2OPTIX™ [29]), the core SiHy structure of DAILIES TOTAL1® can be validated. Finally, partitioning of oleophilic solutes from an oil solvent can be pursued to establish whether or not an aqueous-saturated surface gel can forestall low aqueous-soluble lipid penetration into the core SiHy region.

We measure uptake of six prototypical fluorescent solutes in DAILIES TOTAL1® SCLs. Two-photon fluorescence confocal laser-scanning microscopy (FCLSM) obtains profiles and partition coefficients of both hydrophilic (i.e., fluorescently labeled avidin and dextrans) and oleophilic (i.e., Nile Red and fluorescently labeled cholesterol) solutes. For the hydrophilic solutes in DAILIES TOTAL1®, FCLSM measurements confirm consistently greater solute partitioning in the surface-gel layers and, hence, higher water content compared to that in the SiHy core. FCLSM confirms both the layered structure and establishes the surface-gel-layer thickness. Higher surface-layer water content was validated using attenuated total-reflectance Fourier-transform infrared spectroscopy. Penetration of two oleophilic solutes from silicone oil into the SiHy core was not prevented by the surface-gel layers. To establish a baseline, solute-uptake and water-content measurements were also performed on a single-water-content prototype SiHy SCL: O_2OPTIX™.

6.3 Materials and Methods

6.3.1 Soft Contact Lenses

Two commercially available Alcon (Fort Worth, TX) SiHy SCLs were used in this study: DAILIES TOTAL1® (delefilcon A; composition unpublished) and O_2OPTIX™ (lotrafilcon B; containing N,N-dimethylacrylamide and methacryloxypropyl tris(trimethylsiloxy)silane[29]). The diameter, base curve, and power were 14.1 and 14.2 mm,

8.5 and 8.6 mm, and -0.75 and -2.0, for DAILIES TOTAL1® and O_2OPTIX™, respectively. Prior to each measurement, lenses were extracted in excess pH 7.4 phosphate buffer saline solution (PBS) for at least 48 h to remove preservatives and surfactants from the packaging solutions. PBS was prepared as described previously.[13,16,17] For measurements at pH 4, extracted lenses were subsequently equilibrated for 24 h in excess pH-4 citrate buffer (1.2×10^{-2} M citric acid anhydrous, Cat. No. A940-500, Fisher Scientific; 8.2×10^{-3} M sodium citrate dihydrate, SX0445-1, EMD Chemicals; 0.15 M NaCl, S271-3, Fisher Scientific). All experiments were performed at ambient temperature.

6.3.2 Attenuated Total-Reflectance Fourier-Transform Infrared Spectroscopy (*ATR-FTIR*)

SCL surface water content was determined using attenuated total-reflectance Fourier-transform infrared spectroscopy (ATR-FTIR).[30-32] IR spectra were obtained using a Nicolet 6700 FTIR spectrometer (Thermo Scientific, Madison, WI) equipped with a DTGS-KBr detector and a single-reflection Smart OMNI-Sampler ATR cell (No. 0028-899, Thermo Scientific). In all cases, ambient air was used as the reference spectrum. Prior to each water-content measurement, SCLs were removed from the extraction solution, lightly blotted with Fisherbrand® weighing paper (Fisher Scientific, Pittsburgh, PA), and forced onto the ATR crystal using the instrument supplied fixture or light weights to ensure intimate crystal contact. The applied force was low enough to ensure no gel collapse.[33] Subsequently, FTIR spectra were obtained in the range of wavenumber from 4000 to 650 cm^{-1} during 64 scans, with 2 cm^{-1} resolution. Each measurement was performed in triplicate.

Total internal reflectance probes surface properties through an exponentially decaying evanescent wave of penetration depth, d_p, given by

$$d_P = \frac{\lambda_\ell}{2\pi\, n_1[\sin^2\theta - (n_2/n_1)^2]^{1/2}} \tag{1}$$

where λ_ℓ is the wavelength of light, θ is the angle of incidence (45°), and n_1 and n_2 are the refractive indices of the ATR crystal (Germanium: n_1 = 4) and either the surface-gel layer (approximated as water: $n_2 \sim 1.33$) or O_2OPTIX™ (n_2 = 1.42 [29]), respectively. Over the wavenumbers investigated, penetration depths into the lenses ranged from 0.1 to 1 μm, which are considerably smaller than the observed DAILIES TOTAL1® surface-layer thicknesses.[27] For O_2OPTIX™, however, penetration depths are considerably greater than the 25-nm thick plasma coating.[29] In this case, water contents measured by ATR-FTIR are averaged over the plasma-surface-coated region and the untreated bulk SiHy material.

Figure 6.1 displays ATR-FTIR spectra for PBS solution, DAILIES TOTAL1®, and O_2OPTIX™ over the range of wavenumbers between 4000 and 2500 cm^{-1} where water absorbs strongly. For clarity, the baseline was subtracted. In all cases, the O-H stretching band (3500-3000 cm^{-1} [34]) is clearly observed. Following Wilson et al.,[30] surface water content was calculated from the peak area between 3600 and 3000 cm^{-1}. To account for the contribution of lens polymer to the IR spectra (e.g., at 2950 cm^{-1}), overlapping peaks were deconvoluted utilizing dry-lens spectra; thus, only peak areas corresponding to O-H stretching were used in the calculation. We neglected the O-H bending band because the matrix polymer contributes

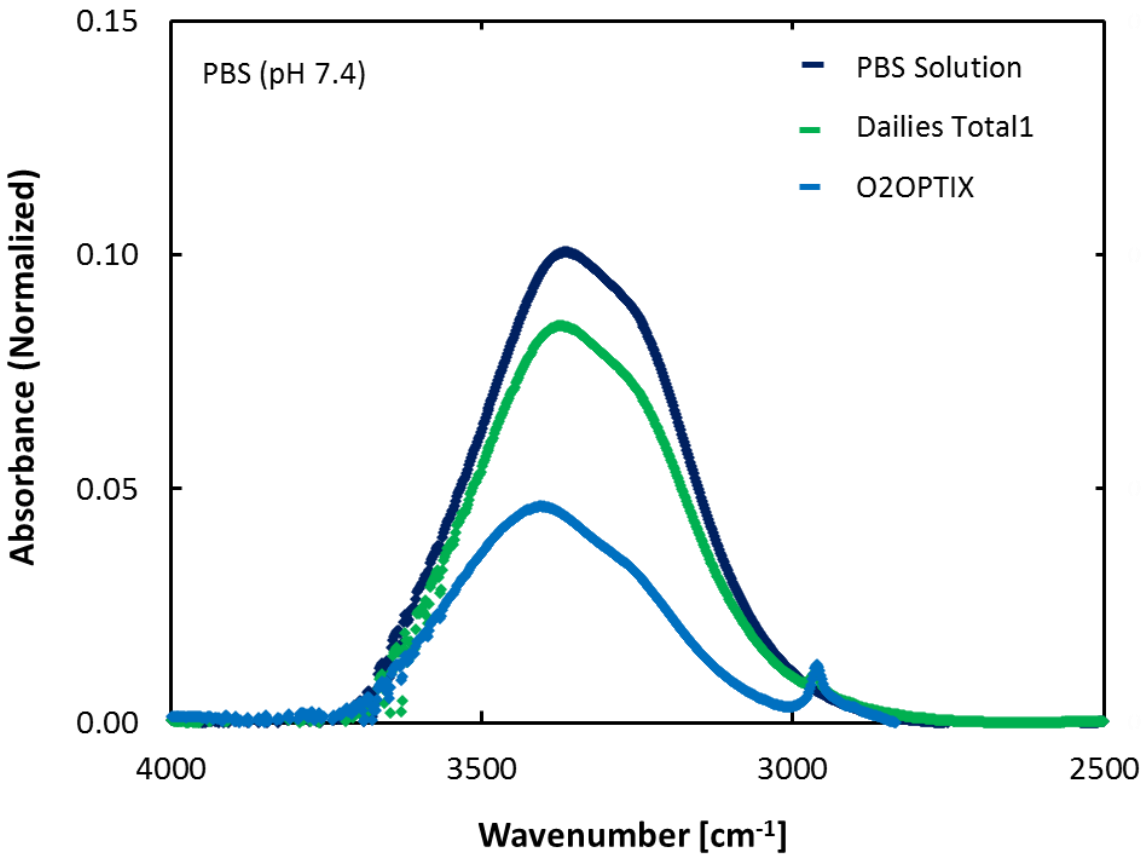

Figure 6.1: Truncated ATR-FTIR spectra for PBS solution, DAILIES TOTAL1®, and O_2OPTIX™ over the range of wavenumbers between 4000 and 2500 cm^{-1}. The measured surface mass water contents of DAILIES TOTAL1® and O_2OPTIX™ were 82 ± 3% and 43 ± 2%, respectively.

significantly at these wavenumbers. ATR-FTIR-measured mass water contents were validated from in-house synthesized 2-hydroxyethyl methacrylate (HEMA)/methacrylic acid (MAA) copolymer hydrogels[13] of known bulk gravimeteric water content. Figure 6.2 plots the ATR-FTIR-measured water content against known gravimetric water content for four HEMA/MAA hydrogels. Water content obtained by ATR-FTIR is in good agreement with that determined gravimetrically over the range of water contents studied.

6.3.3 Fluorescent Solutes

PBS (pH 7.4) and citrate buffer (pH 4) solutions, prepared as described above, were solvents for the hydrophilic fluorescent solutes. Fluorescein isothiocyanate dextrans (FITC-dextran4, MW = 4000 g/mol; FITC-dextran20, MW = 20,000 g/mol; FITC-dextran70, MW = 70,000 g/mol) were obtained from TdBCons (Uppsala, Sweden). To remove free label (i.e., FITC), FITC-dextran solutions were extensively dialyzed in Slide-A-Lyzer Dialysis Cassettes (No. 66212, Thermo Scientific, cutoff MW = 2000 g/mol) for 1 wk at 25 °C, with its surrounding respective dialyzing solution changed daily. Cationic FITC-conjugated avidin (FITC-avidin, MW = 68,000 g/mol) was acquired from Invitrogen (Eugene, OR). In this case, free FITC label was removed by filter centrifugation at 25 °C using an Amicon Ultra-4 membrane (10,000 g/mol, UFC801008, EMD Millipore Corp., Billerica, MA) for 3 cycles at 4000 rpm.

Silicone oil was purchased from Fisher Scientific (500 cSt, S159-500, Pittsburgh, PA) and used as the solvent for oleophilic-fluorescent solutes. Nile Red (N1142) and 25-[N-[(7-nitro-2-1,3-benzoxadiazol-4-yl)methyl]amino]-27-norcholesterol (NBD-cholesterol, 810250P) solutes were purchased from Invitrogen and Avanti Polar Lipids (Alabaster, AL), respectively, and used without further purification. Table 6.1 reports the molecular weight and hydrodynamic radius, a_{is}, of all solutes.

Table 6.1: Solute Properties in Aqueous pH 7.4

Solute	M_w (g/mol)	a_{is} (nm)
Nile Red	320	0.8 [35]
NBD-cholesterol	560	[a] 0.9 [36]
FITC-dextran4	4,000	1.6 [16,17]
FITC-dextran20	20,000	3.4 [16,17]
FITC-avidin	68,000	3.5 [17]
FITC-dextran70	70,000	5.8 [16,17]

[a] approximated as cholesterol in water-saturated chloroform

6.3.4 Solute Partition Coefficients

Solute partition coefficients in the SCLs were obtained using two-photon fluorescence confocal laser-scanning microscopy (FCLSM)[37,38] excited at 780 nm, as described previously.[13,16,17] With the exception of Nile Red, emission for all solutes was detected through

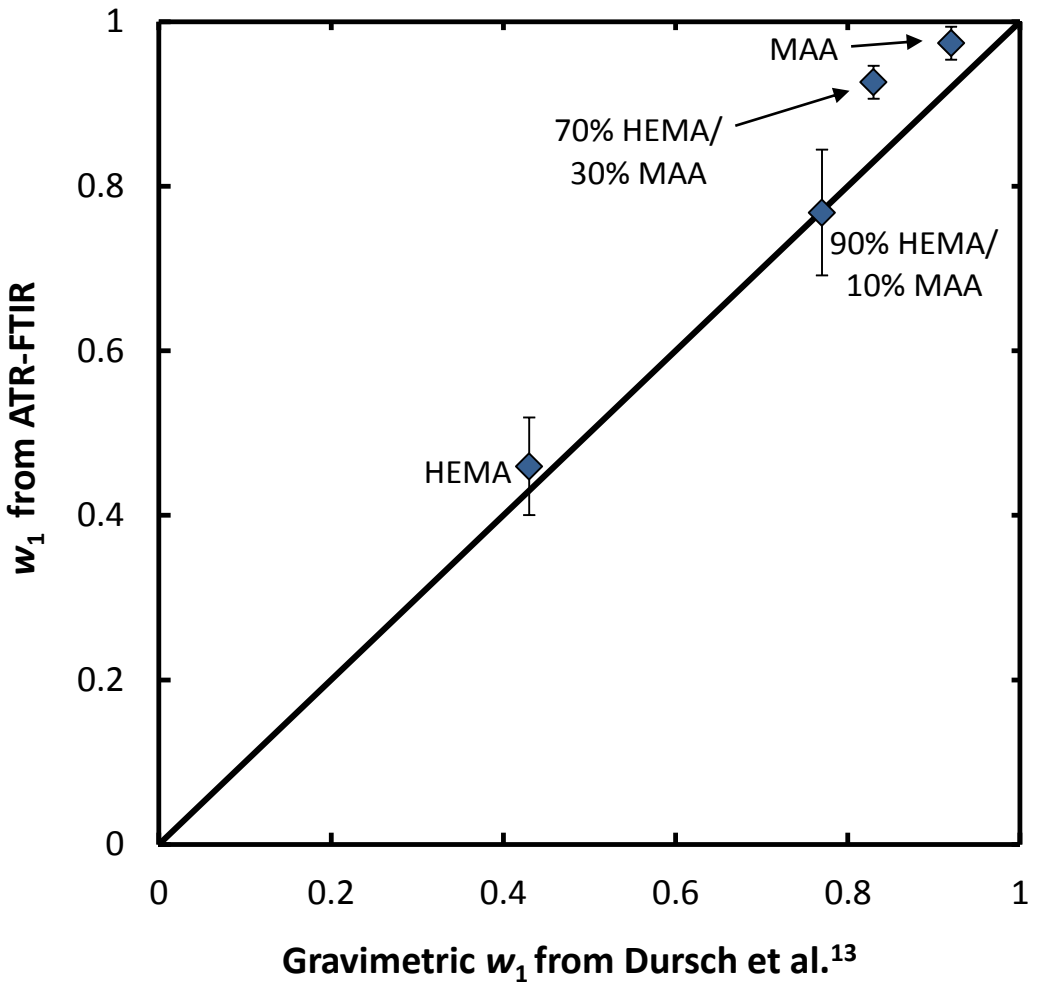

Figure 6.2: ATR-FTIR-measured mass water content as a function of known bulk gravimeteric water content for HEMA/MAA synthesized hydrogels.

a 500-550 nm emission filter. For Nile Red, a 685 nm short-pass emission filter was employed. Prior to the uptake measurement, extracted SCLs were soaked in the pertinent solute-containing solution under magnetic stirring for at least 2 d at 400 rpm. After equilibration, a 1-mm thick layer of the bulk-solute solution in a small Petri dish was placed on the microscope platform and scanned in the vertical (z) direction at 2-μm intervals to a depth of at least 250 μm. Thereafter, a solute-loaded SCL was placed on a microscope slide (48300-047, VWR International, West Chester, PA, USA) and placed on the microscope for scanning in the z-direction at the same laser power and detector setting as those during scanning of the bulk-solute solution. Background fluorescence intensity was recorded and subtracted from solution and SCL signals. In the concentration range studied (i.e., 10^{-5} to 5×10^{-4} M), detected solute intensities inside the SCLs and in the surrounding bulk solution were proportional to dye concentration.[13,16,17] The partition coefficient, k, which is the concentration of solute in the gel phase divided by the concentration in bulk surrounding phase, is thus given by the ratio of solute intensity in the SCL to that in the loading solution. Equilibrium was confirmed for all solutes excluding the protein, FITC-avidin.[17] With the exception of FITC-avidin, loading concentration was varied over a factor of 10 with no change in the measured partition coefficient.

Prior to FCLSM with the oleophilic solutes, SCLs were first saturated with aqueous PBS for 48 h and then immersed in silicone oil containing dissolved Nile Red or NBD-cholesterol. FCLSM was performed as described above. Measured intensity of Nile Red depends strongly on the polarity of its environment.[39] As a result, partition coefficients were confirmed both by back extraction[13] into silicone oil and into decane as an alternate solvent. Agreement was excellent in all cases. Gravimetric oil-uptake measurements reveal little to no swelling of dry SiHy lenses when immersed in 500-cSt silicone oil, likely due to size exclusion from silicone microdomains as a result of the large molecular weight of the oil. Additionally, water-saturated lens thicknesses obtained from FCLSM of oleophilic and hydrophilic solutes verify minimal imbibition of silicone oil into water-saturated DAILIES TOTAL1® and O_2OPTIX™ lenses.

6.4 Results

Table 6.2 reports mass water contents, w_1, obtained by ATR-FTIR for the DAILIES TOTAL1® surface layer and O_2OPTIX™ in aqueous pH 7.4 and 4. Also reported are gravimetric water contents of the DAILIES TOTAL1® SiHy core and O_2OPTIX™. Core water content was obtained from the measured gravimetric water content of the entire lens corrected for the measured water content of the surface layers of known thickness (see below) using a typical core dry-polymer density of 1067 kg/m^3.[16,17] Several features are salient. For both the SiHy core of DAILIES TOTAL1® and O_2OPTIX™, water content does not vary over the range of pH studied. Conversely, for the DAILIES TOTAL1® surface layers, water content rises significantly with increased aqueous pH (i.e., from 63 to 82%) indicating a polyelectrolyte gel.[13] ATR-FTIR water-content measurements at pH 6.5 demonstrate no significant deswelling compared to that at pH 7.4 (data not shown). Therefore, the surface-gel-layer water content does not vary over the reported range of tear-film physiological pH (i.e., 6.5-7.8).[40] In all cases, the DAILIES TOTAL1® surface-layer water content was significantly larger than that of the SiHy core, with core gravimetric water content identical to that of O_2OPTIX™. ATR-FTIR

surface-water content for O_2OPTIX™ is slightly larger than bulk water content obtained gravimetrically, but is not significant due to limitations in deconvoluting the water signature in high-polymer-content SCLs.

Table 6.2: Water Content of DAILIES TOTAL1® and O_2OPTIX™ at Aqueous pH 7.4 / 4

SCL	w_1 pH 7.4/ pH 4	w_1 lit.
DAILIES TOTAL1® (surface layer)	[a] 82 ± 3% / [a] 63 ± 2%	85% [27,28]
DAILIES TOTAL1® (core)	[b] 29 ± 5% / [b] 34 ± 6%	33% [24-28]
O_2OPTIX™	[a] 43 ± 2% / [a] 44 ± 2% [b] 33 ± 6% / [b] 38 ± 3%	33% [29]

[a] obtained from ATR-IR
[b] obtained gravimetrically[13]

As discussed previously,[13,16,17] higher water content reflects larger water-filled meshes and leads to greater solute partitioning into hydrogels, all else being equal. Figure 6.3 displays typical fluorescence-confocal-microscopy images of aqueous FITC-dextran4 in (a) DAILIES TOTAL1® and (b) O_2OPTIX™ equilibrated at pH 7.4. Scale bars represent 20 μm in the vertical direction. Figure 6.3a reveals the layered structure of DAILIES TOTAL1®. Uptake of FITC-dextran4 in the surface-gel layer is clearly greater than that in the SiHy core. The resulting fluorescence intensity profile (not shown) establishes a surface-layer thickness of 11 ± 4 μm. Conversely in Figure 6.3b, FITC-dextran4 uptake in O_2OPTIX™ is spatially uniform. Comparison of intensities in Figures 3a and 3b demonstrates that FITC-dextran4 partitioning in the SiHy core DAILIES TOTAL1® is similar to that in O_2OPTIX™.

Figure 6.4 plots partition coefficients at pH 7.4 as a function of hydrodynamic radius for several fluorescently labeled aqueous solutes in DAILIES TOTAL1® and O_2OPTIX™. At this pH, the aqueous solutes are anionic.[13,41] In all cases, the DAILIES TOTAL1®-core partition coefficients are similar to those of O_2OPTIX™. This result indicates that the chemical and physical structures of the core of DAILIES TOTAL1® and O_2OPTIX™ are similar, confirming the reported SiHy structure of the DAILIES TOTAL1® core.[9,27,28] Hydrophilic solutes partition primarily into the hydrophilic domains of SiHys. Since the water contents of the DAILIES TOTAL1® core and O_2OPTIX™ are identical, corresponding partition coefficients are essentially identical. Larger solutes exhibit progressively smaller partition coefficients, indicative of size exclusion from the water domains of the SCLs.[13,16,17] Importantly, solute partition coefficients in the DAILIES TOTAL1® surface-gel layers are greater than those in the underlying SiHy core, confirming the higher water content in the surface layers. The solid line in Figure 6.4 corresponds to predicted FITC-dextran partition coefficients in the surface-gel layer according to theory below (i.e., Eq. 2).

Figure 6.5 also plots aqueous solute partition coefficients as a function of hydrodynamic radius in DAILIES TOTAL1® and O_2OPTIX™, but now for pH 4. At this lower pH, the hydrophilic solutes are partially anionic.[13,41] Trends are identical to those observed at

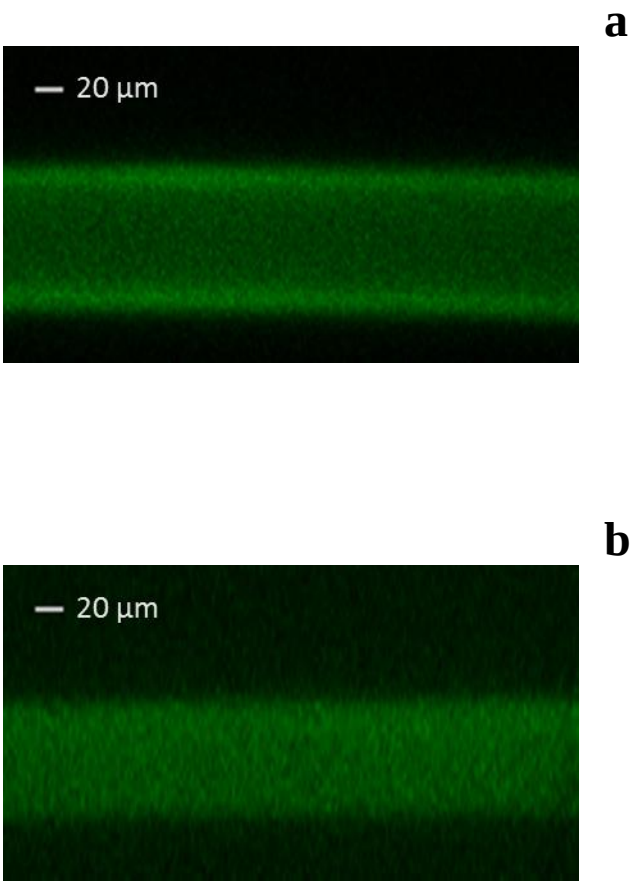

Figure 6.3: Fluorescence-confocal-microscopy images of FITC-dextran4 at equilibrium in DAILIES TOTAL1® (a) and O_2OPTIX™ (b). Scale bars represent 20 µm in the vertical direction.

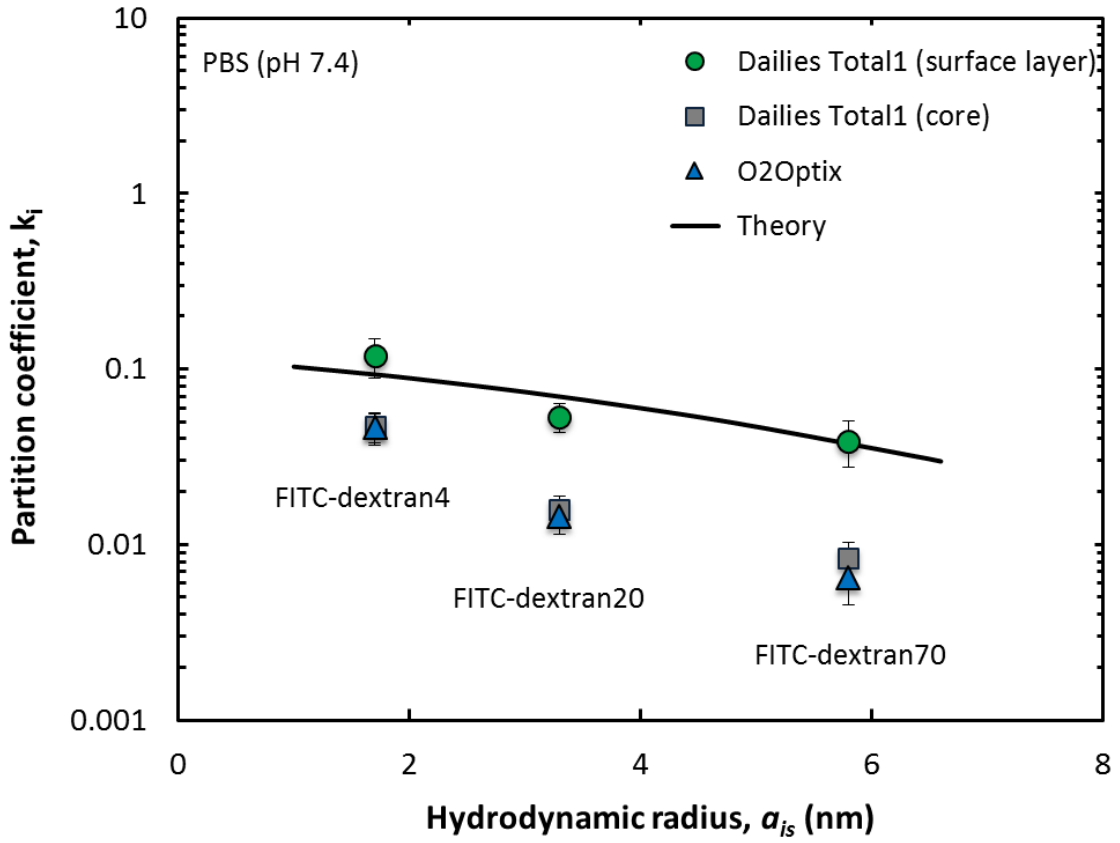

Figure 6.4: Hydrophilic solute partition coefficients, k_i, as a function of hydrodynamic radius, a_{is}, at pH 7.4 for FITC-dextran4, FITC-dextan20, and FITC-dextan70, in DAILIES TOTAL1® and O_2OPTIX™. The line is drawn according to Eq. 2, with $\phi_1 = 0.83$, $a_f = 6.6$ nm, $E_i^{el} = 0.14$, and $E_i^{ad} = 1$.

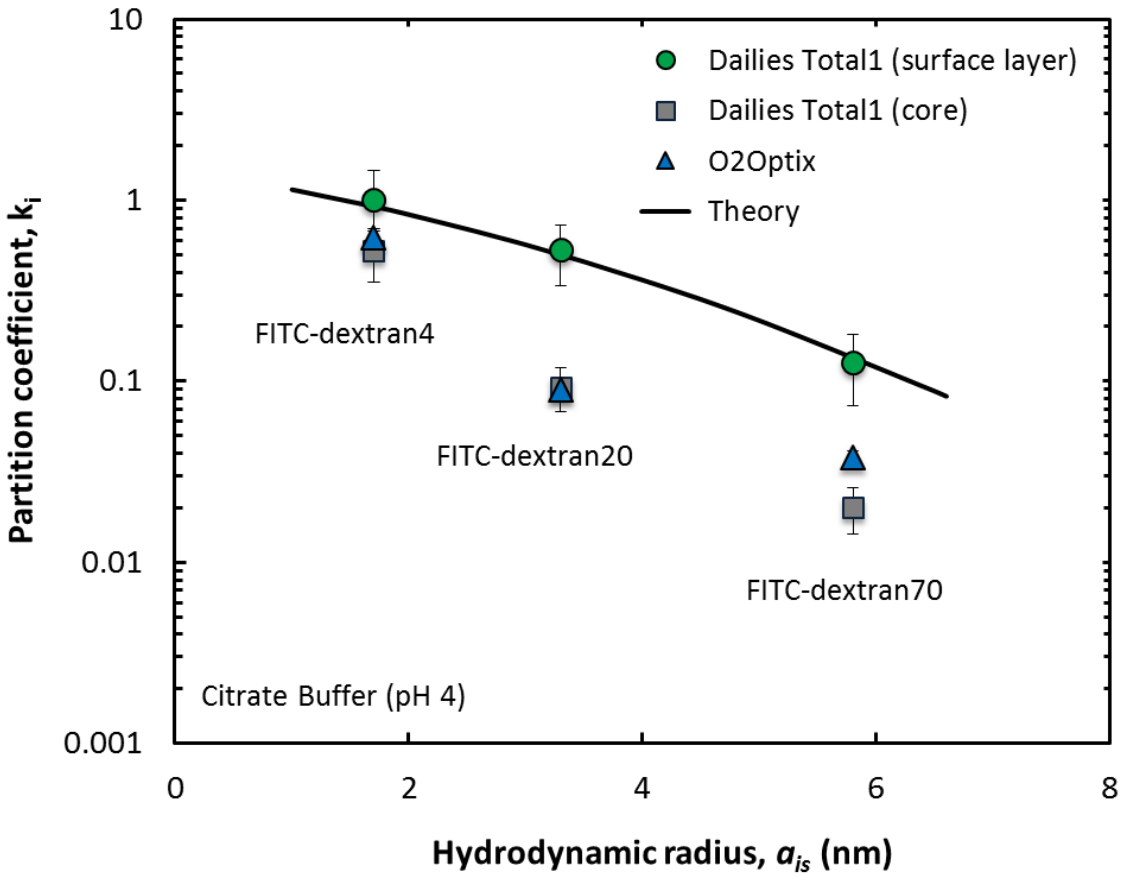

Figure 6.5: Hydrophilic solute partition coefficients, k_i, as a function of hydrodynamic radius, a_{is}, at pH 4 for FITC-dextran4, FITC-dextan20, and FITC-dextan70, in DAILIES TOTAL1® and O_2OPTIX™. The line is drawn according to Eq. 2, with $\phi_1 = 0.64$, $a_f = 6.6$ nm, $E_i^{el} = 1$, and $E_i^{ad} = 2.3$.

pH 7.4: partition coefficients are identical in O_2OPTIX™ and the DAILIES TOTAL1® SiHy core, and higher in the surface layers of DAILIES TOTAL1®. Partition coefficients again decline with increasing solute size. Here too, a solid line is drawn for the predicted FITC-dextran partition coefficients in the surface-gel layer according to Eq. 2 below.

Comparison of Figures 4 and 5 reveals that at pH 4 measured partition coefficients are large (i.e., greater than or equal to the water content), whereas at pH 7.4, measured partition coefficients are small (i.e., less than or equal to the lens water content) for the same solutes. This result is characteristic of aqueous ionized-solute partitioning into SCL materials due to repulsion between solutes and hydrogel strands of like-charge, and/or due to diminished specific interactions between ionized solutes and polymer chains.[13] At pH 7.4, FITC-dextrans (pK_a = 6.7, 4.4 [41]) are dianionic. They are repelled from coionic SCLs and also exhibit weaker specific adsorption to uncharged SCLs compared to that of the counterpart neutral solutes.[13] Conversely at pH 4, the aqueous solutes are predominately neutral, and are taken up more strongly by the SCLs. Measured FITC-dextran partition coefficients in the surface layer of DAILIES TOTAL1® increase more substantially with decreasing pH compared to those of the SiHy core and O_2OPTIX™, despite the larger surface-layer water content. Again, this result suggests that the DAILIES TOTAL1® surface gels are anionic. For O_2OPTIX™ and the SiHy core of DAILIES TOTAL1®, however, increased uptake at pH 4 compared to that at pH 7.4 is most likely explained by greater specific adsorption on a neutral polymer matrix due to decreased solute ionization.

Table 6.3 displays measured partition coefficients for the cationic protein FITC-avidin at pH 7.4. Partitioning of similarly sized FITC-dextran20 is shown for comparison. In the DAILIES TOTAL1® core and O_2OPTIX™, partition coefficients for the positively charged protein FITC-avidin are larger than those of similar-sized FITC-dextran20 again due to specific solute interaction with the polymer matrix. In the DAILIES TOTAL1® surface layer, however, FITC-avidin partition coefficients are nearly 30 times larger than those of FITC-dextran20. Strong specific adsorption of FITC-avidin to the negatively charged surface gel is indicated. We conclude that the high water-content surface-gel layers of DAILIES TOTAL1® are charged anionic, whereas both the SiHy core of DAILIES TOTAL1® and O_2OPTIX™ are nonionic at physiological pH.

Table 6.3: Partition Coefficients of FITC-avidin and FITC-dextran20 in DAILIES TOTAL1® and O_2OPTIX™ at pH 7.4

SCL	FITC-avidin	FITC-dextran20
DAILIES TOTAL1® (surface layer)	1.50 ± 0.75	0.054 ± 0.023
DAILIES TOTAL1® (core)	0.062 ± 0.023	0.016 ± 0.001
O_2OPTIX™	0.12 ± 0.05	0.014 ± 0.003

In contrast to the hydrophilic solutes in Figure 6.4 that exhibit small partition coefficients in the SiHy core (and in O_2OPTIX™)), oleophilic solutes (e.g., wax esters and

sterols) have a high affinity for silicone microdomains.[42] Figure 6.6 shows typical fluorescence-confocal-microscopy images of oleophilic Nile Red absorbed from silicone oil into water-saturated (a) DAILIES TOTAL1® and (b) O_2OPTIX™. Scale bars represent 20 μm in the vertical direction. Clearly, the oleophilic dye penetrates both SCLs after 2 d of loading. Table 6.4 summarizes partition coefficients for Nile Red and NBD-cholesterol in the DAILIES TOTAL1® core and O_2OPTIX™. Partition coefficients in the thin surface gel are not reported, because of the high intensity of the neighboring SiHy core interferes with measured intensities in the surface layer. Nevertheless, opposing fringes of low intensity (i.e., black) at the anterior and posterior of the lens are barely observed, confirming the presence of surface-gel layers.

Table 6.4: Oleophilic Solute Partition Coefficients in DAILIES TOTAL1® and O_2OPTIX™

SCL	Nile Red	NBD-Cholesterol
DAILIES TOTAL1® (core)	7.5 ± 0.5	5.8 ± 0.4
O_2OPTIX™	10.9 ± 0.9	7.4 ± 1.3

Both Nile Red and NBD-cholesterol exhibit greater-than-unity partition coefficients in the SiHy core of DAILIES TOTAL1® and in O_2OPTIX™ apparently owing to strong specific adsorption to silicone moieties.[13] Again, partition coefficients in the SiHy core of DAILIES TOTAL1® and in O_2OPTIX™ are similar (compare Figures 6a and 6b). Delivery of oleophilic solutes from silicone oil into a water-saturated SiHy lens does not mimic that on eye. That process involves lipid-solute delivery from lens-deposited patches or spots of tear-film lipids and proteins, not from continuous oil.[11,43,44] However, since oily deposits on worn SCLs directly contact the lens surface, local oil-soluble solute delivery to a water-saturated bulk lens is not disparate to that from continuous oil.

6.5 Discussion

We successfully implement fluorescent-solute partitioning experiments to characterize the layered structure of DAILIES TOTAL1® water-gradient lenses. Fluorescent-solute loading established a surface-layer thickness of approximately 10 μm, in good agreement with those reported earlier from atomic force microscopy.[27,28] Additionally, FCLSM measurements confirm consistently greater solute partitioning in the surface-gel layer reflecting large water-filled liquid spaces, and therefore, higher water content compared to that in the SiHy core. Surface-layer mass water content was established as 82 ± 3% using attenuated total-reflectance Fourier-transform infrared spectroscopy (ATR-FTIR) compared to a core water content of 34 ± 6%.

Fluorescent-solute partitioning experiments reveal the similarity of the DAILIES TOTAL1® SiHy core and O_2OPTIX™. Both hydrophilic and oleophilic-solute partition coefficients in the SiHy core and in O_2OPTIX™ were nearly identical, regardless of the solute and aqueous pH studied. This is likely due to their similar structure and chemistry giving equal water contents of 33%, reflective of similar-sized water-filled meshes. Likewise, similar SiHy

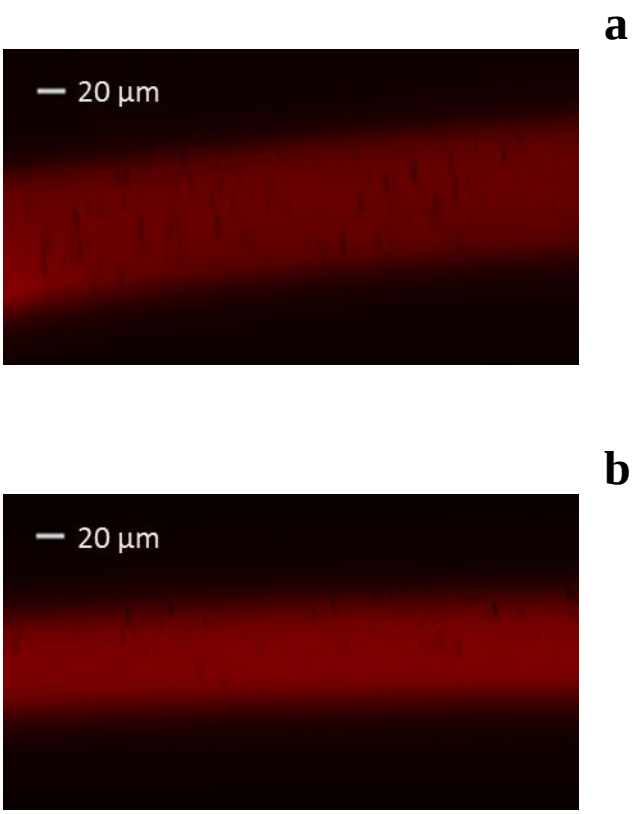

Figure 6.6: Fluorescence-confocal-microscopy images of Nile Red at equilibrium in DAILIES TOTAL1® (a) and O_2OPTIX™ (b). Scale bars represent 20 µm in the vertical direction. The dye is dissolved in silicone oil and delivered to water-saturated lenses.

compositions and structure lead to similar solute-gel interactions.[13,16,17] Additionally, we find that silicone-microdomain size scales as submicron in both O_2OPTIX™ and DAILIES TOTAL1®, since they are smaller than the resolution of the confocal microscope (~1 μm). This is clearly shown by the locally uniform intensities in Figures 3 and 6 and also by lens transparency.

Solute partitioning may also be used to determine the charge valence of SCLs. This chemical property is important to understanding care-solution and tear-film component uptake into lenses, since an ionic lens attracts counterion solutes and repels coion solutes.[9,13,16] Comparison of aqueous-solute partitioning at pH 4 compared to that at pH 7.4 reveals that the surface-gel layers of DAILIES TOTAL1® are anionic at physiological pH 7.4. The large partition coefficient of the positively charged protein, FITC-avidin, further supports this finding and also indicates specific ion binding of the protein to the negatively charged SCL-gel matrix. The large increase in surface-gel water content with increasing pH provides yet more confirmation of charged surface-gel layers.

Theory for hydrophilic-solute partition coefficients further documents our measured water content and charge valence of the DAILIES TOTAL1® surface gels. The partition coefficient, k_i, of an aqueous solute i is the product of the water volume fraction, ϕ_1, and individual enhancement factors[13]

$$k_i = \phi_1 E_i^{ex} E_i^{el} E_i^{ad} \tag{2}$$

where E_i^{ex}, E_i^{el} E_i^{ad} denote size exclusion, electrostatic interaction, and specific solute adsorption to the SCL polymer network strands, respectively. For an ideal point solute, k_i equals the hydrogel water volume fraction (i.e., $E_i^{ex} = E_i^{el} = E_i^{ad} = 1$). Actual solutes, however, are excluded from a gel matrix due to finite size ($E_i^{ex} < 1$), are attracted ($E_i^{el} > 1$) or repelled ($E_i^{el} < 1$) by electrostatic interaction with the polymer chains, and may specifically adsorb to the SCL polymer strands ($E_i^{ad} > 1$).[13] In Eq. 2, ϕ_1 is calculated from measured mass water contents of the surface layers (Table 6.2) and a dry polymer density characteristic of SCLs (1067 kg/m^3 [16]). Following Kotsmar et al.,[16] E_i^{ex} is given by a mesh-size distribution (e.g., see Eq. 8 of Kotsmar et al.[16]) with a fiber radius of 6.6 nm calculated from rubber elastic theory and ϕ_1 (specifically, the fiber radius was calculated using Eqs. 6 and 8 of Kotsmar et al.[16] with the measured surface-layer water volume fraction at pH 7.4 (Table 6.2), the length of a carbon-carbon bond (0.154 nm), the DAILIES TOTAL1® surface-gel elastic-modulus from nanoindentation tribology (0.025 MPa),[25] the Flory characteristic ratio typical of polymers with similar moduli ($C_n = 4$),[45] the dry polymer density characteristic of SCLs (1067 kg/m^3),[16,17] and a typical molecular weight of a repeat unit (300 g/mol)). At pH 4, the surface gels are essentially uncharged (i.e., the overall matrix monomer fractional degree of ionization, $f_{[-]}$, equals zero). Therefore, we take $E_i^{el} = 1$ at pH 4 and fit an average $E_i^{ad} = 2.3$ to the measured solute partition coefficients following Dursch et al.[13] Conversely, $E_i^{ad} = 1$ at pH 7.4, since FITC-dextrans are highly water soluble and not likely to interact specifically with the SCL polymer strands.[16] In this case, the anionic degree of ionization is taken as an

adjustable constant, $f_{[-]} = 0.17$, and $E_i^{el} = 0.14$ is calculated from Eqs. 8 and 9 of Dursch et al.[13] Importantly, all parameters are physically based.[13,16,17]

Lines in Figures 4 and 5 for the surface-gel partition coefficients are predicted from Eq. 2 according to the chosen parameter set. Excellent agreement is found for both pH values studied. Although the calculation is impacted by parameter choice, hydrophilic-solute-partitioning theory confirms the high water content and negative charge of the surface-gel layers at physiologic pH 7.4. Theory is not available for the SiHy gels in Figures 4 and 5.

Despite the high-water-content coating of DAILIES TOTAL1®, oleophilic Nile Red and NBD-cholesterol partition into the underlying SiHy core. In fact, equilibrium partition coefficients in the SiHy core of DAILIES TOTAL1® are similar to those in O_2OPTIX™ (Table 6.3). Oleophilic solutes penetrate the surface-gel layers by three possible mechanisms: (1) dissolution and bulk diffusion through the water fraction; (2) surface diffusion along polymer chains;[17,46] and (3) partial collapse of the surface gel when immersed in the oil allowing more direct access of the Nile Red to the core lens. Significant collapse, however, is unlikely due to the extremely low solubility of water in silicone oil.[47] We saturated DAILIES TOTAL1® lenses with aqueous FITC dextran4, equilibrated with FITC-dextran4-saturated silicone oil, and scanned with FCLSM. To within the precision of the experiment, no decrease in surface-gel thickness was observed demonstrating diffusion through the surface gel as the most likely access mechanism.

Although the aqueous solubilities of Nile Red and NBD-cholesterol are small,[48] they are apparently non-negligible. Bulk diffusion coefficients of similar sized solutes in water are of the order 10^{-6} cm^2/s.[13] Thus, dissolution and diffusion through the water fraction of the surface gel is a likely pathway for oleophilic-solute initial penetration into the supporting SiHy core of the lens.[46] Later saturation of the SiHy core by oleophilic dyes likely involves diffusion in both the hydrophobic silicone and hydrophilic phase-separated microdomains. In our experiments, the presence of a hydrophilic high-water-content surface gel did not prevent lipid penetration into a SiHy-lens core. We further conclude that transport of oil-soluble dyes through SiHy SCLS does not validate a percolated (i.e., gyroid[42]) microstructure for the silicone domains unless the aqueous-solute pathway can be completely eliminated.

6.6 Conclusions

Solute partitioning in SCLs provides valuable information on gel structure and composition in addition to quantifying uptake and release amounts. Using FCLSM and ATR-FTIR, we confirm the layered structure of DAILIES TOTAL1® with hydrophilic surface-gel layers of water content near 82% compared to 33% for the SiHy core. Consequent high aqueous-solute uptake is much higher in the surface gels compared to that in the SiHy-like core. Changes in the ionicity of the aqueous solutes evaluate the charge valence on the surface-gel layers as anionic at physiologic pH 7.4. Despite the high-water-content surface-gel layers, oleophilic Nile Red and NBD-cholesterol partition significantly from continuous oil into the SiHy core of DAILIES TOTAL1® with greater-than-unity partition coefficients because of strong specific adsorption in the silicone domains. Fluorescent-solute partitioning is a useful tool to characterize SCLs, especially those with surface coatings within the micron resolution of FCLSM.

6.7 Acknowledgements

We thank the CRL Molecular Imaging Center and NIH grant number 3R01EY015514-01S1 for use of the confocal microscope.

6.8 References

1. Jones, L.; Brennan, N. A.; González-Méijome, J.; Lally, J.; Maldonado-Codina, C.; Schmidt, T. A.; al., e. The TFOS international workshop on contact lens discomfort: Report of the contact lens materials, design, and care subcommittee. *Investigative Ophthalmology & Visual Science* **2013,** 54, (11), TFOS37-TFOS70.
2. Ketelson, H. A.; Meadows, D. L.; Stone, R. P. Dynamic wettability properties of a soft contact lens hydrogel. *Colloids and Surfaces B: Biointerfaces* **2005,** 40, (1), 1-9.
3. Tran, V. B.; Sung, Y. S.; Copley, K.; Radke, C. J. Effects of aqueous polymeric surfactants on silicone-hydrogel soft- contact-lens wettability and bacterial adhesion of Pseudomonas aeruginosa. *Contact Lens and Anterior Eye* **2012,** 35, (4), 155-162.
4. Tonge, S.; Jones, L.; Goodall, S.; Tighe, B. The ex vivo wettability of soft contact lenses. *Current Eye Research* **2001,** 23, (1), 51-59.
5. Peterson, R. C.; Wolffsohn, J. S.; Nick, J.; Winterton, L.; Lally, J. Clinical performance of daily disposable soft contact lenses using sustained release technology. *Contact Lens and Anterior Eye* **2006,** 29, (3), 127-134.
6. Szczotka-Flynn, L. B. Chemical properties of contact lens rewetters. *Contact Lens Spectrum* **2006,** 21, (4), 40.
7. Luensmann, D.; Jones, L. Protein deposition on contact lenses: The past, the present, and the future. *Contact Lens and Anterior Eye* **2012,** 35, (2), 53-64.
8. Bengani, L. C.; Leclerc, J.; Chauhan, A. Lysozyme transport in p-HEMA hydrogel contact lenses. *Journal of Colloid and Interface Science* **2012,** 386, (1), 441-450.
9. Guan, L.; Jiménez, M. E. G.; Walowski, C.; Boushehri, A.; Prausnitz, J. M.; Radke, C. J. Permeability and partition coefficient of aqueous sodium chloride in soft contact lenses. *Journal of Applied Polymer Science* **2011,** 122, (3), 1457-1471.
10. Lorentz, H.; Jones, L. Lipid deposition on hydrogel contact lenses: How history can help us today. *Optometry & Vision Science* **2007,** 84, (4), 286-295.
11. Peng, C.-C.; Lim, P. S.; Chong, H.; Dursch, T. J.; Radke, C. J. Critical coefficient of friction of in-vitro spoiled soft contact lenses. *Investigative Ophthalmology & Visual Science* **2014,** 55, (13), [ARVO E-Abstract 4652].
12. Alvarez-Lorenzo, C.; Hiratani, H.; Concheiro, A. Contact lenses for drug delivery: achieving sustained release with novel systems. *American Journal of Drug Delivery* **2006** 4, (3), 131-151.
13. Dursch, T. J.; Taylor, N. O.; Liu, D. E.; Wu, R. Y.; Prausnitz, J. M.; Radke, C. J. Water-soluble drug partitioning and adsorption in HEMA/MAA hydrogels. *Biomaterials* **2014,** 35, (2), 620-629.

14. Peng, C.-C.; Burke, M. T.; Chauhan, A. Transport of topical anesthetics in vitamin E loaded silicone hydrogel contact lenses. *Langmuir* **2011,** 28, (2), 1478-1487.

15. Kapoor, Y.; Thomas, J. C.; Tan, G.; John, V. T.; Chauhan, A. Surfactant-laden soft contact lenses for extended delivery of ophthalmic drugs. *Biomaterials* **2009,** 30, (5), 867-878.

16. Kotsmar, C.; Sells, T.; Taylor, N.; Liu, D. E.; Prausnitz, J. M.; Radke, C. J. Aqueous solute partitioning and mesh size in HEMA/MAA hydrogels. *Macromolecules* **2012,** 45, (22), 9177-9187.

17. Liu, D. E.; Kotsmar, C.; Nguyen, F.; Sells, T.; Taylor, N. O.; Prausnitz, J. M.; Radke, C. J. Macromolecule sorption and diffusion in HEMA/MAA hydrogels. *Industrial & Engineering Chemistry Research* **2013,** 52, (50), 18109-18120.

18. Am Ende, M. T.; Peppas, N. A. Transport of ionizable drugs and proteins in crosslinked poly (acrylic acid) and poly (acrylic acid-co-2-hydroxyethyl methacrylate) hydrogels. II. Diffusion and release studies. *Journal of Controlled Release* **1997,** 48, (1), 47-56.

19. Fatin-Rouge, N.; Milon, A.; Buffle, J.; Goulet, R. R.; Tessier, A. Diffusion and partitioning of solutes in agarose hydrogels: The relative influence of electrostatic and specific interactions. *The Journal of Physical Chemistry B* **2003,** 107, (44), 12126-12137.

20. Amsden, B. Solute diffusion within hydrogels: Mechanisms and models. *Macromolecules* **1998,** 31, (23), 8382-8395.

21. Watkins, A. W.; Southard, S. L.; Anseth, K. S. Characterizing multilaminated hydrogels with spatially varying network structure and solute loading using confocal laser scanning microscopy. *Acta Biomaterialia* **2007,** 3, (4), 439-448.

22. Walther, D. H.; Sin, G. H.; Blanch, H. W.; Prausnitz, J. M. Pore-size distributions of cationic polyacrylamide hydrogels of different compositions maintained at the same swelling capacity. *Journal of Macromolecular Science, Part B* **1994,** 33, (3-4), 267-286.

23. Walther, D. H.; Sin, G. H.; Blanch, H. W.; Prausnitz, J. M. Pore-size distributions of cationic 2-hydroxyethyl methacrylate (HEMA) hydrogels. *Polymer Gels and Networks* **1995,** 3, (1), 29-45.

24. Pruitt, J.; Bauman, E. The development of Dailies Total1 water gradient contact lenses. *Contact Lens Spectrum* **2013,** 28, (13), 40-44.

25. Dunn, A. C.; Urueña, J. M.; Huo, Y.; Perry, S. S.; Angelini, T. E.; Sawyer, W. G. Lubricity of surface hydrogel layers. *Tribology Letters* **2012,** 49, (2), 371-378.

26. Stone, R. P. Introducing water gradient technology. *Contact Lens Spectrum* **2013,** 28, (13), 34-38.

27. Pruitt, J.; Qiu, Y.; Thekveli, S.; Hart, R. Surface characterization of a water gradient silicone hydrogel contact lens (delefilcon A). *Investigative Ophthalmology & Visual Science* **2012,** 53, (14), [ARVO E-Abstract 6107].

28. Qiu, Y.; Pruitt, J. D.; Thekveli, S. J.; Tucker, R. C.; Nelson, J. Silicone hydrogel lenses with water-rich surfaces. USA Patent 20120026458, 2012.

29. Jones, L.; Dumbleton, K. Contact lenses. In *Optometry: Science, Techniques and Clinical Management*, Rosenfield, M.; Logan, N.; Edwards, K. H., Eds. Butterworth-Heinemann: 2009; p 341.

30. Wilson, T.; Coles-Brennan, C.; Xu, J.; Kakkassery, J. A novel method for evaluating ex vivo dehydration of contact lenses. *Contact Lens and Anterior Eye* **2013,** 36, Supplement 2, e20.

31. Hallinan, D. T.; Elabd, Y. A. Diffusion and sorption of methanol and water in nafion using time-resolved fourier transform infrared−attenuated total reflectance spectroscopy. *The Journal of Physical Chemistry B* **2007,** 111, (46), 13221-13230.

32. Ide, M.; Mori, T.; Ichikawa, K.; Kitano, H.; Tanaka, M.; Mochizuki, A.; Oshiyama, H.; Mizuno, W. Structure of water sorbed into poly(MEA-co-HEMA) films as examined by ATR−IR spectroscopy. *Langmuir* **2003,** 19, (2), 429-435.

33. Angelini, T.; Nixon, R.; Dunn, A.; Uruena, J.; Pruitt, J.; Sawyer, W. Viscoelasticity and mesh-size at the surface of hydrogels characterized with microrheology. *Investigative Ophthalmology & Visual Science* **2013,** 54, (15), [ARVO E-Abstract 500].

34. Smith, B. C. *Infrared spectral interpretation: A systematic approach*. CRC press: 1998.

35. Poole, R. A.; Hawe, A.; Jiskoot, W.; Braeckmans, K. Fluorescence spectroscopy to characterize protein aggregates and particles. In *Analysis of Aggregates and Particles in Protein Pharmaceuticals*, John Wiley & Sons, Inc.: 2012; pp 201-226.

36. Giordani, C.; Wakai, C.; Okamura, E.; Matubayasi, N.; Nakahara, M. Dynamic and 2D NMR Studies on Hydrogen-Bonding Aggregates of Cholesterol in Low-Polarity Organic Solvents. *The Journal of Physical Chemistry B* **2006,** 110, (31), 15205-15211.

37. Luensmann, D.; Zhang, F.; Subbaraman, L.; Sheardown, H.; Jones, L. Localization of lysozyme sorption to conventional and silicone hydrogel contact lenses using confocal microscopy. *Current Eye Research* **2009,** 34, (8), 683-697.

38. Luensmann, D.; Glasier, M.-A.; Zhang, F.; Bantseev, V.; Simpson, T.; Jones, L. Confocal microscopy and albumin penetration into contact lenses. *Optometry & Vision Science* **2007,** 84, (9), 839-847.

39. Sackett, D. L.; Wolff, J. Nile red as a polarity-sensitive fluorescent probe of hydrophobic protein surfaces. *Analytical Biochemistry* **1987,** 167, (2), 228-234.

40. Craig, J. P.; Willcox, M. D. P.; Argüeso, P.; Maissa, C.; Stahl, U.; Tomlinson, A.; Wang, J.; Yokoi, N.; Stapleton, F. The TFOS international workshop on contact lens discomfort: Report of the contact lens interactions with the tear film subcommittee. *Investigative Ophthalmology & Visual Science* **2013,** 54, (11), TFOS123-TFOS156.

41. Cole, L.; Coleman, J.; Evans, D.; Hawes, C. Internalisation of fluorescein isothiocyanate and fluorescein isothiocyanatedextran by suspension-cultured plant cells. *Journal of Cell Science* **1990,** 96, (4), 721-730.

42. Nicolson, P. C.; Vogt, J. Soft contact lens polymers: An evolution. *Biomaterials* **2001,** 22, (24), 3273-3283.

43. Hart, D. E.; Lane, B. C.; Josephson, J. E.; Tisdale, R. R.; Gzik, M.; Leahy, R.; Dennis, R. Spoliage of hydrogel contact lenses by lipid deposits: Tear-film potassium depression, fat, protein, and alcohol consumption. *Ophthalmology* **1987,** 94, (10), 1315-1321.

44. Copley, K. A.; Zhang, Y.; Radke, C. J. Wettability of SCLs assessed in a model blink–cycle cell. *Investigative Ophthalmology & Visual Science* **2006,** 47, (13), [ARVO E-Abstract 2407].

45. Raeber, G. P.; Lutolf, M. P.; Hubbell, J. A. Molecularly engineered PEG hydrogels: A novel model system for proteolytically mediated cell migration. *Biophysical Journal* **2005,** 89, (2), 1374-1388.

46. Petersen, S.; Fahr, A.; Bunjes, H. Flow cytometry as a new approach to investigate drug transfer between lipid particles. *Molecular Pharmaceutics* **2010,** 7, (2), 350-363.

47. Lee, J. N.; Park, C.; Whitesides, G. M. Solvent compatibility of poly(dimethylsiloxane)-based microfluidic devices. *Analytical Chemistry* **2003,** 75, (23), 6544-6554.

48. Castro, G. R.; Larson, B. K.; Panilaitis, B.; Kaplan, D. L. Emulsan quantitation by nile red quenching fluorescence assay. *Applied Microbiology and Biotechnology* **2004,** 67, (6), 767-770.

Appendix A

Confocal Microscopy Procedure

Fluorescent solute equilibrium partition coefficients and diffusivities in hydrogels may be obtained by two-photon fluorescence confocal microscopy. We employed a Carl Zeiss (Jena, Germany) 510 LSM META NLO AxioImager Confocal Microscope equipped with a Spectra-Physics (Santa Clara, CA) MaiTai HP DeepSee Laser at the UC Berkeley CRL Molecular Imaging Center. The procedure for measurement is described below.

A1. Initializing the Laser and Microscope

1. On the remote control, turn System/PC and Components switches **ON**. This provides power for the computer and initializes components utilized by the microscope software (**ZEN 2009**).

Figure A.1

2. Once computer loads, **open** MaiTai HP DeepSee Laser software (**Spectra-Physics Mai Tai Control rev E**) and select COM Port **4**.

Figure A.2

3. Through the software interface shown below, click **ON** to turn on the Spectra-Physics (Santa Clara, CA) MaiTai HP DeepSee Laser. It will say **EMISSION** once turned on.

Also, set the desired wavelength (**780 nm** for sodium fluorescein, FITC, Bodipy Green and riboflavin; **800 nm** for Nile Red).

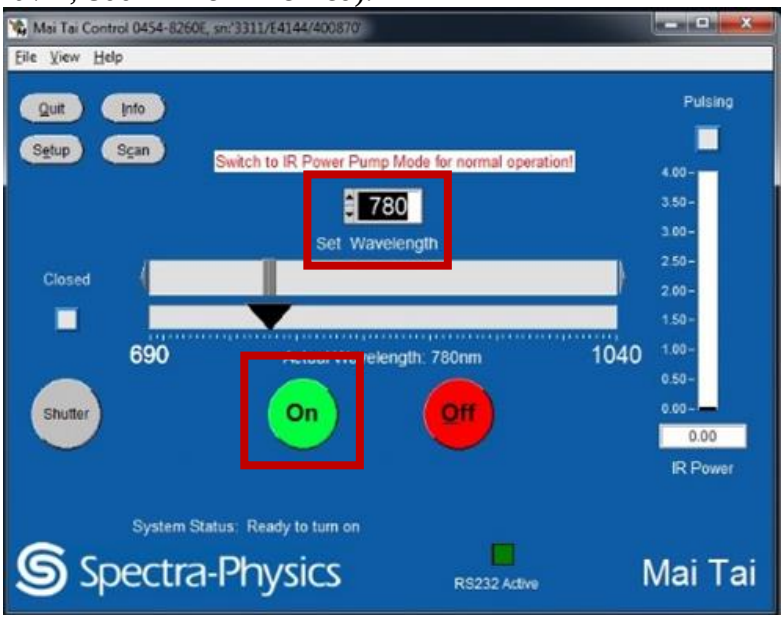

Figure A.3

4. **Close** MaiTai HP DeepSee Laser software (MaiTai controller software and **ZEN 2009** cannot be run concurrently). Click **Close shutter and exit** in the pop-up window.
5. **Open** microscope software (**ZEN 2009**) and click **Start System** to initialize the system hardware that will be used for imaging.

Figure A.4

6. **Important:** Wait at least **15 minutes** for laser power to become steady. Fluctuations in laser intensity will infect fluorescence intensity measurements.
7. Inside **ZEN 2009** click **Acquisition**.

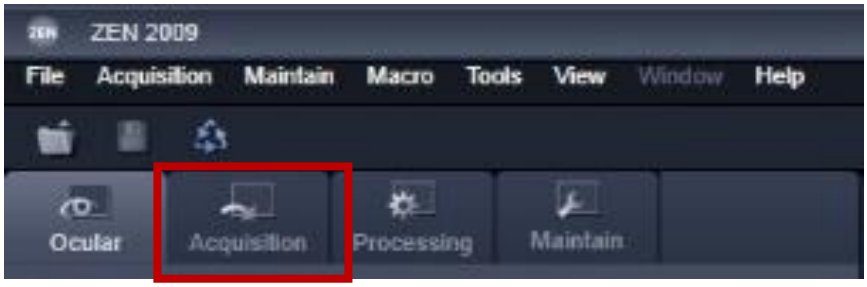

Figure A.5

8. Click the **Laser** tool and ensure **Power** is set to **On** and **Status** reads **Mode-locked**

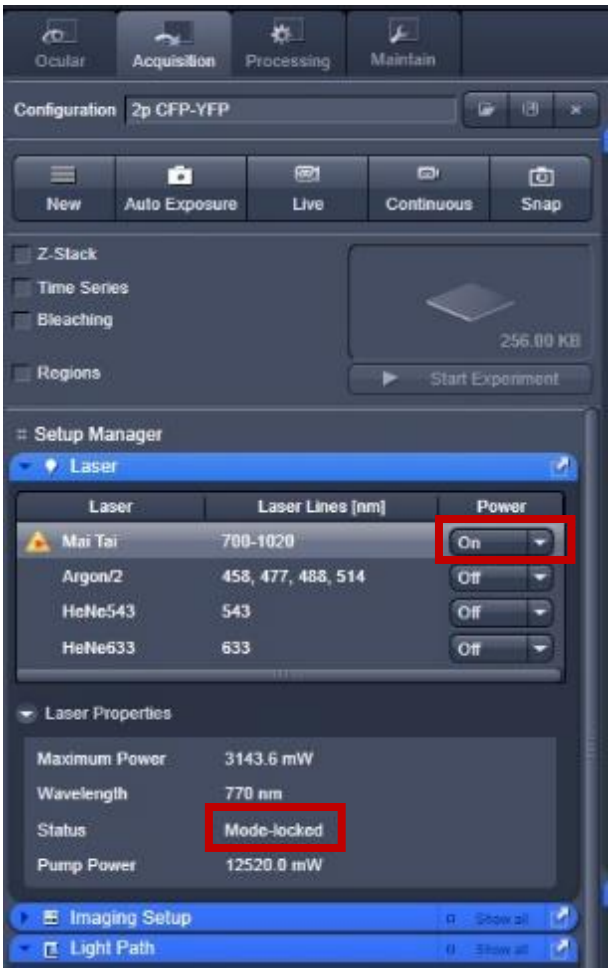

Figure A.6

9. If have configuration previously stored, then load it. Otherwise click **Light Path** and set it to the configuration shown below:

9a. For sodium fluorescein, FITC, Bodipy Green and riboflavin:

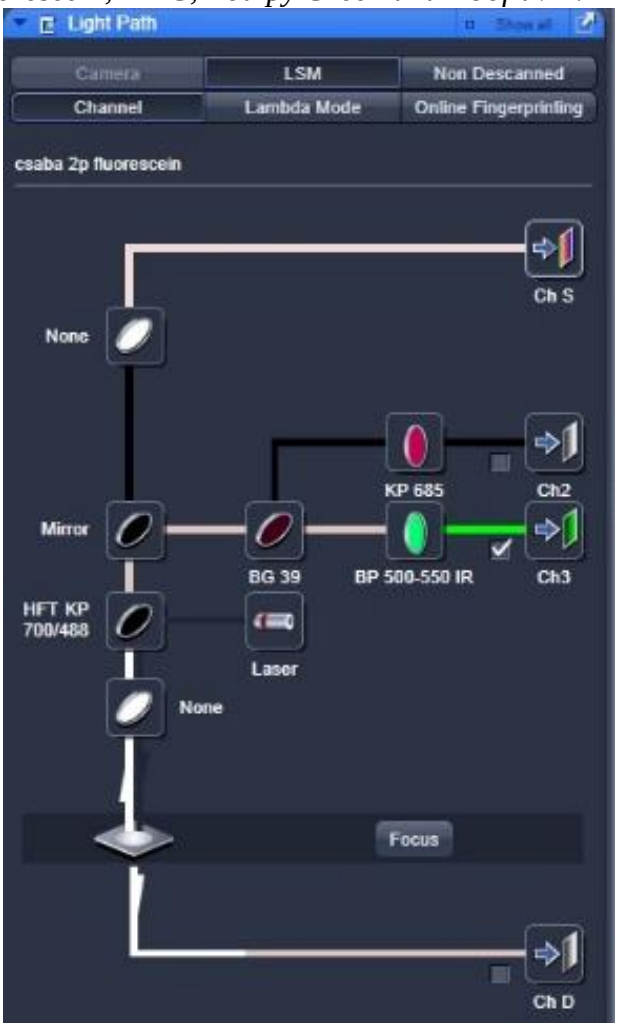

Figure A.7

9b. For Nile Red:

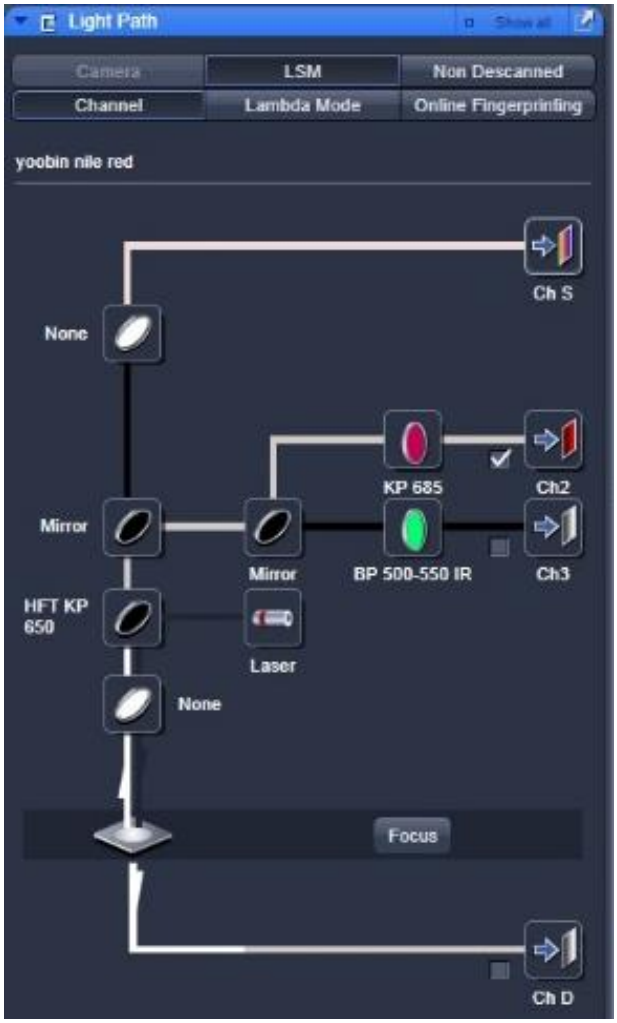

Figure A.8

A2. Initial Imaging Procedure

10. Ensure 10x-air objective is used for imaging (~3 cm focal distance)
11. Under **Acquisition** menu select **Live** to begin fast-scanning. Place Kimwipe® on microscope stage and see if red light is transmitted through the objective onto the Kimwipe®. If no light is visible, imaging cannot be performed due to laser misalignment or errors in microscope setup. Contact facility administrator if this is the case.

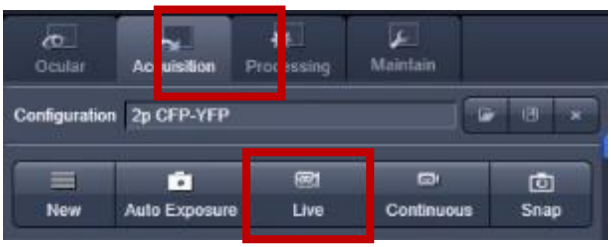

Figure A.9

12. Place microscope slide (VWR Micro Slides, 48300-04) on microscope stage. Pipette pertinent solute-containing-solution from vile into petri dish or vial cap and place on microscope slide with care not to spill.
13. Adjust stage height with care so objective does not touch solution. Once within the focal distance of the objective, fluorescence should be detected and the image on the screen will appear brighter. Intensity values of the image will also increase. Signal may be seen by the naked eye as a bright light coming from the sample (e.g., green for Fluorescein). If no intensity is detected, open the **Channels** dropdown and adjust transmission % (by the slide bar next to the laser) and detector **Gain.** Transmission % is the amount of laser output. Detector gain is the sensitivity of the detector employed. Increasing either will increase detected signal but also background signal. If no intensity is observed with these adjustments, the concentration of fluorescent solute in the sample may be too low and should be raised. Detection depends on several parameters including the solute concentration in the sample, the laser power employed, as well as the cleanliness of the objective lens employed.

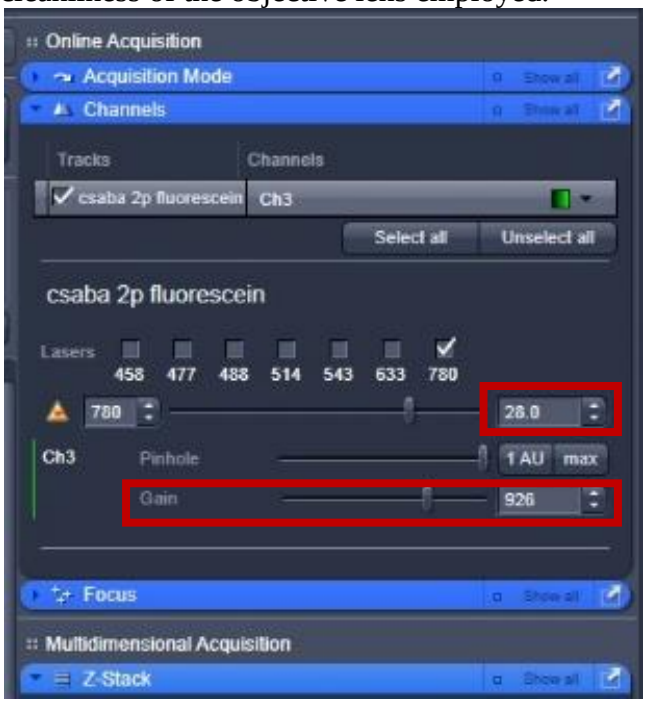

Figure A.10

Note: In this image, detector **Gain** is set extremely high (926) to show its range. At this high a value it is likely to saturate the detector. Typical Gain values during experimentation are 100-500.

14. Click **Stop** to stop scanning.

A3. Concentration Detection: 2D Imaging in the Vertical (z-) Direction

15. Check the **Z-Stack** box and click **Live** for fast-scanning. Then prepare sample as described below:

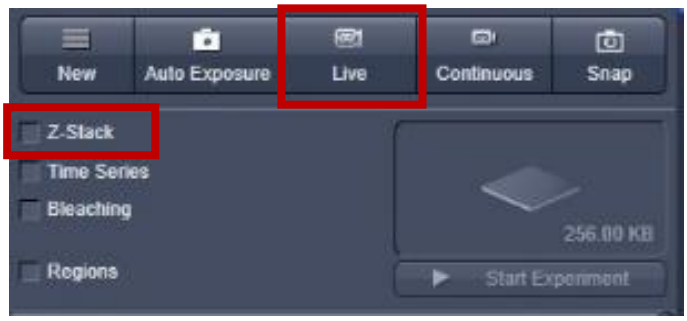

Figure A.11

15a. *For Liquids:* Prepare sample for measurement by Step 12.

15b. *For Hydrogels:* Remove hydrogel from solution and place on microscope slide. Quickly measure (before it dries out) by Steps 16-17. Ideally, total measurement time should be < 2 minutes.

16. Open the **Z-Stack** drop-down menu. Adjust stage height to adjust scanning region. Click **Set First** and **Set Last** to adjust the limits of the vertical measurement region. Also, choose **Interval** size for measurement (typically 2-10µm is suitable but choose wisely to obtain enough intensity points (> 20 inside the solution or gel sample) and scanning time is not too long (~1-2 min). When setting the upper limit, obtain intensities in the space above the sample for background florescence intensity. For hydrogel measurements, also obtain intensities below the sample to ensure scanning through the whole gel thickness. Background florescence intensity arises due to the light from the surroundings.

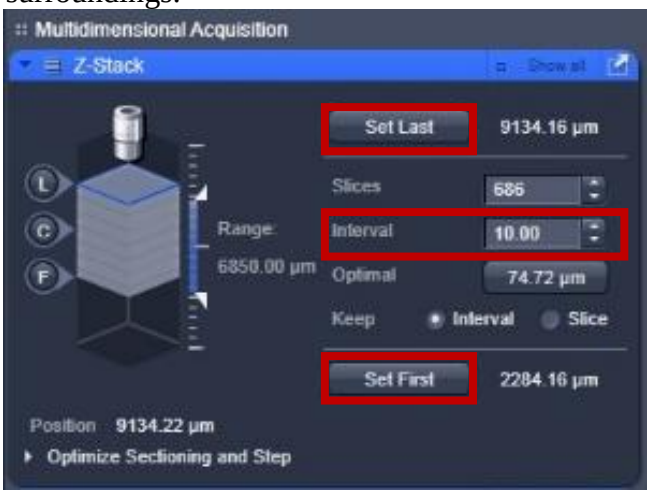

Figure A.12

17. Click **Start Experiment** to begin scanning. When scanning is completed **save** the image. It will save as an LSM file.

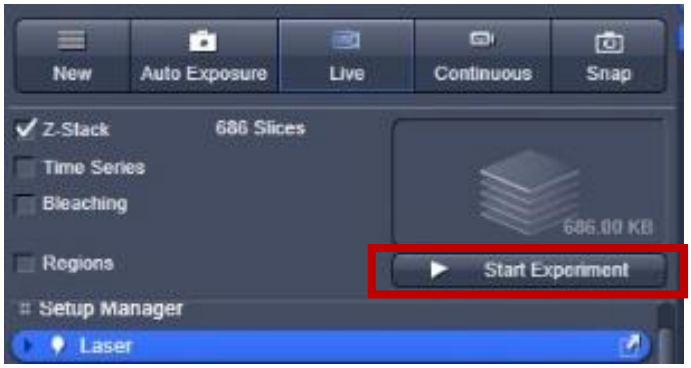

Figure A.13

A4. Obtaining Fluorescence Intensities

18. Fluorescence Intensities may be extracted in either **ZEN 2009** or **ImageJ.** Each method is described below

18a. In **ZEN 2009** click the **Profile** tab. Ensure the **line** tool is selected. Then, inside the image click (and hold), and drag your mouse across the image. Pixel intensities in the region where you dragged (the red line that appears on the screen) will be shown and may be saved for later use.

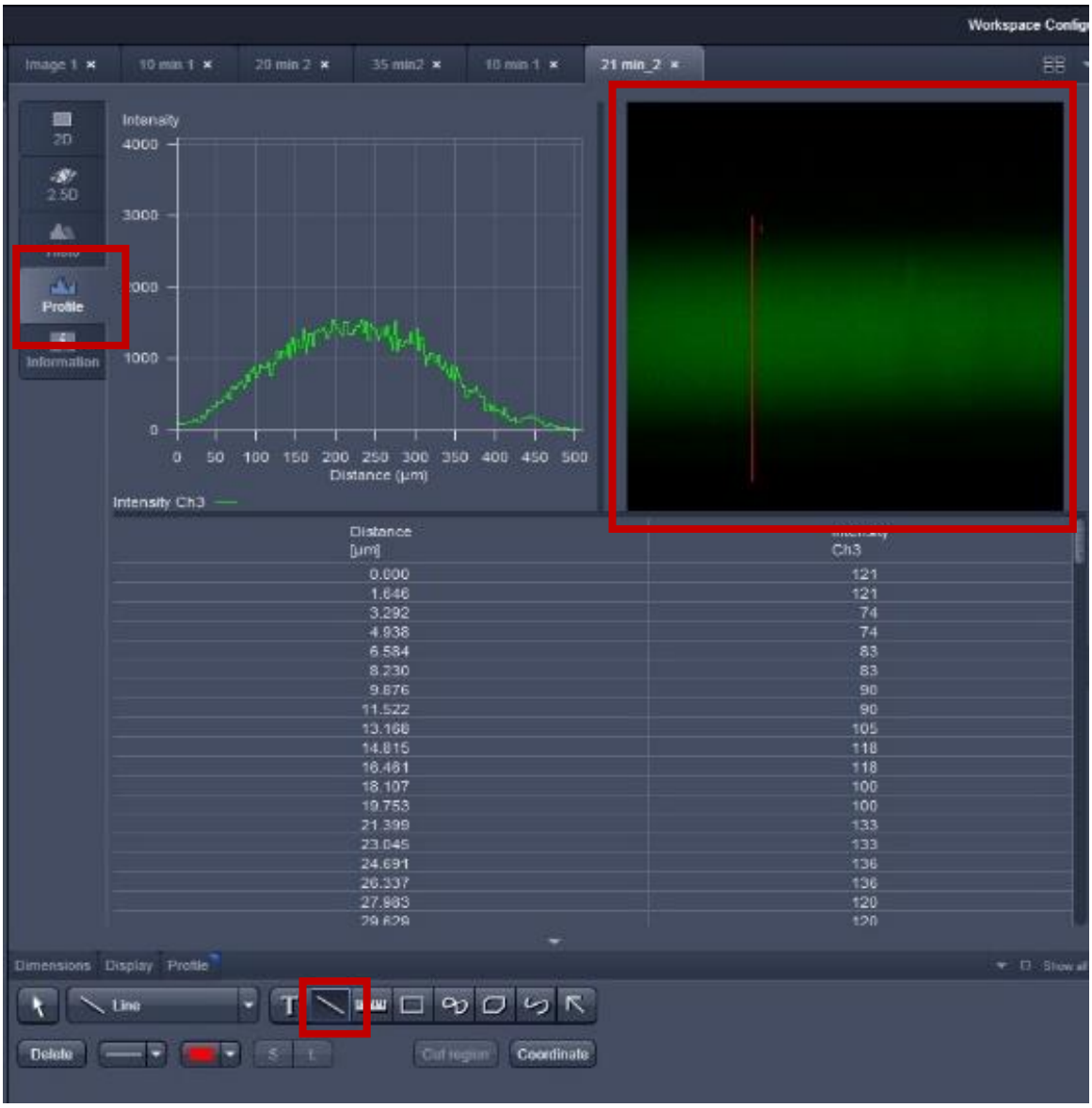

Figure A.14

18b. In ImageJ,

i. Open the image (LSM file) and select the **Rectangular** selection tool.

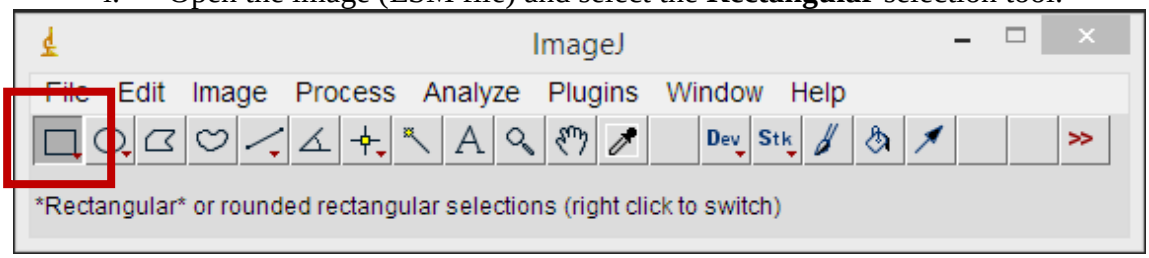

Figure A.15

ii. Select the desired region in the image for fluorescence intensity extraction. In the **Analyze** drop down click **Plot Profile.** A profile will appear for averages of all fluorescence intensities in the z-direction as a function of position in the x-direction.

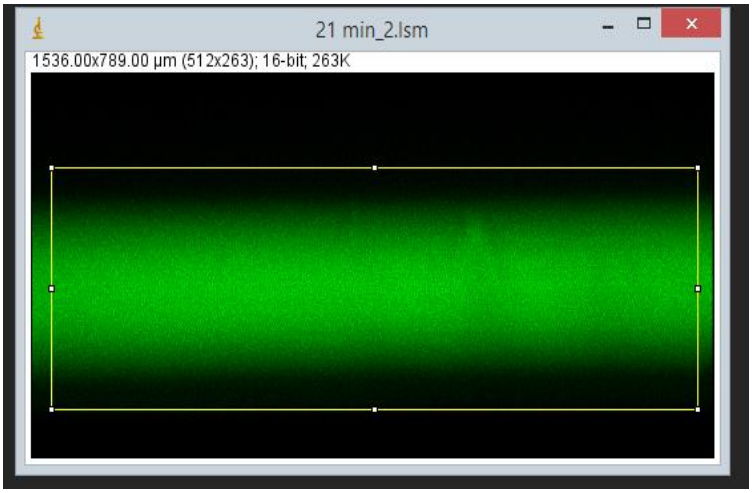

Figure A.16

iii. Click **Live**. Hold **alt** and click the corner of your selection rectangle to plot averages of all fluorescence intensities in the x-direction as a function of position in the z-direction. While holding **alt** unclick **Live.**

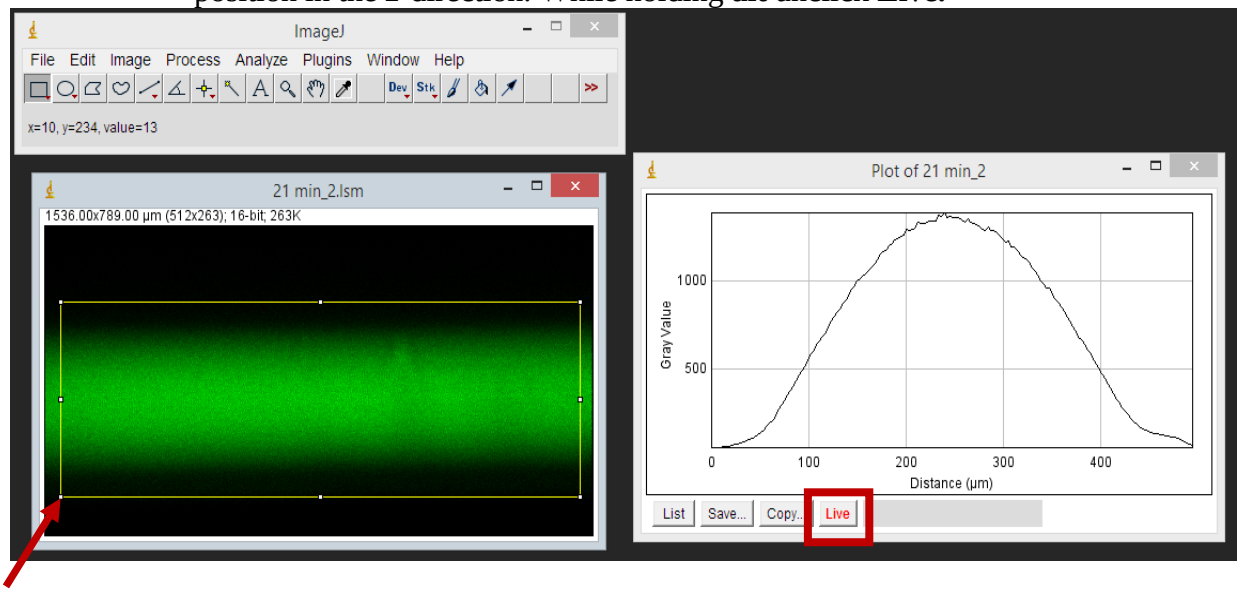

Figure A.17

19. Before analysis, subtract background fluorescence intensity from all values. Ensure detected sample intensities are each at least twice the background intensity value. If detected intensities blend with the background, measurement becomes inaccurate.

A5. Calibration: Ensure Florescence Intensity and Solute Concentration are Linearly Proportional

20. Prepare solutions of the same composition (e.g., buffer, dilute HCl, silicone oil) and dissolve varying amounts of pertinent fluorescent solute in each. Typically the fluorescent solute concentrations should span a few orders of magnitude.
21. Measure fluorescence intensity of solutions with similar fluorescent solute concentrations by Steps 15-19 with the same microscope settings (same transmission % and detector gain). If intensity is outside of the detectable range, adjust microscope settings (transmission % and detector gain) until detection is possible. See Step 13 to adjust microscope settings. **Please note if using more than one microscope setting:** Must have repeat measurements of the same solute concentration solution at different microscope settings so comparison between settings is possible.
22. Repeat Step 21 until all solutions are accounted for and extract fluorescence intensities by Step 18-19.
23. Compare concentrations of prepared solutions to measured florescent intensities to determine the linear regime.

A6. Partition Coefficient Measurement

Note: Partition coefficient measurement should only be performed where fluorescence intensity and concentration are linearly proportional

24. Prepare pertinent solute-containing solution of at least 10 mL in 20mL scintillation vials. Place desired hydrogel (6 x 6 mm, 100μm-2.5mm thick) in solution under magnetic stirring at 400 rpm and allow time to equilibrate. **For solute-hydrogel systems with extremely pronounced specific adsorption**, solute-containing bulk solution may need to be changed periodically to ensure solution concentration does not deplete and remains in the measurable range.
25. After equilibration, measure florescent solute concentrations in the hydrogel and surrounding bulk solution by Steps 15-19.

A7. In-Gel Diffusivity Measurement

Note: Diffusivity measurement should only be performed where fluorescence intensity and concentration are linearly proportional

Absorption Measurements

26. Soak aqueous-solution equilibrated gel sheets (6 x 6 mm, 100μm-2.5mm thick) in solute-containing aqueous solution under magnetic stirring at 400 rpm. Each gel should be in its own 20mL scintillation vial with ~20mL of solute-containing aqueous solution.
27. At selected times, remove a gel sheet from solution, lightly blot on both faces, and place flat on a microscope slide (VWR Micro Slides, 48300-047, VWR International, West Chester, PA, USA). A microscope cover-glass (#12-541-B, Fisher Scientific, Fair Lawn, New Jersey, USA) to prevent water evaporation is optional. However, keep the total measurement time to a minimum as described in Steps 15 and 16.
    a. Blotting must be lightly performed to not infect measurements. Alternatively, a gel may be lightly dragged across a microscope slide on both faces to remove excess solution.

b. Selected times should be greater than 10 minutes for accurate diffusion coefficient measurement. In the first ten minutes, times may be inaccurate as measurement time is ~1 min. Further, within the first 5 minutes, measurements may also be infected slightly by initial placement into the solute-containing solution. Although early time measurements are not recommended, if desired, infection may be mitigated by turning on and off the magnetic stirring 2-3 times quickly upon gel placement. We find no change in measured diffusivities from this procedure.
c. Selected times should be spaced out so that profiles from each time point are distinct from each other.
d. Selected times should be small enough so the concentration in the gel has not equilibrated. If measurement is taken too close to equilibrium, diffusivity measurement may become inaccurate. Hence, thicknesses must be chosen wisely to allow for suitable measurement times.

28. Follow steps 15-18 and scan downward through the gel at selected intervals over the entire hydrogel slab thickness. To minimize edge effects, perform scans in the middle of the hydrogel slab. After scanning is complete, do a second back-up scan at a different point in the middle of the gel slab for good measure.
    a. A diffraction pattern may be observed (due to solute dried on the surface from blotting or inhomogeneities in the gel sample) when scanning through the gel. These scans are inaccurate for concentration measurement and should not be used.

Desorption Measurements

29. Soak nascent swollen gels sheets in the pertinent solute solution under magnetic stirring to complete saturation. Confirmed saturation through measuring the gel partition coefficient and a uniform-equilibrated concentration profile.
30. After equilibration, place solute-saturated gel sheets in a large volume of solute-free pertinent solution under magnetic stirring at 400 rpm.
31. At selected release times, scan a gel sheet similarly to the absorption measurements, but without blotting. The same considerations as in absorption are important for desorption.

Diffusion Analysis

32. Convert micrographs obtained from two-photon confocal microscopy into fluorescence-intensity-versus-position profiles by Steps 18 and 19. For each image, multiple intensity vs position measurements should be averaged into one profile (either by extracting intensities from multiple vertical lines drawn in **ZEN 2009** or through the rectangular selection tool in **ImageJ**). If extracting intensities from drawn vertical lines in **ZEN 2009**, averaged intensities must be smoothed with nearby points by an adjacent-averaging smoothing technique. If **ImageJ** is used, smoothing averaged intensities with nearby points is not necessary.
    a. Because of signal attenuation, intensities near the bottom of the gel slab are slightly lower than those near the top of the slab. Detected fluorescence intensities decline when a thick sample is scanned deeply. The magnitude of

signal attenuation depends on hydrogel composition, water contents, and solute concentration. Lower hydrogel water contents and higher solute concentrations are more prone to this decline. To overcome the lack of uniform signal detection at the solute concentrations studied, data measured only in the top one-half of the gel where intensities are practically independent of sample depth should be analyzed. Gel thicknesses were also chosen so signal attenuation is negligible in the top half of the gel.

b. A second artifact arises in the experimental intensity data directly at the top surface of the gel. Solute concentrations at the top surface should be large and remain at a single large value during loading. In some cases, however, the maximum fluorescence intensity measured in the gel sample is not exactly at the top surface of the gel, but sometimes is observed downward to a depth of 50 μm. Most likely, the gel surface is locally dried due to the blotting procedure. Consequently, do not directly use the measured surface intensities in the fitting procedure to obtain solute/gel diffusion coefficients. We find that stirring the surrounding bulk aqueous phase at higher speeds, or even no stirring, has no influence on the measured concentration profiles, confirming negligible external mass-transfer resistance.

33. Extract diffusion coefficients from fluorescence vs intensity profiles by application of Fick's Second law and a least squares fitting algorithm as described in Chapter 2.

Appendix B

Transient Intensity Profiles Measured by Confocal Microscopy

This appendix presents typical absorption/desorption transient intensity profiles for fluorescent solutes in 2-hydroxyethyl methacrylate/methacrylic acid (HEMA / MAA) hydrogels. These profiles illustrate the importance of specific steps taken in Appendix A.

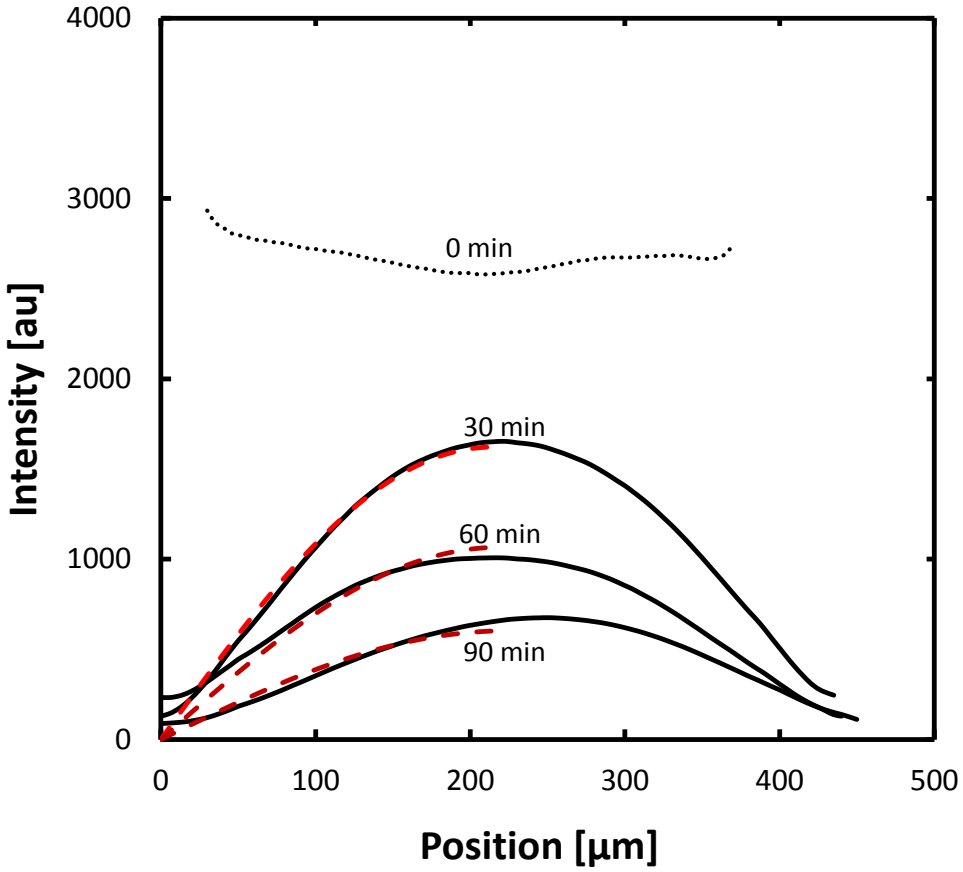

Figure B.1: Transient intensity profiles of FITC-dextran20 desorption from 70 wt % HEMA/30 wt % MAA hydrogels with 1 wt % cross-link density at pH 7.4. Solid and dashed lines represent measured profiles and best fits to Fick's law, respectively. Hydrogel thicknesses and measurement times are chosen appropriately (Appendix A Steps 27b-d). Selected measurement times are >10 min but less than the time to reach equilibrium. Additionally, chosen times are spread out to obtain distinct intensity profiles as shown here.

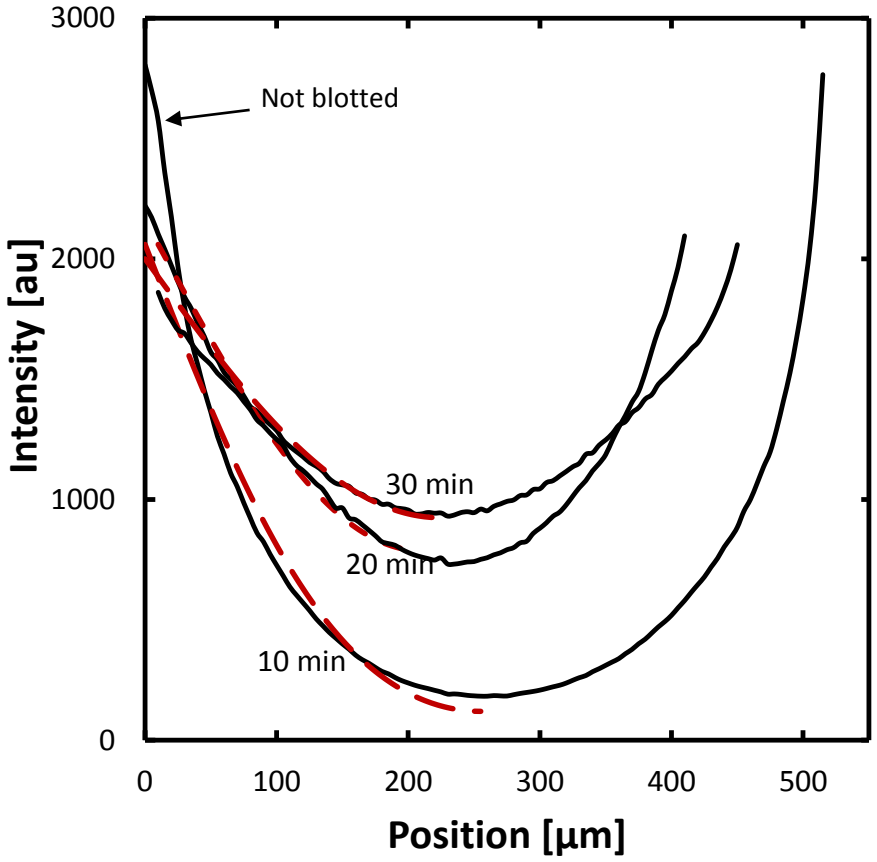

Figure B.2: Transient intensity profiles of FITC-dextran20 absorption into 70 wt % HEMA/30 wt % MAA hydrogels with 0.05 wt % cross-link density at pH 7.4. Solid and dashed lines represent measured profiles and best fits to Fick's law, respectively. As described in Appendix A, measurements at each time point are of a different sample (and here, each has a different thickness). Note the 10 min profile shown has much higher measured surface concentrations as it was not blotted and is infected by the high intensities of outside solution present on the gel surface. Clearly, surface blotting is important in absorption profile measurement (Appendix A Step 27a).

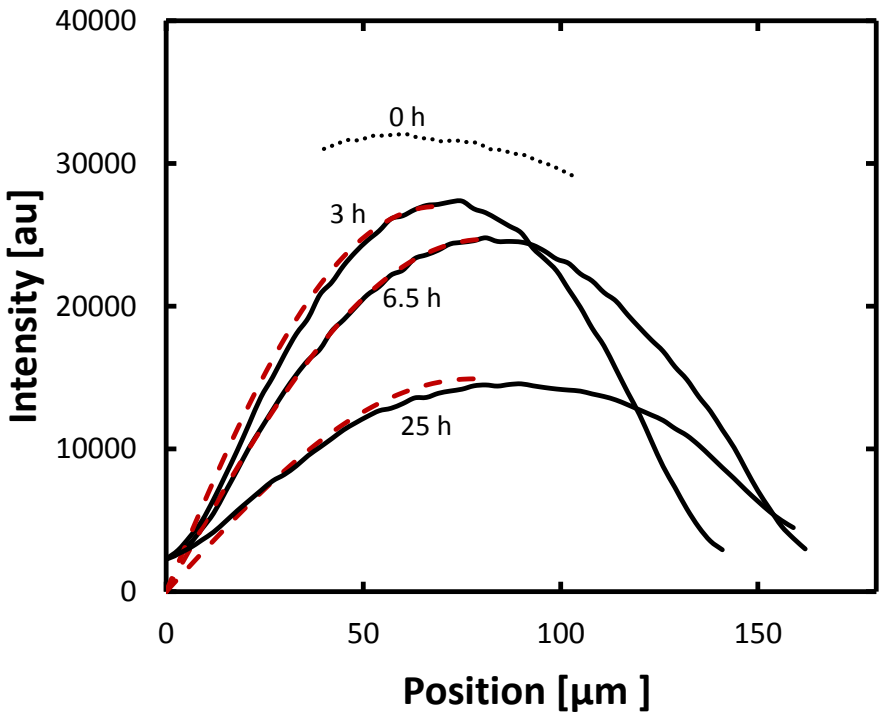

Figure B.3: Transient intensity profiles of sodium fluorescein desorption from 100 wt % HEMA/ 0 wt % MAA hydrogels with 0.25 wt % cross-link density at pH 2. For strongly adsorbing solutes with extremely low effective diffusion coefficients, it is imperative to choose suitable microscope settings (Appendix A Step 21), hydrogel thicknesses, and measurement times (Appendix A Step 27). Note if laser power varies between measurement times, scans of a saturated gel at each measurement time must also be performed and the profiles renormalized.

Appendix C

Steric Obstruction Factor Derivation

Following Brady[1], the relative diffusion coefficient of dilute solute i in a liquid-saturated gel may be expressed as a product of a hydrodynamic factor, F_i, and a steric obstruction factor, S_i, or

$$\frac{D_i}{D_{io}} = F_i S_i, \tag{C1}$$

where D_i and D_{io} are the solute diffusion coefficient inside the hydrogel and in bulk solution, respectively. This appendix presents our derivation of the steric obstruction factor (Chapter 2 Eq. 13) used in Large-Pore Effective-Medium (LPEM) theory. We adopt the analytical cylindrical-cell methodology presented in Belloni et al.,[2] Nilsson et al.,[3] and Johansson et al.[4] Section C1 calculates the diffusion coefficient of solute transporting across a single cylindrical cell. In Section C2, the overall steric obstruction factor is calculated by integrating over the distribution of cylindrical cells in the Ogston mesh-size distribution.[5] For clarity, throughout this appendix we drop the subscript i.

C1. Single Cylindrical-Cell Diffusion Coefficient

To determine the steric obstruction factor, we first calculate the diffusion coefficient of a point solute transporting across a single cylindrical cell. A cylindrical cell of radius R was constructed over an infinitely long polymer strand of radius a_f and subjected to a constant perpendicularly-imposed bulk concentration gradient (in the x-direction) of magnitude E. Let x_0 be the macroscopic rectangular coordinate on the length scale of the medium. On this scale, x_0 locates center of a polymer strand. Origin of the local or microscopic length scale x is set at the center of the cylinder. Figure C.1 displays a diagram of the cylindrical cell. In this appendix, let c and $< c >$ denote the microscopic and bulk concentrations, respectively. The steady-state diffusion equation under these conditions is

$$0 = \nabla^2 c(r,\theta), \tag{C2}$$

and macroscopically,

$$\frac{\partial < c >}{\partial x_0} = E, \tag{C3}$$

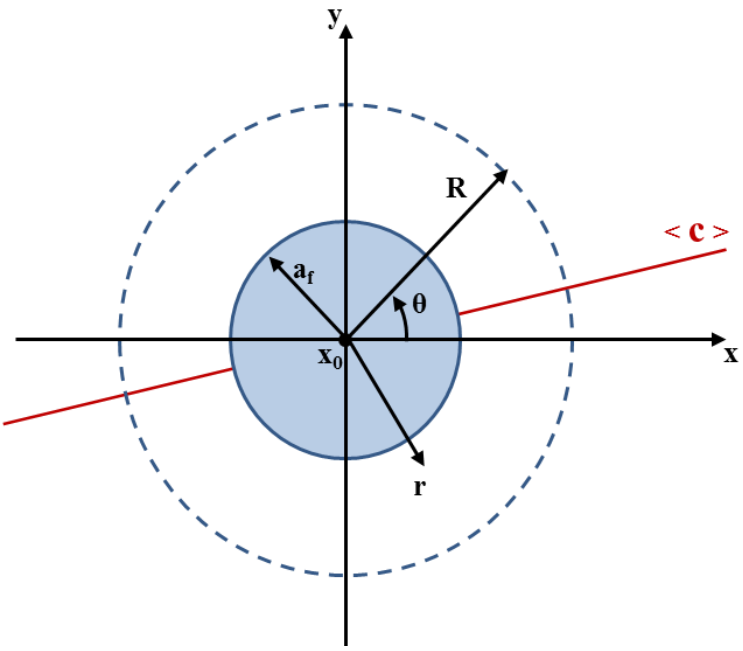

Figure C.1: Cylindrical-cell diagram

subject to the boundary conditions,

$$\text{BC 1.} \qquad c(r=R,\theta) = < c > = E(x_0 + R\cos\theta) \tag{C4}$$

$$\text{BC 2.} \qquad \frac{\partial c}{\partial r}(r=a_f,\theta) = 0 \tag{C5}$$

$$\text{BC 3.} \qquad \frac{\partial c}{\partial \theta}(r, \quad \theta = 0,\pi) = 0\,. \tag{C6}$$

At the edge of the cylindrical cell (i.e., at $r = R$), the microscopic variation in concentration due to the obstructing polymer strand is negligible. Accordingly, the concentration at $r = R$ is equivalent to the macroscopic bulk concentration (BC 1). Additionally, at the surface of the polymer strand (i.e., $r = a_f$), there is zero flux (BC 2).

From Eq. C4, we assume a solution of the following form:

$$c(r,\theta) = f_0(r) + f_1(r)\cos\theta\,. \tag{C7}$$

BCs 1 and 2 now become

$$\text{BC 1.} \qquad f_0(R) = Ex_0 \quad , \quad f_1(R) = ER \tag{C8}$$

$$\text{BC 2.} \qquad \frac{\partial f_0}{\partial r}(a_f,\theta) = 0 \quad , \quad \frac{\partial f_1}{\partial r}(a_f,\theta) = 0 \quad . \tag{C9}$$

Substitution of Eq. C7 into Eq. C2 and setting each part equal to zero gives

$$\frac{1}{r}\frac{d}{dr}\left(r\frac{df_0}{dr}\right) = 0 \tag{C10}$$

$$\text{and } r^2\frac{d^2 f_1}{dr^2} + r\frac{df_1}{dr} - f_1 = 0\,. \tag{C11}$$

Eq. C11 is of the form of Cauchy-Euler. Applying the BCs to Eqs. C10 and C11 and solving for the microscopic concentration in the cylindrical cell yields

$$c(r,\theta) = Ex_0 + \frac{E\left(r + \dfrac{a_f{}^2}{r}\right)}{1 + \dfrac{a_f{}^2}{R^2}}\cos\theta\,. \tag{C12}$$

To obtain the diffusion coefficient over a single cylindrical cell, we first relate the microscopic flux to the overall macroscopic flux in the x-direction. The macroscopic flux in the x-direction is defined as,

$$< j_x >= -D_\perp \frac{\partial < c >}{\partial x_0} = -D_\perp E, \tag{C13}$$

whereas the microscopic flux is defined as,

$$\underline{j} = -D_o \nabla c = -D_o \left[\frac{\partial c}{\partial r} \underline{i}_r + \frac{1}{r} \frac{\partial c}{\partial \theta} \underline{i}_\theta \right] \tag{C14}$$

where $D_\perp$ and D_o are the diffusion coefficients over a single cylindrical cell and in free-solution, respectively. Gauss's divergence theorem dictates,

$$0 = \int \nabla \cdot \underline{j} dV = \int_{S_1} \mathbf{n} \cdot j_r dS_1 + \int_{S_2} \mathbf{n} \cdot j_x dS_2 \tag{C15}$$

where **n** is a unit outward normal, V is the volume of the cylindrical cell, j_r and j_x denote fluxes in the r and x directions, respectively, and S_1 and S_2 are surfaces enclosing the polymer strand with normal vectors in the r and x directions, respectively. For clarity, Figure C.2 displays a diagram of the fluxes and the S_1 and S_2 surfaces. Here,

$$\int_{S_1} \mathbf{n} \cdot j_r dS_1 = \int_{S_1} -D_o \frac{\partial c}{\partial r}|_R \, dS_1 = L \int_\theta^{2\pi-\theta} -D_o \frac{E \cos\theta \left(1 - \frac{a_f{}^2}{R^2} \right)}{\left(1 + \frac{a_f{}^2}{R^2} \right)} R d\theta \tag{C16}$$

Substituting C16 into C15 gives,

$$\int_{S_2} \mathbf{n} \cdot j_x dS_2 = -D_0 2L(\sin\theta) R f_1'(R) \tag{C17}$$

where $f_1'(R) = E \left(1 - \frac{a_f{}^2}{R^2} \right) \Big/ \left(1 + \frac{a_f{}^2}{R^2} \right)$.

Solving for average flux in the x-direction over the control volume yields the macroscopic flux, or

$$< j_x >= \frac{\int_{-R}^{R} \left[\int_{S_2} \mathbf{n} \cdot j_x dS_2 \right] dx}{\int dV} = -D_0 f_1'(R). \tag{C18}$$

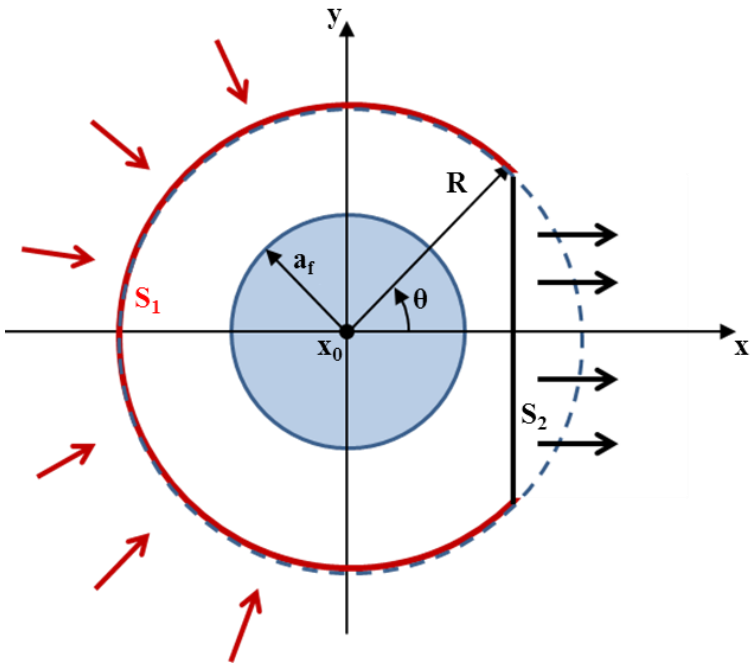

Figure C.2: Flux through cylindrical cell

Please note in Eq. C18 that the total volume of the cylindrical cell is used and not only that surrounding the polymer strand. We desire the average value over all space and not that in an annulus.

Equating Eqs. C13 and C18 with slight rearrangement yields the relative diffusion coefficient over a single cylindrical cell, or

$$\frac{D_{\perp}}{D_0} = \frac{f_1'(R)}{E} = \frac{\left(1-\frac{a_f{}^2}{R^2}\right)}{\left(1+\frac{a_f{}^2}{R^2}\right)}. \tag{C19}$$

Extending Eq. C19 for finite solute size gives Chapter 2 Eq. 12, or

$$\frac{D_{\perp}^{*}(R)}{D_0} = \frac{\left(1-\frac{(a_S+a_f)^2}{R^2}\right)}{\left(1+\frac{(a_S+a_f)^2}{R^2}\right)}, \tag{C20}$$

where a_S is the hydrodynamic radius of the diffusing solute and * denotes finite solute size.

C2. Evaluation of the steric obstruction factor

Following Johansson et al.,[4] a correlation function is employed to relate the diffusion coefficient over a single cylindrical cell to an overall steric obstruction factor. To compute the correlation function, we start with the void-volume distribution function in a single cylindrical cell, or

$$g^{CC}(r',R) = \frac{2(r'+a_f)}{R^2}\sigma\left(r'-(R-a_f)\right), \tag{C21}$$

where

$$\sigma\left(r'-(R-a_f)\right) = \begin{Bmatrix} 1 & r' \le (R-a_f) \\ 0 & r' > (R-a_f) \end{Bmatrix}$$

and r' is a vector normal to the polymer strand beginning at a_f and pointing radially outward (i.e., $r' = r - a_f$).[4] The step function, $\sigma\left(r'-(R-a_f)\right)$ ensures $g^{CC}(r',R)$ has a nonzero value only within the cylindrical cell. Figure C.3 displays a diagram of the cylindrical cell with r' labeled. Figure C.4 graphs the step function, $\sigma\left(r'-(R-a_f)\right)$. The validity of Eq. C21 was confirmed as integrating over all space gave the void-volume fraction of the cylindrical cell (i.e., $1-\frac{a_f^2}{R^2}$).

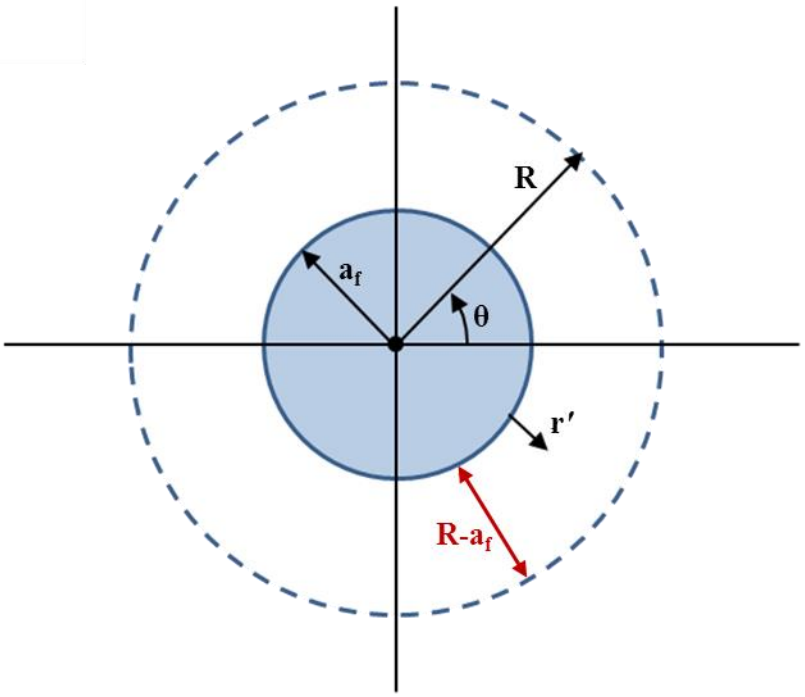

Figure C.3: Cylindrical-cell diagram illustrating *r*'

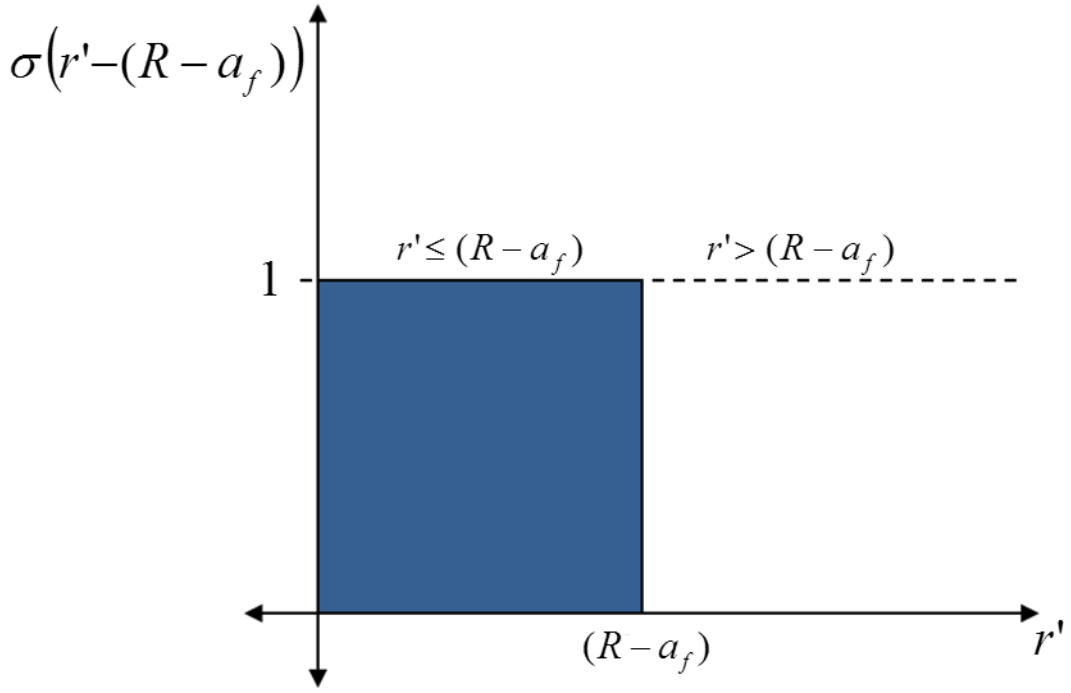

Figure C.4: The step function, $\sigma\left(r'-(R-a_f)\right)$ as a function of r'

Ogston's distribution,[5] derived for randomly oriented infinitely long fibers, is given by

$$g_0(r') = \frac{2\phi_2}{a_f}(1+\frac{r'}{a_f})\exp[-\phi_2(1+\frac{r'}{a_f})^2], \tag{C22}$$

where ϕ_2 is the overall polymer volume fraction. The correlation function, $\zeta(R)$, is defined such that

$$g_0(r') = \int_{a_f}^{\infty} \zeta(R) g^{CC}(r', R) dR. \tag{C23}$$

Deconvolution[4] of Eq. C23 yields the correlation function

$$\zeta(R) = \frac{2\varphi_2{}^2 R^3}{a_f^4} \exp\left[-\varphi_2 \frac{R^2}{a_f^2}\right]. \tag{C24}$$

Correcting for excluded volume due to finite solute size, Eqs. C21 and C23 become

$$g^{*CC}(r,b) = \frac{2(r + a_f + a_S)}{R^2} \sigma\big(r - (R - a_f - a_S)\big) \tag{C25}$$

$$\text{and } g_0{}^*(r) = \frac{2\phi_2}{a_f}(1+\frac{r}{a_f}+\frac{a_S}{a_f})\exp[-\phi_2(1+\frac{r}{a_f}+\frac{a_S}{a_f})^2], \tag{C26}$$

respectively. The validity of Eq. C25 was confirmed as integrating over all space gave the void-volume fraction available to a size-excluded solute in a cylindrical cell (i.e., $1-\frac{(a_S + a_f)^2}{R^2}$).

Following the deconvolution procedure with Eqs C25 and C26 yielded the correlation function accounting for finite solute size, or

$$\zeta^*(R) = \frac{2\varphi_2{}^2 R^3}{a_f^4} \exp\left[-\varphi_2 \frac{R^2}{a_f^2}\right]. \tag{C27}$$

Comparison of Eqs. C27 and C24 reveals the correlation functions for point solutes and for size-excluded solutes are identical.

The overall steric obstruction factor, S, was obtained by taking the product of the cylindrical-cell relative diffusivity and the correlation function and integrating, or

$$S = \int_{a_f}^{\infty} \frac{D_{\perp}^*(R)}{D_0} \zeta^*(R) dR \tag{C28}$$

Substitution of Eqs. C20 and C27 into Eq. C28 and integrating yields,

$$S(\alpha) = [1-\alpha]e^{-\alpha} + 2\alpha^2 e^{\alpha} E_1(2\alpha) \qquad \text{(C29)}$$

where $\alpha = \phi_2(1+\frac{a_S}{a_f})^2$ and E_1 is the exponential integral, $E_1 = \int_x^{\infty} \frac{e^{-u}}{u} du$.

References

1. Brady, J. F. Hindered diffusion. In *Extended Abstracts, AIChE Annual Meeting, San Fransisco, CA 1994*, AIChE: p 320.
2. Belloni, L.; Drifford, M.; Turq, P. Counterion diffusion in polyelectrolyte solutions. *Chemical Physics* **1984,** 83, (1), 147-154.
3. Nilsson, L. G.; Nordenskioeld, L.; Stilbs, P.; Braunlin, W. H. Macroscopic counterion diffusion in solutions of cylindrical polyelectrolytes. *The Journal of Physical Chemistry* **1985,** 89, (15), 3385-3391.
4. Johansson, L.; Elvingson, C.; Löfroth, J. E. Diffusion and interaction in gels and solutions. 3. Theoretical results on the obstruction effect. *Macromolecules* **1991,** 24, (22), 6024-6029.
5. Ogston, A. G. The spaces in a uniform random suspension of fibres. *Transactions of the Faraday Society* **1958,** 54, 1754-1757.

Appendix D

Hydrodynamic Permeability of Hydrogels

Abstract

The hydrodynamic (Darcy) permeability, κ, is a necessary parameter in Large-Pore-Effective Medium (LPEM) theory for *a priori* diffusion-coefficient prediction. This appendix reports experimentally measured hydrodynamic permeabilities of co-polymer hydroxyethyl methacrylate (HEMA) / methacrylic acid (MAA) hydrogels studied in Chapters 2-4. Invoking the Carman-Kozeny expression for porous-medium absolute permeability (Chapter 2 Eq. 7) yields excellent agreement with experimental values validating its application with a hydrodynamic tortuosity, $\tau_H \sim 4.7$ for our HEMA/MAA hydrogels. Also presented are experimentally measured and theoretically predicted hydrodynamic permeabilities of HEMA/MAA-based silicone hydrogels (SiHys). The silicone monomer and amphiphilic compatibilizer employed in SiHy synthesis were 3-methacryloxypropyltris (trimethylsiloxy)silane (TRIS) and acryloxy-terminated ethyleneoxide dimethylsiloxane-ethyleneoxide ABA triblock copolymer (DBE-U12), respectively. For the SiHys, measured hydrodynamic permeabilities rise linearly with increasing solvent-free hydrophilic-polymer volume fraction. Similar to the water and solute uptake models presented in Chapter 5, hydrodynamic permeability is predicted assuming water flow occurs only though the hydrophilic microdomains. In all cases, excellent agreement is found between theory and experiment.

The work presented in this appendix was performed in collaboration with Kevin Jia-Yu Hou and Nina Widjaja. Included with permission

D1 Experimental Methods

D1.1 Hydrogel Synthesis

HEMA/MAA hydrogels were synthesized by thermal-initiated free radical polymerization as described in Chapters 2 and 3. However, SiHys in this appendix were synthesized utilizing photo-initiation rather than the thermal initiation described in Chapter 5. The hydrodynamic permeability measurement requires large surface-area hydrogel slabs without defects or holes, which lead to artificially high measured permeabilities. Regions with holes sometimes develop when synthesizing SiHys by thermal-initiated free-radical polymerization. Hole formation is likely due to solvent boiling during polymerization. The solvent, ethanol, has a boiling point (78°C) very similar to the decomposition temperature of the thermal initiator, 4,4-Azobis(4-cyanovaleric acid) (~70 °C). Nevertheless, water uptake in SiHys synthesized by photo-initiation were similar to those in SiHys synthesized by the thermal-initiation procedure described in Chapter 5.

Unlike solute and water uptake presented in Chapter 5, measurement of hydrodynamic permeabilities require SiHys of large surface area without any holes/defects. Because fluid-flow takes the path of least resistance, even a single hole renders the hydrodynamic permeability measurement inaccurate by orders of magnitude. Accordingly, SiHys were synthesized using photo-initiation. For photo-initiated free radical polymerization, hydrogel composition was varied by altering the relative amounts of silicone monomer (i.e., TRIS), macromer (i.e., DBE-U12), and hydrophilic monomer (i.e., HEMA, MAA, or a mixture of 2 vol % MAA and 98 vol % HEMA denoted as 2%MAA/98%HEMA) in the volume ratios reported in Table D.1. Typical reaction solutions consisted of monomer, macromer, 0.25 vol % ethylene glycol dimethacrylate (EGDMA), 0.5 wt% of 2-Hydroxy-2-methylpropiophenone (97%, Sigma Aldrich, St. Louis, MO), and 100 wt% ethanol as the solvent, where percentages are of total monomer plus macromer. Hydrogels are referred to by their corresponding solvent-free volume fraction of hydrophilic monomer, ν_{hyphil}, where the volume fraction of hydrophilic monomer, macromer ($\nu_{macromer}$), and hydrophobic monomer (ν_{hyphob}) sum to unity (i.e., $1 = \nu_{hyphil} + \nu_{macromer} + \nu_{hyphob}$). The solution was stirred magnetically, and subsequently bubbled with nitrogen gas for 15 min to remove dissolved oxygen. The stripped reaction mixture was injected between two upright glass plates separated by a spacer (100 μm-250 μm thick), and previously hydrophobized with RainX® Original (Sopus Products, Houston, TX). The solution-filled glass molds were exposed to UV light ($\lambda = 312$ nm; Spectroline Bi-O-Vision TVD-1000R, Spectronics Corp., Westbury, MY) at 70% intensity until synthesis was complete. Typical exposure times were ~40 min. However, longer exposure times were necessary for high-silicone-fraction SiHys (up to 120 min). After synthesis, SiHys were swelled in phosphate buffered saline (PBS) for a minimum of 48 hours changing solution daily until equilibrium was reached. Equilibrium water contents of all SiHys were obtained prior to permeability measurement to ensure consistency between batches.

Table D.1: SiHy Composition and Hydrophilic-Monomer Volume Fraction, ν_{hyphil}

Constituent Volume Parts			ν_{hyphil}
[a] Silicone Monomer	Macromer	[b] Hydrophilic Monomer	
10	[c]1 or 2	1	~0.08
5	1	1	0.14
1	1	1	0.33
1	1	5	0.71

[a] TRIS

[b] HEMA, MAA, or 2%MAA/98%HEMA

[c] 1 macromer volume part is used for HEMA-based hydrogels, whereas 2 macromer volume parts are used for MAA- and 2%MAA/98%HEMA- based hydrogels.

D1.2. Hydrodynamic Permeability Measurement

Hydrogel hydrodynamic permeabilities were measured using a custom-built apparatus adapted from that of Monticelli et al.[1] Figure D.1 diagrams the permeameter. To maintain constant inlet pressure, compressed air was supplied through a house line to a constant-head aqueous solution reservoir modulated by a pressure regulator (Veriflo Corp., Richmond, CA). A 170-kPa safety check valve (1.27-cm Swagelok SS-802-25; Solon OH) prevented over-pressurization. A digital pressure gauge (SSI Technologies, Inc., Janesville, WI) was installed to detect and to ensure constant-head pressures. Due to vessel pressurization, aqueous solution flowed from the pressurized tank, through the custom-built membrane holder, described in detail below, and up a precision-bore vertical glass capillary tube (ID 1 mm, Wilmad LabGlass, Buena, NJ) open to ambient pressure. The membrane holder was situated at equal elevation with the air-line exit in the constant-head reservoir. Accordingly, pressure upstream of the hydrogel slab equals that detected by the digital pressure gauge. Thus, the pressure drop across the hydrogel slab is that between the pressure-gauge reading and the liquid head equivalent generated from liquid-height rise in the capillary tube. Liquid-height rise was measured with a precision cathetometer (Wild Heerbrugg, KM347, Gains, Switzerland).

For steady flow through porous media, Darcy's law dictates the relationship between applied pressure and fluid-flow velocity,

$$v = -\frac{\kappa}{\mu}\frac{\Delta P}{L}, \tag{D1}$$

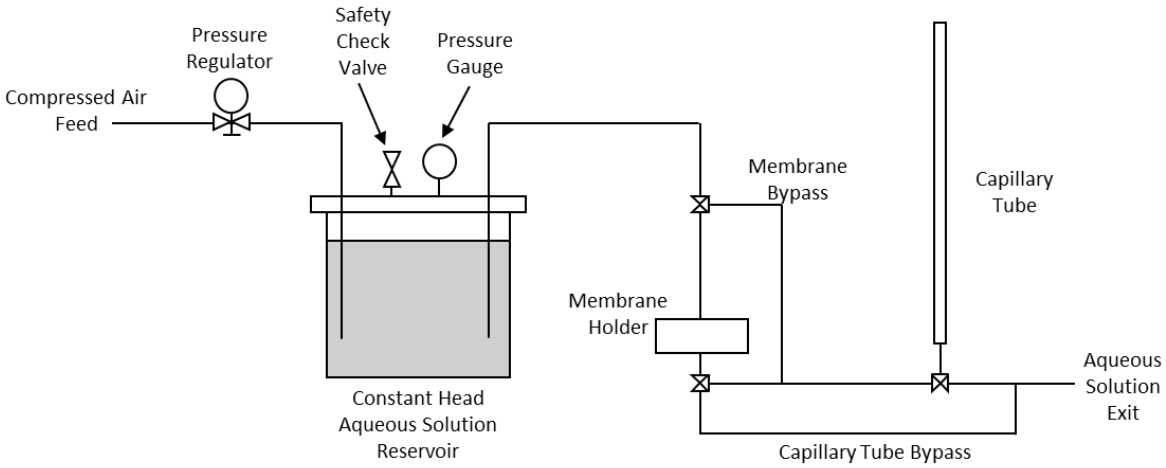

Figure D.1: Diagram of the permeameter apparatus

where v and μ are the fluid superficial velocity and viscosity, respectively, κ is the porous-medium hydrodynamic permeability, ΔP is the pressure difference across the hydrogel slab, and L is the slab thickness. Here $\Delta P = P_2 - P_1$ where P_1 and P_2 are the pressures just upstream and downstream of the hydrogel slab.

Prior to measurement, hydrogels were swollen to equilibrium in phosphate-buffered saline (PBS) as described in Chapters 2-5. Equilibrium swollen hydrogel slabs were subsequently cut into circles of 5.5 cm diameter and placed into the custom-built membrane holder. Figure D.2 displays a diagram of the membrane cell. The hydrogel slab sat atop a Whatman filter paper (Cat No 1001 150) and beneath a silicone-rubber gasket (ID 2.54 cm) that prevent hydrogel deformation and define the flow area, respectively. The silicone-rubber gasket also provides a leak-tight seal for the hydrogels. Gasket thickness was chosen accordingly (500 μm and 330 μm for hydrogels synthesized with 100 μm and 250 μm spacers, respectively). A solid plastic gasket (ID 2.54 cm, 380μm thick) was positioned above the rubber gasket. All internal components are housed within the membrane cell and are sandwiched between porous plastic distributers (from 47 mm Millipore filter holders) to ensure uniform water flow. The membrane cell was held together by four screws near the periphery that compress the three O-rings and silicone rubber-gasket to prevent leakage. Additionally, cell assembly took place under water to eliminate trapped air bubbles that interfere with hydrodynamic permeability measurement.

Following membrane-holder assembly, constant-head pressure was applied to the upstream side of the hydrogel slab and monitored by the installed pressure gauge. Concomitantly, the flowrate through the membrane cell was determined by the height rise in the capillary tube. To obtain accurate hydrodynamic permeabilities, flowrate data were analyzed under steady-state conditions (when both the flowrate and applied pressure remained constant with time). Time to steady state varied depending upon hydrogel composition and the upstream pressures applied but typically required ~4 hours. After steady state was achieved, height readings were taken at regular time intervals of 20-90 minutes chosen for accurate fluid-height changes (i.e., > 2 mm). For each hydrogel composition, hydrodynamic permeabilities were measured as a function pressure drop. Moderate pressures drops (20-150 kPa) were employed to prevent hydrogel deformation/tearing.

Figure D.3 displays typical measured hydrodynamic permeabilities as a function of pressure drop for 3 MAA-based SiHys. Measured hydrodynamic permeabilities decrease linearly with rising pressure drop, likely due to hydrogel compression. Identical trends were observed in agarose hydrogels.[2] We desire the zero-pressure-drop hydrodynamic permeability, κ_0, as hindered solute diffusion in hydrogels occurs without an external applied pressure. Following Johnson and Deen,[2] κ_0 was evaluated by fitting a straight line to the measured hydrodynamic permeabilities as a function of pressure drop and extrapolating to the ordinate intercept.

D2. Results and Discussion

D2.1 Hydrodynamic Permeabilities of HEMA/MAA Homopolymer Hydrogels

Figure D.4 plots κ_0 as a function of water content expressed in the form $(1-\phi_2)^3/\phi_2^2$ (per Carman-Kozeny theory) on log-log scales for HEMA/MAA hydrogels at pH 7.4. Measured

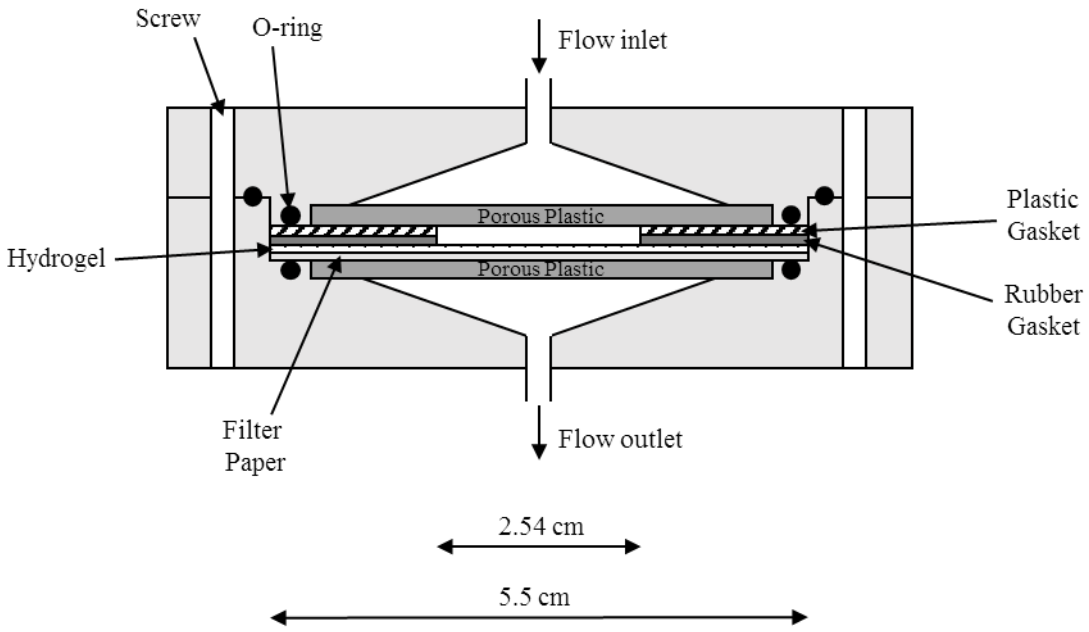

Figure D.2: Diagram of the hydrodynamic permeability membrane cell

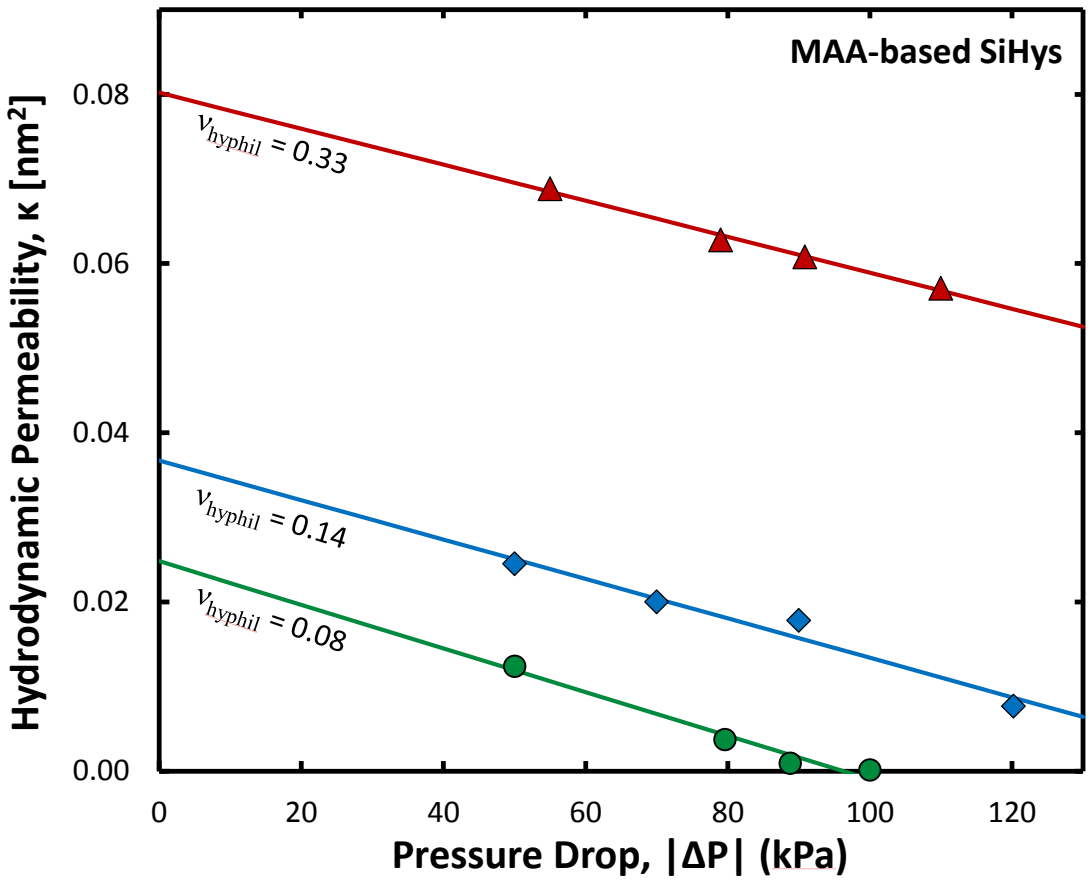

Figure D.3: Typical measured hydrodynamic permeabilities as a function of pressure drop for three MAA-based SiHys at pH 7.4. Least-squares-fit straight lines permit extrapolation to zero pressure drop to give κ_0.

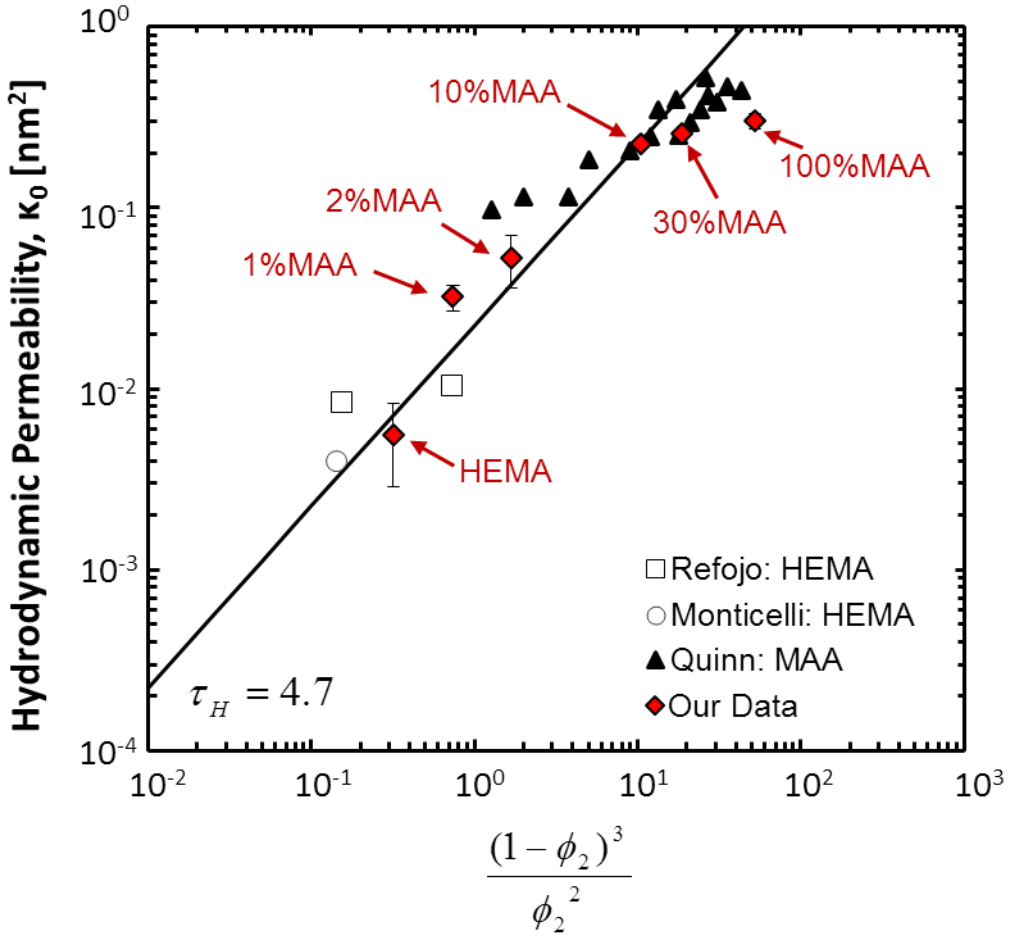

Figure D.4: Hydrodynamic permeabilities at zero pressure drop, κ_0, as a function of water contents expressed as $(1-\phi_2)^3/\phi_2^2$ for the HEMA/MAA hydrogels studied in Chapters 2-4 at pH 7.4. Also shown are measured hydrodynamic permeabilities for HEMA hydrogels by Refojo[3] (□) and Monticelli et al.[1] (○), and for MAA hydrogels by Quinn and Grodzinsky[4] (▲).With a_f = 2 nm, the best-fit unity-slope straight line gives a hydrodynamic tortuosity of τ_H = 4.7.

hydrodynamic permeabilities of HEMA/MAA hydrogels rise with increasing water content due to increased aqueous void volume. Also shown are literature values for HEMA hydrogels[1,3] and MAA hydrogels.[4] Our measurements are consistent with the literature values for both HEMA and MAA hydrogels. Significantly, HEMA/MAA hydrogels exhibit remarkably low hydrodynamic permeabilities, smaller than that of both sandstone (10^2-10^4 nm^2) and limestone (10^0-10^2 nm^2).[5] The straight-line fit in Figure D.4 indicates agreement with the Carman-Kozeny expression (Chapter 2 Eq. 7) as discussed below.

In Chapter 2, we invoked the Carman-Kozeny expression for hydrodynamic permeability in porous media, or $\kappa = (1-\phi_2)\langle r_H^2 \rangle / 2\tau_H^2$, where $\langle r_H^2 \rangle$ is the mean square hydraulic radius and τ_H is the gel hydrodynamic tortuosity. Application to a random array of fibers yielded

$$\kappa = \frac{(1-\phi_2)^3}{8\phi_2{}^2\tau_H^2} a_f^2 \quad , \tag{D2}$$

where, a_f is the gel fiber radius. For HEMA/MAA hydrogels, a_f is fixed at 2 nm.[6] As described in Chapter 2, τ_H of 4.7 was obtained by a best-fit of Eq. D2 to literature data. In Figure D.4, excellent agreement is seen between theory and our experimental values over several orders of magnitude. Clearly, the Carman-Kozeny expression quantitatively describes hydrodynamic permeabilities of HEMA/MAA hydrogels and may be employed in effective medium theory.

D2.2 Hydrodynamic Permeabilities of HEMA/MAA-Based SiHys

As discussed in Chapter 5, SiHys are microphase-separated materials with hydrophobic silicone domains and hydrophilic-polymer domains. Water and aqueous solutes reside in the hydrophilic-polymer domains and uptake is dictated by the solvent-free volume fraction of hydrophilic monomer during synthesis, ν_{hyphil}. Similarly, water transport occurs within the SiHy hydrophilic domains. Figure D.5 plots κ_0 as a function of ν_{hyphil} on a log-log scale for HEMA/MAA-based SiHys at pH 7.4. The hydrophilic-monomer fraction consists of HEMA (triangles), MAA (squares), or a mixture of 2 vol % MAA and 98 vol % HEMA (diamonds), denoted as 2%MAA/99%HEMA. Hydrodynamic permeabilities for conventional hydrogels that contain no silicone monomer or macromer (i.e., where $\nu_{hyphil} = 1$) are also shown. Solid lines are drawn according to theory discussed below. In all cases, κ_0 rises linearly with increasing ν_{hyphil}. As expected, The MAA-based hydrogels display consistently higher κ_0 than the HEMA-based and 2% MAA/98%HEMA-based hydrogels. Figure D.4 reveals MAA-based hydrogels have higher water contents than HEMA- and 2%MAA/98%HEMA-based hydrogels at pH 7.4. Greater hydrogel water contents lead to larger κ_0 due to the increased available volume for water flow.

In Chapter 5 we proposed a linear dependence of SiHy water and aqueous solute uptake on solvent-free hydrophilic-phase volume fraction. Similarly, hydrodynamic permeabilities in Figure D.5 rise linearly with increasing solvent-free hydrophilic-phase volume fraction. When $\nu_{hyphil} = 0$ (not shown), hydrodynamic permeabilities approach zero. When $\nu_{hyphil} = 1$,

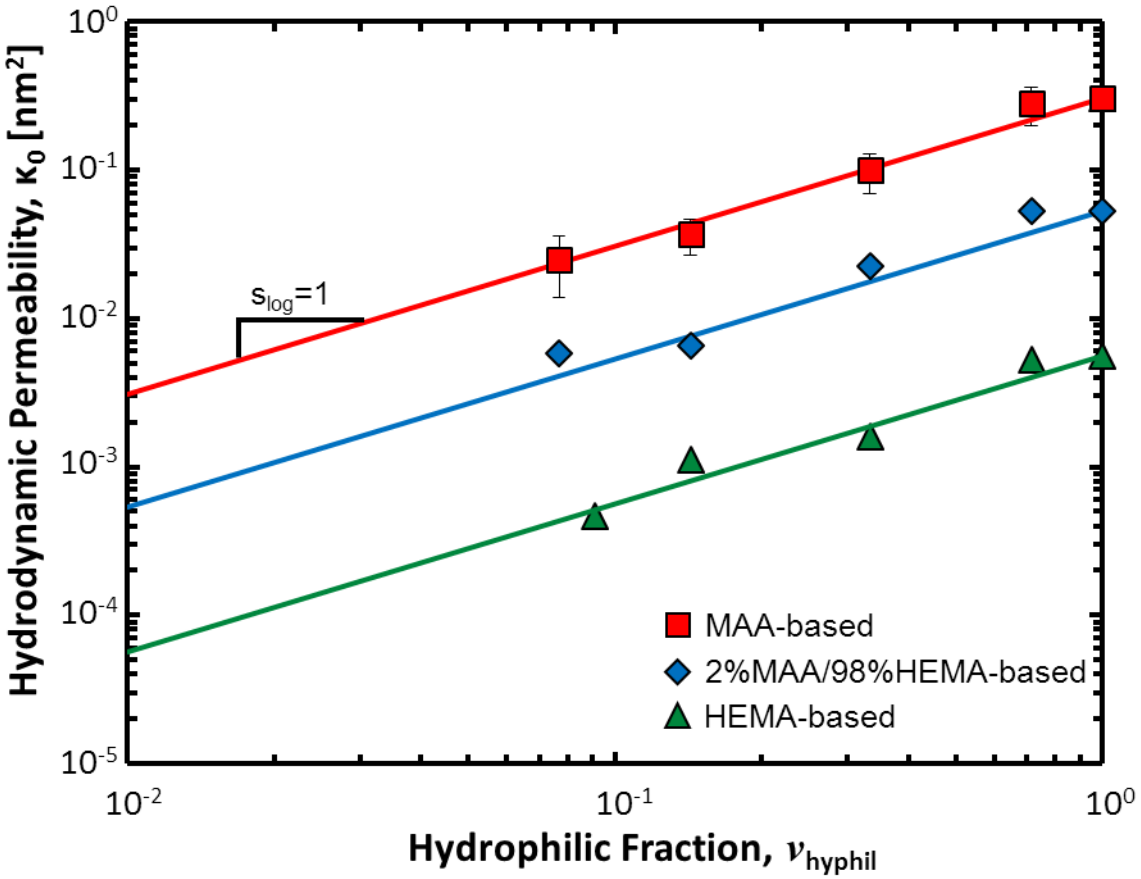

Figure D.5: Hydrodynamic permeabilities at zero pressure drop, κ_0, as a function of the solvent-free volume fraction of hydrophilic monomer, ν_{hyphil}, for HEMA- (triangles), MAA- (squares), and 10%MAA/90%HEMA-based (diamonds) SiHys at pH 7.4. Typical error bars are shown.

hydrodynamic permeabilities are simply the permeabilities of the conventional hydrophilic hydrogel of the corresponding type (i.e., HEMA, MAA, or 2%MAA/98%HEMA). Accordingly, SiHy hydrodynamic permeabilities are given by

$$\kappa_0 = \nu_{hyphil}\,\kappa_{0,hyphil}, \tag{D3}$$

where $\kappa_{0,hyphil}$ is the extrapolated hydrodynamic permeability of the conventional hydrophilic hydrogel. Solid lines in Figure D.5 are drawn according to Eq. D3 using no adjustable parameters. In all cases, excellent agreement is found between theory and experiment. Eq. D3 demonstrates water transport occurs primarily through the hydrophilic-polymer microdomains. Estimation of SiHy hydrodynamic permeabilities is now possible, based solely on the relative monomer fractions added during synthesis.

D3. References

1. Monticelli, M. V.; Chauhan, A.; Radke, C. J. The effect of water hydraulic permeability on the settling of a soft contact lens on the eye. *Current Eye Research* **2005,** 30, (5), 329-336.
2. Johnson, E. M.; Deen, W. M. Hydraulic permeability of agarose gels. *AIChE Journal* **1996,** 42, (5), 1220-1224.
3. Refojo, M. F. Permeation of water through some hydrogels. *Journal of Applied Polymer Science* **1965,** 9, (10), 3417-3426.
4. Quinn, T. M.; Grodzinsky, A. J. Longitudinal modulus and hydraulic permeability of poly (methacrylic acid) gels: Effects of charge density and solvent content. *Macromolecules* **1993,** 26, (16), 4332-4338.
5. Bear, J. *Dynamics of fluids in porous media*. Courier Corporation: New York, 1972.
6. Kotsmar, C.; Sells, T.; Taylor, N.; Liu, D. E.; Prausnitz, J. M.; Radke, C. J. Aqueous Solute Partitioning and Mesh Size in HEMA/MAA Hydrogels. *Macromolecules* **2012,** 45, (22), 9177-9187.